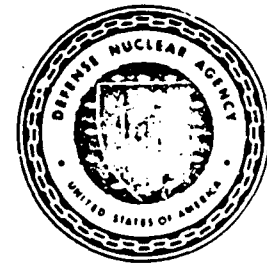




Defense Nuclear Agency
Alexandria, VA 22310-3398



C

AD-A278 837



DNA-TR-93-74

HYDROPLUS Experimental Study of Dry, Saturated, and Frozen Geological Materials

Edward S. Gaffney
Eric A. Smith
Kasch Corporation
901 Pennsylvania Avenue, NE
Albuquerque, NM 87110-7491

DTIC
SELECTE
MAY 04 1994
S B D

April 1994

Technical Report

DTIC

CONTRACT No. DNA 001-92-C-0057

Approved for public release;
distribution is unlimited.

1292 94-13321



94 5 03 054

DISCLAIMER:

Throughout this document references are made to commercial products. These references are provided to define the materials and products used in the test series report herein. In no way are these references to be construed as an endorsement or recommendation of these products by either the Defense Nuclear Agency or Ktech Corporation.

Destroy this report when it is no longer needed. Do not return to sender.

PLEASE NOTIFY THE DEFENSE NUCLEAR AGENCY,
ATTN: CSTI, 6801 TELEGRAPH ROAD, ALEXANDRIA, VA
22310-3398, IF YOUR ADDRESS IS INCORRECT, IF YOU
WISH IT DELETED FROM THE DISTRIBUTION LIST, OR
IF THE ADDRESSEE IS NO LONGER EMPLOYED BY YOUR
ORGANIZATION.



DISTRIBUTION LIST UPDATE

This mailer is provided to enable DNA to maintain current distribution lists for reports. (We would appreciate your providing the requested information.)

- Add the individual listed to your distribution list.
- Delete the cited organization/individual.
- Change of address.

NOTE:
Please return the mailing label from the document so that any additions, changes, corrections or deletions can be made easily.

NAME: _____

ORGANIZATION: _____

OLD ADDRESS

CURRENT ADDRESS

_____	_____
_____	_____
_____	_____

TELEPHONE NUMBER: () _____

DNA PUBLICATION NUMBER/TITLE

CHANGES/DELETIONS/ADDITIONS, etc.)
(Attach Sheet if more Space is Required)

_____	_____
_____	_____
_____	_____

DNA OR OTHER GOVERNMENT CONTRACT NUMBER: _____

CERTIFICATION OF NEED-TO-KNOW BY GOVERNMENT SPONSOR (If other than DNA):

SPONSORING ORGANIZATION: _____

CONTRACTING OFFICER OR REPRESENTATIVE: _____

SIGNATURE: _____

CUT HERE AND RETURN



DEFENSE NUCLEAR AGENCY
ATTN: TITL
6801 TELEGRAPH ROAD
ALEXANDRIA, VA 22310-3398

DEFENSE NUCLEAR AGENCY
ATTN: TITL
6801 TELEGRAPH ROAD
ALEXANDRIA, VA 22310-3398

REPORT DOCUMENTATION PAGE

Form Approved
OMB No. 0704-0188

Public reporting burden for this collection of information is estimated to average 1 hour per response including the time for reviewing instructions, searching existing data sources, gathering and maintaining the data needed, and completing and reviewing the collection of information. Send comments regarding this burden estimate or any other aspect of this collection of information, including suggestions for reducing this burden, to Washington Headquarters Services, Directorate for Information Operations and Reports, 1215 Jefferson Davis Highway, Suite 1204, Arlington, VA 22202-4302, and to the Office of Management and Budget, Paperwork Reduction Project (0704-0188), Washington, DC 20503.

1. AGENCY USE ONLY (Leave blank)		2. REPORT DATE 940401	3. REPORT TYPE AND DATES COVERED Technical 910715 - 920930	
4. TITLE AND SUBTITLE HYDROPLUS Experimental Study of Dry, Saturated, and Frozen Geological Materials			5. FUNDING NUMBERS C - DNA 001-92-C-0057 PE - 62715H PR - AB TA - CC WU - DH328750	
6. AUTHOR(S) Edward S. Gaffney and Eric A. Smith				
7. PERFORMING ORGANIZATION NAME(S) AND ADDRESS(ES) Ktech Corporation 901 Pennsylvania Avenue, NE Albuquerque, NM 87110-7491			8. PERFORMING ORGANIZATION REPORT NUMBER KTECH TR92-26	
9. SPONSORING/MONITORING AGENCY NAME(S) AND ADDRESS(ES) Defense Nuclear Agency 6801 Telegraph Road Alexandria, VA 22310-3398 FCTP/Martinez			10. SPONSORING/MONITORING AGENCY REPORT NUMBER DNA-TR-93-74	
11. SUPPLEMENTARY NOTES This work was sponsored by the Defense Nuclear Agency under RDT&E RMC Code B4662D AB CC 00007 5200A 25904D.				
12a. DISTRIBUTION/AVAILABILITY STATEMENT Approved for public release; distribution is unlimited.			12b. DISTRIBUTION CODE	
13. ABSTRACT (Maximum 200 words) The dynamic shock responses of eight (8) types of rock and grouts were determined from one-dimensional plate impact experiments to support the Defense Nuclear Agency (DNA) HYDROPLUS program. Hugoniot data and loading and release paths were measured using in-situ stress gauges or VISAR interferometry. Two NTS tuffs from the DISTANT ZENITH and HUNTERS TROPHY test beds, a grout, MJ-2, which was designed to match the DISTANT ZENITH tuff and three carbonate rocks, Danby marble, Fort Knox carbonates and Salem limestone were characterized. All of these materials were tested in a water saturated condition at ambient and frozen conditions. Additionally, the Salem limestone was characterized dry. Hugoniot data for ice was also measured. Experiments that simulated jointed rock formation were conducted using Danby marble to evaluate the effects of water- or ice-filled joints on the amplitude of a stress wave propagating through the formation. Hugoniot data, release adiabats, and propagated waveshapes are presented for the rocks, grout, and ice. The effects of freezing, porosity, and dolomitization of the limestones on the Hugoniot and wave propagation characteristics of these materials are detailed. Propagated wave profiles and measured attenuation rates are given for the simulated jointed rock experiments. <i>DISCONTINUED</i>				
14. SUBJECT TERMS Hugoniot DISTANT ZENITH Tuff Release Adiat MJ-2 Grout Ice Jointed Rocks			HUNTERS TROPHY Tuff Danby Marble Fort Knox Carbonates	
			15. NUMBER OF PAGES 170	
			16. PRICE CODE	
17. SECURITY CLASSIFICATION OF REPORT UNCLASSIFIED	18. SECURITY CLASSIFICATION OF THIS PAGE UNCLASSIFIED	19. SECURITY CLASSIFICATION OF ABSTRACT UNCLASSIFIED	20. LIMITATION OF ABSTRACT SAR	

UNCLASSIFIED

SECURITY CLASSIFICATION OF THIS PAGE

CLASSIFIED BY:

N/A since Unclassified.

DECLASSIFY ON:

N/A since Unclassified.

PREFACE

Ktech Corporation was tasked under Contract DNA001-92-C-0057, Subtask 01-19/04 to measure the dynamic response of materials relevant to the Defense Nuclear Agency (DNA) HYDROPLUS yield verification program. This work was conducted at the Materials Response Impact Facility at Kirtland Air Force Base. The Facility was a USAF Phillips Laboratory facility at the start of the effort (Mr. David Hillard, PL/WSSH, Contracting Officer Representative (COR)) and was a DNA Facility (Mr. Doug Seemann, DNA/Experimental Shock Physics (DNA/FCTP), Contracting Officer Technical Representative (COTR)) at the end of the effort. The work was monitored by Ms. Audrey Martinez, DNA/FCTP. During the course of the program the work was reviewed by the High Pressure Equation of State Working Group (HPEOS WG) chaired by Dr. George Baladi, DNA/FCTP. The HPEOS WG provided many helpful comments which have assisted in interpreting the data, and they have also provided direction on the content of the program. The authors are thankful for the careful review of the text by A. Martinez, E. Rinehart, (DNA/FCTP) and F. Davies (Ktech). Russell Hallett, Sherri Heyborne, John Liwski, and Tom Thornhill of Ktech provided valuable assistance in the fabrication, test, and analysis of the experiments.

Accession For	
NTIS GRA&I	<input checked="" type="checkbox"/>
DTIC TAB	<input type="checkbox"/>
Unannounced	<input type="checkbox"/>
Justification	
By _____	
Distribution/ _____	
Availability Codes	
Dist	Avail and/or Special
A-1	

CONVERSION TABLE

Conversion factors for U.S. customary to metric (SI) units of measurement.

MULTIPLY _____ > BY _____ > TO GET
 TO GET < _____ BY < _____ DIVIDE

angstrom	1.000 000 X E -10	meters (m)
atmosphere (normal)	1.013 25 X E +2	kilo pascal (kPa)
bar	1.000 000 X E +2	kilo pascal (kPa)
barn	1.000 000 X E -28	meter ² (m ²)
British thermal unit (thermochemical)	1.054 350 X E +3	joule (J)
calorie (thermochemical)	4.184 000	joule (J)
cal (thermochemical/cm ²)	4.184 000 X E -2	mega joule/m ² (MJ/m ²)
curie	3.700 000 X E +1	*giga becquerel (GBa)
degree (angle)	1.745 329 X E -2	radian (rad)
degree Fahrenheit	$t_c = (t_f + 459.67)/1.8$	degree kelvin (K)
electron volt	1.602 19 X E -19	joule (J)
erg	1.000 000 X E -7	joule (J)
erg/second	1.000 000 X E -7	watt (W)
foot	3.048 000 X E -1	meter (m)
foot/pound-force	1.355 818	joule (J)
gallon (U.S. liquid)	3.785 412 X E -3	meter ³ (m ³)
inch	2.540 000 X E -2	meter (m)
jerk	1.000 000 X E +9	joule (J)
joule/kilogram (J/kg) radiation dose absorbed	1.000 000	Gray (Gy)
kilotons	4.183	terajoules
kip (1000 lbf)	4.448 222 X E +3	newton (N)
kip/inch ² (ksi)	6.894 757 X E +3	kilo pascal (kPa)
ktop	1.000 000 X E +2	newton-second/m ² (N-s/m ²)
micron	1.000 000 X E -6	meter (m)
mil	2.540 000 X E -5	meter (m)
mile (international)	1.609 344 X E +3	meter (m)
ounce	2.834 952 X E -2	kilogram (kg)
pound-force (lbf avoirdupois)	4.448 222	newton (N)
pound-force inch	1.129 848 X E -1	newton-meter (N-m)
pound-force/inch	1.751 268 X E +2	newton/meter (N/m)
pound-force/foot ²	4.788 026 X E -2	kilo pascal (kPa)
pound-force/inch ² (psi)	6.894 757	kilo pascal (kPa)
pound-mass (lbm avoirdupois)	4.535 924 X E -1	kilogram (kg)
pound-mass-foot ² (moment of inertia)	4.214 011 X E -2	kilogram-meter ² (kg-m ²)
pound-mass/foot ³	1.601 846 X E +1	kilogram/meter ³ (kg/m ³)
rad (radiation dose absorbed)	1.000 000 X E -2	**Gray (Gy)
roentgen	2.579 760 X E -4	coulomb/kilogram (C/kg)
shake	1.000 000 X E -8	second (s)
slug	1.459 390 X E +1	kilogram (kg)
torr (mm Hg, 0°C)	1.333 22 X E -1	kilo pascal (kPa)

* The becquerel (Bq) is the SI unit of radioactivity; 1 Bq = 1 event/s.

** The Gray (Gy) is the SI unit of absorbed radiation.

TABLE OF CONTENTS

Section	Page
PREFACE	iii
CONVERSION TABLE	iv
FIGURES	vii
TABLES	x
1 INTRODUCTION	1
1.1 BACKGROUND	1
1.2 PROGRAM SCOPE	2
1.3 DOCUMENT ROADMAP	6
2 EXPERIMENTAL AND ANALYTICAL TECHNIQUES	7
2.1 SAMPLE CHARACTERIZATION	7
2.2 GAS GUN TECHNIQUES	8
2.2.1 Equation of State Tests	9
2.2.2 Artificial Joints	16
2.3 LAGRANGIAN ANALYSIS	18
3 EXPERIMENTAL RESULTS FOR TUFF AND TUFF-MATCHING GROUT	22
3.1 HUNTERS TROPHY TUFF (GI-1)	22
3.2 DISTANT ZENITH TUFF	31
3.3 MJ-2 (NSF-6) GROUT	34
3.4 DISTANT ZENITH TUFF AND MJ-2 (NSF-6) GROUT COMPARISON	36
4 EXPERIMENTAL RESULTS FOR CARBONATE ROCKS	43
4.1 DANBY MARBLE	43
4.2 FT. KNOX CARBONATES	49
4.3 SALEM LIMESTONE	53
4.4 DISCUSSION	60
5 EXPERIMENTAL RESULTS FOR ICE	79
5.1 RESULTS	79
5.2 DISCUSSION	89

Section	Page
6 EXPERIMENTAL RESULTS FOR JOINT EXPERIMENTS	91
7 CONCLUSIONS	98
8 REFERENCES	101
Appendix	
STRESS AND PARTICLE VELOCITY WAVEFORMS	103

FIGURES

Figure	Page
2-1 Rock equation of state experimental arrangement with Lagrangian stress gauges.	10
2-2 Ice equation of state experimental arrangement with Lagrangian stress gauges.	14
2-3 Equation of state experimental arrangement for VISAR particle velocity measurement.	15
2-4 Jointed target experiment configuration.	17
2-5 The generation of path lines in the loading process for the Lagrangian analysis.	20
3-1 Photograph of typical Hunters Trophy tuff (GI-1) sample	23
3-2 HUNTERS TROPHY tuff (GI-1) stress-particle velocity Hugoniot data and release paths	26
3-3 HUNTERS TROPHY tuff (GI-1) stress- ρ/ρ_0 Hugoniot data and release paths	27
3-4 HUNTERS TROPHY tuff (GI-1) shock velocity-particle velocity Hugoniot data	28
3-5 HUNTERS TROPHY tuff (GI-1), shot 3520.	29
3-6 HUNTERS TROPHY tuff (GI-1), shots 3518 and 3519.	29
3-7 HUNTERS TROPHY tuff (GI-1), shots 3516 and 3517.	30
3-8 HUNTERS TROPHY tuff (GI-1), shots 3521 and 3522.	30
3-9 Photograph of typical DISTANT ZENITH tuff sample	32
3-10 VISAR data for MJ-2 (NSF-6) grout 5-mm (shot 3512 and 3514) and 10 mm (shot 3506) samples.	37
3-11 DISTANT ZENITH tuff and MJ-2 (NSF-6) grout stress-particle velocity Hugoniot data with partial loading and release paths.	38
3-12 DISTANT ZENITH tuff and MJ-2 (NSF-6) grout stress- ρ/ρ_0 Hugoniot data with partial loading and release paths.	39
3-13 DISTANT ZENITH tuff and MJ-2 (NSF-6) grout shock velocity-particle velocity Hugoniot data.	40
3-14 Comparison between VISAR particle velocity profiles for MJ-2 (NSF-6) grout and DZ tuff.	42
4-1 Danby marble stress-particle velocity Hugoniot data with partial loading and release paths.	46
4-2 Danby marble stress- ρ/ρ_0 Hugoniot data with partial loading and release paths.	47
4-3 Danby marble shock velocity-particle velocity Hugoniot data.	48
4-4 Stress histories for Danby marble	50
4-5 Photograph of typical Jeffersonville-2 sample.	51
4-6 Ft. Knox carbonates stress-particle velocity Hugoniot data with partial loading and release paths	56
4-7 Ft. Knox carbonates stress- ρ/ρ_0 Hugoniot data with partial loading and release paths	57
4-8 Ft. Knox carbonates shock velocity-particle velocity Hugoniot data.	58
4-9 Salem limestone stress-particle velocity Hugoniot data and release paths	63
4-10 Salem limestone stress- ρ/ρ_0 Hugoniot data and release paths	64
4-11 Salem limestone shock velocity-particle velocity Hugoniot data	65
4-12 Dry Salem limestone data at 8 mm depth.	66
4-13 Saturated Salem limestone data at 8 mm depth.	66
4-14 Frozen Salem limestone data at 8 mm depth.	67
4-15 Frozen Louisville and frozen Jeffersonville-1 comparison.	68
4-16 Saturated Louisville and saturated Jeffersonville-2 comparison.	68
4-17 Shot 3489 (saturated) and 3490 (frozen) comparison.	70
4-18 Shot 3499 (saturated) and 3492 (frozen) comparison.	70
4-19 Shot 3503 (saturated) and 3505 (frozen) comparison.	71
4-20 Shot 3497 (saturated) and 3498 (frozen) comparison.	71

FIGURES (Continued)

Figures	Page
4-21 Comparison of stress profiles with peaks near 2.5 GPa at 8 mm depths in each type of Salem limestone.	72
4-22 Comparison of the response of dry, saturated, and frozen Salem limestone at a nominal impact velocity of 0.14 km/s	74
4-23 Comparison of the response of dry, saturated, and frozen Salem limestone at a nominal impact velocity of 0.29 km/s	75
4-24 Comparison of the response of dry, saturated, and frozen Salem limestone at a nominal impact velocity of 0.5 km/s	76
4-25 Comparison of the response of dry, saturated, and frozen Salem limestone at a nominal impact velocity of 0.79 km/s	77
4-26 Shot 3562 (saturated) and 3577 (frozen) comparison.	78
5-1 Ice stress-particle velocity Hugoniot EOS data with loading and release paths	81
5-2 Ice stress-density Hugoniot EOS data with loading and release paths	82
5-3 Ice shock velocity-particle velocity Hugoniot EOS data	83
5-4 Shot 3539, stress-time data	84
5-5 Shot 3536, stress-time data	85
5-6 Shot 3538, stress-time data	86
5-7 Shot 3540, stress-time data	87
5-8 Stress histories (dotted line) and Lagrangian code input (solid line) for gauges #1 and #2 on shot 3538	88
6-1 Stress wave profiles transmitted through single-jointed samples for 1.2 GPa input stress	94
6-2 Stress wave profiles transmitted through single-jointed samples for 6 GPa input stress	95
6-3 Stress wave profiles transmitted through triple-jointed samples for 6 GPa input stress	96
A-1 HUNTERS TROPHY tuff shot 3520	105
A-2 HUNTERS TROPHY tuff shot 3518	106
A-3 HUNTERS TROPHY tuff shot 3519	107
A-4 HUNTERS TROPHY tuff shot 3516	108
A-5 HUNTERS TROPHY tuff shot 3517	109
A-6 HUNTERS TROPHY tuff shot 3521	110
A-7 HUNTERS TROPHY tuff shot 3522	111
A-8 DISTANT ZENITH shot 3437	112
A-9 DISTANT ZENITH shot 3447	113
A-10 DISTANT ZENITH shot 3515	114
A-11 MJ-2 (NSF-6) grout shot 3449	115
A-12 MJ-2 (NSF-6) grout shot 3506	116
A-13 MJ-2 (NSF-6) grout shot 3512	117
A-14 MJ-2 (NSF-6) grout shot 3514	118
A-15 MJ-2 (NSF-6) grout shot 3528	119
A-16 Danby marble shot 3467	120
A-17 Danby marble shot 3469	121
A-18 Danby marble shot 3513	122
A-19 Danby marble shot 3527	123
A-20 Ft. Knox carbonates shot 3489	124
A-21 Ft. Knox carbonates shot 3490	125
A-22 Ft. Knox carbonates shot 3499	126

TABLES

Table	Page
1-1 Material core sample summary	4
i-2 Shot summary	5
2-1 Impactor and buffer materials (Hugoniot)	9
3-1 Material properties for HUNTERS TROPHY tuff (GI-1)	23
3-2 HUNTERS TROPHY tuff shot configuration data	25
3-3 HUNTERS TROPHY tuff Lagrangian stress gauge Hugoniot data	25
3-4 Material properties for DISTANT ZENITH tuff	32
3-5 DISTANT ZENITH tuff shot configuration data	33
3-6 DISTANT ZENITH tuff Hugoniot data	33
3-7 Material properties for DISTANT ZENITH MJ-2 (NSF-6) grout	34
3-8 MJ-2 (NSF-6) grout shot configuration data	35
3-9 MJ-2 grout Hugoniot data	35
4-1 Material properties for Danby marble	44
4-2 Danby marble shot configuration data	45
4-3 Danby marble Lagrangian stress gauge Hugoniot data	45
4-4 Material properties for Ft. Knox carbonates	52
4-5 Ft. Knox carbonates shot configuration data	54
4-6 Ft. Knox carbonates (UTP site) Lagrangian stress gauge Hugoniot data	55
4-7 Material properties for Salem limestone	59
4-8 Salem Limestone shot configuration data	61
4-9 Salem Limestone Lagrangian Hugoniot data	62
5-1 Ice shot configuration data	80
5-2 Ice equation of state data	80
6-1 Danby marble joint experiment shot configuration summary	91
6-2 Danby marble joint experiment target configuration data	92

FIGURES (Continued)

Figures	Page
A-23 Ft. Knox carbonates shot 3492	127
A-24 Ft. Knox carbonates shot 3491	128
A-25 Ft. Knox carbonates shot 3503	129
A-26 Ft. Knox carbonates shot 3505	130
A-27 Ft. Knox carbonates shot 3504	131
A-28 Ft. Knox carbonates shot 3497	132
A-29 Ft. Knox carbonates shot 3498	133
A-30 Salem limestone shot 3554	134
A-31 Salem limestone shot 3556	135
A-32 Salem limestone shot 3564	136
A-33 Salem limestone shot 3558	137
A-34 Salem limestone shot 3561	138
A-35 Salem limestone shot 3555	139
A-36 Salem limestone shot 3563	140
A-37 Salem limestone shot 3557	141
A-38 Salem limestone shot 3560	142
A-39 Salem limestone shot 3559	143
A-40 Salem limestone shot 3562	144
A-41 Salem limestone shot 3583	145
A-42 Salem limestone shot 3573	146
A-43 Salem limestone shot 3576	147
A-44 Salem limestone shot 3574	148
A-45 Salem limestone shot 3575	149
A-46 Salem limestone shot 3582	150
A-47 Salem limestone shot 3577	151
A-48 Danby marble with joints shot 3470	152
A-49 Danby marble with joints shot 3471	153
A-50 Danby marble with joints shot 3473	154
A-51 Danby marble with joints shot 3474	155
A-52 Danby marble with joints shot 3475	156
A-53 Danby marble with joints shot 3476	157

SECTION 1 INTRODUCTION

The Defense Nuclear Agency (DNA) has developed a method of verifying the yield of non-standard underground nuclear tests using peak radial stress and velocity at several ranges from the working point in conjunction with hydrocode calculations. This method, which is known as "HYDROPLUS," requires measurements of the dynamic material properties of the geologic materials between the working point and the measurement locations as input to the hydrocode calculations. In support of this effort, the dynamic shock response for different rock types and man-made grouts was determined from plate impact experiments at the DNA Impact Facility at Kirtland AFB, New Mexico. This report describes the experimental techniques used and details the experimental results and analysis.

1.1 BACKGROUND.

The verification protocol of the Threshold Test Ban Treaty (TTBT) is based on the use of on-site verification techniques. The HYDROPLUS method uses stress and velocity gauges to measure the peak stress and particle velocity at known ranges. Experience at the Nevada Test Site (NTS) and calculations have shown that the rate of decay of peak values vs. range is dependent on the unloading behavior from the peak state. Therefore, successful application of the HYDROPLUS method requires knowledge of the response of rocks and grouts to dynamic loading and also to the subsequent release.

Underground nuclear tests conducted by DNA at the NTS in the last three years have included fielding of instrumentation to exercise the HYDROPLUS method. In support of these experiments, data were needed on the shock response of tuffs from the DISTANT ZENITH and HUNTERS TROPHY test beds and on MJ-2 (NSF-6) grout which was used to stem the gauge emplacements on DISTANT ZENITH. The Hugoniot and loading and release paths were measured for these materials from 1.5 to 12.1 GPa.

The numerical hydrocodes used for HYDROPLUS and the techniques of gauge emplacement were both exercised in the DISTANT MOUNTAIN high explosive tests series. These tests used large, carefully machined blocks of marble from Danby, Vermont, loaded by a shock produced by

nitromethane. Equation of state (EOS) and constitutive property data on Danby marble were measured at stress levels between 1.2 and 15.6 GPa to support the DISTANT MOUNTAIN tests.

Since underground nuclear testing began, there have been many publications of shock wave data for rocks (Ahrens, 1964 and McQueen, 1967). These data have made possible considerable advances in the understanding of nuclear test technology including better containment designs and hydrodynamic yield determinations. However, much of the Russian nuclear test site in Novaya Zemlya is underlain by permafrost. Although there are a few publications on shocks in frozen soils (e.g., Gaffney, 1979), there are no published data on shock propagation in frozen rocks. To fill this void, experiments were conducted on low porosity (~2 percent) carbonates from the Underground Technology Program (UTP) test site at Ft. Knox, Kentucky, and Salem limestone (16 percent porosity); rocks were tested in both water saturated and frozen states. The Salem limestone was also tested dry.

Understanding of the propagation of shocks in frozen media entails a knowledge of the response of pure ice. Gaffney (1985) provided a compilation of shock data available in 1985. There is considerable complexity between 0.2 and 4.0 GPa due to the occurrence of plastic yielding and many solid state phase changes. To provide more detail, plate impact tests were also conducted for ice at stresses ranging from 0.7 to 3.0 GPa.

Real rocks are not continuous, but rather are masses of heterogeneous material separated by fractures or joints which may be open. If these joints are filled with water or ice and/or other materials with acoustic impedances much less than the intact rock, they will affect the propagation of shocks across them. These effects are complex, and probably pressure dependent. At pressures below 0.2 GPa, an ice-filled joint would be expected to have less effect than a water-filled one because the impedance of ice is greater than the impedance of water. But at higher pressures, the situation is reversed, and the ice-filled joint should have a greater effect than a water-filled one. Consequently six tests were conducted with artificial joints, both ice-filled and water-filled, to elucidate the phenomena associated with shock propagation in frozen, jointed rock.

1.2 PROGRAM SCOPE.

This report documents fifty-nine (59) gas gun tests conducted on 8 materials and two special target configurations in support of DNA's HYDROPLUS yield verification program. All samples were

obtained from cores provided by DNA. Test samples were prepared by Ktecii, Terra Tek, and the USACE/Waterways Experiment Station (WES). Table 1-1 describes the sources of the cores. Table 1-2 defines the 59 tests performed. It lists the materials tested, stress ranges examined, the number of shots, and the sections of this document where the results and discussion are presented. Experiments were conducted to characterize four material categories: tuffs and grout, carbonate rocks, ice, and simulated jointed rocks. Hugoniot data were obtained for: ice; MJ-2 (NSF-6) grout from DISTANT ZENITH; DISTANT ZENITH tuff; HUNTERS TROPHY tuff; and three carbonate rocks, Danby marble, Fort Knox carbonates, and Salem limestone. The Hugoniot data are supplemented with loading and release paths derived from Lagrangian analyses for at least one shot on each material. All rocks and grout experiments were tested in a water saturated condition at ambient conditions. The Fort Knox carbonates and the Salem Limestone were also tested frozen. Only Salem limestone was tested dry. The response of Danby marble slabs, separated by spacers to simulate rock containing joints, was examined in six tests. The joints were filled with either water or ice.

There is a significant difference (20%) between the Hugoniots of the DISTANT ZENITH and HUNTERS TROPHY tuffs, even though densities and ultrasonic wavespeeds match. The Hugoniots of the DISTANT ZENITH and the MJ-2 (NSF-6) grout are close even though the acoustic impedances differ by 30 percent.

Differences in the response of dry and saturated 16% porosity Salem limestone were pronounced. Studies on saturated limestone at both room temperature and $\sim -7^{\circ}\text{C}$ indicated that the importance of freezing depends on the porosity of the rock. Negligible effects of freezing were identified in the low porosity (~ 2 percent) Ft. Knox carbonates, but freezing did cause noticeable (10%) changes in the response of the 16-percent porous Salem limestone at modest pressures; both wavespeeds and stress profiles were controlled by the phase of the interstitial water. Porosity and saturation of the geology must be known to develop adequate dynamic material properties for use in hydrocode calculations.

The Ft. Knox carbonates were obtained from the Jeffersonville and Louisville formations. Comparison of the data from the Jeffersonville formation, a calcite limestone, with that from the Louisville formation, which is partly dolomitized, indicate that dolomitization has a marked effect

Table 1-1. Material core sample summary.

Core	Source Location	Hole Number	Interval* (feet)
DISTANT ZENITH tuff	NTS	U12p.04 IH-20	144.4 - 145.8
DISTANT ZENITH MJ-2 (NSF-6) grout	USACE/WES Vicksburg, MS	U12p.04 pour #21 Mix: MJ-2 (NSF-6) Car #3 & #9 7-17-91	
HUNTERS TROPHY tuff	Area 12, NTS (Stratigraphic Designator T14H)	U12n.24 GI-1	211.4 - 212.5
Danby Marble	Vermont Marble Company, Proctor, VT		
Ft. Knox carbonates	Ft. Knox, KY UTP Site		
Louisville formation (preserved)		CB-7 (Section #1-3) CB-7 (Section #4)	601.2 - 602.3 642.3 - 642.9
Jeffersonville-1 formation (preserved)		CB-7	523.6 - 523.9
Jeffersonville-2 formation (unpreserved)		GWMH-3A	521.6 - 522.3
Salem Limestone	Elliot Stone Company, Inc., Bedford, IN (Gefken, 1992)		
Ice	Samples were made by Ktech from de-aired distilled water.		

* Interval is (1) the distance along the satellite hole from the drill collar to the core sample for the tuff from NTS, and (2) the distance from the surface for the Ft. Knox carbonates.

Table 1-2. Shot summary.

Results Section	Material	Nominal Stress Range (GPa)	No. of Shots		
			Ambient	Frozen	Dry
3	<u>Tuffs and Grouts</u>				
3.1	DISTANT ZENITH tuff	1.5 — 10.4	4	0	0
3.2	HUNTERS TROPHY tuff	1.6 — 5.0	7	0	0
3.3	MJ-2 (NSF-6) grout	4.2 — 12.1	6	0	0
4	<u>Carbonate Rocks</u>				
4.1	Danby Marble	1.2 — 15.6	4	0	0
4.2	Ft. Knox Carbonates	1.8 — 6.0	5	5	0
4.3	Salem Limestone	0.6 — 5.2	6	7	5
5	<u>Ice</u>	0.7 — 2.9	0	4	0
6	<u>Joint Experiments in Danby Marble</u>	1.2 — 5.6	3	3	0

Note: Ambient and frozen shot samples were saturated. Dry Salem limestone experiments were conducted at ambient temperature.

on the Hugoniot (~40% increase in impedance). Since dolomitization is frequently inhomogeneous, its presence at any location will be difficult to predict.

Four Hugoniot and transmitted stress wave experiments were conducted on ice in the stress range of 0.5 to 3.0 GPa. The results, when combined with previously available data, provide a good definition of the Hugoniot of ice from 1.5 to 3.0 GPa. As with previous investigations, the results between 0.7 GPa and 1.5 GPa are less satisfying. Unloading of ice compressed to a density of about 1.35 g/cc at 1.5 GPa trends toward the density of ices II and III, although the apparent modulus is too low for any of the high pressure phases.

In the simulated joint tests, water-filled joints caused more rapid attenuation than no joints. Ice-filled joints caused even more attenuation than water-filled joints. These effects were seen at 1 GPa and 5 GPa. However, the effects may be scale dependent. The pulse durations in the simulation experiments were orders of magnitude shorter than those generated by nuclear events, but the joints were also thinner.

1.3 DOCUMENT ROADMAP.

This document is divided into seven major sections. The experimental configurations and the analysis techniques are presented in Section 2 for the experiments performed in this study. The experimental data are detailed in Sections 3, 4, 5, and 6. Section 3 presents the tuff and tuff-matching grout results, Section 4 the carbonate rocks data, Section 5 the ice data, and finally Section 6 the jointed experiments results. Within each of these sections a description of each geological material and its derived material properties (Hugoniot points and loading and release curves data) are presented. A discussion of each individual set of results is also given in these sections. Conclusions that can be drawn from these measurements are summarized in Section 7. Recorded waveforms are presented individually in Appendix A by material type.

SECTION 2 EXPERIMENTAL AND ANALYTICAL TECHNIQUES

This section presents descriptions of the experimental techniques used to measure the dynamic material properties of the rocks and grout evaluated in this program and details the analytic techniques used to interpret the measured data. The nondestructive evaluation (NDE) techniques used to evaluate the test samples are detailed in Section 2.1. Gas gun techniques used to measure the Hugoniot are presented in Section 2.2 which specifies the experimental configurations, the material properties of the impactors and buffers, and the instrumentation techniques used in these tests. Two basic instrumentation techniques, in-situ stress gauges and interferometry, were used. The measurement techniques and their associated steady-state analysis techniques are presented. Section 2.3 describes the Lagrangian analysis techniques used to analyze the attenuating stress waves measured by the in-situ stress gauges.

2.1 SAMPLE CHARACTERIZATION.

Nondestructive evaluation (NDE) of samples prior to testing was limited to bulk density measurements and ultrasonic longitudinal velocity measurements. All of these measurements were taken at ambient temperature including those samples later frozen. Sample saturation was maintained during handling and measurements. Tabulations of sample thickness, density, and longitudinal velocity for each material are shown in Sections 3 and 4. Average and standard deviation (std) values for density and longitudinal velocity are also given for each material. Prepared samples were nominally 5 or 10 mm thick and 48 or 64 mm in diameter. Bulk densities were determined from sample weight and volume measurements. Two techniques for measuring sample volume were used: geometric and immersion. The geometric method was based on sample thickness and diameter measurements. The immersion method employed Archimedes principle of buoyancy where the samples were immersed in water and the buoyant force (F_b) was measured. Since the volume of the sample is equal to the volume of the water displaced, the volume can be determined from the buoyant force and density of water (ρ_w) by:

$$\text{Sample volume} = \frac{F_b}{\rho_w} \quad (2.1)$$

For dry samples, the geometric method was used for density measurement. The immersion method was used on saturated samples which were not perfect cylinders (e.g., chipped or pitted edges). For example, pebbles were dislodged from the perimeter of tuff samples after they were

loosened from the matrix during the machining process. This resulted in pits or voids in the edges which would yield a low density measurement if the geometric method was used. The accuracy of these density measurements is $\pm 1\%$.

Ultrasonic velocity measurements were made to check sample integrity and to estimate shock impedances for experiment design. Sample longitudinal ultrasonic velocity measurements were taken in the through-the-thickness direction by measuring the transit time through the sample of a pulse generated by a 19.1-mm-diameter 10-MHz quartz crystal transducer clamped to one face of a disk and detected by a similar transducer on the opposite face. The coupling medium between the transducers and sample was water.

2.2 GAS GUN TECHNIQUES.

Plane shock wave experiments were conducted on the 105-mm diameter, single stage, light gas gun at the DNA Material Response Impact Facility at Kirtland AFB, New Mexico. Stress wave propagation characteristics in geologic or man-made materials were measured using standard plate impact techniques (Lee, 1989). These transmitted wave experiments provided wave propagation and Hugoniot data for the materials. At lower stresses, in-material gauge techniques were used while an interferometric technique provided Hugoniot data above 6 GPa. These techniques are discussed in more detail later in this section. The materials were examined in dry or water saturated states at ambient or frozen temperatures.

The samples were mounted at the end of the gas gun in a sealed target holder. Sample and impactor were carefully aligned prior to each shot to provide planar impact. Tilt between impactor and sample, as determined by tilt pins, was generally less than 1.0 mrad. Precisely spaced shorting pins were placed near the muzzle of the gun to measure projectile velocity. Prior to impact, signals were generated when the pins were shorted by projectile contact. These data signals, and the data signals generated by the in-situ stress gauges and interferometry, were recorded on Tektronix¹ 7612D and LeCroy² 9450 digitizers. The target chamber and barrel of the gun were evacuated to below 0.1 mtorr prior to each shot to eliminate air cushion effects.

¹ Tektronix, Inc., P.O. Box 500, Beaverton, OR.

² LeCroy Research Corporation, Chestnut Ridge, NY.

2.2.1 Equation of State Tests.

Thin-plate impactors of either tungsten carbide (WC), 4340 steel, or 6061-T6 aluminum were used. The Hugoniot coefficients for these materials are listed in Table 2-1.

Table 2-1. Impactor and buffer materials (Hugoniots).

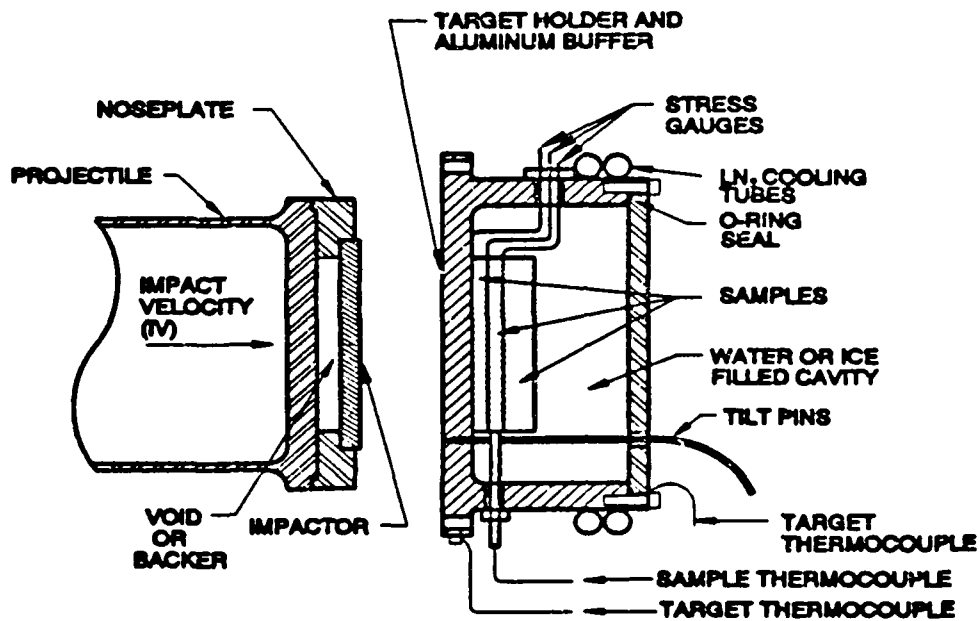
Hugoniot Coefficients ^a				Initial Density (g/cc)	Range (GPa)
A	B	C	D		
6061-T6 Al (Christman^o, 1971, and Marsh^m, 1979)					
0.0	17.50	0.00	0.0	2.706	0.0 - 0.6 ^e
1.0	14.04	3.77	0.0	2.706	0.6 - 16.0 ^e
0.0	14.46	3.62	0.0	2.703	7.0 - 107.8 ^m
Tungsten Carbide (WC) (Karnes, Private Communication)					
0.00	102.50	0.00	0.00	14.85	0.0 - 3.0
-0.21	106.22	-95.69	124.70	14.85	3.0 - 27.5
4340 Steel, Rc54 hardness (Butcher, 1964)					
0.00	455.00	0.00	0.00	7.85	0.0 - 2.7
2.56	415.84	0.00	0.00	7.85	2.7 - 6.2

$$^a \text{Stress (GPa)} = A + Bu_p + Cu_p^2 + Du_p^3$$

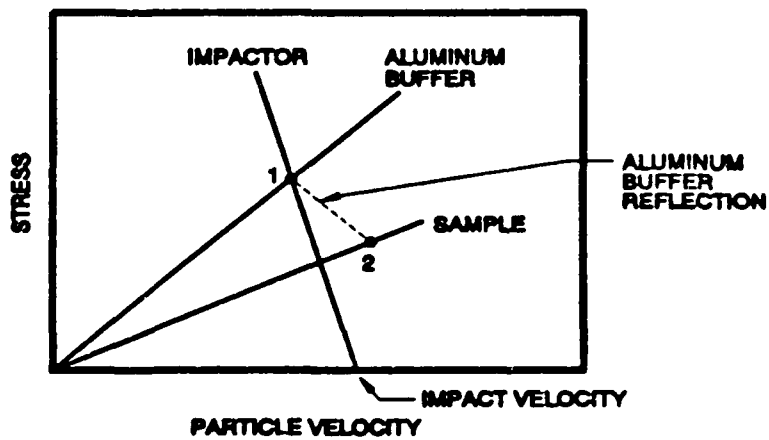
2.2.1.1 Lagrangian Stress Measurements. The experimental configuration is shown in Figure 2-1(a). The impactor was contained in an aluminum nose plate and mounted on the front of the projectile. When necessary, low density (0.27 g/cc) carbon foam or PMMA³ backed the impactor to keep it from bowing as it accelerated down the barrel.

The target holders in which the geological samples were mounted consisted of a vacuum-tight aluminum housing sealed to prevent the water or ice from evaporating or subliming in the vacuum. The target holders were filled with water for the saturated rock sample tests. The four tilt pins were equally spaced around the perimeter of the sample, and were lapped flush with the front surface of the target holder.

³ Rohm & Haas Type II UVA polymethyl methacrylate (PMMA) obtained in sheet stock.



(a) Experimental configuration.



(b) Relative shock response diagram.

Figure 2-1. Rock equation of state experimental arrangement with Lagrangian stress gauges.

For the frozen shots, the target and sample temperatures were maintained at -10 or $-7^{\circ}\text{C} \pm 1^{\circ}\text{C}$ by cold nitrogen gas flowing through tubes bonded to the outside of the target holder with thermally conductive epoxy. Sample and target holder thermocouples (Figure 2-1(a)) were used to monitor the sample and target temperatures during target transportation and shot preparation. The thermocouples were connected to a strip chart recorder to monitor and record target and sample temperatures through shot time. One target thermocouple was attached to a controller (Greb, 1990) which controlled the nitrogen flow rate.

For the ice experiments, the discs of ice were made by freezing de-aired distilled water in a mold, with freezing progressing from one side to another. After freezing, the surface ice was shaved to produce discs with the desired thickness and a flat surface. The shaving technique removed a thin, bubbly layer near the final freezing surface. Target holders used in these experiments were identical to those used for frozen rock.

Dynasen⁴ model C300-50--EK RTE carbon gauges (Lee, 1981) were used to make Lagrangian stress measurements at three depths in the rock as shown in Figure 2-1(a). The carbon gauge packages consisted of a 0.064-mm-thick carbon gauge bonded between two 0.013 mm thick sheets of teflon with Hysol⁵ 2038 epoxy. This resulted in a total gauge package thickness that ranged from 0.10 to 0.11 mm and a gauge package diameter equal to that of the sample. Gauge packages were bonded to samples and aluminum buffer with super glue⁶. Super glue was used because it adheres well to wet and frozen materials. Material thicknesses were measured before and after each assembly step. A press was used in each of these processes to ensure thin glue bonds. Bonds were generally less than .01 mm thick. Target holders were then filled with water to maintain sample saturation. For frozen experiments, targets were then placed into a freezer and allowed to freeze overnight.

Figure 2-1(b) is a schematic that illustrates the Hugoniot of the impactor and target materials in stress-particle velocity space and shows the states achieved in the target after impact. The material Hugoniot shown are linear approximations. Point 1 represents the impact stress in the aluminum buffer and Point 2 is the stress transmitted into the sample and measured with the carbon gauges. The stress histories measured by these in-situ gauges were reduced to histories of particle velocity,

⁴ Dynasen, Inc., 20 Arnold Place, Goleta, CA.

⁵ Hysol Division of Dexter, Inc., Andover, MA.

⁶ Pronto CAS Instant Adhesive, 3M, St. Paul, MN.

specific volume, relative volume, and other related variables of the one-dimensional flow using both steady-state assumptions and the Lagrangian gauge analysis method of Seaman (1987). The Lagrangian analysis is described in Section 2.3.

Since the raw data are in terms of stress vs. time at fixed Lagrangian positions, two flow parameters, stress (σ) and shock velocity (U_s), are directly related to the data. Other flow parameters for steady waves such as particle velocity (u), relative density (ρ/ρ_0), or energy (E) can be derived using the Hugoniot expressions for conservation of momentum, mass, and energy:

$$\sigma - \sigma_0 = \rho_0(U_s - u)(u - u_0) \quad (2.2)$$

$$\rho/\rho_0 = (U_s - u_0) / (U_s - u) \quad (2.3)$$

$$E - E_0 = \Delta E = \frac{1}{2}(\sigma + \sigma_0) \left(\frac{1}{\rho_0} - \frac{1}{\rho} \right) \quad (2.4)$$

where subscript 0 denotes the state ahead of the shockwave.

For a single shock traveling into undisturbed material with an initial density (ρ_0), these equations reduce to:

$$\Delta \sigma = \rho_0 U_s u, \quad \rho/\rho_0 = \frac{U_s}{U_s - u}, \quad \Delta E = \frac{1}{2} u^2 \quad (2.5)$$

Alternatively, these parameters can be derived from the Lagrangian analysis which takes the non-steady nature of the flow into account. Therefore, two values for the particle velocity are reported throughout this document. One is taken from the Hugoniot relationship (Equation 2.2) and is listed as " u_p ." The other, listed as " u_s ," is taken from the Lagrangian analysis results along with relative density, stress, and shock velocity.

The shock velocity listed is the Lagrangian velocity. For single shocks this is equivalent to the Eulerian velocity. For shocks with precursors, such as are seen in marble, limestone, and ice, the main shock state must be derived by referencing all values to those behind the precursor using the Hugoniot relationships (Equations 2.2 - 2.4).

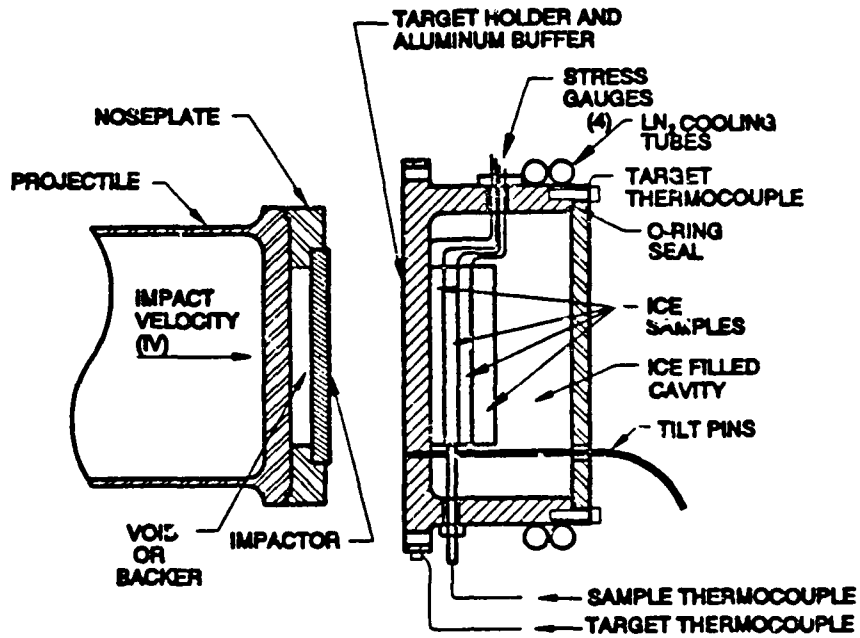
For the ice targets, four gauges were employed instead of three, as shown in Figure 2-2(a). Hugoniot data presented for ice were derived from the Hugoniot relations using impedance matching techniques based on the equilibrium stress measured at the aluminum-sample interface, the impact velocity, and the known impactor and buffer Hugoniots. This is shown in Figure 2-2(b). Point 1 represents the impact stress in aluminum and Point 2 represents the stress transmitted into the ice. Point 2 is the Hugoniot point and was determined from the intercept of the buffer reflection and the measured stress (σ_2) at the aluminum-ice interface. The release adiabat accounted for the elastic-plastic behavior of the aluminum.

2.2.1.2 VISAR Measurements. Particle velocity measurements were made on the high pressure EOS experiments (above 6.0 GPa) using a Velocity Interferometer System for Any Reflector (VISAR) (Barker, 1972, and Smith, 1989). The particle velocity histories were recorded to determine the material EOS and to support shock response model efforts. The VISAR system (Smith, 1989) had a double delay leg that enabled acquisition of two independent velocity measurements (identified as Leg 1 and Leg 2 throughout this report).

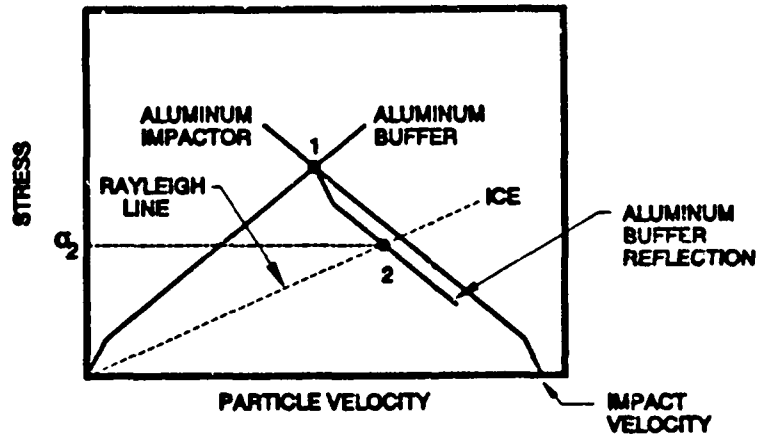
The target configuration for VISAR experiments is shown in Figure 2-3(a). A diffuse mirror was applied directly to the surface of a window of either PMMA (Barker, 1970) or lithium fluoride (LiF) (Wise, 1986). The LiF windows were bonded directly to the sample. When PMMA was used, a thin (0.75 mm) buffer of PMMA was located between the sample and window. The PMMA window assemblies were used for the lower impedance materials such as the tuffs and grouts, whereas LiF was used for the higher impedance marble. The PMMA buffer served to smooth out stress waves from heterogeneous materials such as the tuffs. The VISAR measured the change in particle velocity induced by the stress wave propagation across the sample-LiF window interface or in the PMMA window. The sample-window assembly was placed into the target as shown in Figure 2-3(a) and the sample was bonded directly to the aluminum buffer. A press was used in the bonding process to achieve a thin glue bond which was typically less than 0.01 mm thick. Thickness measurements were made before and after each glueing step to determine sample and bond thickness.

For VISAR experiments, shock velocities were derived from the measurements of shock transit time through the sample. The transit time was derived from the tilt pin data which defined impact time and the arrival time of the half amplitude of the stress wave at the VISAR mirror. Hugoniot data were derived from the measured shock velocity and sample density using standard impedance match techniques and the Hugoniot relationships. The shock response diagram in Figure 2-3(b)

88019-3.WPG

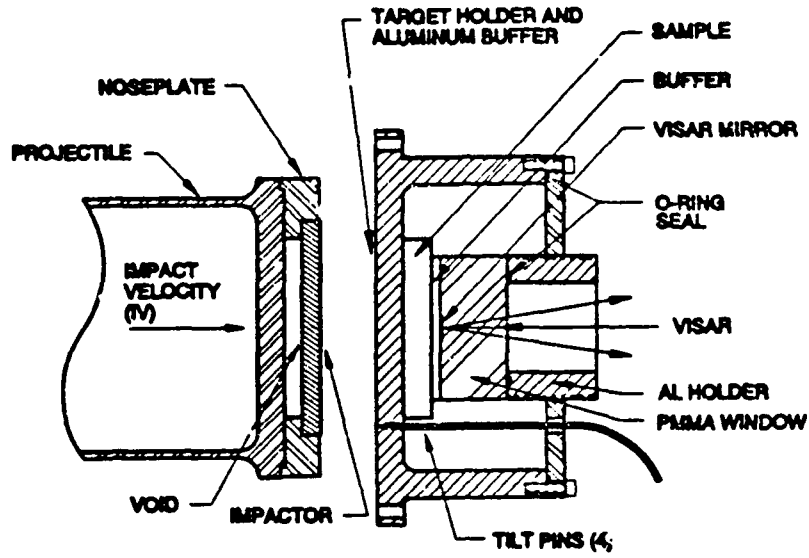


(a) Experimental arrangement.

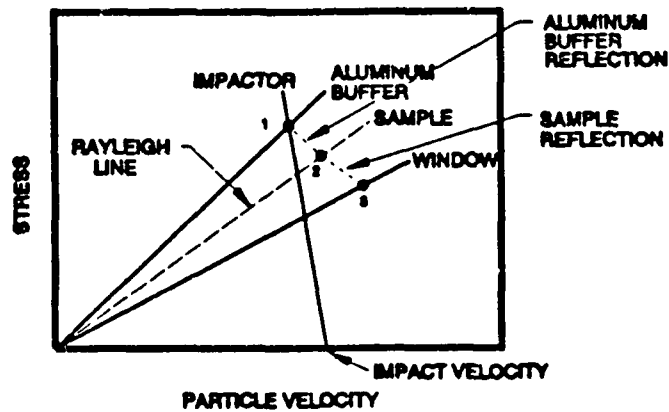


(b) Shock response diagram

Figure 2-2. Ice equation of state experimental arrangement with Lagrangian stress gauges.



(a) Experimental configuration.



(b) Shock response diagram.

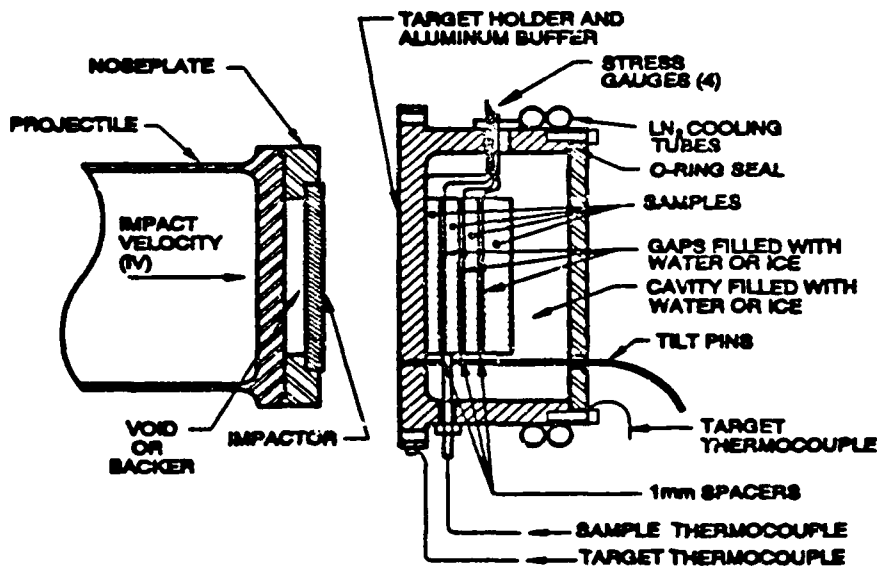
Figure 2-3. Equation of state experimental arrangement for VISAR particle velocity measurement.

shows the stress and particle velocity states in the materials for a given impact velocity. The Hugoniot has been approximated by the mechanical impedances of the respective materials. The release adiabat of the aluminum was approximated by a reflection of the 6061-T6 aluminum Hugoniot sample. The equilibrium impact stress in the aluminum target-holder buffer is represented by Point 1, and the stress and particle velocity states transmitted into the sample are represented by Point 2. The slope of the Rayleigh Line was determined by the measured shock velocity, and the Hugoniot point was defined as the intersection between the sample Rayleigh line and the unloading path of the 6061-T6 aluminum buffer. The states transmitted into the window and measured with the VISAR interferometer are represented by Point 3. The VISAR particle velocity profile can be compared to hydrocode calculated stress and particle velocity profiles at Point 3 to check validity of data.

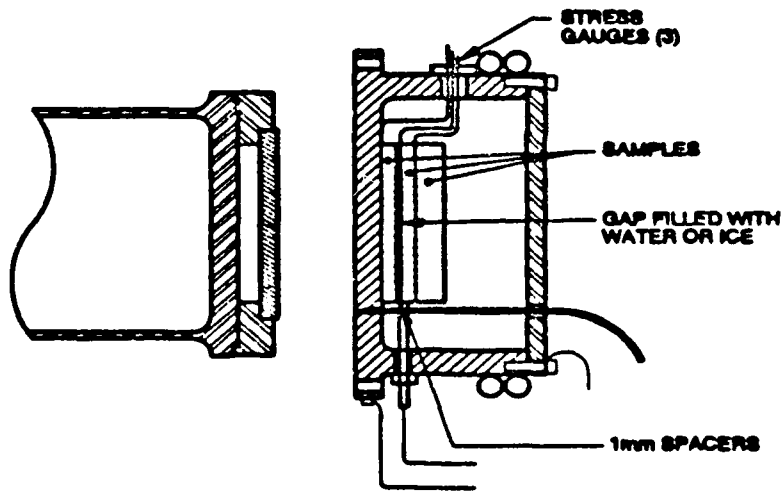
2.2.2 Artificial Joints.

To study the phenomena associated with shock propagation in jointed rock, tests were conducted with artificially jointed test samples. Single and multiple water-filled joint experiments were conducted at ambient temperature or at -7°C . Figure 2-4 shows the target configurations for these experiments. The targets consisted of three or four discs of marble separated by 1-mm-thick shims to produce one or three gaps. The marble discs were 5-mm thick except for the last one which was 10 mm thick. The shims were bonded between the samples to hold the stack in place and the gaps were filled with water. Thickness measurements were made to determine individual material thicknesses. Thin-film carbon gauge packages were mounted at the interface between the aluminum buffer and the first marble disc and on the downstream side of the joints. On the single-joint tests with the gap between the two 5-mm samples, as shown in Figure 2-4(b), a carbon gauge package was also bonded between the second 5-mm sample and the 10-mm backing sample.

For all six of the jointed tests, high-impedance flyers were employed, which produced an incident wave profile at the aluminum-target interface with a $1\text{-}\mu\text{s}$ flat tops followed by a series of unloading steps, each about $1\text{-}\mu\text{s}$ duration. The impact velocities were such that a precursor developed in the aluminum in all instances.



(a) Multiple joints



(b) Single joint

Figure 2-4. Jointed-target experiment configuration.

2.3 LAGRANGIAN ANALYSIS.

The stress histories measured by the in-situ stress gauges were used to calculate histories of particle velocities, specific volume, and other relatable variables in a one-dimensional flow using the non-steady Lagrangian analysis method of Seaman (1987). The computed stress-particle velocity and stress-specific volume paths can be extremely useful in developing equations of state or constitutive relations. The loading portions generally follow Rayleigh lines and may reveal precursors and rate dependence. The unloading paths can usually be taken as adiabats and therefore as curves on the equation of state surface after the presence of the deviator stress has been accounted for. Seaman's Lagrangian analysis method is derived from earlier work by Fowles and Williams (Fowles, 1970) and Grady (1973). The basic equations upon which the Lagrangian analysis techniques rest are the conservation laws of mass, momentum, and energy. In Lagrangian coordinates, these relations are:

$$\left(\frac{\partial v}{\partial t}\right)_h - \frac{1}{\rho_o} \left(\frac{\partial u}{\partial h}\right)_t = 0 \quad \text{Mass} \quad (2.6)$$

$$\left(\frac{\partial u}{\partial t}\right)_h + \frac{1}{\rho_o} \left(\frac{\partial \sigma}{\partial h}\right)_t = 0 \quad \text{Momentum} \quad (2.7)$$

$$\left(\frac{\partial E}{\partial t}\right)_h + \frac{\sigma}{\rho_o} \left(\frac{\partial u}{\partial h}\right)_t = 0 \quad \text{Energy} \quad (2.8)$$

where ρ_o is the initial density, u is the particle velocity, v is the specific volume, σ is the stress in the direction of propagation, t is time, h is the initial or Lagrangian position, and E is the internal energy.

To determine the stress, velocity, volume, and energy histories at each gauge plane, the preceding equations are integrated along lines of constant h (the gauge path). The integrated forms of the above equations are:

$$v_2 = v_1 + \frac{1}{\rho_o} \int_{t_1}^{t_2} \left(\frac{\partial u}{\partial h}\right)_t dt \quad (2.9)$$

$$u_2 = u_1 - \frac{1}{\rho_o} \int_{t_1}^{t_2} \left(\frac{\partial \sigma}{\partial h} \right)_t dt \quad (2.10)$$

$$E_2 = E_1 - \frac{1}{\rho_o} \int_{t_1}^{t_2} \sigma \left(\frac{\partial u}{\partial h} \right)_t dt \quad (2.11)$$

For each of these integrals, the terms under the integral sign are evaluated numerically from the gauge records. Thus, volume histories are determined from velocity records, velocity histories from stress records, and energy histories from stress and velocity data. Since only stress data were obtained in this program, the velocities were computed from the stress data and then the volume histories were derived.

The integration of equations 2.9, 2.10, and 2.11 requires the smoothing and digitization of the measured stress profiles into discrete time intervals and the numerical evaluation of the partial derivatives. The approach is illustrated in Figure 2-5 which shows a series of stress histories obtained from in-situ Lagrangian gauges. A series of smooth curves are imagined to connect the records in such a way that the lines are approximately in the directions of wave propagation. These lines, termed path lines, are generally located with equal increments of stress and connect similar flow features in each stress profile (e.g., precursors and inflections). Figure 2-5 shows the path lines for the loading segment of the profiles. At each intersection of a path line with a gauge line the time (T_p) associated with the stress (σ_p) is calculated from a smoothed fit through nearby stress-time points defined in the digitization process.

The partial derivative $\left(\frac{\partial \sigma}{\partial h} \right)_t$ can next be obtained using the identity

$$\left(\frac{\partial \sigma}{\partial h} \right)_t = \frac{d\sigma}{dh} - \left(\frac{\partial \sigma}{\partial t} \right)_h \frac{\partial t}{\partial h} \quad (2.12)$$

The derivatives on the right-hand side of equation 2.12 are derived by fitting the stress and time data to functions of h on each path line and by fitting the stress data to a function of t on each gauge line.

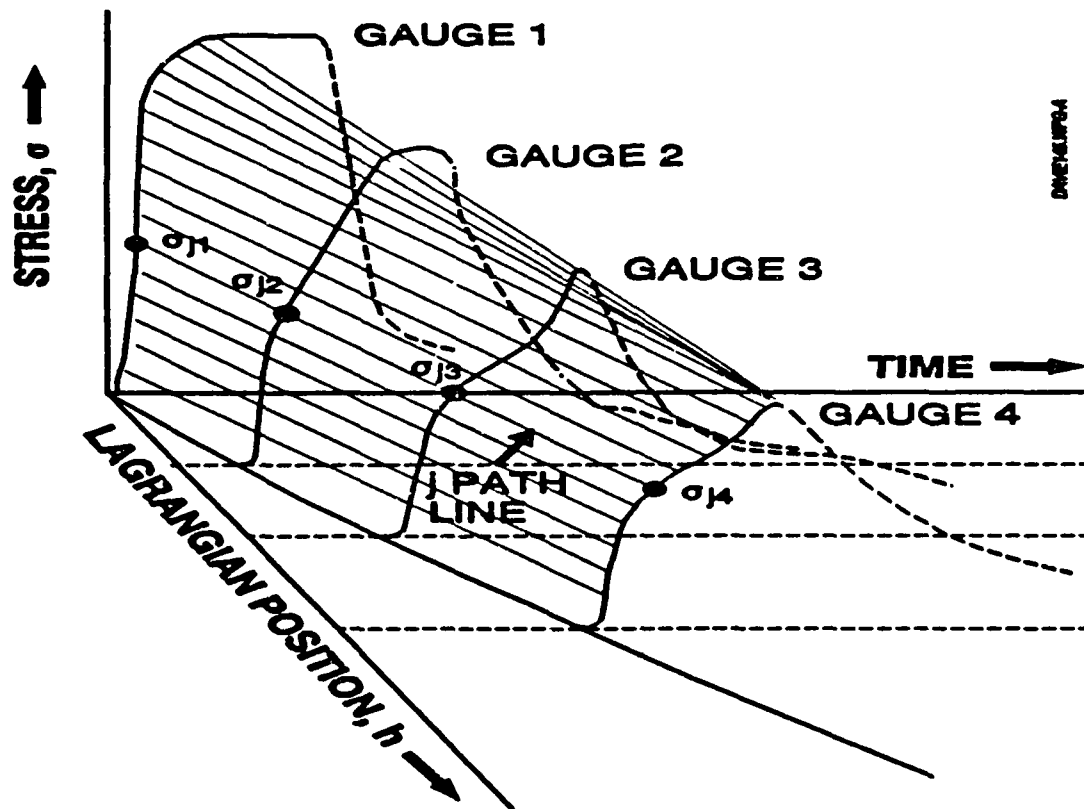


Figure 2-5. The generation of path lines in the loading process for the Lagrangian analysis.

The numerical approximation

$$u_{j+1,k} - u_{j,k} = -\frac{1}{2\rho_0} \left[\left(\frac{d\bar{\sigma}_k}{dh} + \frac{d\bar{\sigma}_{j+1,k}}{dh} \right) (T_{j+1,k} - T_k) - (\sigma_{j+1,k} - \sigma_k) \left(\frac{dt_k}{dh} + \frac{dt_{j+1,k}}{dh} \right) \right] \quad (2.13)$$

is used to evaluate equation 2.10 and obtain the velocity histories where $\sigma_{j,k}$ is the fitted value on the j th path line. Seaman's code GUINSY3 (Seaman, 1987) was used with linear fits for both stress-position and position-time, and fits up to fifth order for stress-time.

The tabulated data presented in this report were derived from the output of GUINSY3. Two values are given for the particle velocity in each data set. The particle velocity listed as " u_p " was derived by the Lagrangian analysis (GUINSY3); the other, " u_{pH} ," was derived from the steady-state Hugoniot relationships.

In many cases, the Lagrangian analysis, involving one flat-topped (or nearly flat-topped) wave and two attenuated wave resulted in a loading curve that was initially linear and then flattened to a final state before unloading. These curves are considered to be evidence of rate dependent behavior. In these cases, the "Hugoniot" state was taken as the state at the end of the linear loading. This point is considered to lie on the instantaneous Hugoniot as is the Hugoniot state derived from the steady state analysis. They are not, however, necessarily the same point, but do lie on the same Hugoniot.

SECTION 3

EXPERIMENTAL RESULTS FOR TUFF AND TUFF-MATCHING GROUT

This section presents the experimental results on two tuffs from NTS; HUNTERS TROPHY tuff and DISTANT ZENITH tuff, and on MJ-2 (NSF-6) grout which was a tuff-matching grout used as a gauge stemming material for the DISTANT ZENITH event at NTS. Hugoniot data and relief paths are presented in this section together with shot configuration tables showing details of impactor and buffer material thicknesses, and sample number, density, and thickness. All recorded waveforms are illustrated in Appendix A and are also available from the DNA HYDROPLUS data archive on the DNA CRAY storage system at Los Alamos National Laboratory. Comparisons of the results of the DISTANT ZENITH tuff with the MJ-2 (NSF-6) grout results are presented. In addition to the present HUNTERS TROPHY tuff ($\rho_o = 1.86 \text{ g/cc}$) experiments, a higher density HUNTERS TROPHY tuff ($\rho_o = 2.05 \text{ g/cc}$) has also been tested. These results will be published at a later date (Smith, 1993). The lower density tuff, referred to in this report as HUNTERS TROPHY tuff (GI-1), has the stratigraphic designation Tt-4H (see Table 1-1), and the higher density tuff has the stratigraphic designation Tt-4J. Both of these HUNTERS TROPHY tuffs, as well as the DISTANT ZENITH tuff, were also tested by Sandia National Laboratories (Furnish, 1993).

3.1 HUNTERS TROPHY TUFF (GI-1).

HUNTERS TROPHY tuff (GI-1) core material was obtained from the interval 211.4 - 212.5 feet in hole U12n.24 GI-1 at NTS. The average sample density was 1.86 g/cc^3 (std = 0.020) and the average ultrasonic longitudinal velocity was 3.34 km/s (std = 0.24). Sample characterization data are presented in Table 3-1 which defines the as-received condition of the samples. The accuracy of each measurement is indicated at the top of each column. The samples were heterogeneous with up to 5-mm-diameter inclusions as shown in the photograph of a typical HUNTERS TROPHY tuff (GI-1) sample in Figure 3-1. In order to minimize variability, samples used in a given target were matched as closely as possible according to density. The samples were in a saturated condition when received by Ktech. This saturation was maintained at all times.

Table 3-1. Material properties for HUNTERS TROPHY tuff (GI-1).

Sample No.	Avg. Thick. (mm) ±1%	Bulk Density (g/cc) ±1%	Longitudinal Velocity (km/s) ±5%	Sample No.	Ave. Thick. (mm) ±1%	Bulk Density (g/cc) ±1%	Longitudinal Velocity (km/s) ±5%
HT-1	5.03	1.87	3.38	HT-14*	5.04	1.88	4.19
HT-2	5.03	1.88	3.24	HT-15	9.98	1.89	3.41
HT-3	10.00	1.84	3.39	HT-16	5.03	1.88	3.28
HT-4	5.05	1.88	3.11	HT-17	5.04	1.87	3.37
HT-5	5.05	1.86	3.57	HT-18	10.00	1.86	3.31
HT-6	10.00	1.85	3.36	HT-19	5.02	1.88	3.37
HT-7	5.04	1.88	3.43	HT-20	5.04	1.82	3.34
HT-8	5.02	1.88	3.30	HT-21	10.01	1.84	3.26
HT-9	10.01	1.88	3.37	HT-22	5.03	1.80	3.14
HT-10	5.03	1.88	3.09	HT-23	5.06	1.87	3.11
HT-11	5.04	1.87	3.76	HT-24	10.00	1.85	3.14
HT-12	9.98	1.87	3.57	HT-25	5.06	1.85	3.31
HT-13	5.04	1.85	3.30	HT-26	5.05	1.86	3.09
				HT-27	9.96	1.85	2.94

* The relatively high ultrasonic velocity on Sample HT-14 was due to a 5 mm diameter rock in the center of the sample. This sample was not used.

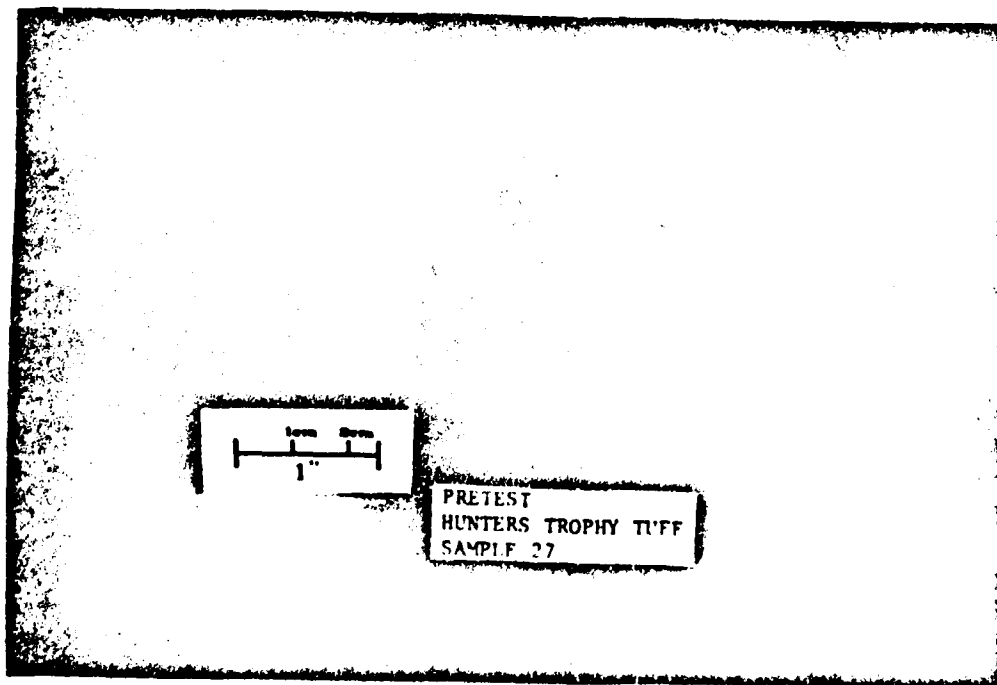


Figure 3-1. Photograph of typical Hunters Trophy tuff (GI-1) sample.

Seven (7) ambient temperature experiments below 5 GPa were conducted on HUNTERS TROPHY tuff (GI-1) with Lagrangian stress gauges. Table 3-2 contains shot configuration information for each of these experiments. The impactor and buffer material thicknesses and thicknesses and densities of the individual samples used to fabricate each target are listed. Note that the material thickness may differ from those presented in Table 3-1 due to the lapping processes that were necessary to obtain adequately flat samples. Stress-time profile plots for each experiment are presented in Appendix A. Hugoniot data was obtained by Lagrangian analysis and is presented in Table 3-3 along with measured density and impact velocity. The initial sample density listed is an average sample density which was used in the Lagrangian analysis. The shock velocity listed was calculated by the Lagrangian analysis for the half-amplitude stress measured by gauge-1. This table also presents the particle velocity (u_{pu}) obtained by steady-state analyses. Hugoniot data from Table 3-3 and release paths are plotted in Figures 3-2, 3-3, and 3-4. The scatter in the data, which is greater than the expected experimental uncertainties ($\pm 5\%$), is attributed to local and sample-to-sample inhomogeneity.

Figure 3-5 shows the slow main wave and an emerging precursor that developed on shot 3520 as the shock progressed into the target; however, on the higher stress-level shots (Figures 3-6, 3-7, and 3-8) the precursor was overrun by the main wave. In Figure 3-5, the dip in the equilibrium stress level of gauge-1 may be due to a low density inclusion or void in the sample near the gauge location since the $1\text{-}\mu\text{s}$ pulse width is consistent with all of the other experiments on HUNTERS TROPHY tuff (GI-1). A well defined precursor from the 6061-T6 aluminum buffer can be seen on gauge-1 on all shots.

Stress-time histories for tests conducted at nominally the same impact velocity are overlaid in Figures 3-6, 3-7, and 3-8. The comparisons show the similarity in material shock response at each of the three stress levels despite the material heterogeneity. A slightly lower shock velocity (6%) was measured on shot 3519 than 3518 although the profiles are otherwise very similar.

Table 3-2. HUNTERS TROPHY tuff (GI-1) shot configuration data.

Shot No.	6061-T6		Thickness (mm) and Density (g/cc)								
	Impact Thick	Buffer Thick	Sample 1			Sample 2			Sample 3		
			No.	Thick	ρ_s	No.	Thick	ρ_s	No.	Thick	ρ_s
3520	4.79	9.40	HT-26	5.05	1.86	HT-25	5.06	1.85	HT-6	9.99	1.85
3518	4.82	9.41	HT-1	5.03	1.87	HT-5	5.05	1.86	HT-3	9.99	1.84
3519	4.78	9.39	HT-10	5.02	1.88	HT-17	5.03	1.87	HT-15	9.96	1.89
3516	4.81	9.46	HT-2	5.03	1.88	HT-4	5.05	1.88	HT-9	10.00	1.88
3517	4.88	9.40	HT-7	5.03	1.88	HT-8	5.01	1.88	HT-12	9.97	1.87
3521	4.78	9.38	HT-16	5.03	1.88	HT-19	5.01	1.88	HT-18	10.00	1.86
3522	4.74	9.41	HT-20	5.04	1.82	HT-22	5.01	1.80	HT-21	10.00	1.84

Table 3-3. HUNTERS TROPHY tuff (GI-1) Lagrangian stress gauge Hugoniot data.

Shot Number	Impact Velocity (km/s)	Initial Density (g/cc)	Stress (GPa)	Hugoniot			
				U_s ($\frac{1}{2}$ amp) ^m (km/s)	u_p (m/s)	u_{ps} (m/s)	ρ/ρ_s
3520*	0.468	1.85	1.62	2.41	351	363	1.166
3518	0.643	1.86	2.79	3.22	462	466	1.169
3519	0.647	1.88	2.71	3.04	477	474	1.189
3516	0.876	1.88	3.76	3.07	653	651	1.272
3517	0.881	1.88	3.92	3.17	654	658	1.261
3521	1.045	1.88	5.01	3.46	749	770	1.277
3522	1.040	1.83	4.79	3.45	760	759	1.283

Configuration: CF/6061-T6 → 6061-T6/CG/Sample/CG/Sample/CG/Sample

* On shot 3520 a void was behind the impactor instead of carbon foam.

^m Shock velocity taken as dh/dt at gauge 1 half-amplitude loading stress from Lagrangian analysis.

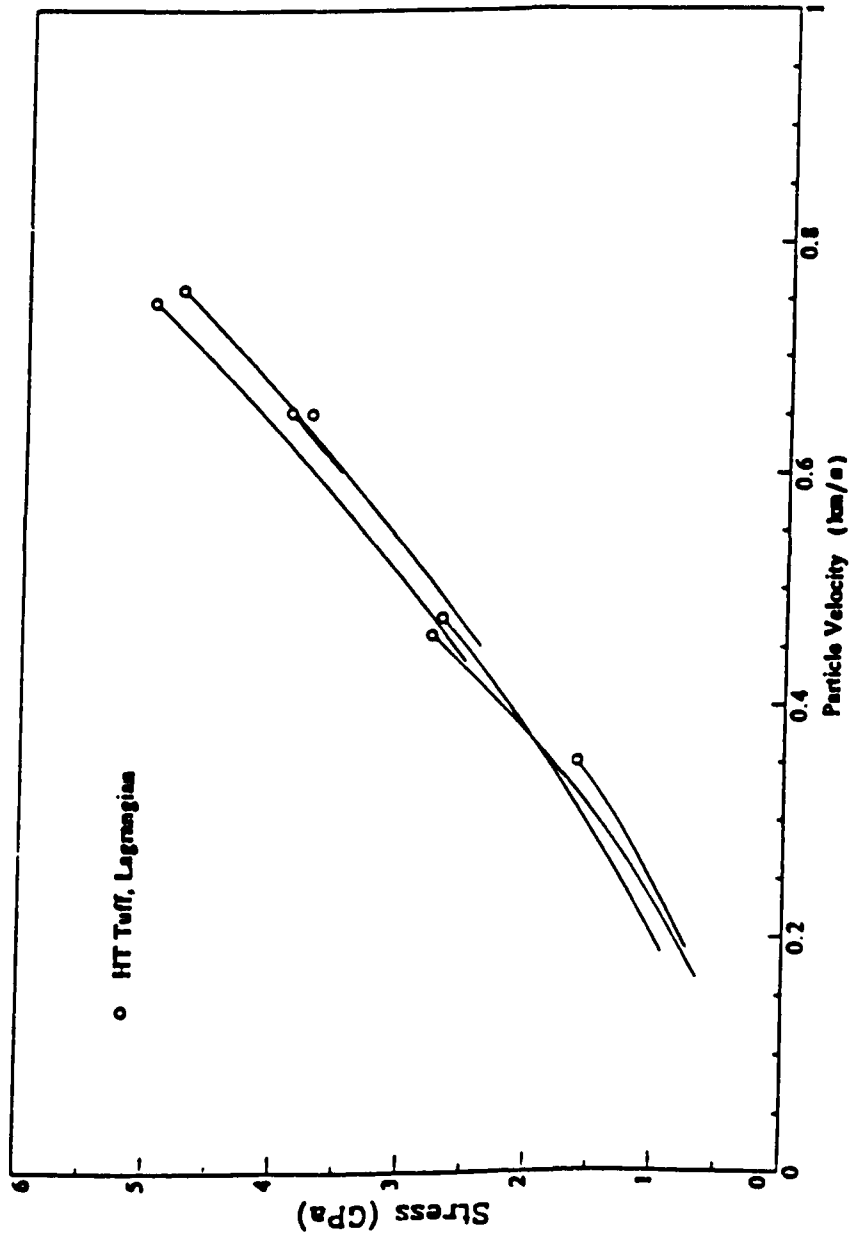


Figure 3-2. HUNTERS TROPHY tuff (GI-1) stress-particle velocity Hugoniot data and release paths.

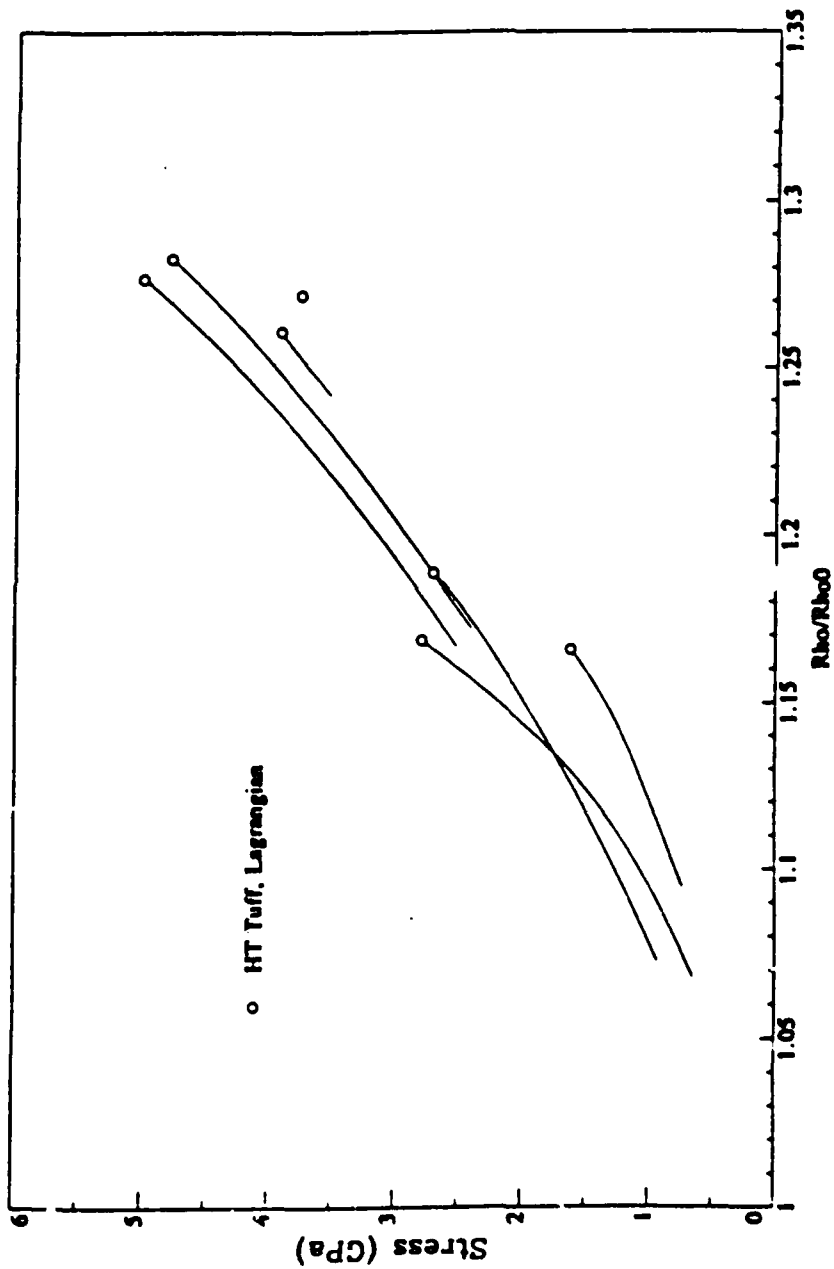


Figure 3-3. HUNTERS TROPHY tuff (GI-1) stress- ρ , Hugoniot data and release paths.

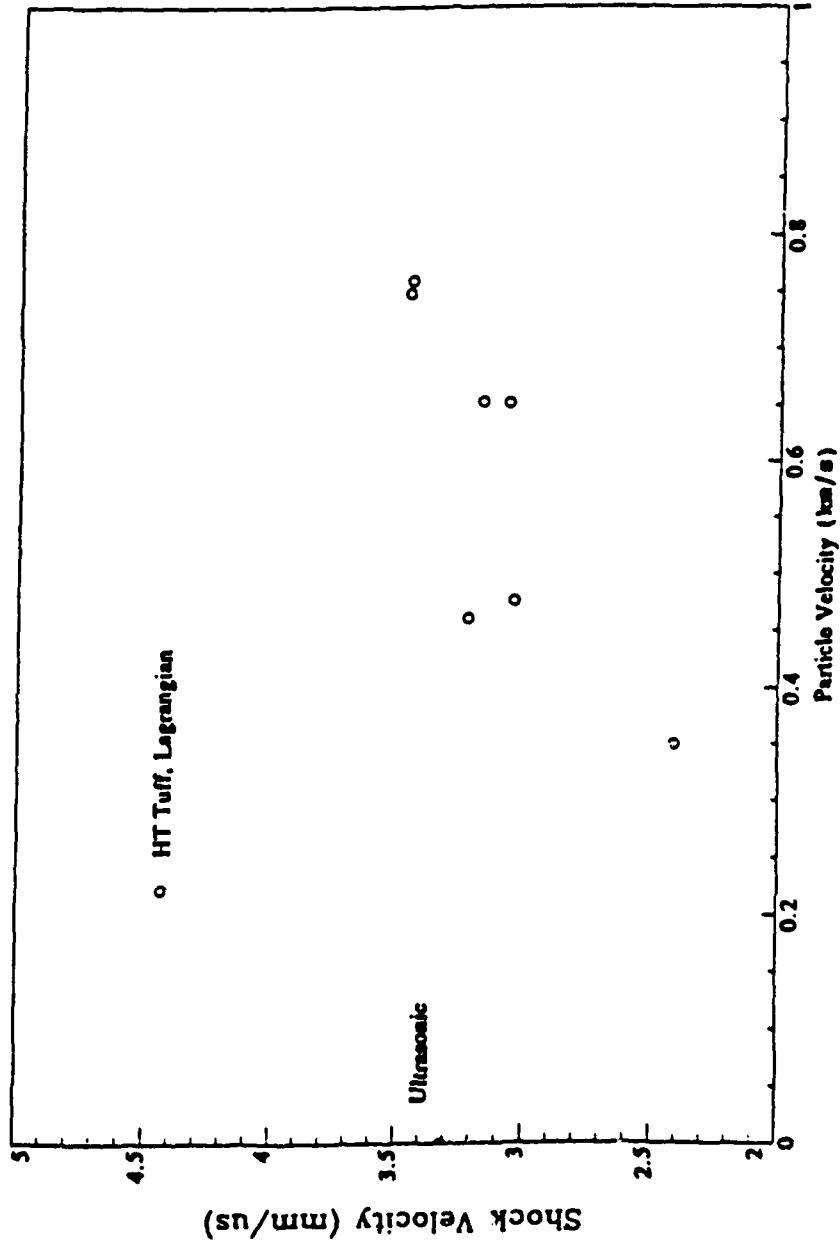


Figure 3-4. HUNTERS TROPHY tuff (GI-1) shock velocity-particle velocity Hugoniot data.

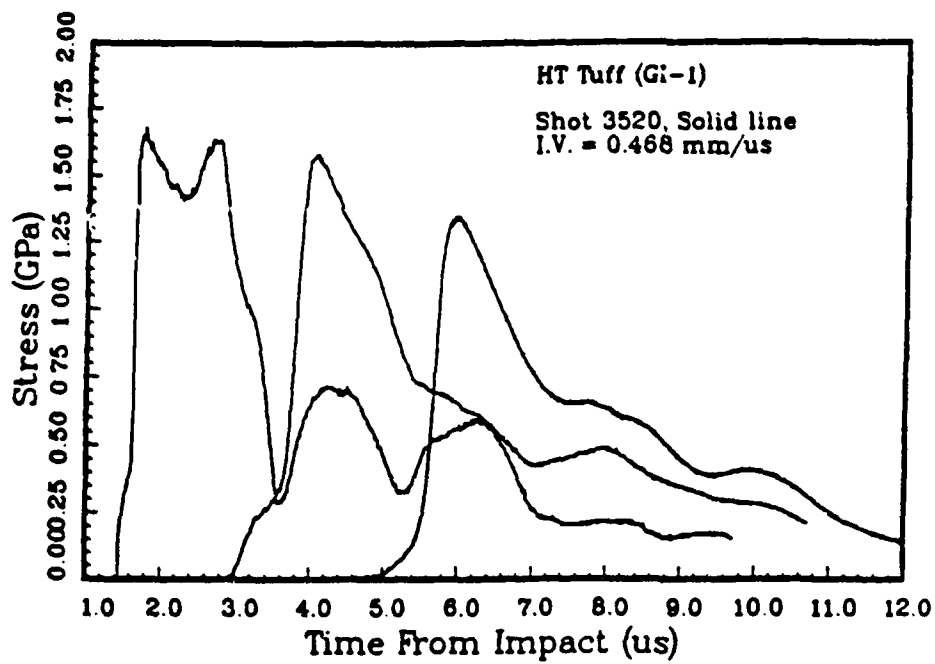


Figure 3-5. HUNTERS TROPHY tuff (GI-1), shot 3520.

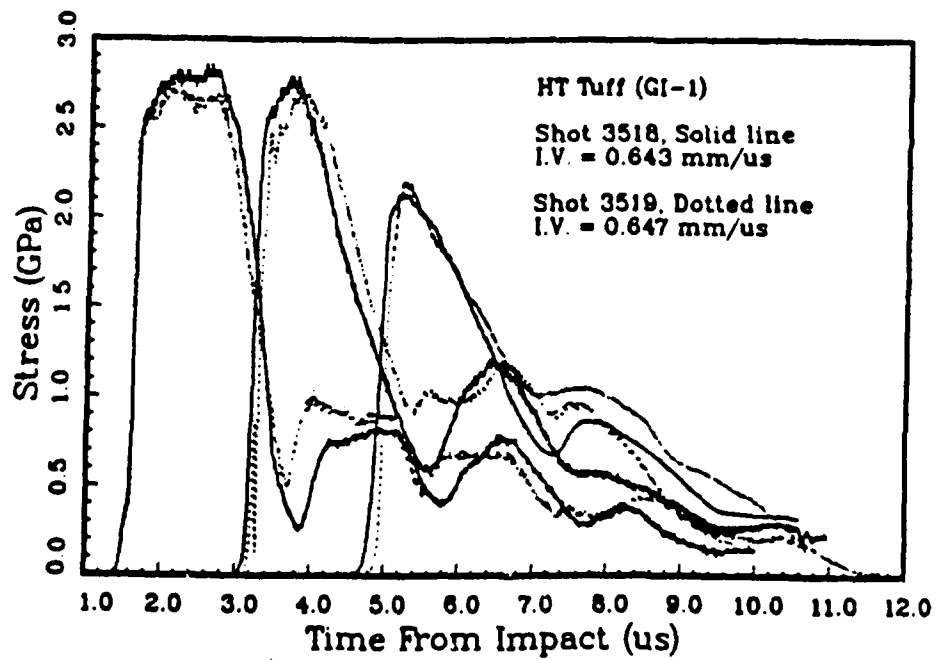


Figure 3-6. HUNTERS TROPHY tuff (GI-1), shots 3518 and 3519.

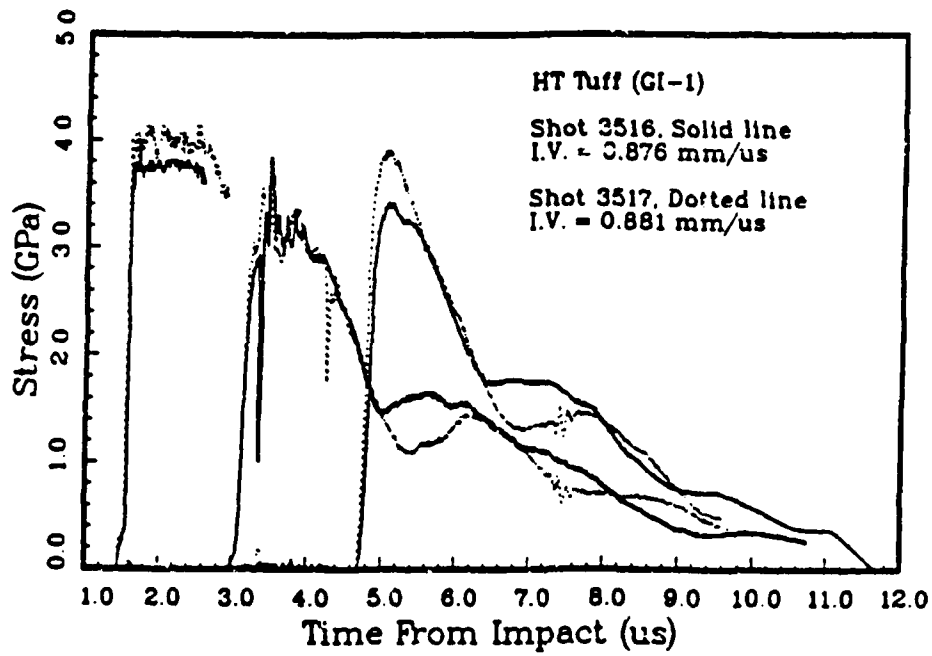


Figure 3-7. HUNTERS TROPHY tuff (GI-1), shots 3516 and 3517.

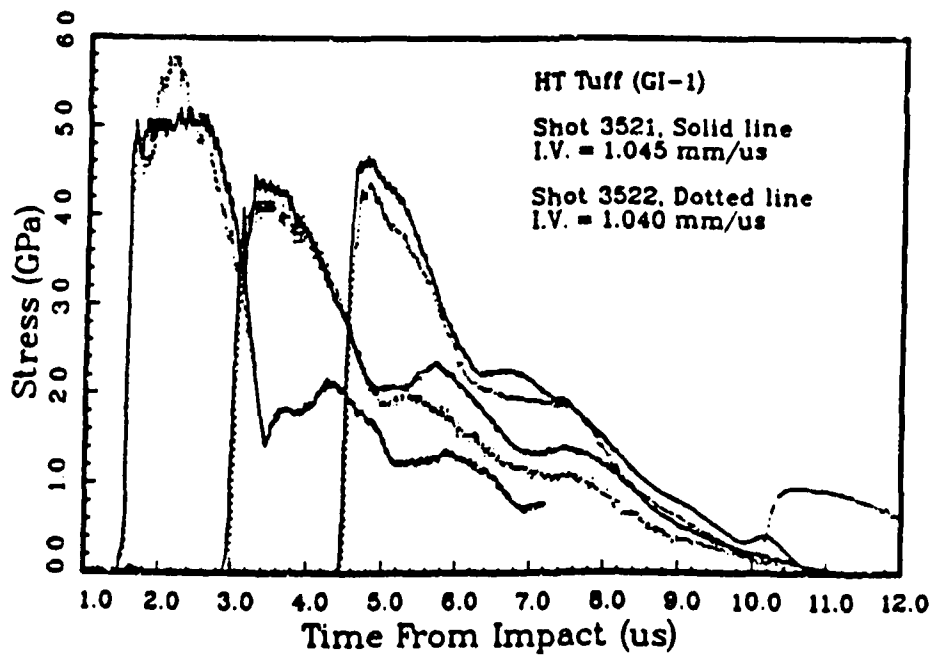


Figure 3-8. HUNTERS TROPHY tuff (GI-1), shots 3521 and 3522.

3.2 DISTANT ZENITH TUFF.

The DISTANT ZENITH core material was obtained from NTS. The average sample density was 1.87 g/cc (std = 0.009) and the average ultrasonic longitudinal velocity was 3.46 km/s (std = 0.09). Sample characterization data are presented in Table 3-4 which defines the as-received condition of the samples. The DISTANT ZENITH tuff was heterogeneous, containing up to 5 mm diameter inclusions as shown in Figure 3-9. The samples were stored in water to maintain saturation and tested at ambient temperature.

Four experiments were conducted on DISTANT ZENITH tuff; two used Lagrangian stress gauges and two used VISAR particle velocity measurements. All experiments used tungsten carbide (WC) impactors. Table 3-5 contains shot configuration information such as material thicknesses and sample densities. Note that the material thickness may differ from those presented in Table 3-4 due to the lapping processes that were necessary to obtain adequately flat samples. Stress-time profiles for each experiment are presented in Appendix A. The data obtained from the Lagrangian analysis along with density and impact velocity are given in Table 3-6. The shock velocity listed was calculated by the Lagrangian analysis for the half-amplitude stress measured by gauge-1. Table 3-6 also presents the particle velocity, u_{pH} , derived from the steady state analysis.

The peak stress was attenuated on shot 3507 before the wave propagated through the 10-mm-thick sample. This conclusion was based on two facts: (a) no flat top was observed on the measured stress profile, and (b) the calculated peak particle velocity was lower than results from other tests. Hugoniot data are therefore not reported for this experiment. A five-millimeter-thick sample was used on shot 3515 to ensure that a steady wave was obtained for analysis.

For shot 3437 (DISTANT ZENITH tuff), we observed a sharp shock to about 1.76 GPa, then an ~80 ns wide step, followed by a slower compression to about 2.56 GPa. The step was caused by an abnormally thick epoxy bond between the target holder and the sample. In this case, the lower value is reported as the Hugoniot state. The unloading paths derived from the Lagrangian analyses are presented in Figure 3-10 and 3-11. These plots also show the loading path of the slower compression up to the peak stress.

Table 3-4. Material properties for DISTANT ZENITH tuff.

Sample No.	Thick. (mm) ±1%	Density (g/cc) ±1%	Longitudinal		Sample No.	Thick. (mm) ±1%	Density (g/cc) ±1%	Longitudinal	
			Velocity (km/s) ±5%					Velocity (km/s) ±5%	
NTS-1	5.00	1.86	3.48		NTS-8	5.02	1.87	3.43	
NTS-2	5.02	1.85	3.58		NTS-9	5.02	1.86	3.53	
NTS-3	5.00	1.86	3.53		NTS-10	5.04	1.87	3.52	
NTS-4	4.99	1.86	3.59		NTS-11	10.02	1.87	3.41	
NTS-5	5.01	1.86	3.43		NTS-12	10.01	1.88	3.32	
NTS-6	5.01	1.87	3.47		NTS-13	10.00	1.87	3.29	
NTS-7	4.99	1.88	3.56		NTS-14	10.05	1.88	3.48	
					NTS-15	9.98	1.86	3.31	

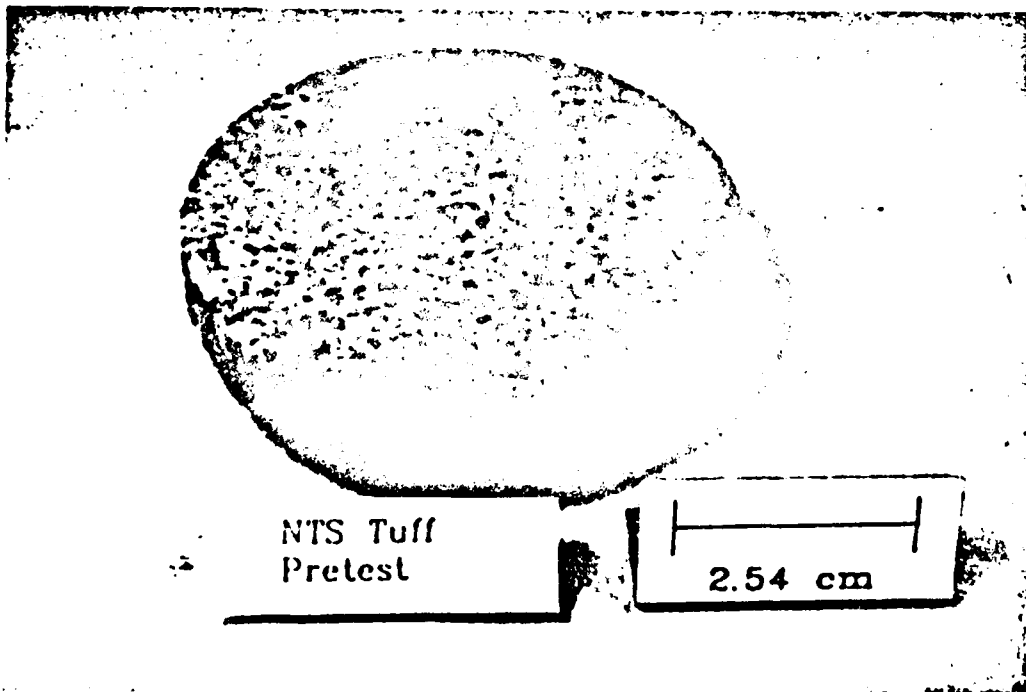


Figure 3-9. Photograph of typical DISTANT ZENITH tuff sample.

Table 3-5. DISTANT ZENITH tuff shot configuration data.

Shot No.	WC Impact Thick	6061-T6 Buffer Thick	Thickness (mm) and Density (g/cc)								
			Sample 1			Sample 2			Sample 3		
			No.	Thick	ρ_0	No.	Thick	ρ_0	No.	Thick	ρ_0
3437	4.78	9.42	NTS-1	5.00	1.86	NTS-2	5.02	1.85	NTS-15	9.98	1.86
3447	4.79	9.40	NTS-8	5.01	1.87	NTS-4	4.99	1.86	NTS-14	10.04	1.88
3507	6.35	9.40	NTS-13	10.00	1.87	PMMA	0.77	1.18	PMMA	25.40	1.18
3515	6.35*	9.40	NTS-10	5.03	1.87	PMMA	0.77	1.18	PMMA	25.40	1.18

* Shot 3515 impactor was backed with PMMA

Table 3-6. DISTANT ZENITH tuff Hugoniot data.

Shot Number	Impact Velocity (km/s)	Initial Density (g/cc)	Conf.†	Stress (GPa)	Hugoniot			
					u_s ½ amp (km/s)	u_p (m/s)	u_{pH} (m/s)	ρ/ρ_0
3437	0.311	1.86	a	1.49*	3.02	260	266	1.093
3447	0.602	1.87	a	4.73*	3.53	711	717	1.252
3507†	1.286	1.87	b	—	4.31	—	—	—
3515	1.134	1.87	b	10.37	4.33	—	1280	1.418

† Configuration: a) WC → 6061-T6/CG/Sample/CG/Sample/CG/Sample

b) WC → 6061-T6/Sample/PMMA Buffer/VISAR Mirror/PMMA

* Stress is an initial shock stress level from the Lagrangian analysis and does not represent peak or equilibrium stress.

† Stress attenuated before arrival at measurement station; no Hugoniot data

3.3 MJ-2 (NSF-6) GROUT.

MJ-2 (NSF-6) grout was a stemming material for HYDROPLUS gauges on the DISTANT ZENITH test event and was selected to closely match the shock impedance of the DISTANT ZENITH tuff. The average sample density was 2.014 g/cc (std = 0.011) and the average ultrasonic longitudinal velocity was 4.19 km/s (std = 0.12). Sample characterization data are given in Table 3-7 which defines the as-received condition of the samples. The accuracy of each measurement is listed at the top of each column of this table. The MJ-2 (NSF-6) grout samples were machined from 100-mm-diameter cylinders poured during stemming operations at the DISTANT ZENITH site at NTS. They were stored in water to maintain saturation and tested at ambient temperature. Many of the machined samples contained up to 2.0-mm-diameter voids in the surface caused apparently from entrapped air bubbles. Samples with surface bubbles visible in the center region near the gauge location were not used but voids below the surface may have been present in the test samples.

Table 3-7. Material properties for DISTANT ZENITH MJ-2 (NSF-6) grout.

Sample No.	Thick. (mm) ±1%	Density (g/cc) ±1%	Longitudinal		Sample No.	Thick. (mm) ±1%	Density (g/cc) ±1%	Velocity (km/s) ±5%
			Velocity (km/s) ±5%	Velocity (km/s) ±5%				
MJ-2-1	10.04	2.03	4.09		MJ-2-16	5.01	2.01	4.18
MJ-2-2	10.02	2.03	4.03		MJ-2-17	5.03	2.04	4.28
MJ-2-3	10.01	2.02	3.99		MJ-2-18	5.03	2.03	4.21
MJ-2-4	10.03	2.03	4.09		MJ-2-B-1	5.01	2.02	4.45
MJ-2-5	10.01	2.02	4.05		MJ-2-B-2	5.00	2.01	4.32
MJ-2-6	5.01	2.01	4.16		MJ-2-B-3	5.01	2.01	4.31
MJ-2-7	5.01	2.02	4.22		MJ-2-B-4	5.01	2.01	4.35
MJ-2-8	5.02	1.99	3.96		MJ-2-B-5	5.01	2.02	4.37
MJ-2-9	5.01	2.01	4.15		MJ-2-B-6	5.00	2.01	4.30
MJ-2-10	5.02	2.01	4.16		MJ-2-B-7	5.01	2.01	4.38
MJ-2-11	5.02	2.01	4.24		MJ-2-B-8	5.01	2.01	4.22
MJ-2-12	5.01	2.01	4.18		MJ-2-B-9	10.00	2.00	4.19
MJ-2-13	10.03	2.03	4.06		MJ-2-B-10	9.99	2.00	4.10
MJ-2-14	5.01	2.00	4.18		MJ-2-B-11	10.01	2.01	4.21
MJ-2-15	5.02	2.00	4.14		MJ-2-B-12	9.97	2.01	4.15

Six (6) experiments were conducted on MJ-2 (NSF-6) grout; two used Lagrangian stress gauges and four used the VISAR interferometer. Table 3-8 details the shot configuration information. Note that the material thickness may differ from those presented in Table 3-7 due to the lapping

Table 3-8. MJ-2 (NSF-6) grout shot configuration data.

Shot No.	Impactor Thick	6061-T6 Buffer Thick	Thickness (mm) and Density (g/cc)								
			Sample 1			Sample 2			Sample 3		
			No.	Thick	ρ_0	No.	Thick	ρ_0	No.	Thick	ρ_0
3449	4.78	9.41	MJ2-1	10.02	2.03	MJ2-14	5.00	2.00	MJ2-6	5.01	2.01
3506	6.35	9.40	MJ2-4	10.04	2.03	PMMA	0.77	1.18	PMMA	25.40	1.18
3511	6.35	9.40	MJ2-11	10.00	2.02	PMMA	0.77	1.18	PMMA	25.40	1.18
3512	6.35	9.40	MJ2-B1	4.99	2.02	PMMA	0.77	1.18	PMMA	25.40	1.18
3514	6.35	9.40	MJ2-12	5.01	2.01	PMMA	0.77	1.18	PMMA	25.40	1.18
3528	4.78	9.36	MJ2-B7	4.99	2.01	MJ2-B8	5.01	2.01	MJ2-B9	10.00	2.00

Table 3-9. MJ-2 grout Hugoniot data.

Shot Number	Impact Velocity (km/s)	Initial Density (g/cc)	Conf.	Hugoniot				
				Stress (GPa)	$U_{\frac{1}{2} \text{ amp}}$ (km/s)	u_p (m/s)	u_{pH} (m/s)	ρ/ρ_0
3449	0.600	2.01	a	4.23*	3.54	589	594	1.202
3506	1.200	2.03	b	12.08	4.59	—	1300	1.391
3511*	1.318	2.02	b	—	3.52	—	—	—
3512	1.211	2.02	c	11.87	4.44	—	1320	1.426
3514	1.206	2.01	c	11.82	4.46	—	1320	1.420
3528	0.597	2.01	a	5.22*	3.67	707	708	1.239

Configuration: a) WC → 6061-T6/CG/Sample/CG/Sample/CG/Sample

b) WC → 6061-T6/Sample/PMMA buffer/VISAR mirror/PMMA

c) PMMA/WC → 6061-T6/Sample/PMMA buffer/VISAR mirror/PMMA

* Stress is an initial shock stress level from the Lagrangian analysis and does not represent peak or equilibrium stress.

* Stress attenuated before arrival at measurement station, no Hugoniot data.

processes that were necessary to obtain adequately flat samples. Table 3-9 summarizes the Hugoniot data obtained from each of the analysis techniques.

Particle velocity profiles from three MJ-2 (NSF-6) grout VISAR shots conducted at about 12 GPa are shown in Figure 3-12 (shots 3506, 3514, and 3512). The two shots containing 5-mm-thick samples (shots 3512 and 3514) resulted in nearly identical responses. The other shot (3506) was conducted with a 10-mm-thick sample and resulted in a narrower pulse width than was observed at the 5-mm-range. This is due to catchup of the loading wave by the faster release rarefaction. Comparison of the pulse widths shows the release velocity was 6.2 km/s at 12 GPa. The stress was attenuated on shot 3511 before the wave propagated through the 10-mm-thick sample. This conclusion was based on two facts: (1) no flat top was observed on the measured stress profile, and (2) the calculated peak particle velocity was lower than results from other data. Hugoniot data were therefore not obtained from this experiment. Five-millimeter-thick samples were used on shots 3512 and 3514 to ensure that a steady wave was obtained for analysis.

The data measured on Lagrangian-gauge shot 3449 for MJ-2 (NSF-6) grout did not permit a credible analysis with GUINSY3. Shot 3449 had an attenuated wave arriving at the second gauge location, although it is not readily apparent because of the questionable sensitivity of this gauge. Release paths were not included for this shot. The measured wave profiles for this shot and shot 3528 showed a steep front followed by a gradual rise. The Hugoniot data points for these two shots were defined as this pronounced inflection of the stress profiles as measured by gauge-1.

3.4 DISTANT ZENITH TUFF AND MJ-2 (NSF-6) GROUT COMPARISON.

Since MJ-2 (NSF-6) grout was an impedance-matching grout for the DISTANT ZENITH tuff, experimental results for these two materials have been compared and plotted together. The Hugoniot data listed in Table 3-5 for DISTANT ZENITH tuff and Table 3-9 for MJ-2 (NSF-6) grout are plotted in Figures 3-11, 3-12, and 3-13. The Hugoniot points shown were based upon a stress measured at the end of the fast rise time portion of the wave profile. The slower compression up to the peak stress is shown as a loading path. Release paths from the peak stress are also shown.

Comparison of results for the DISTANT ZENITH tuff and the MJ-2 (NSF-6) grout indicate that a fair match to the Hugoniot has been achieved. Figure 3-11 shows the MJ-2 (NSF-6) grout to have a higher impedance than the DISTANT ZENITH tuff by about 10 percent in the 4 to 10 GPa stress range.

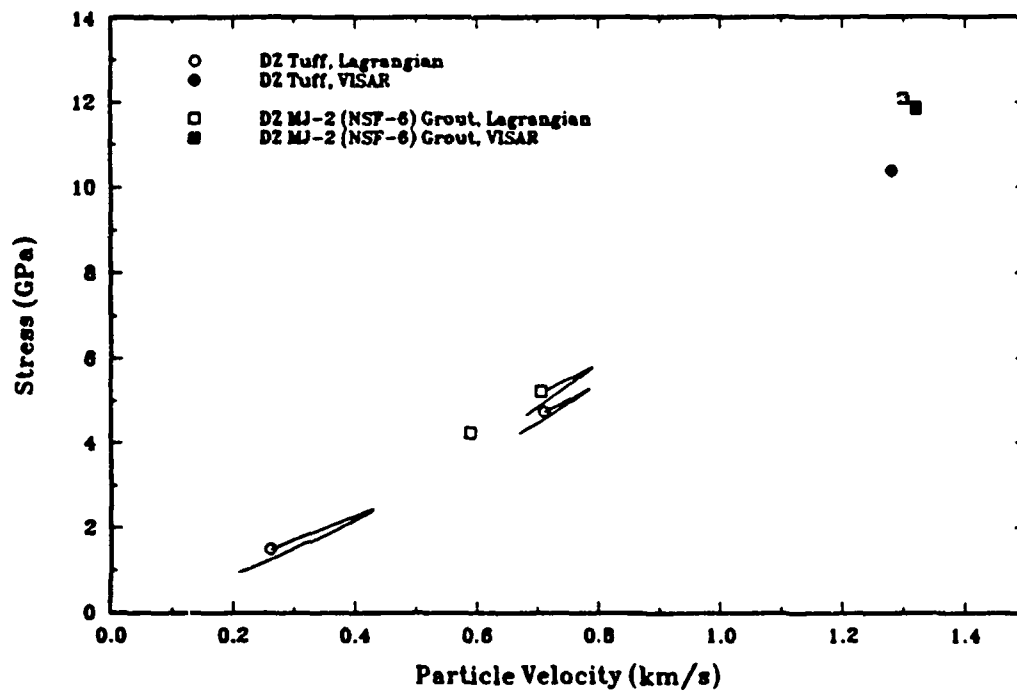


Figure 3-10. DISTANT ZENITH tuff and MJ-2 (NSF-6) grout stress-particle velocity Hugoniot data with partial loading and release paths.

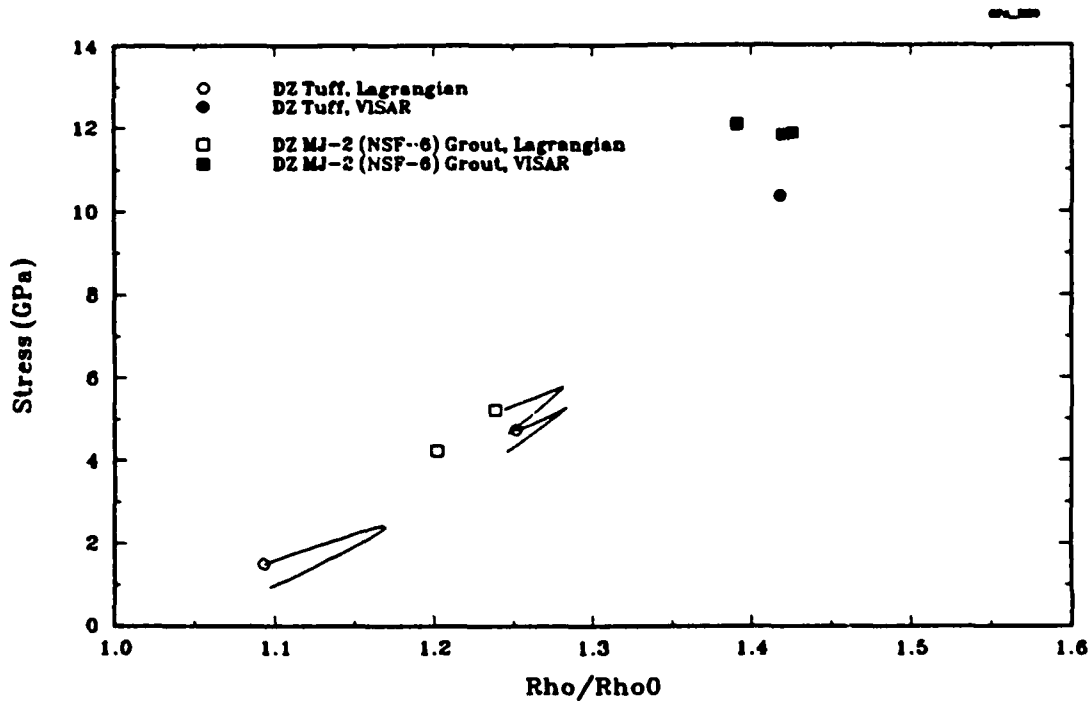


Figure 3-11. DISTANT ZENITH tuff and MJ-2 (NSF-6) grout stress- ρ/ρ_0 Hugoniot data with partial loading and release paths.

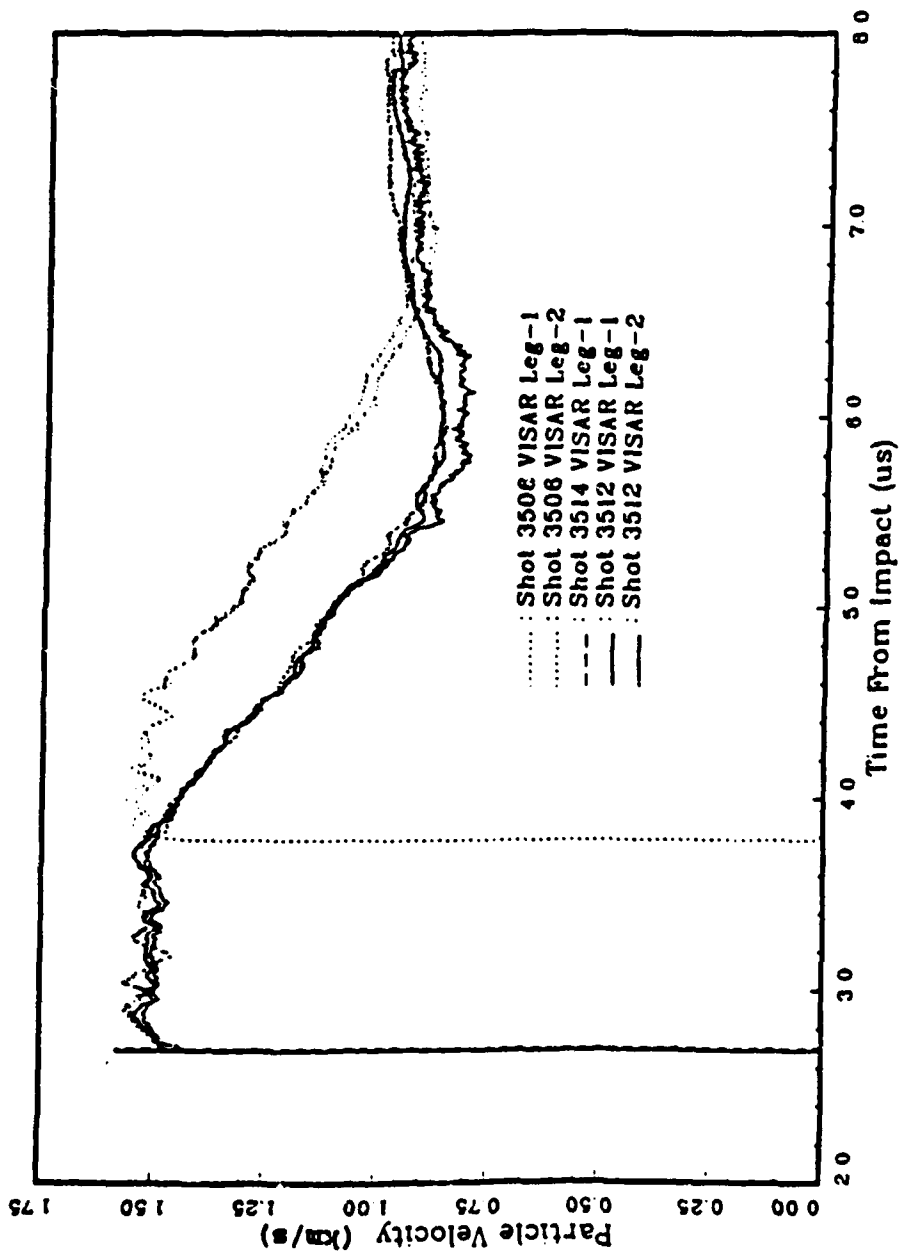


Figure 3-12. VISAR data for MJ-2 (NSF-6) group 5-mm (shot 3512 and 3514) and 10-mm (shot 350E).

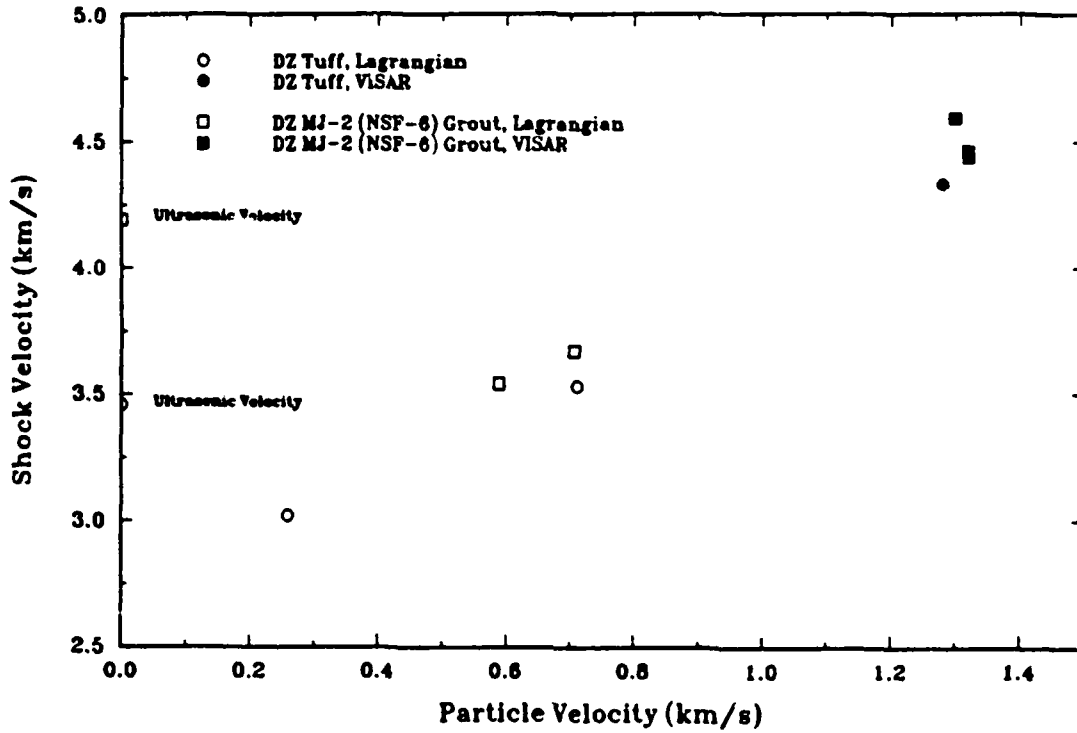


Figure 3-13. DISTANT ZENITH tuff and MJ-2 (NSF-6) grout shock velocity-particle velocity Hugoniot data.

The grout ultrasonic velocity is 20 percent higher than that for the DISTANT ZENITH tuff. However, the shock velocity is in much closer agreement (~5%) as shown in Figure 3-13. Since the grout density was 8 percent higher than the tuff density, it is concluded that the bulk sound speeds are in good agreement.

Figure 3-14 is a comparison of the results for DISTANT ZENITH tuff (shot 3515) and MJ-2 (NSF-6) grout (shot 3512) in the 10 to 12 GPa range. The wave profiles show similar responses for the two 5-mm-thick samples.

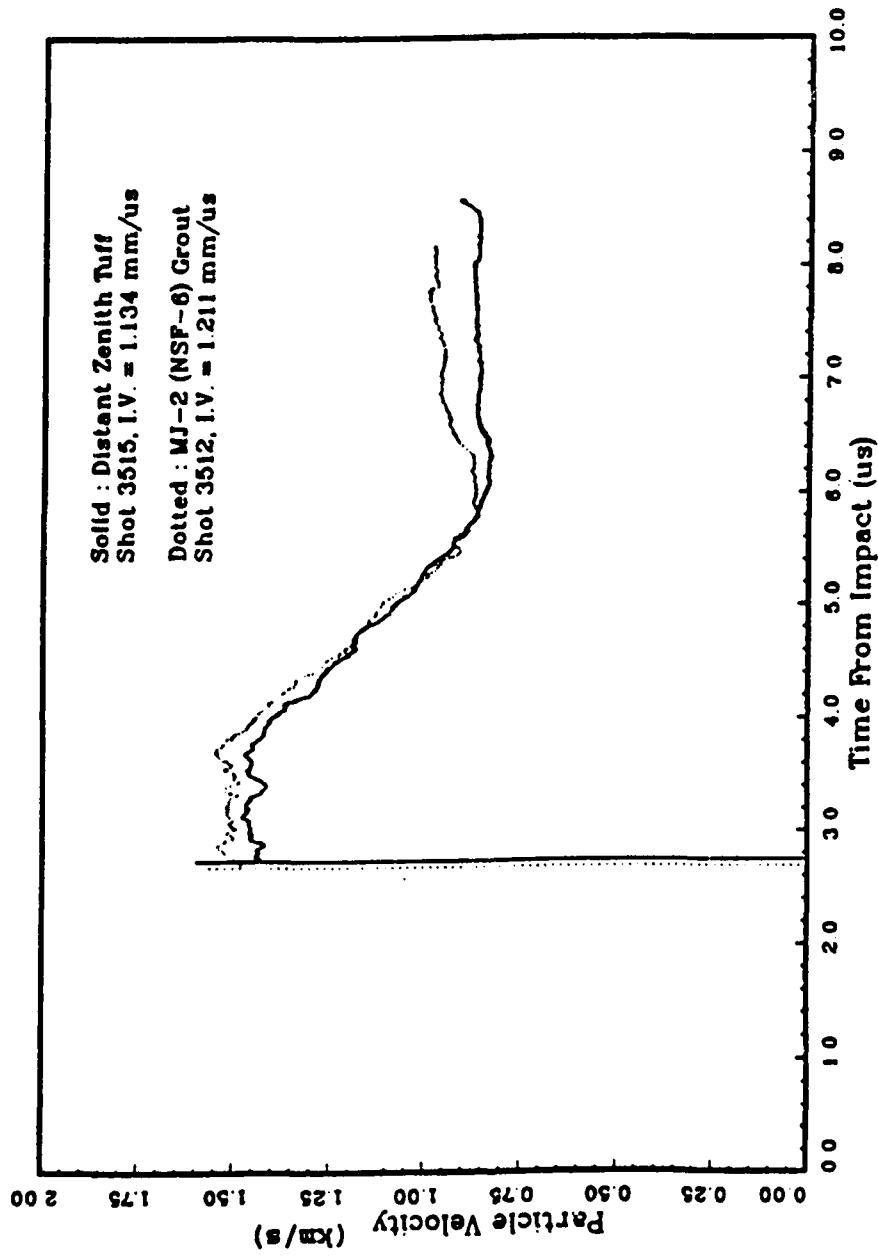


Figure 3-14. Comparison between VISAR particle velocity profiles for MJ-2 (NSF-6) grout and DZ tuff.

SECTION 4

EXPERIMENTAL RESULTS FOR CARBONATE ROCKS

Equation of state data were obtained for four carbonate rocks: Danby marble from Proctor, VT, carbonates from the UTP site at Fort Knox, KY (Louisville and Jefferson formations), and Salem limestone from Eedford, IN. Hugoniot data and loading and relief paths are presented in this section together with shot configuration tables showing details of impactor and buffer material thicknesses, and sample number, density, and thickness. All recorded waveforms are illustrated in Appendix A and are also available from the DNA HYDROPLUS data archive on the DNA CRAY storage system at Los Alamos National Laboratory. Danby marble and Ft. Knox carbonates were also tested by Sandia National Laboratories (Furnish, 1993).

4.1 DANBY MARBLE.

The Danby marble samples were cut from tiles supplied by the Vermont Marble Company in Proctor, VT. The Danby marble is a calcite marble streaked with dark minerals which appear to be primarily mica. These dark streaks were avoided as much as possible in the selection of the samples. This led to a highly reproducible set of samples. Although the porosity was less than 1 percent the marble was saturated by evacuating it, purging it with CO₂, and immediately placing it in water. Pretest material properties data are summarized in Table 4-1 which defines the as-received condition of the samples. The average density was 2.695 g/cc (std = 0.004) and the average ultrasonic velocity was 6.20 km/s (std = 0.11).

Two equation of state tests, at nominal stresses of 1.2 GPa and 6 GPa, were performed with three Lagrangian stress gauges located at nominal ranges of 0, 5, and 10 mm from an aluminum buffer. Two other tests, at 10.25 GPa and at 15.64 GPa, used VISAR interferometry. Table 4-2 contains information on the experimental configurations such as material thickness and density data. Note that the material thickness may differ from those presented in Table 4-1 due to the lapping processes that were necessary to obtain adequately flat samples. Table 4-3 contains the Hugoniot data from these tests. The Hugoniot data and some release paths are plotted in stress-particle velocity, stress-relative density, and shock velocity-particle velocity spaces in Figures 4-1, 4-2, and 4-3, respectively.

Table 4-1. Material properties for Danby marble.

Sample No.	Avg. Thick. (mm) ±1%	Density (g/cc) ±1%	Longitudinal Velocity (km/s) ±5%	Sample No.	Avg. Thick. (mm) ±1%	Density (g/cc) ±1%	Longitudinal Velocity (km/s) ±5%
DM-1	5.02	2.69	6.21	DM-21	5.01	2.69	6.09
DM-2	5.02	2.70	6.21	DM-22	5.01	2.69	6.11
DM-3	5.02	2.69	6.19	DM-23	5.01	2.69	6.31
DM-4	5.00	2.69	6.46	DM-24	5.01	2.70	6.10
DM-5	5.01	2.69	6.37	DM-25	5.01	2.70	6.18
DM-6	5.02	2.69	6.13	DM-26	5.01	2.69	6.14
DM-7	5.00	2.69	6.21	DM-27	5.01	2.69	N/A
DM-8	5.01	2.69	6.11	DM-28	9.00	2.70	6.11
DM-9	5.02	2.70	6.25	DM-29	9.01	2.70	6.12
DM-10	5.01	2.70	6.24	DM-30	9.00	2.70	6.03
DM-11	5.01	2.69	6.30	DM-31	9.02	2.70	6.31
DM-12	5.02	2.69	6.40	DM-32	9.01	2.70	6.28
DM-13	5.00	2.69	6.21	DM-33	9.00	2.70	6.08
DM-14	5.01	2.70	6.18	DM-34	9.01	2.70	6.04
DM-15	5.02	2.69	6.04	DM-35	9.02	2.70	6.45
DM-16	5.01	2.70	6.15	DM-36	9.01	2.70	6.04
DM-17	5.01	2.70	6.21	DM-37	9.00	2.70	6.31
DM-18	5.01	2.69	6.13	DM-38	9.01	2.70	6.22
DM-19	5.01	2.69	6.19	DM-39	9.00	2.70	6.26
DM-20	5.00	2.69	6.17				

Table 4-2. Danby marble shot configuration data.

Shot No.	Impact Thick	6061-T6 Buffer Thick	Thickness (mm) and Density (g/cc)								
			Sample 1			Sample 2			Sample 3		
			No.	Center Thick	ρ_s	No.	Center Thick	ρ_s	No.	Center Thick	ρ_s
3467	3.19	9.39	DM-2	5.01	2.70	DM-1	5.01	2.69	DM-28	9.00	2.70
3469	4.78	9.38	DM-27	5.01	2.69	DM-24	5.01	2.70	DM-30	9.00	2.70
3513	6.35	9.40	DM-3	5.02	2.69	LiF	25.40	2.64			
3527	6.35	9.40	DM-9	5.01	2.70	LiF	25.40	2.64			

Table 4-3. Danby marble Lagrangian stress gauge Hugoniot data.

Shot Number	Impact Velocity (km/s)	Initial Density (g/cc)	Conf. [†]	Stress (GPa)	Hugoniot			ρ/ρ_s
					U_s ($\frac{1}{2}$ amp) (km/s)	u_p (km/s)	u_{pH} (km/s)	
3467	0.097	2.696	a	1.172 $\pm .013$	6.094 $\pm .063$	0.077 $\pm .003$	0.071 $\pm .001$	1.0142 $\pm .0005$
3469	0.515	2.696*	b	1.430*	4.797* $\pm .586$	0.107*	0.111*	1.0223*
		(2.76)	b	5.43	4.00	0.475	0.479	1.133
		(2.76)		5.30	4.00	0.458	0.467	1.122
3527	0.899	2.70	c	10.25	4.21	—	0.91	1.274
3513	1.200	2.69	d	15.64	5.20	—	1.12	1.274

* precursor

† Configuration: a) 4340 → 6061-T6/CG/Sample/CG/Sample/CG/Sample

b) WC → 6061-T6/CG/Sample/CG/Sample/CG/Sample

c) WC → 6061-T6/Sample/VISAR Mirror/LiF

d) PMMA/WC → 6061-T6/Sample/VISAR Mirror/LiF

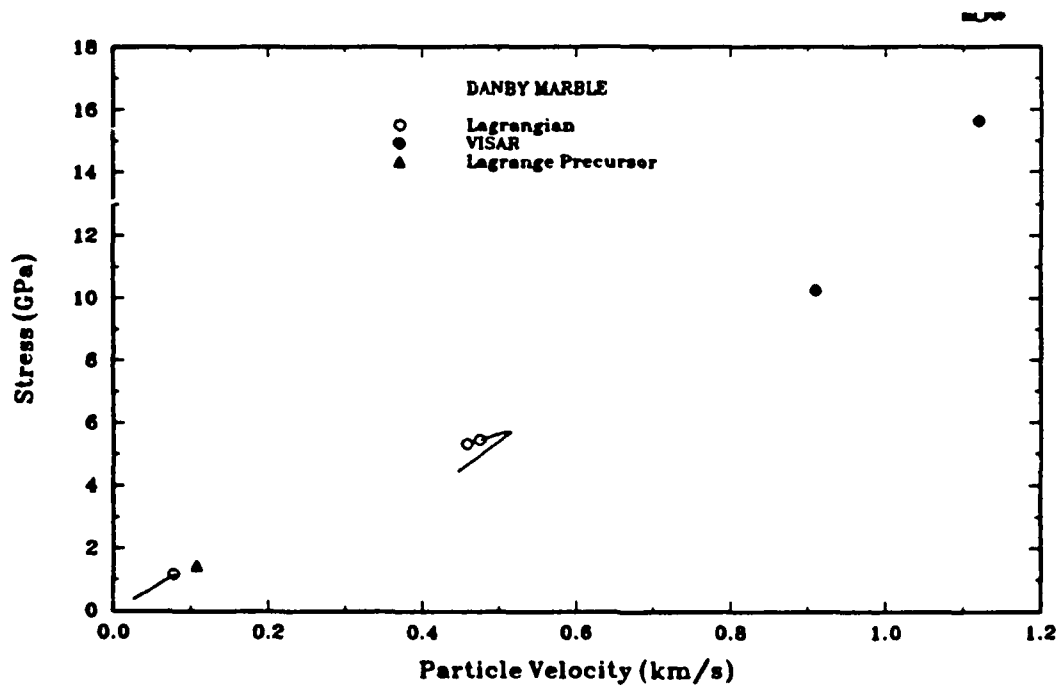


Figure 4-1. Danby marble stress-particle velocity Hugoniot data with partial loading and release paths.

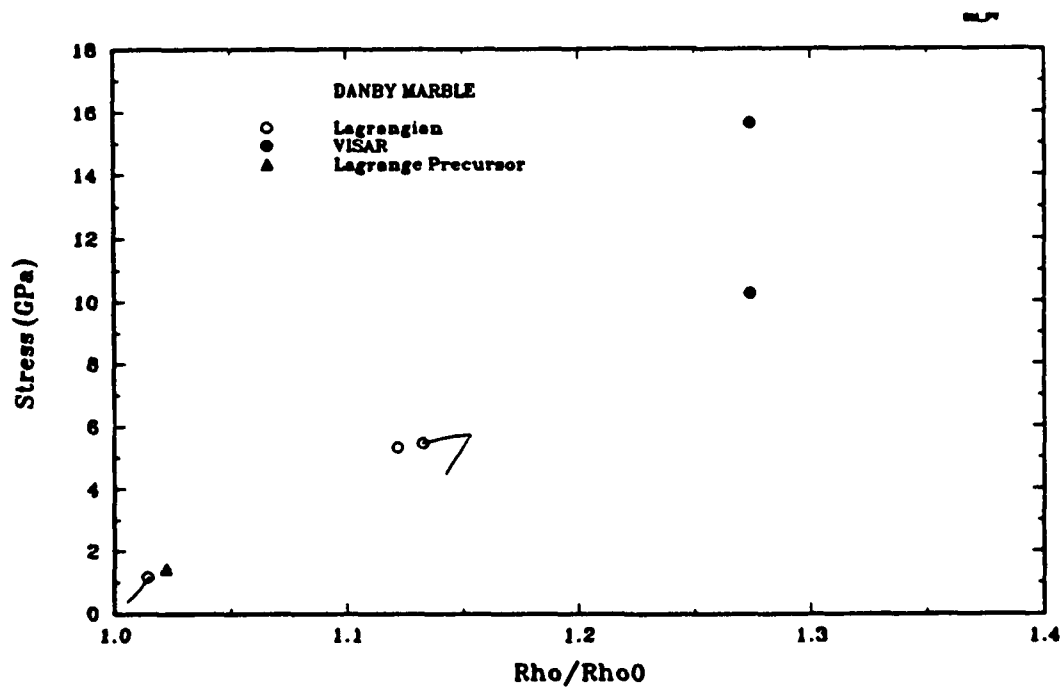


Figure 4-2. Danby marble stress- ρ/ρ_0 Hugoniot data with partial loading and release paths.

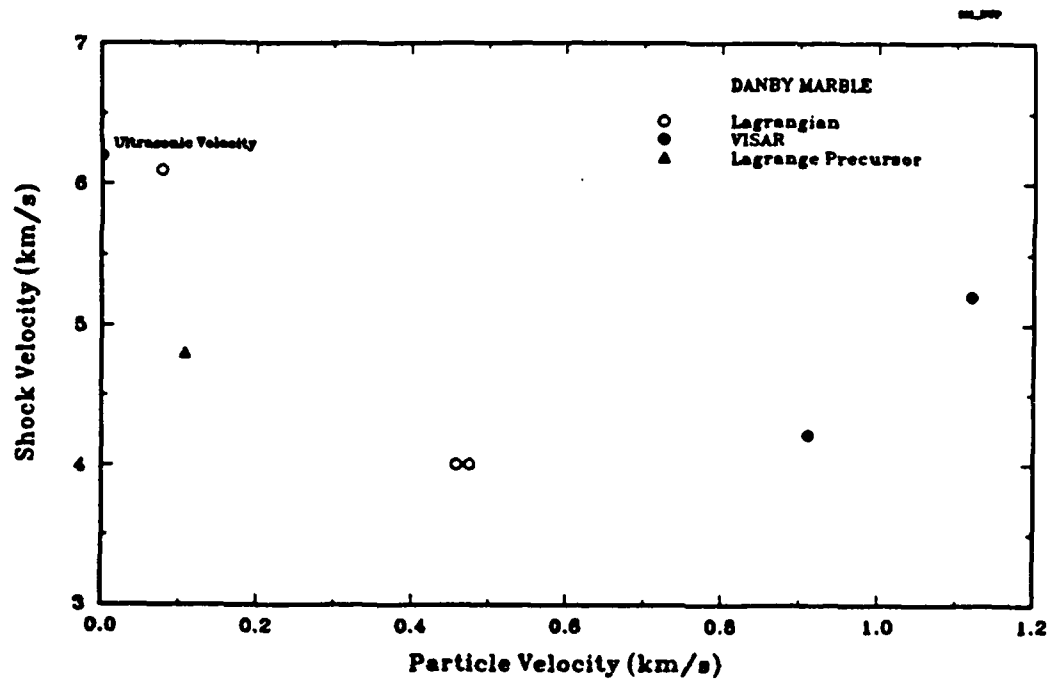


Figure 4-3. Danby marble shock velocity-particle velocity Hugoniot data.

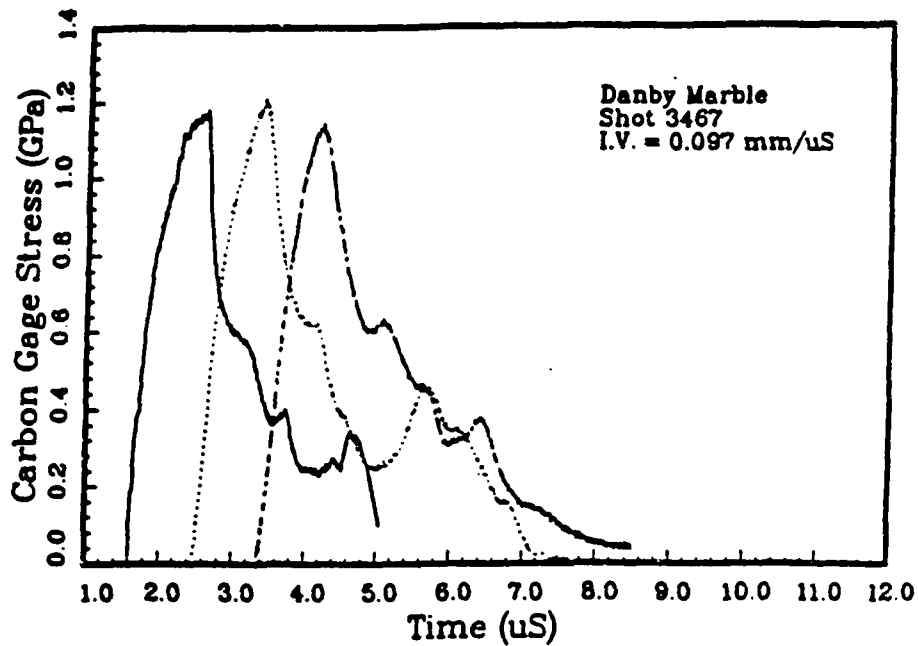
Lagrangian stress histories for Danby marble (shots 3467 and 3469) are shown in Figure 4-4. The response of Danby marble is very different for 1 GPa shocks than for 6 GPa shocks. The 1 GPa data indicate nearly perfectly elastic propagation at 5.2 km/s for loading and 5.5 km/s for unloading. In contrast, the 6 GPa records show a marked precursor with an amplitude of about 1.5 GPa, due to calcite I \rightarrow calcite II \rightarrow calcite III phase changes. The precursor is followed by a main loading wave traveling at about 3.85 km/s. The unloading signal again travels at about 5.5 km/s, so that it very rapidly overtakes the loading wave. After about 10 mm of propagation, the peak has attenuated from 4.8 GPa to only 4.2 GPa.

4-2 FT. KNOX CARBONATES.

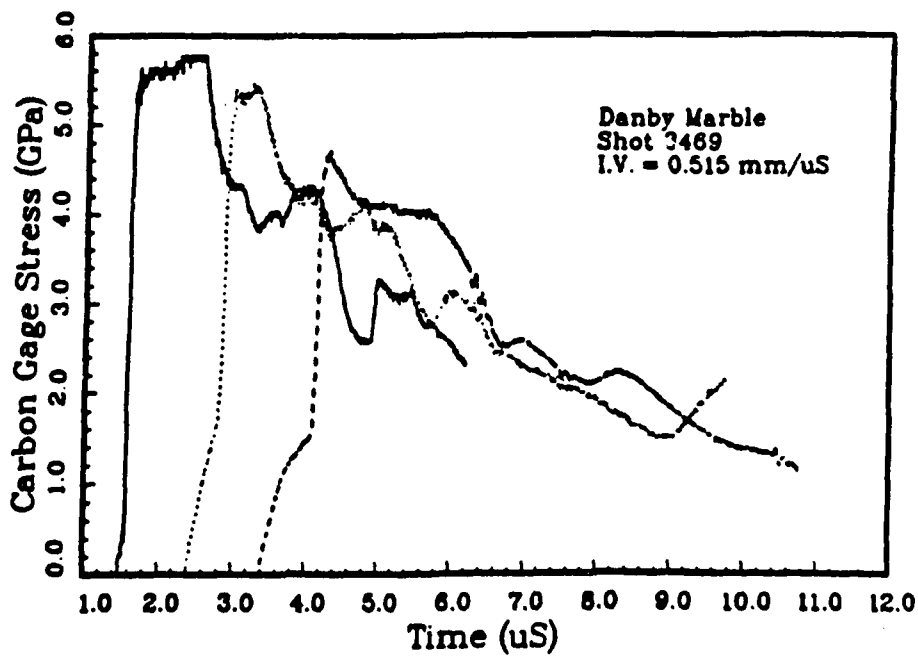
Ft. Knox Carbonates Hugoniot data were obtained from three different core samples from the Louisville and Jeffersonville formations at the UTP site in Ft. Knox, Kentucky. The porosity of each of the cores was approximately 2 percent. The Louisville formation was fine grained and mottled with patches of dolomite. Two different Jeffersonville cores were supplied for testing. Neither was dolomitized. The first Jeffersonville core received was fine grained and homogeneous without inclusions. This core was designated Jeffersonville-1. The second core, referred to as Jeffersonville-2, contained abundant inclusions in the form of crinoid fragments which can be clearly seen in Figure 4-5.

Samples were received saturated with water. Saturation was maintained throughout the sample evaluation and target assembly process. Frozen targets were assembled at ambient temperature and then frozen overnight to -12°C . The frozen targets were removed from the freezer, mounted on the gun, and maintained at $-7 \pm 1^{\circ}\text{C}$ until impact. Thermocouples in the target were monitored during the freezing and shot preparation processes.

The average as-received densities of the Ft. Knox Carbonate samples from the Louisville, Jeffersonville-1, and Jeffersonville-2 formations were 2.753 (std = 0.041), 2.703 (std = 0.008), and 2.738 (std = 0.008) g/cc, respectively. The average ultrasonic velocities were 6.63 (std = 0.22), 6.39 (std = 0.05), and 6.41 (std = 0.23) km/s, respectively. A complete listing of pretest material properties is given in Table 4-4 which defines the as-received condition of the samples.



(a) Shot 3467, elastic propagation is observed at a stress of 1.16 GPa.



(b) Shot 3469, precursor and attenuation due to catch-up is observed above 2GPa.

Figure 4-4. Stress histories for Danby marble.

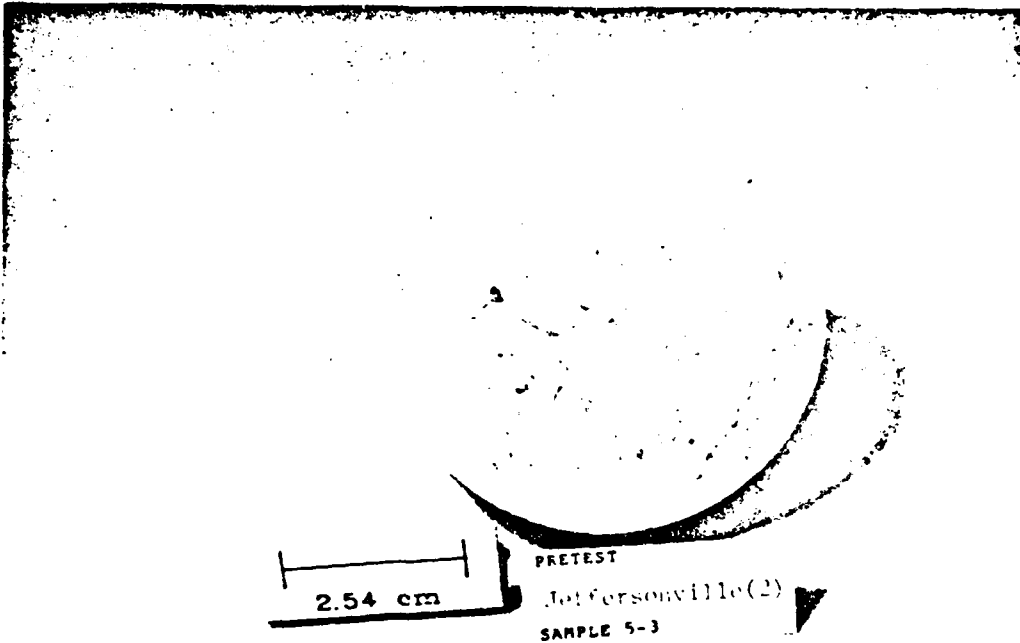


Figure 4-5. Photograph of typical Jeffersonville-2 sample.

Table 4-4. Material properties for Ft. Knox carbonates.

Sample No.	Avg. Thick. (mm) ±1%	Density (g/cc) ±1%	Longitudinal Velocity (km/s) ±5%	Sample No.	Avg. Thick. (mm) ±1%	Density (g/cc) ±1%	Longitudinal Velocity (km/s) ±5%
<u>Louisville Carbonate</u>				<u>Jeffersonville-1 limestone</u>			
Hole: CB-7, Depth: 601.2 - 602.3				Hole: CB-7, Depth: 523.6 - 523.9			
1-4	4.99	2.76	6.54	LS-1	5.03	2.71	6.34
1-5	9.98	2.75	6.13	LS-2	5.07	2.69	6.44
1-6	4.98	2.75	6.19	LS-3	5.04	2.70	6.37
1-9	10.02	2.81	6.87	LS-4	5.02	2.71	6.41
1-11	4.98	2.79	6.89	LS-5	5.02	2.71	6.35
1-12	5.00	2.80	6.74	LS-6	4.98	2.71	6.29
3-2	5.00	2.69	6.45	LS-7	10.08	2.70	6.43
3-3	4.91	2.72	6.90	LS-8	10.02	2.69	6.41
3-4	10.04	2.68	6.56	LS-9	9.90	2.70	6.45
3-6	5.00	2.75	6.85	<u>Jeffersonville-2 limestone</u>			
3-7	10.01	2.74	6.81	Hole: GWMH-3A, Depth: 521.6 - 522.3			
3-8	4.97	2.68	6.50	5-2	4.97	2.73	6.30
Hole: CB-7, Depth: 642.3 - 642.9				5-3	10.03	2.73	6.55
4-7	10.02	2.78	6.53	5-5	5.03	2.73	6.50
4-8	5.02	2.74	6.75	5-7	5.03	2.74	6.51
4-10	5.00	2.78	6.70	5-8	4.99	2.75	6.43
4-11	10.06	2.79	6.69	5-13	10.04	2.73	6.27
4-12	5.00	2.79	6.62	6-2	5.01	2.75	6.71
Nominal sample diameter = 47mm				6-4	10.03	2.75	6.58
				6-5	5.00	2.73	5.88
				Nominal sample diameter = 63.3 mm			

The experimental configurations and results are summarized in Tables 4-5 and 4-6, respectively. Note that the material thickness presented in Table 4-5 may differ from those presented in Table 4-4 due to the lapping processes that were necessary to obtain adequately flat samples. Hugoniot data points in Table 4-6 were extracted from the Lagrangian analysis. Plots of the Hugoniot data in the stress-particle velocity, stress-relative volume, and shock velocity-particle velocity planes are presented in Figures 4-6, 4-7, and 4-8 for all three types of Ft. Knox carbonate tested. Individual stress-time profiles for each shot are in Appendix A. Comparison of the results show the Louisville and Jeffersonville carbonate shock responses are different, as can be seen in the stress histories. The data indicate the Louisville formation has a higher impedance than the Jeffersonville. This is consistent with the dolomitization reported for the Louisville formation.

The Hugoniot data points are derived from stresses taken at the top of the initial fast rise on the first gauge. The stress increased more slowly above the Hugoniot point up to the peak gauge stress before releasing. This rounding of the peak may be due to strain rate effects. The results of the Lagrangian analyses have been overlaid on the stress-particle velocity and stress-volume plots. Continued loading and compression above the Hugoniot point is most evident in the stress-volume plots.

4.3 SALEM LIMESTONE.

The Salem limestone was from the Elliott Stone Company, Inc.⁷, quarry in Indiana. The samples were cut from a block of Salem limestone obtained by SRI International (Gefken, 1992) by WES personnel. These samples were then lapped by Ktech to acceptable flatness for uniaxial strain impact tests. The Salem limestone samples which were nominally 16 percent porous were tested in dry, saturated, and saturated frozen states. Samples for saturated and frozen tests were received saturated at ambient temperature and when appropriate were frozen prior to target assembly. In consideration of the high porosity of the samples, procedures were developed so that freezing commenced from one side and proceeded to the other to force any air bubbles or excess water out of the sample. The thin surface layers of ice that resulted from the freezing procedure were removed by lapping. Measured material properties for the limestone samples are found in Table 4-7 which defines the as-received condition of the samples. Average densities at room temperature of the dry, and saturated samples were 2.282 (std = 0.014) and 2.427 (std = 0.006) g/cc, respectively, and average longitudinal ultrasonic velocities were 5.03 (std = 0.12) and 5.14 (std = 0.12) km/s, respectively.

⁷ Elliott Stone Company, Inc., 3326 Mitchell Road, P.O. Box 756, Bedford, IN.

Table 4-5. Ft. Knox carbonates shot configuration data.

Shot No.	WC* Impact Thick	6061-T6 Buffer Thick	Thickness (mm) and Density (g/cc) at Ambient Temperature								
			Sample 1			Sample 2			Sample 3		
			No.	Center Thick	ρ_s	No.	Center Thick	ρ_s	No.	Center Thick	ρ_s
3489	3.16*	9.40	1-11	4.99	2.79	1-12	5.01	2.80	1-9	10.04	2.81
3490	3.19*	9.39	4-10	5.02	2.78	4-12	5.00	2.79	4-11	10.07	2.79
3499	3.17	9.41	LS5	5.02	2.71	LS6	4.97	2.71	LS9	9.90	2.70
3492	3.18	9.39	LS2	5.07	2.69	LS3	5.04	2.70	LS8	10.02	2.69
3491	3.17	9.40	3-2	5.01	2.69	3-8	4.98	2.68	3-4	10.04	2.68
3503	4.78	9.40	5-2	5.01	2.73	6-5	5.00	2.73	5-3	10.06	2.73
3505	4.78	9.41	5-7	5.03	2.74	5-5	5.05	2.73	5-13	10.06	2.73
3504	4.78	9.40	6-2	5.04	2.75	5-8	5.02	2.75	6-4	10.06	2.75
3497	4.78	9.39	1-4	5.00	2.76	1-6	4.99	2.75	1-5	10.00	2.75
3498	4.78	9.44	4-8	5.02	2.74	3-6	5.01	2.75	3-7	10.01	2.74

* Impactors were 4340 steel on shots 3489 and 3490

Table 4-6. Ft. Knox carbonates (UTP site) Lagrangian stress gauge Hugoniot data.

Shot Number	Config. †	Impact Velocity (km/s)	Hugoniot Data				
			Initial Density (g/cc)	Stress (GPa)	U_s^{**} (1/2 amp) (km/s)	u_p (km/s)	ρ/ρ_0
3489	a(L)	0.154	2.80	2.01	6.48°	0.118	1.020
3490	a(L) _f	0.156	2.79	1.83	5.84°	0.119	1.022
3499	b(J)	0.232	2.71	2.43	4.21°	0.200	1.043
3492	b(J) _f	0.232	2.69	2.61	4.15°	0.223	1.069
3491	b(L) _f	0.233	2.68	2.87	5.22°	0.220	1.052
3503	c(J2)	0.346	2.73	3.44	3.96	0.293	1.081
3505	c(J2) _f	0.346	2.73	3.92	3.74	0.345	1.095
3504	c(J2)	0.502	2.75	5.47	4.59	0.415	1.097
3497	c(L)	0.507	2.75	5.42	5.24	0.372	1.076
3498	c(L) _f	0.505	2.74	5.97	5.65	0.377	1.071

† Configuration:

- a) 4340 (3.2 mm) → 6061 - T6/CG/Sample/CG/Sample/CG/Sample
- b) WC (3.2 mm) → 6061 - T6/CG/Sample/CG/Sample/CG/Sample
- c) WC (4.8 mm) → 6061 - T6/CG Sample/CG/Sample/CG/Sample

- (L) = Louisville carbonate
- (J) = Jeffersonville-1 limestone
- (J2) = Jeffersonville-2 limestone
- f = Frozen target temperature was -7°C for these shots.
All others were shot at ambient temperature

° 1/2 amplitude shock velocity is in precursor or ramped portion of stress wave.

** Shock velocity taken as dh/dt at gauge 1 half-amplitude loading stress from Lagrangian analysis.

Note: Stress is an initial shock stress level from the Lagrangian analysis and does not represent peak or equilibrium stress.

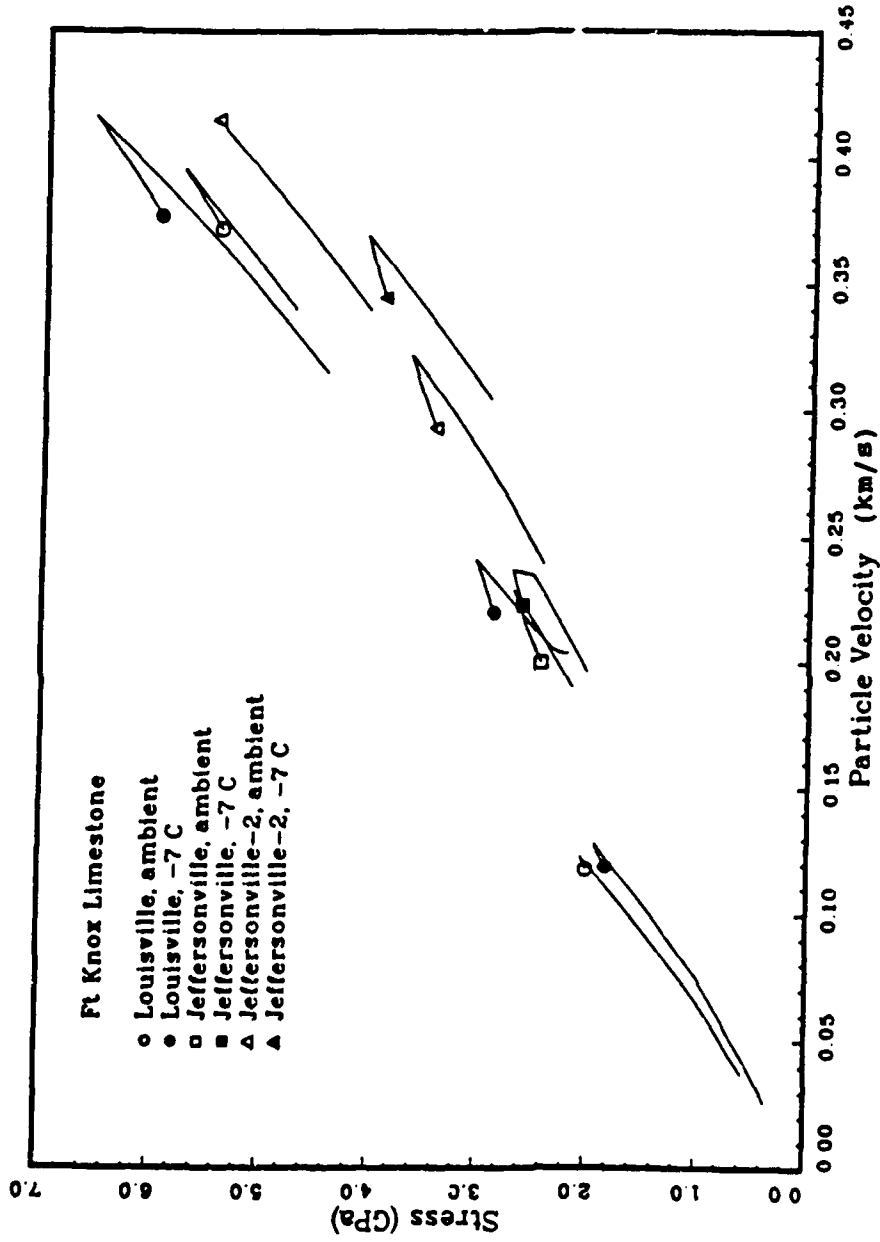


Figure 4-6. Ft. Knox carbonate stress-particle velocity Hugoniot data with partial loading and release paths.

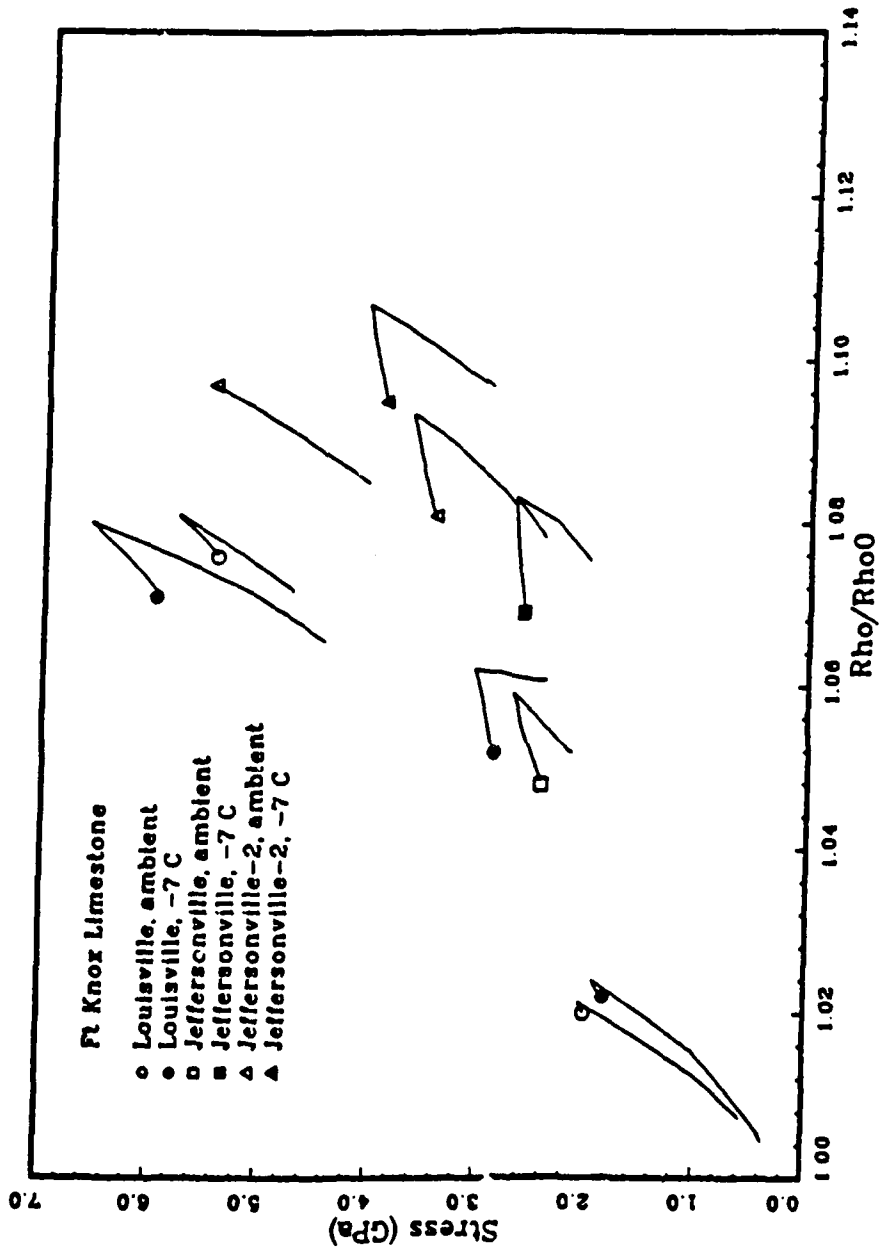


Figure 4-7. Ft. Knox carbonate stress- ρ/ρ_0 Hugoniot data with partial loading and release paths.

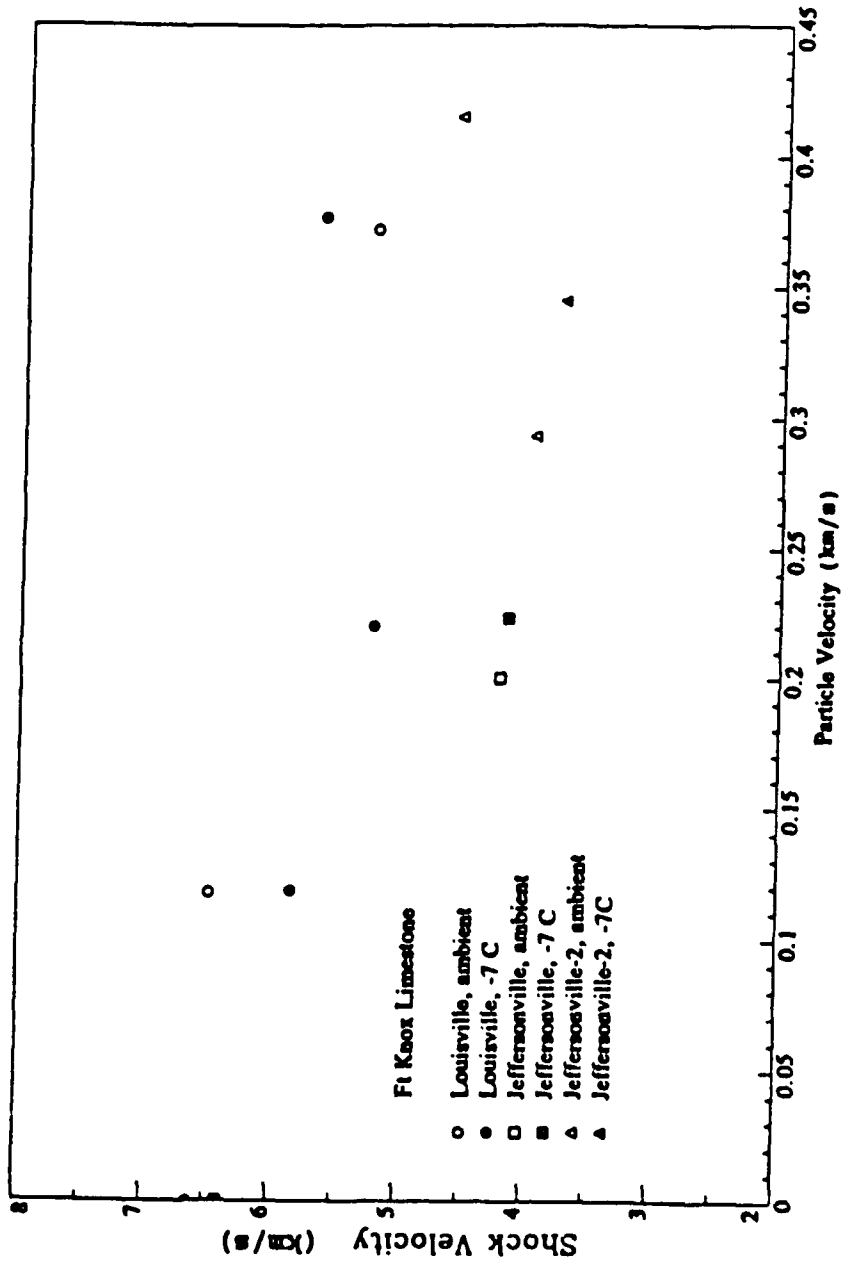


Figure 4-8. Ft. Knox carbonate shock velocity-particle velocity Hugoniot data.

Table 4-7. Material properties for Salem limestone.

Sample No.	Avg. Thick. (mm) ±1%	Density (g/cc) ±1%	Longitudinal Velocity (km/s) ±5%	Sample No.	Avg. Thick. (mm) ±1%	Density (g/cc) ±1%	Longitudinal Velocity (km/s) ±5%
Salem Limestone - Dry							
SL-D3-27	9.88	2.29	4.96	SL-D8-02	9.61	2.26	4.81
SL-D3-28	3.84	2.29	5.16	SL-D8-03	3.62	2.26	5.02
SL-D3-30	9.81	2.29	4.88	SL-D8-04	3.83	2.25	5.00
SL-D3-31	3.77	2.29	5.19	SL-D8-05	9.92	2.27	4.95
SL-D3-32	3.84	2.29	5.13	SL-D8-08	9.90	2.28	4.84
SL-D3-33	9.92	2.30	4.98	SL-D8-09	3.85	2.29	5.16
SL-D3-34	3.88	2.29	5.19	SL-D8-10	3.90	2.29	5.11
SL-D3-35	3.85	2.29	5.14	SL-D8-11	9.91	2.30	4.99
				SL-D8-12	3.80	2.29	5.04
Salem Limestone - Saturated							
SL-D3-02	9.58	2.43	5.03	SL-D3-25	3.83	2.42	5.09
SL-D3-03	3.82	2.42	5.22	SL-D3-26	3.81	2.42	5.10
SL-D3-04	3.83	2.42	4.99	SL-D8-06	3.81	2.41	5.24
SL-D3-05	9.88	2.42	4.89	SL-D8-14	9.93	2.43	5.09
SL-D3-07	3.75	2.42	5.22	SL-D8-15	3.88	2.43	5.34
SL-D3-08	9.10	2.43	4.94	SL-D8-16	3.88	2.42	5.20
SL-D3-09	3.80	2.44	5.01	SL-D8-17	9.86	2.44	5.16
SL-D3-10	3.76	2.44	4.96	SL-D8-18	3.92	2.43	5.27
SL-D3-11	9.90	2.43	5.02	SL-D8-19	3.84	2.43	5.38
SL-D3-12	3.81	2.43	5.28	SL-D8-22	9.89	2.43	5.04
SL-D3-13	3.81	2.43	5.27	SL-D8-23	3.81	2.42	5.16
SL-D3-14	9.86	2.42	4.99	SL-D8-24	3.89	2.42	5.30
SL-D3-16	3.46	2.43	5.08	SL-D8-25	9.88	2.43	5.09
SL-D3-17	3.73	2.42	5.18	SL-D8-26	3.82	2.43	5.23
SL-D3-18	10.03	2.43	4.95	SL-D8-27	3.78	2.43	5.19
SL-D3-19	3.80	2.43	5.20	SL-D8-28	9.97	2.43	5.31
SL-D3-20	3.79	2.43	5.17	SL-D8-29	3.78	2.42	5.23
SL-D3-21	9.98	2.43	5.07	SL-D8-30	3.89	2.43	5.19
SL-D3-22	3.77	2.42	5.12	SL-D8-31	9.85	2.44	5.14
SL-D3-23	3.82	2.43	5.12	SL-D8-32	3.84	2.42	5.35
SL-D3-24	9.88	2.42	5.00	SL-D8-33	3.84	2.42	5.18

Table 4-8 contains shot configuration data such as material thicknesses and sample densities. Note that the material thickness may differ from those presented in Table 4-7 due to the lapping processes that were necessary to obtain adequately flat samples. Table 4-9 contains Hugoniot data. The Salem limestone results are summarized graphically in Figures 4-9 through 4-11. The plotted points are Hugoniot points and the curves are unloading paths. In all three representations of the data it is clear that the dry material has a very different response from both saturated materials (ambient and frozen). This is not surprising since ice-filled pores will be nearly as incompressible as water-filled ones. The stress-density plots also show another interesting feature for both saturated rocks; namely, there are two inflections in the unloading curves. The unloading between 2.5 and 1.7 GPa, shows a marked decrease in stiffness when compared to stress regimes above this range. This is followed by stiffer response for unloading down to as low as 0.5 GPa. The absence of this feature in the dry limestone suggests that this is a reversible phase change involving or facilitated by water.

Stress wave profile data obtained at the 8-mm depth from shots at the different stress levels are shown in Figure 4-12 for dry samples, Figure 4-13 for saturated samples, and Figure 4-14 for saturated frozen samples. These three data sets all show excellent consistency from one sample to another and clearly show the differences between the dry, ambient saturated, and frozen saturated materials. Figure 4-12 shows the establishment of a ramped precursor with the toe moving at 3.96 km/s before compaction leads to shocking up. The precursors for the saturated and frozen samples have measured velocities of 4.23 and 5.03 km/s, respectively. The stress profiles show the influence of the water or ice filling the pores; the precursor velocities are higher and both saturated materials (water- or ice-filled) begin shocking up earlier than the dry porous limestone. In contrast, the stress waves attenuated more rapidly in the dry material. All three sample types show increased main wave velocities at increased stresses.

4.4 DISCUSSION.

The waveforms observed in the Louisville formation carbonates were distinctly different from those measured in calcite rocks. The Louisville formation carbonates were a dolomite (or dolomite limestone). The difference in the responses of the Louisville and Jeffersonville formation materials can be seen clearly in Figures 4-15 and 4-16. For a given impact velocity, the stress in the dolomitized Louisville formation is about 13 to 15 percent higher than in the Jeffersonville calcite

Table 4-8. Salem Limestone shot configuration data.

Thickness (mm) and Density (g/cc) at Ambient Temperature											
Shot No.	6061-T6 Impact Thick	6061-T6 Buffer Thick	Sample 1			Sample 2			Sample 3		
			No.	Center Thick	ρ_s	No.	Center Thick	ρ_s	No.	Center Thick	ρ_s
Ambient Dry											
3554	6.29	9.59	D3-28	3.83	2.29	D3-31	3.78	2.29	D3-27	9.88	2.29
3556	6.28	9.58	D3-32	3.84	2.29	D3-34	3.88	2.29	D3-30	9.81	2.29
3564	6.24	9.63	D8-03	3.61	2.26	D8-04	3.83	2.25	D8-02	9.62	2.26
3558	6.25	9.57	D3-35	3.86	2.29	D8-09	3.86	2.29	D3-33	9.92	2.30
3561	6.43	9.58	D8-10	3.90	2.29	D8-12	3.80	2.29	D8-05	9.93	2.27
Ambient Saturated											
3555	6.28	9.58	D3-03	3.83	2.42	D3-04	3.84	2.42	D3-02	9.58	2.43
3563	6.25	9.64	D3-25	3.83	2.42	D3-26	3.81	2.42	D3-21	9.99	2.43
3557	6.33	9.76	D3-09	3.81	2.44	D3-07	3.75	2.42	D3-05	9.89	2.42
3560	6.32	9.61	D3-13	3.81	2.43	D3-16	3.47	2.43	D3-08	9.06	2.43
3559	6.28	9.58	D3-10	3.77	2.44	D3-12	3.80	2.43	D3-11	9.91	2.43
3562	6.30	9.62	D3-19	3.80	2.43	D3-20	3.79	2.43	D3-14	9.86	2.42
Frozen Saturated											
3583	6.27	9.60	D8-06	3.83	2.41	D3-17	3.74	2.42	D3-24	9.89	2.42
3573	6.25	9.95	D8-15	3.88	2.43	D8-18	3.91	2.43	D8-22	9.88	2.43
3576	6.28	9.60	D8-16	3.88	2.42	D8-19	3.87	2.43	D8-14	9.94	2.43
3574	6.28	9.63	D8-27	3.78	2.43	D8-26	3.83	2.43	D8-25	9.91	2.43
3575	6.29	9.63	D8-32	3.84	2.42	D8-33	3.85	2.42	D8-31	9.88	2.44
3582	6.30	9.63	D3-22	3.78	2.42	D3-23	3.83	2.43	D3-18	10.03	2.43
3577	6.26	9.60	D8-29	3.81	2.42	D8-30	3.92	2.43	D8-28	10.00	2.43

Table 4-9. Salem Limestone Lagrangian Hugoniot data.

Shot Number	Impact Velocity (km/s)	Hugoniot Data				
		Initial ¹ Density (g/cc)	Stress ² (GPa)	U _s ½ amp. ³ (km/s)	u _p (m/s)	ρ/ρ_0
Ambient Dry						
3554 ⁵	0.144	2.29	0.55	3.02 ⁴	88	1.038
3556	0.254	2.29	0.88	2.40 ⁴	161	1.081
3564	0.295	2.26	1.03	2.00	203	1.111
3558	0.533	2.29	2.06	2.35	361	1.177
3561	0.790	2.29	3.57	2.52	573	1.276
Ambient Saturated						
3555	0.144	2.42	0.77	3.62 ⁴	88	1.027
3563	0.292	2.42	1.51	3.39	195	1.062
3557	0.480	2.44	2.47	3.26	308	1.105
3560	0.794	2.43	4.25	3.52	496	1.165
3559	0.802	2.44	4.31	3.45	509	1.175
3562 ⁷	0.928	2.43	5.06	3.50	588	1.200
		2.43	5.06	3.62	577	1.192
Frozen Saturated						
3583 ⁵	0.143	2.41	0.61	3.66 ⁴	75	1.024
3573 ⁶	0.144	2.43	---	---	---	---
3576	0.289	2.42	1.50	3.25 ⁴	190	1.069
3574	0.507	2.43	2.61	3.04	331	1.120
3575	0.777	2.42	4.27	3.27	518	1.184
3582	0.784	2.42	4.29	3.30	524	1.191
3577 ⁷	0.934	2.42	5.19	3.57	583	1.193
			5.19	3.59	581	1.189

Configuration:

CF/6061-T6 → 6061-T6/CG/Sample/CG/Sample/CG/Sample

- Notes:
- ¹ Initial density is of the first sample in the stack.
 - ² Stress is the average equilibrium stress from gauges 1, 2, and 3.
 - ³ Shock velocity taken as dh/dt at gauge 1 half-amplitude loading stress from Lagrangian analysis.
 - ⁴ Half-amplitude velocity was in the ramp portion of the loading wave.
 - ⁵ Gauges 2 and 3 were analyzed since they had similar structure and were very different from gauge 1. Note the stress is from gauge 2 and does not represent the peak input stress.
 - ⁶ Lagrangian analysis was not performed on shot 3573 because a slow rise was observed at aluminum buffer/sample interface which was due to a poor impact condition.
 - ⁷ Gauges 2 and 3 were analyzed for a release path and 2nd Hugoniot point.

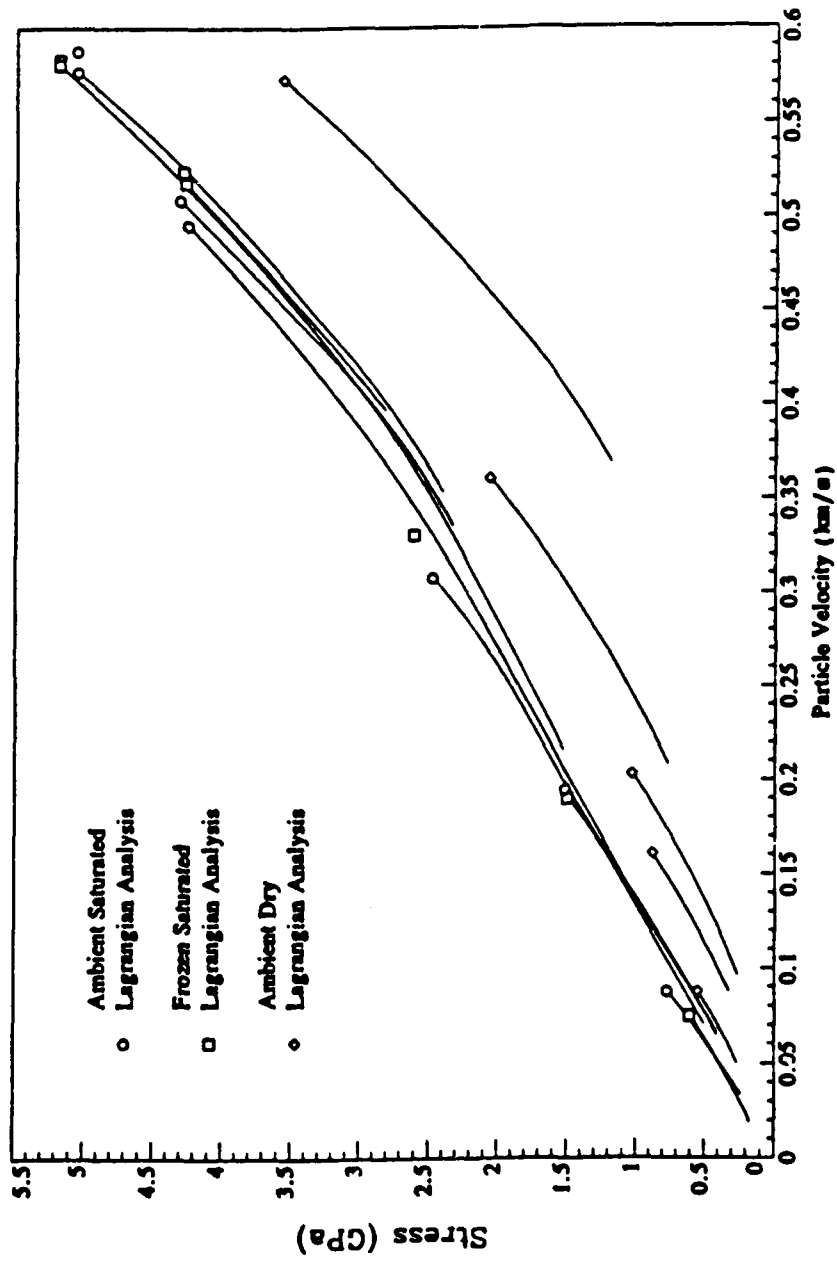


Figure 4-9. Salem limestone stress-particle velocity Hugoniot data and release paths.

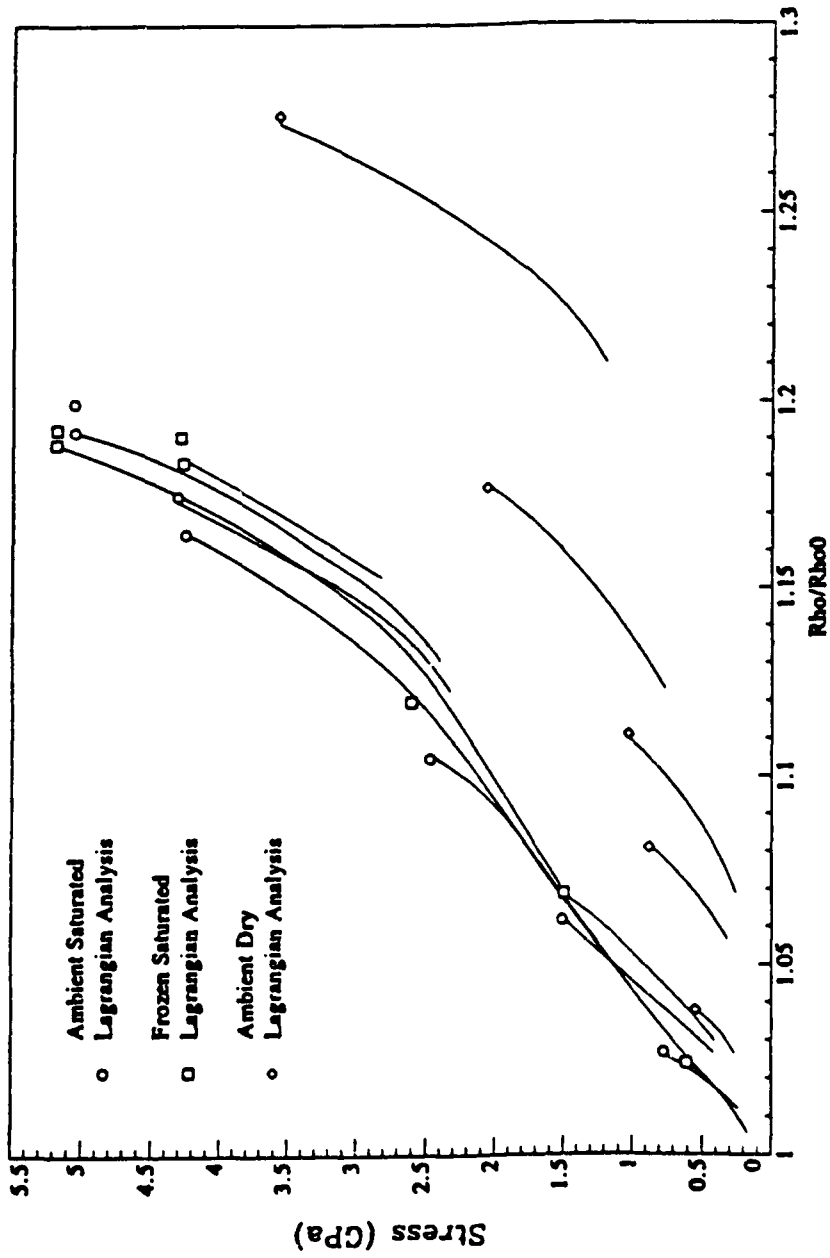


Figure 4-10. Salem limestone stress- ρ/ρ_0 Hugoniot data and release paths.

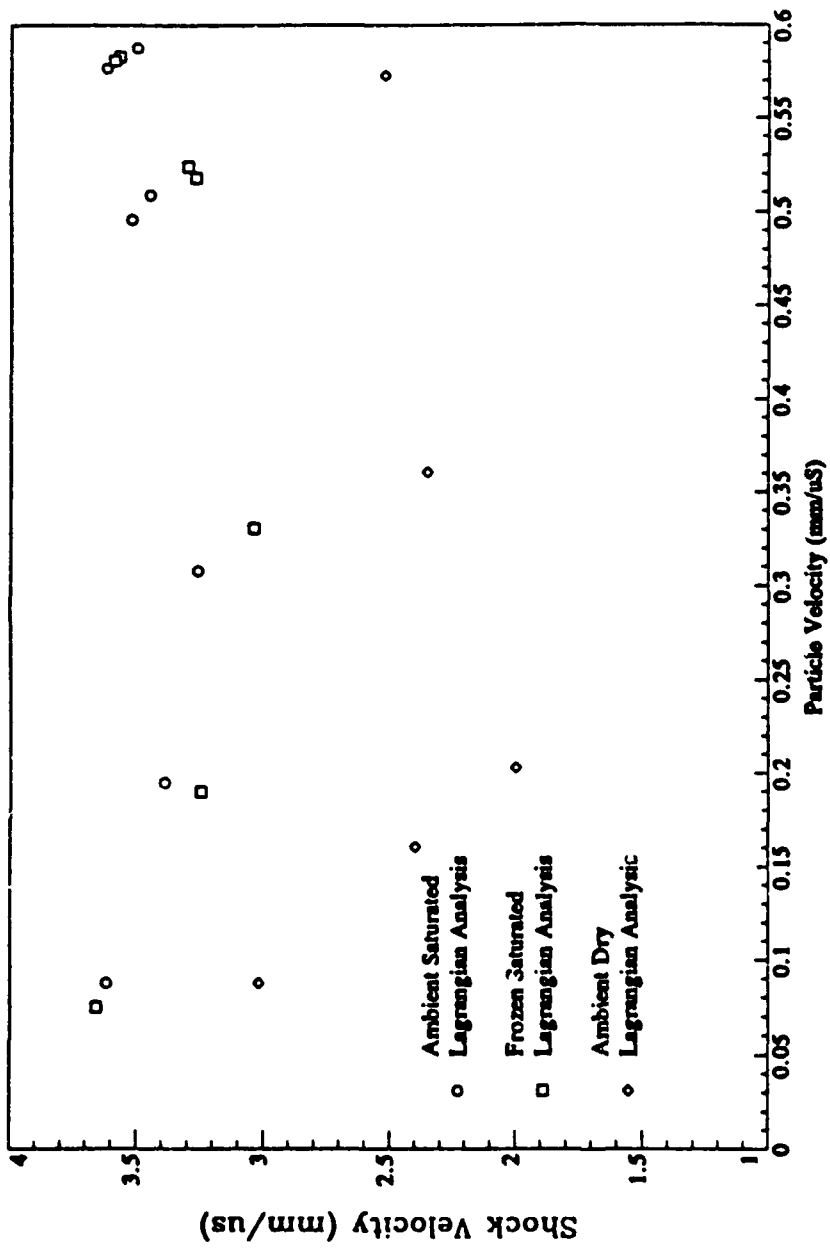


Figure 4-11. Salem limestone shock velocity-particle velocity Hugoniot data.

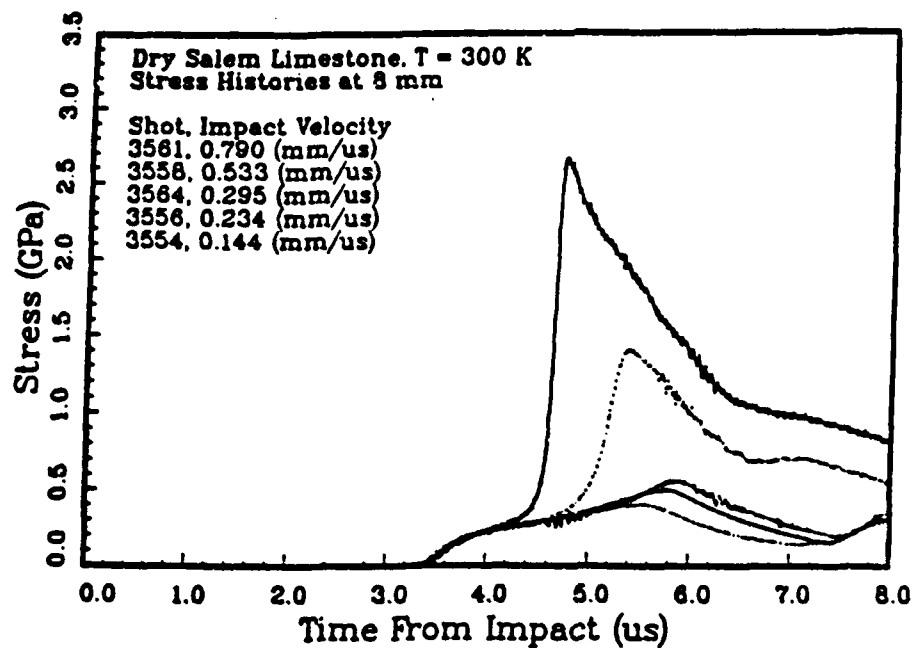


Figure 4-12. Dry Salem limestone data at 8 mm depth.

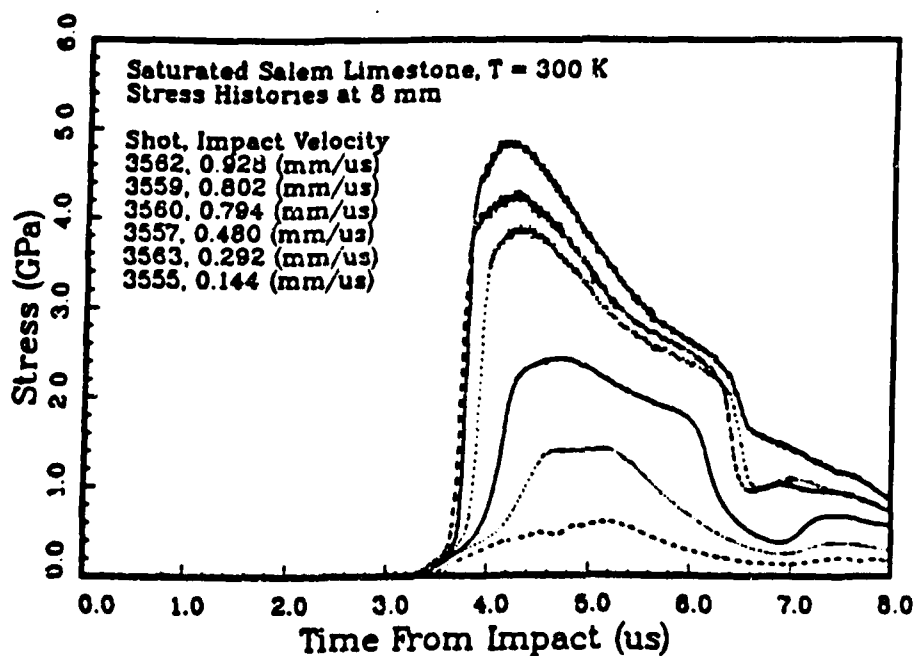


Figure 4-13. Saturated Salem limestone data at 8 mm depth.

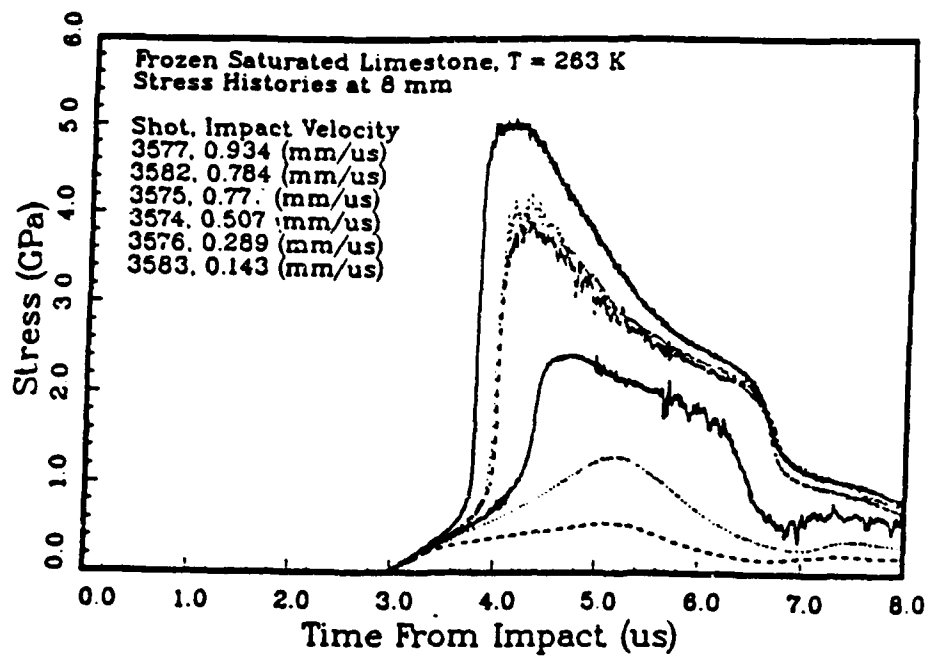


Figure 4-14. Frozen Salem limestone data at 8 mm depth.

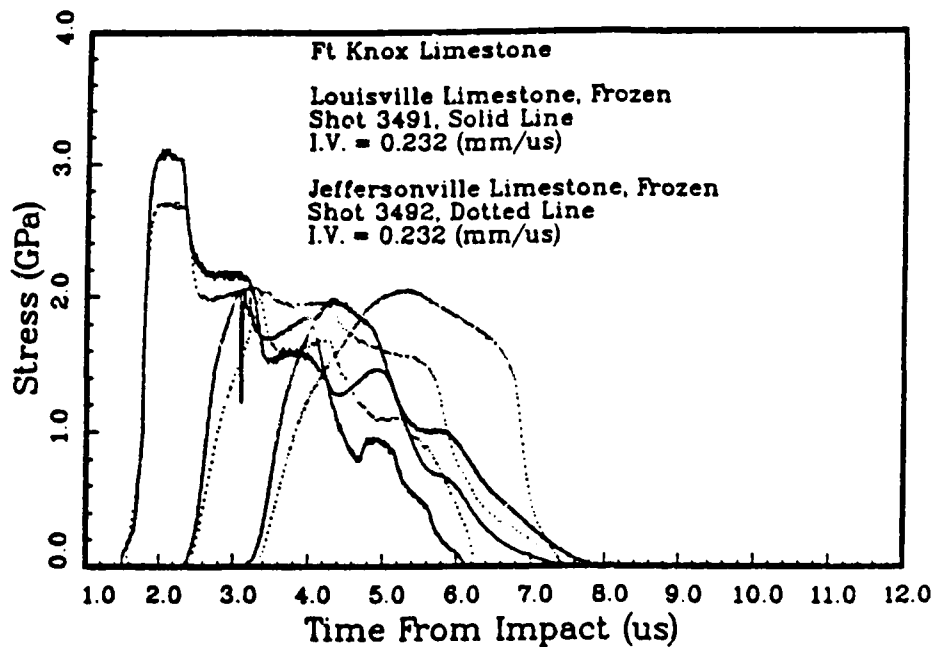


Figure 4-15. Frozen Louisville and frozen Jeffersonville-1 comparison.

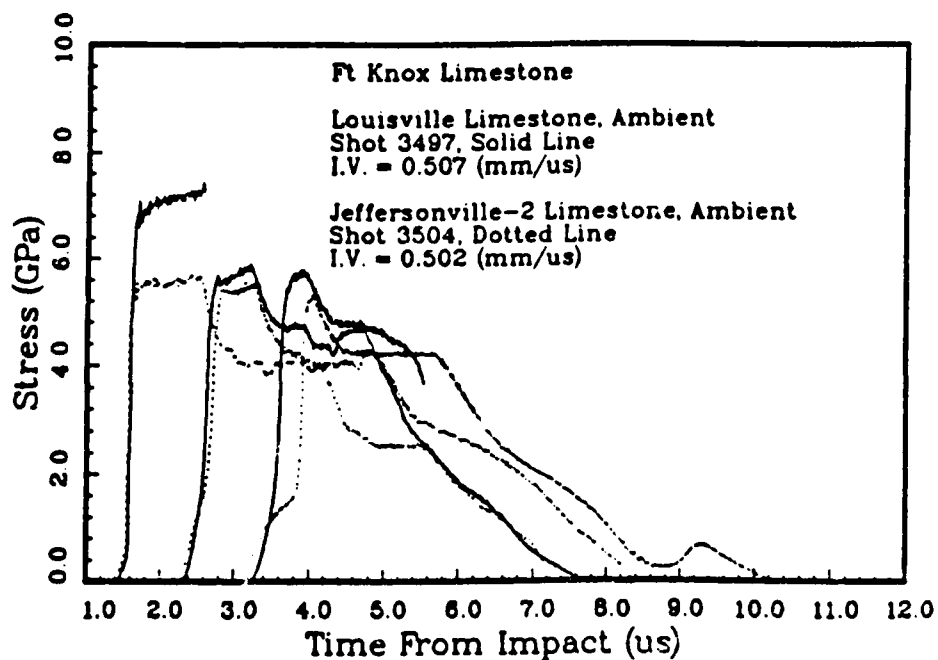


Figure 4-16. Saturated Louisville and saturated Jeffersonville-2 comparison.

formation. Furthermore, above 1.2 GPa the Jeffersonville formation shows a marked softening with the development of a pronounced precursor (especially evident in Figure 4-16) which is caused by the phase transition calcite I \rightarrow calcite II \rightarrow calcite III. The same transition is found in all of the calcite rocks studied.

The 6.3-mm-thick aluminum alloy impactor generated a flat-topped, one microsecond long shock pulse. Rapid attenuation of this stress profile was observed in all the carbonates studied. Even the Louisville carbonate (which does not have a phase change to slow the velocity of the loading wave) suffers complete attenuation of the flat-top of the wave prior to arrival at the second gauge plane at 5-mm-depth for incident stresses of 3 GPa or higher. This is the result of a high initial unloading wave speed.

The differences due to initial temperature are subtle (Figures 4-17 through 4-20) for the Fort Knox carbonates. The largest difference in stress at the buffer/rock interface is approximately 10 percent (Figure 4-19), and at 2.7 GPa there is no difference at all (Figure 4-18). This is not surprising in light of the small fraction of water (or ice) in these samples.

The freezing of low porosity (2-3 percent) saturated limestone has little effect on its equation of state or on the attenuation of shock waves at pressures above about 2 GPa. In the stress regime of 1.5 to 2 GPa, the Ft. Knox frozen limestone shows a slight increase in attenuation.

For the Salem limestone, with 16 percent porosity, the effects of saturation and freezing are quite pronounced. Figure 4-21 shows stress profiles recorded at the 8-mm-depths in each type of rock with peaks near 2.5 GPa. Wave speeds are lowest for the dry material. Below 0.7 GPa the frozen sample shows higher wave speeds than the unfrozen sample, which is a reflection of the higher wave speed of ice (~ 4 km/s) relative to water (~ 1.5 km/s). However, above 0.7 GPa the wave profile in the frozen sample lags behind that in the unfrozen one. This probably reflects a phase change in the H_2O constituent producing high compressibility (and, hence, low wave speed). The data do not permit direct determination of whether the phase change is a melting or a solid-solid transition. Upon unloading, both saturated media show a decompression shock front developing at about 1.7 GPa. This is a result of the concave downwards unloading path noted earlier.

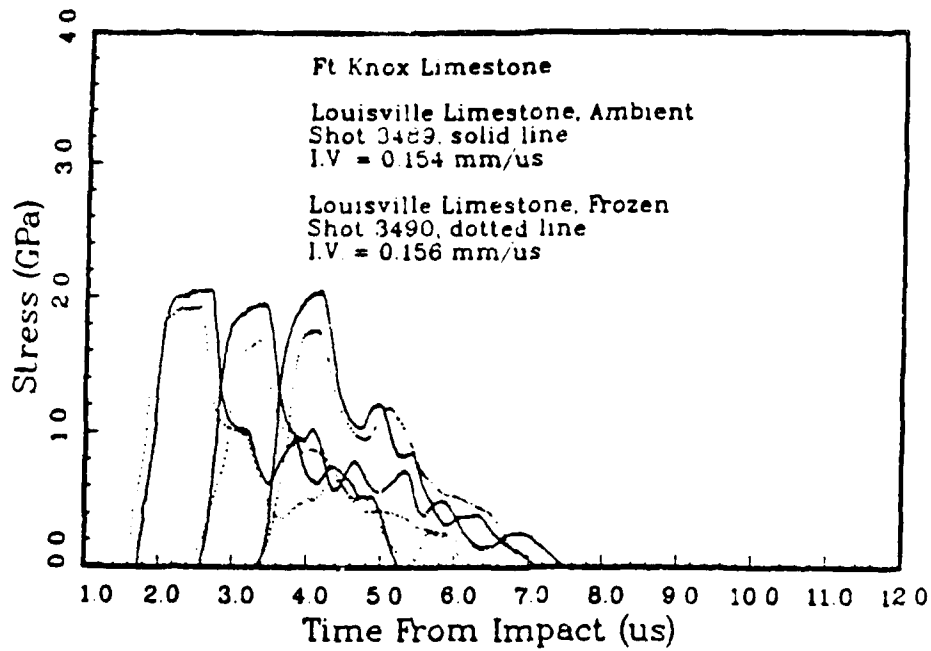


Figure 4-17. Shot 3489 (saturated) and 3490 (frozen) comparison.

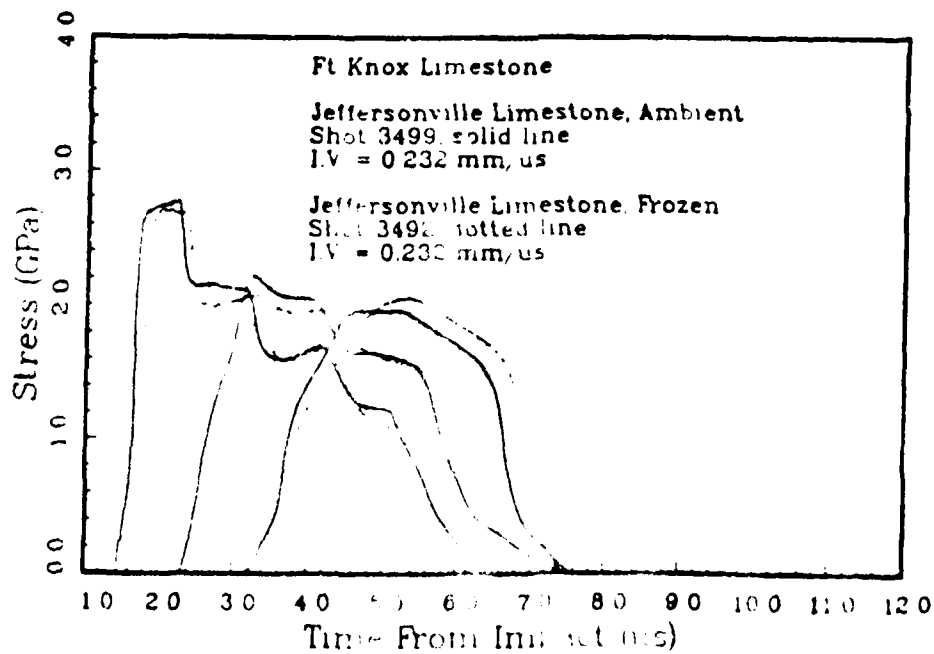


Figure 4-18 Shot 3499 (saturated) and 3492 (frozen) comparison

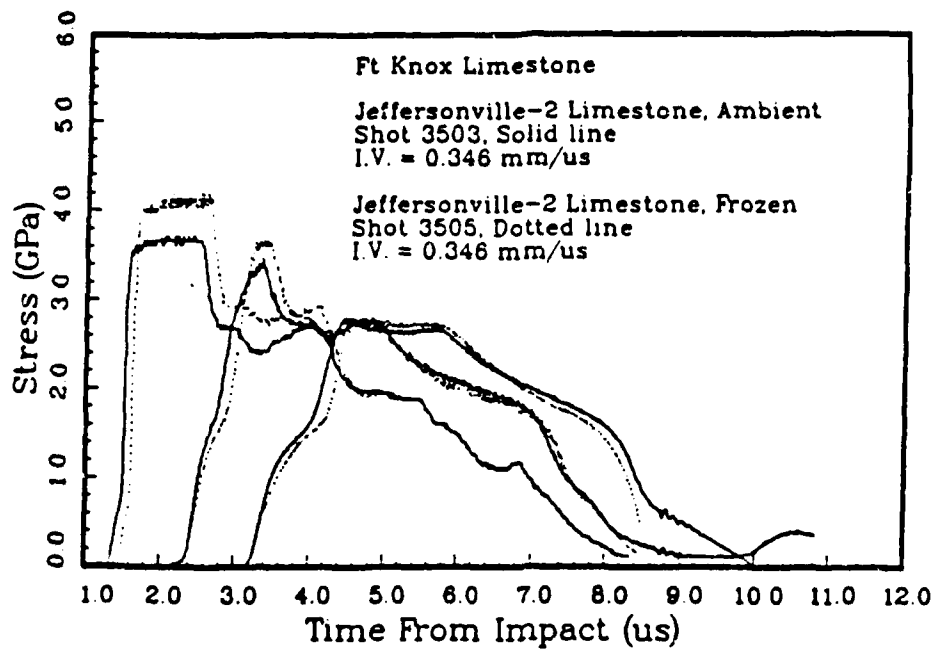


Figure 4-19. Shot 3503 (saturated) and 3505 (frozen) comparison.

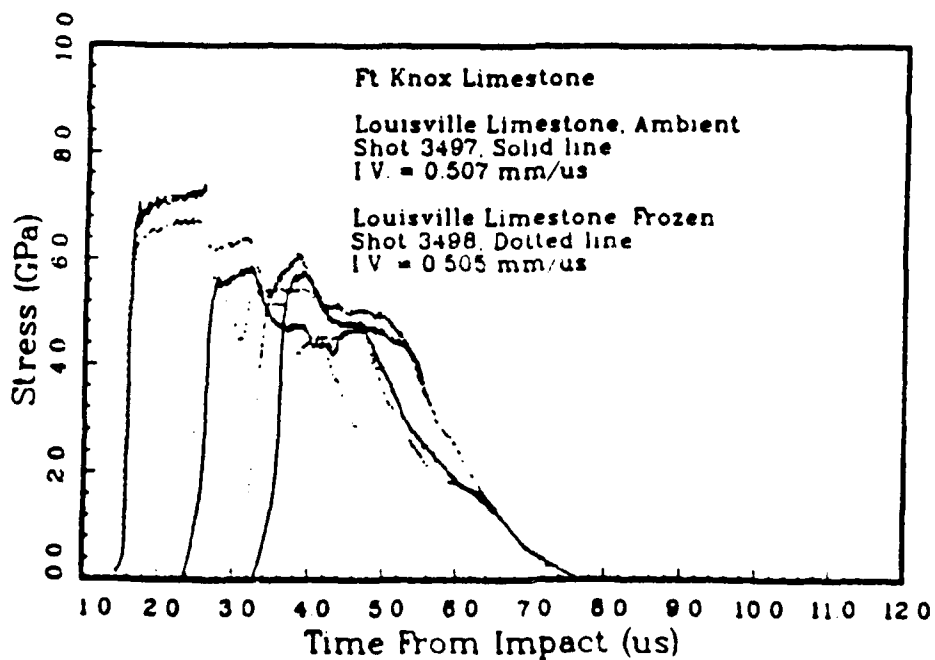


Figure 4-20. Shot 3497 (saturated) and 3498 (frozen) comparison.

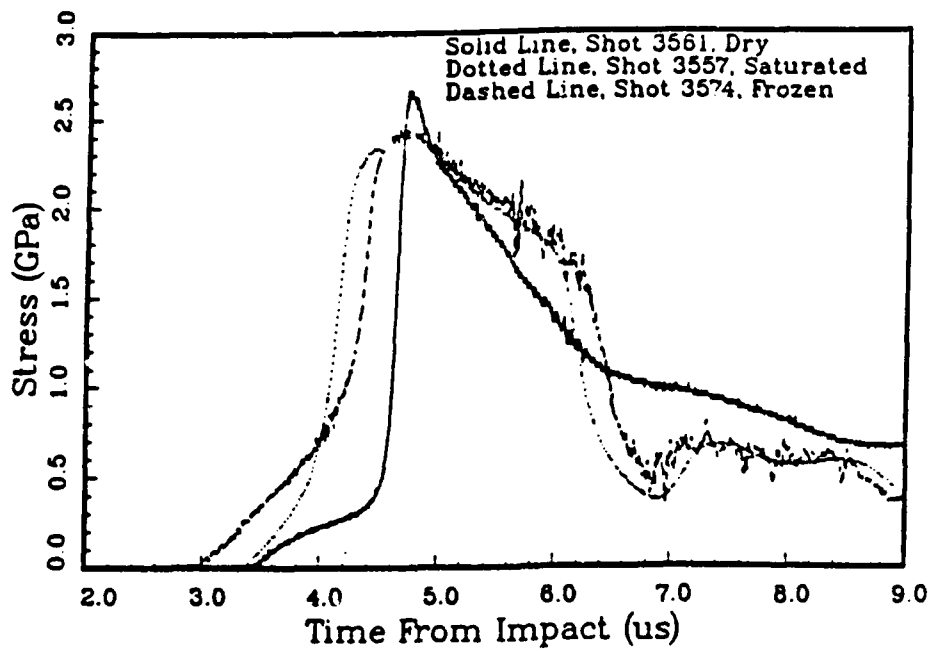


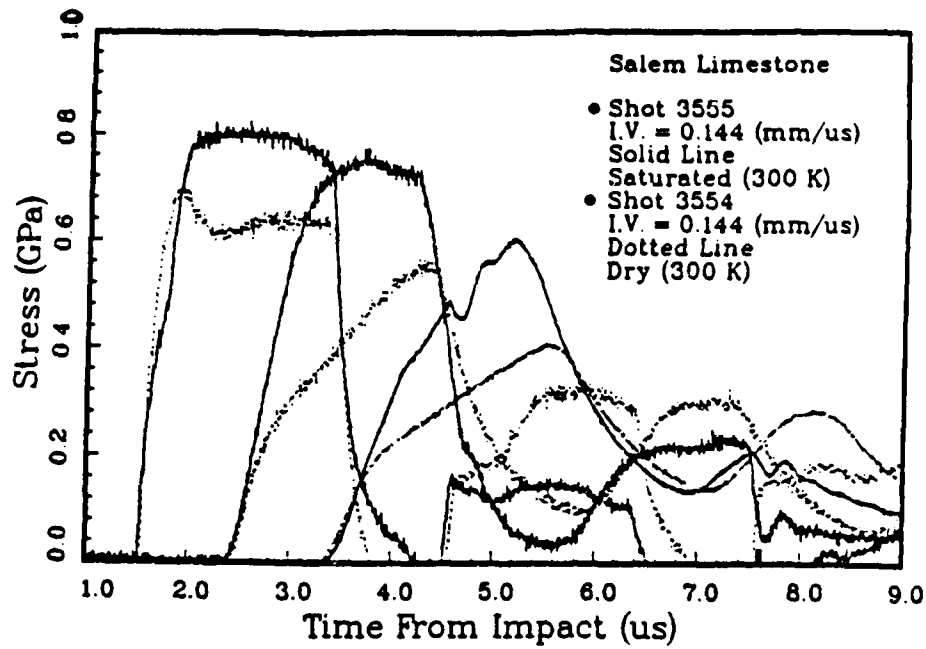
Figure 4-21. Comparison of stress profiles with peaks near 2.5 GPa at 8 mm depths in each type of Salem limestone.

Comparisons of the responses of dry, ambient saturated, and frozen saturated Salem limestone are provided in Figures 4-22, 4-23, 4-24, and 4-25 for the range of impact velocities tested. Figure 4-22a shows the stress profiles measured for saturated (shot 3554) and dry (shot 3555) samples when the impact velocity was 144 m/s. The input stress achieved for dry Salem limestone was 0.64 GPa compared to 0.8 GPa for saturated limestone. The loadings at the 5 and 10-mm-depths coincide until yielding of the dry samples begins at about 0.15 GPa. This response is also seen in the comparisons of higher impact velocity experiments in Figures 4-23a, 4-24a, and 4-25a. A common feature of all dry sample data is a 0.1 - 0.2 μ s wide overshoot on gauge-1. This was due to glue soaking about 0.2 mm into the surface of the porous, dry samples. The equilibrium stress achieved in the dry rock is consistently lower than in the saturated rock by about 0.4 GPa at impacts of 0.3 km/s and above. The dry samples began shocking up after compaction at about 0.45 GPa, whereas the saturated sample loading consists of a near linear ramp up to about 0.45 GPa where shocking up begins (Figures 4-24a and 4-25a).

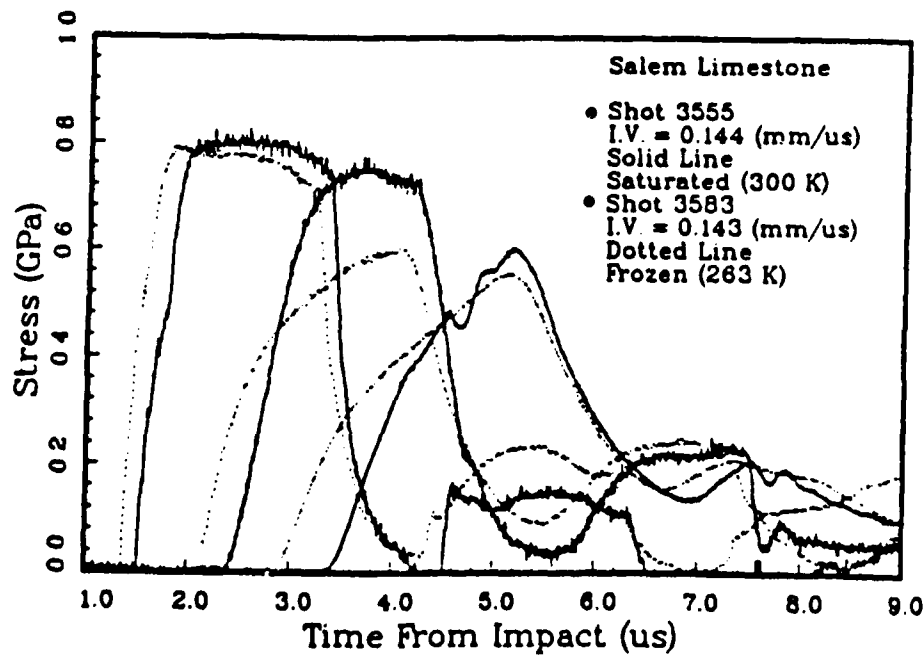
The difference between data from ambient saturated and frozen samples is less distinct, yet some important conclusions can be made. The most significant differences are below 1.0 GPa. Figure 4-22b is a comparison of saturated and frozen data generated at a 0.14 km/s impact velocity. The input stress achieved was 0.8 GPa for both samples but differences in wave velocities are seen in the transmitted waves at the 4 and 8-mm-depths. These differences are also apparent in data at higher pressures as shown in Figures 4-23b, 4-24b, and 4-25b. Below 0.6 to 0.8 GPa, the ramped loading wave velocity is faster in the frozen sample than in the ambient are due to the greater stiffness of ice compared to water.

In the frozen targets, the ramped precursor continues linearly up to the input stress of 1.5 GPa (Figure 4-23b). The linear ramp ends and shock-up begins at about 1 GPa for a stress of 2.5 GPa (Figure 4-24b) and sooner at higher stresses (Figures 4-24b, 4-25b, and 4-26b) as the main wave begins to overtake the precursor. The ambient sample, in contrast, begins shocking up earlier as a result of the faster main wave which is due to greater density of water than ice (Figure 4-24b).

The main wave velocity in the frozen sample is slower than the ambient between 1 and 4 GPa; however, at 5 GPa (Figure 4-26) the main wave velocities are nearly identical as are the overall stress wave profiles.

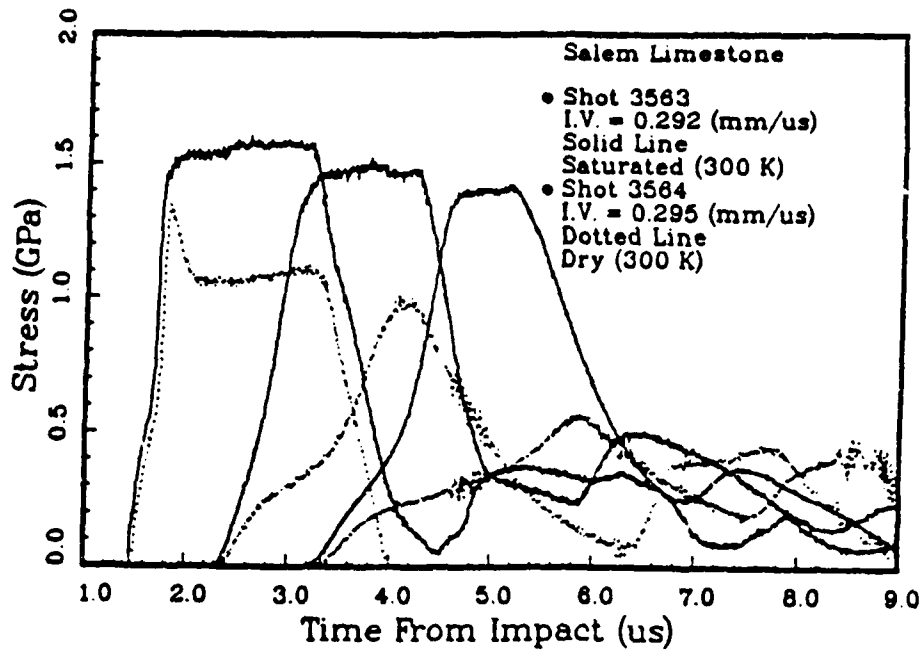


a. Shot 3555 (saturated) and 3554 (dry) comparison.

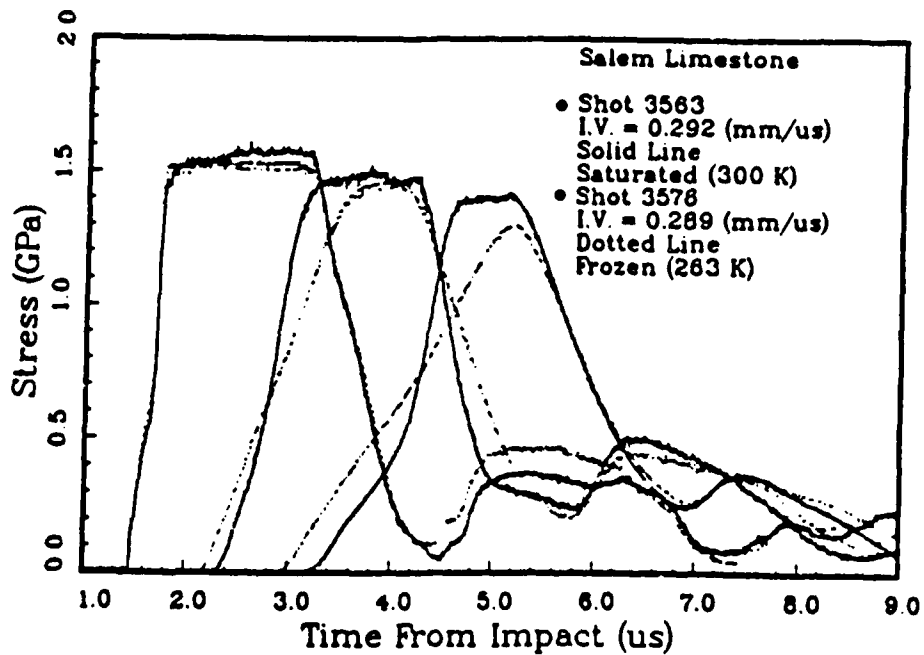


b. Shot 3555 (saturated) and 3583 (frozen) comparison.

Figure 4-22. Comparison of the response of dry, saturated, and frozen Salem limestone at a nominal impact velocity of 0.14 km/s.

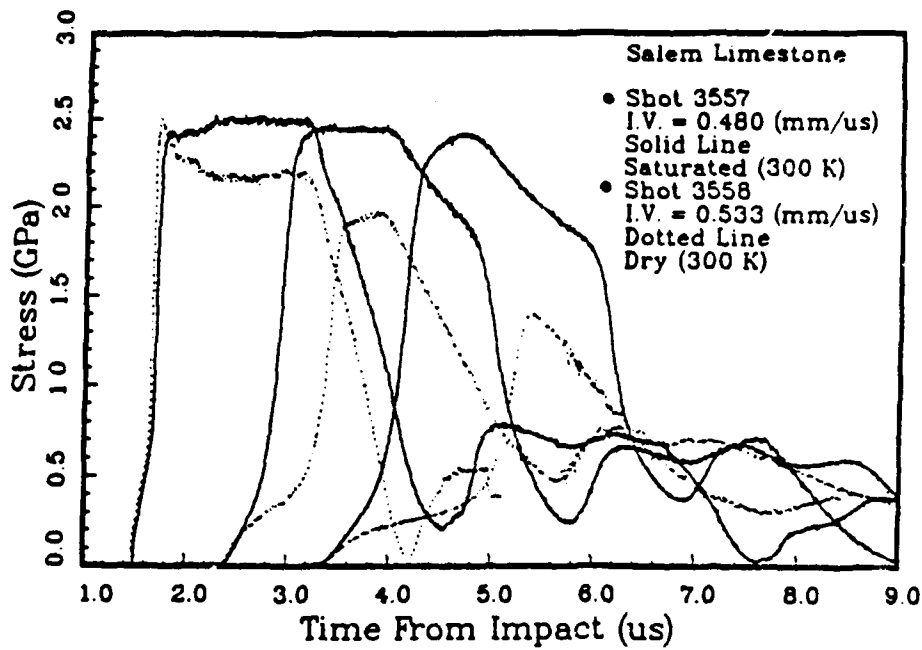


a. Shot 3563 (saturated) and 3564 (dry) comparison.

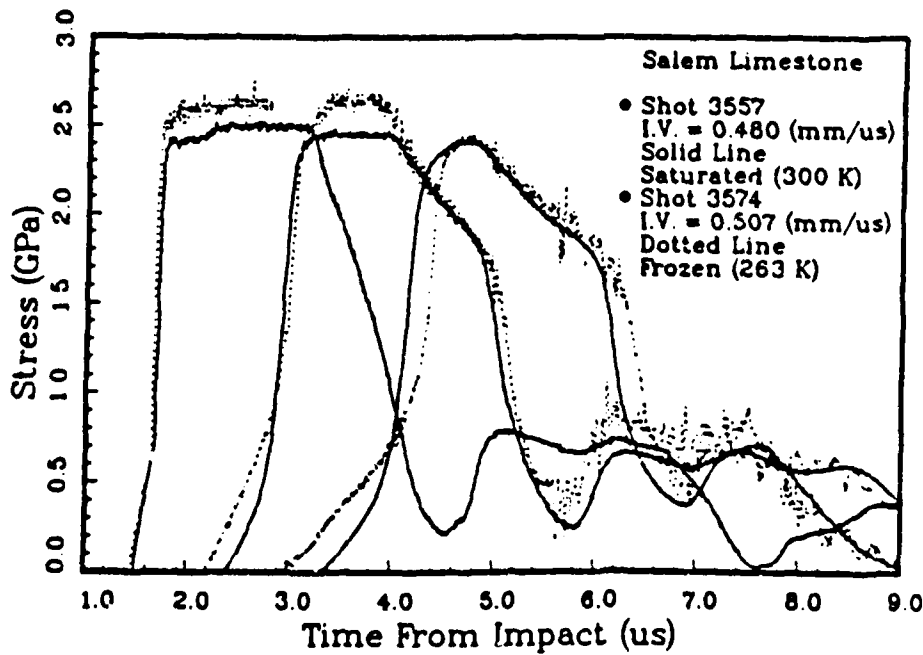


b. Shot 3563 (saturated) and 3576 (frozen) comparison.

Figure 4-23. Comparison of the response of dry, saturated, and frozen Salem limestone at a nominal impact velocity of 0.29 km/s.

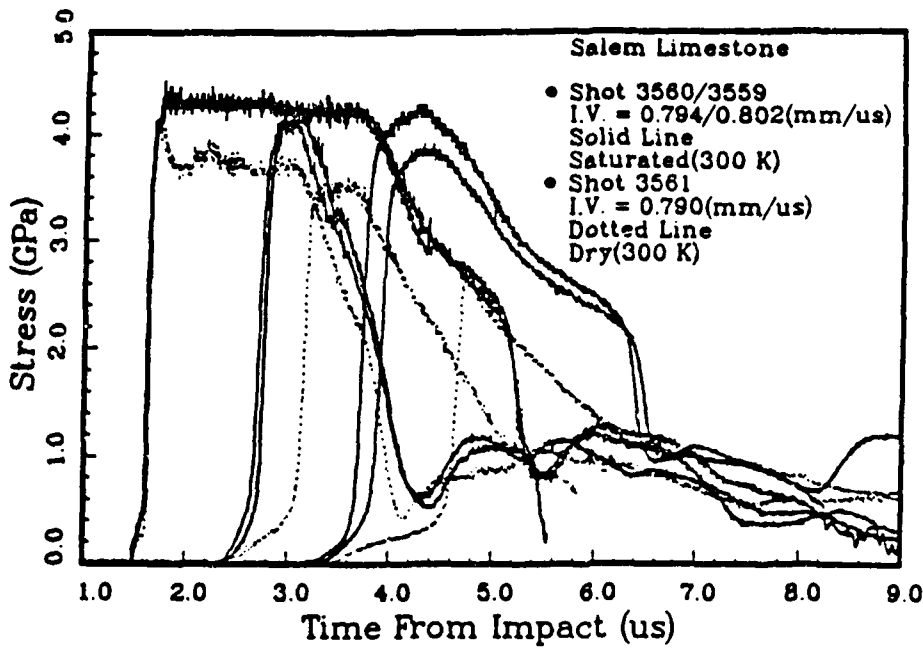


a. Shot 3557 (saturated) and 3558 (dry) comparison.

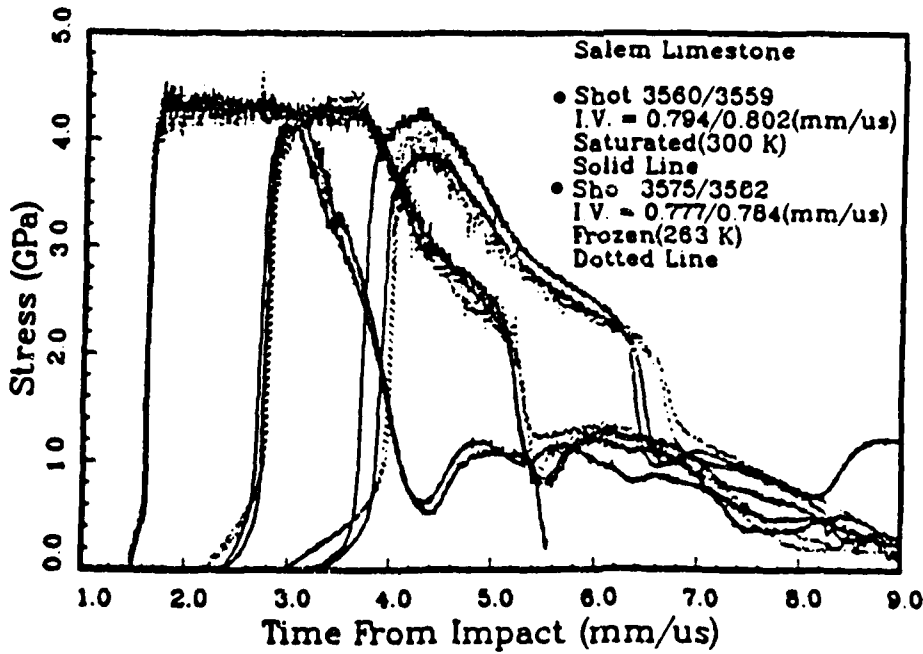


b. Shot 3557 (saturated) and 3574 (frozen) comparison.

Figure 4-24. Comparison of the response of dry, saturated, and frozen Salem limestone at a nominal impact velocity of 0.5 km/s.



a. Shots 3559 and 3560 (saturated) and 3561 (dry) comparison.



b. Shots 3559 and 3560 (saturated) and shots 3575 and 3582 (frozen) comparison.

Figure 4-25. Comparison of the response of dry, saturated, and frozen Salem limestone at a nominal impact velocity of 0.79 km/s.

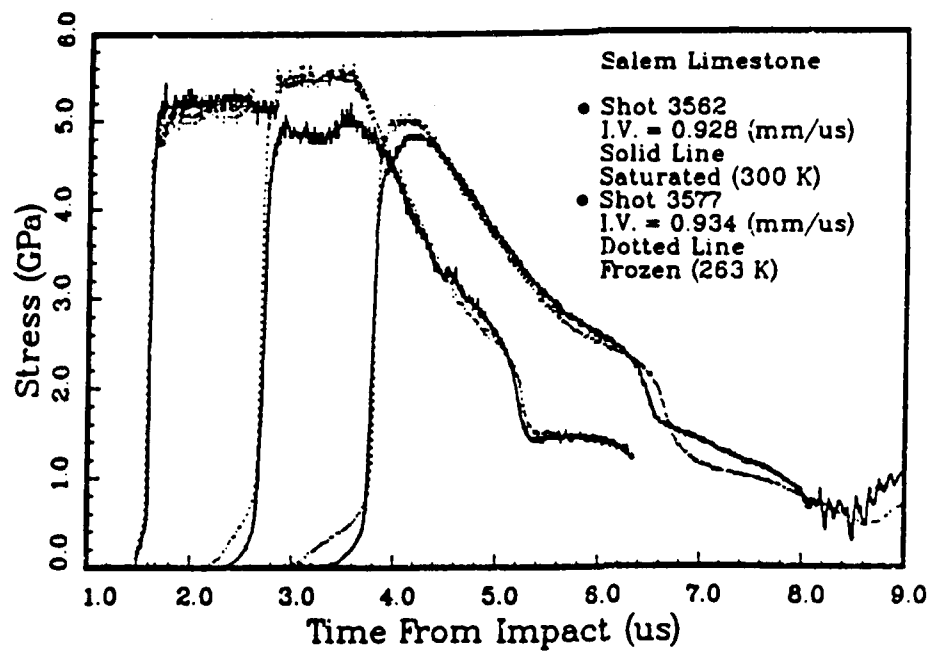


Figure 4-26. Shot 3562 (saturated) and 3577 (frozen) comparison.

SECTION 5

EXPERIMENTAL RESULTS FOR ICE

Measurements were conducted in ice at stresses ranging from 0.7 to 3.0 GPa. Hugoniot data and loading and relief paths are presented in this section together with a shot configuration table showing details of impactor, buffer, and sample material thicknesses. All recorded waveforms are illustrated and are also available from the DNA HYDROPLUS data archive on the DNA CRAY storage system at Los Alamos National Laboratory.

5.1 RESULTS.

Four (4) experiments were conducted with ice. Table 5-1 contains shot configuration details of impactor, buffer, and sample thicknesses. The results are summarized in Table 5-2. Hugoniot data were obtained by both impedance matching and Lagrangian analysis. The Hugoniot elastic limit data was obtained by Lagrangian analysis. The unloading state was determined from the first release plateau on gauge-1 by impedance matching.

The results in Table 5-2 from the four shots on ice are presented in graphical form in Figures 5-1 through 5-3. Also included in these figures are results of several previous investigations of shockwaves in ice from a compilation for a NATO Workshop in 1984 (Gaffney, 1985). Figure 5-1 shows the data in stress-particle velocity space. Lagrangian loading and release paths, and impedance-match Hugoniot and unloading states are shown. Stress-density data for ice are compared in Figure 5-2 with static high-pressure data for five phases of ice (Gagnon, 1987). These static data, plotted as squares, are for Ice III, Ice II, Ice V, and Ice VI, from left to right, respectively. Other than for Ice I, there is no clear correspondence between the static data and our own. Figure 5-3 presents the data in terms of shock velocity and particle velocity.

The stress histories for each of the four shots are presented in Figures 5-4 through 5-7. Figure 5-8 shows the measured data for gauges 1 and 2 from shot 3538 along with the fits to that data used in the Lagrangian analysis. For shot 3538, both the first and second gauges provided flat-topped records, so the Lagrangian analysis could be carried to the Hugoniot state for comparison with the impedance match solution. For the other shots, only the first gauge recorded a flat top. For shot

Table 5-1. Ice shot configuration data.

Shot No.	Thickness (mm)					
	6061-T6 Impact Thick	6061-T6 Buffer Thick	Sample 1 Thickness	Sample 2 Thickness	Sample 3 Thickness	Sample 4 Thickness
3539	7.52	9.58	5.06	4.90	4.90	10.19
3536	7.48	9.40	5.39	4.76	5.13	10.04
3538	7.46	9.62	5.04	4.81	4.77	10.26
3540	7.41	9.57	4.91	5.19	5.25	10.27

Table 5-2. Ice equation of state data.

Shot Number	Impact Velocity (km/s)	Hugoniot Data				
		Initial Density (g/cc)	Stress (GPa)	U_p (1/2 amp.) (km/s)	u_p (km/s)	ρ (g/cc)
<u>Lagrangian Hugoniot elastic limit state</u>						
3539	0.427	0.92	0.050	3.37	0.0170	0.925
3536	0.561	0.92	0.105	3.74	0.0288	0.927
3538	0.797	0.92	0.112	3.52	0.0337	0.929
<u>Impedance match Hugoniot data</u>						
3539	0.427	0.92	0.678 ± .003	1.94	0.380	1.144
3536	0.561	0.92	1.01 ± .05	2.24	0.491	1.179
3538	0.797	0.92	1.51 ± .09	2.37	0.693	1.300
3540	1.297	0.92	2.92 ± .14	2.93	1.083	1.459
<u>Lagrangian analysis peak stress state</u>						
3538	0.797	0.92	1.50	2.14	0.718 ± .001	1.366 ± .010
<u>Impedance match unloading state</u>						
3539			0.42		0.315	
3536			0.63		0.390	
3538			0.92		0.537	
3540			2.00		0.761	

Configuration: 6061-T6 → 6061-T6/cg/ice/cg/ice/cg/ice/cg/ice

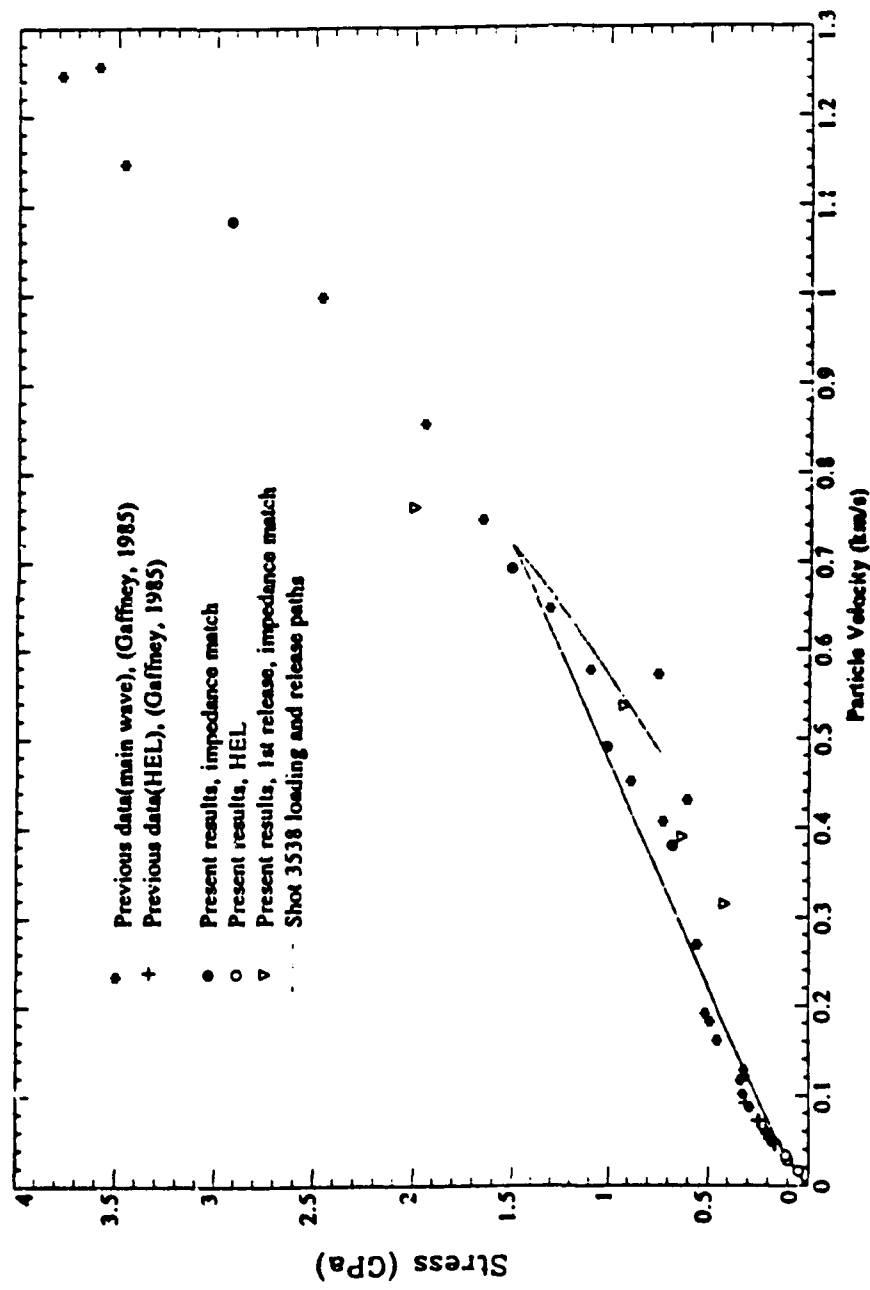


Figure 5-1. Ice stress-particle velocity Hugoniot EOS data with loading and release paths.

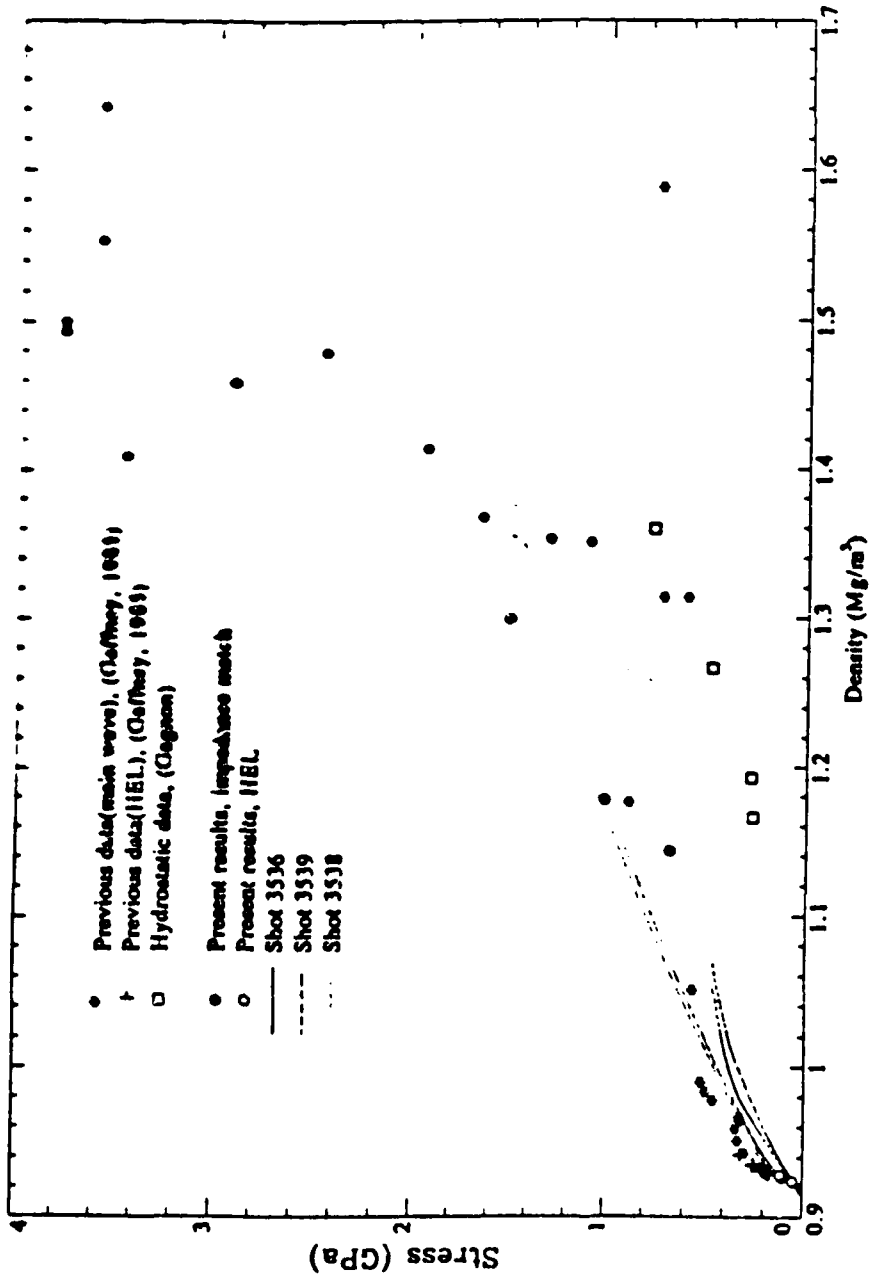


Figure 5-2. Ice stress-density Hugoniot EOS data with loading and release paths.

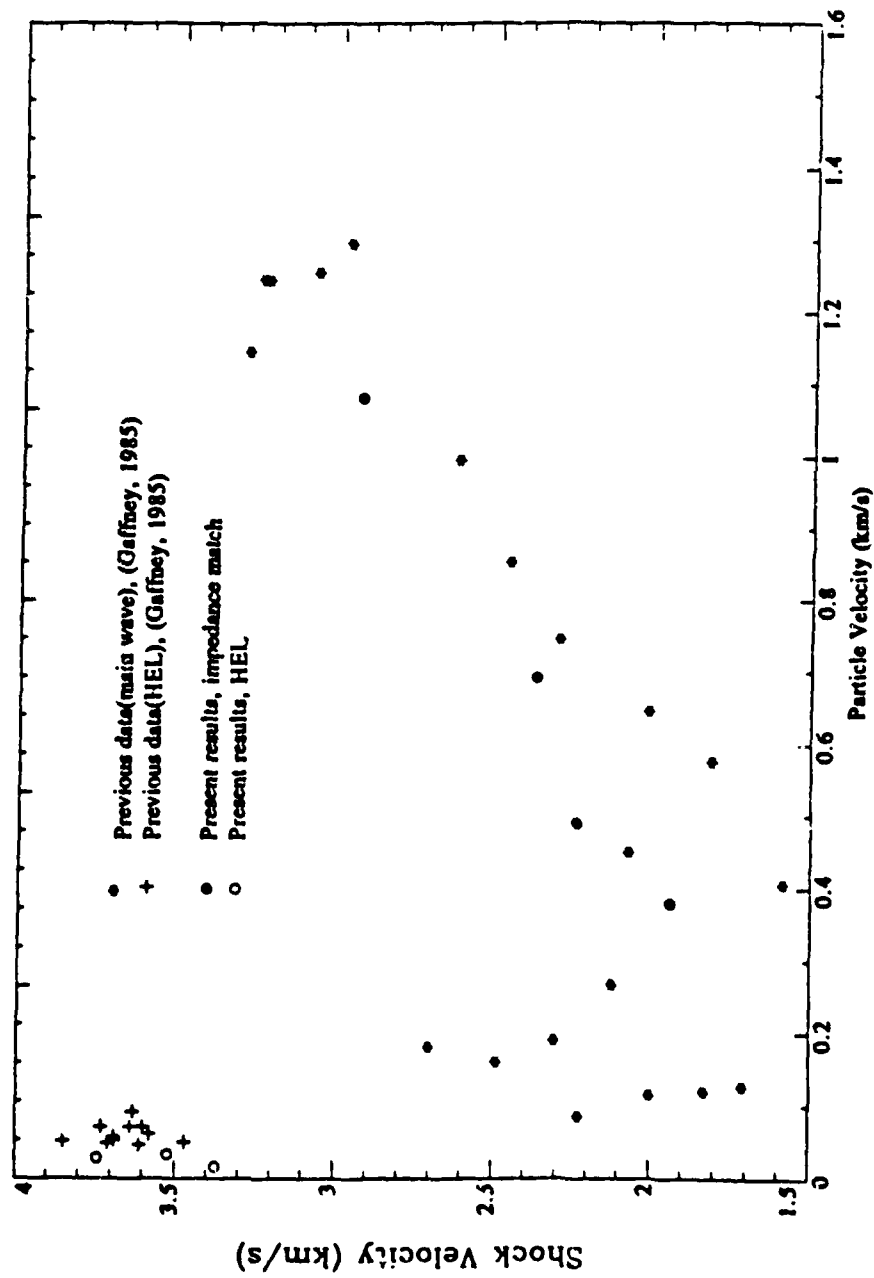


Figure 5-3. Ice shock velocity-particle velocity Hugoniot EOS data.

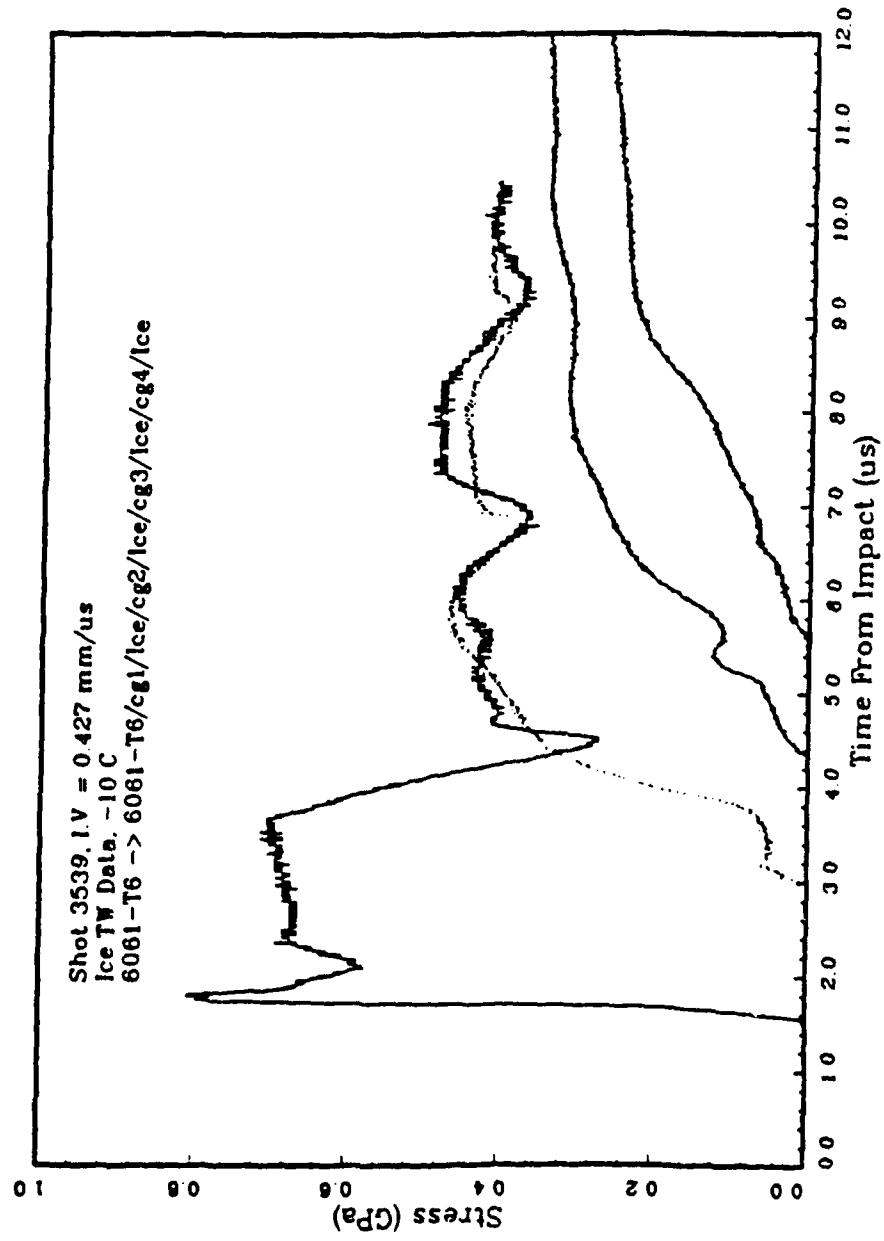


Figure 5-4. Shot 3539, stress-time data.

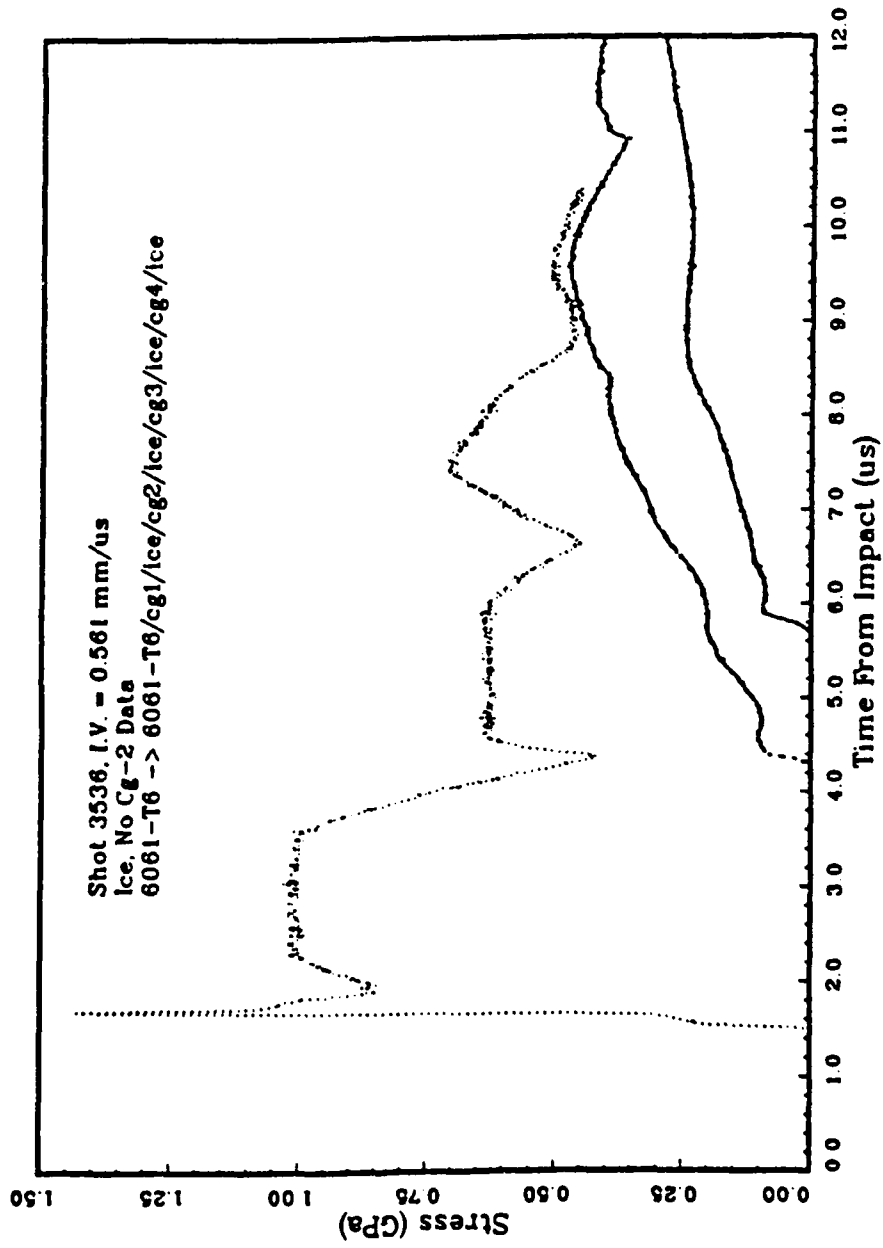


Figure 5-5. Shot 3536, stress-time data.

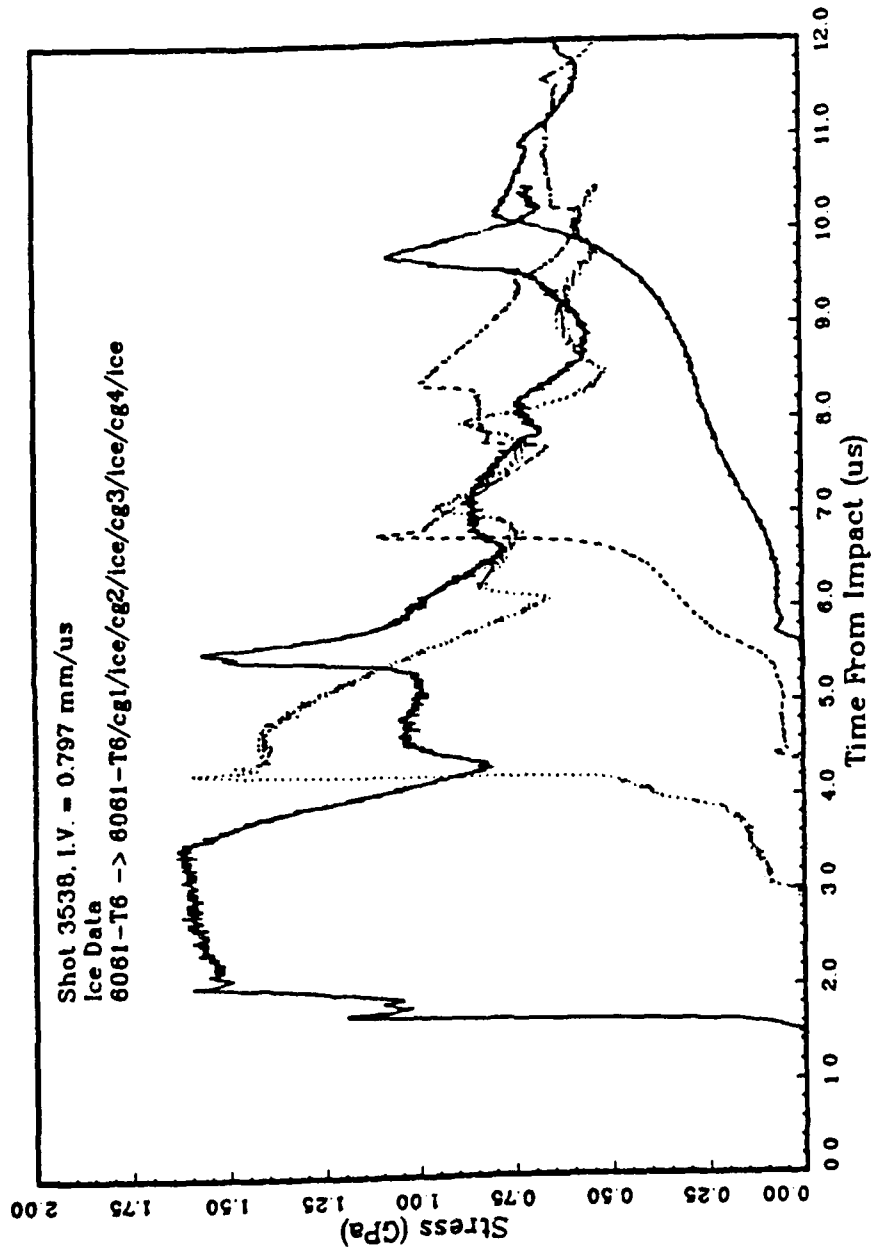


Figure 5-6. Shot 3538, stress-time data.

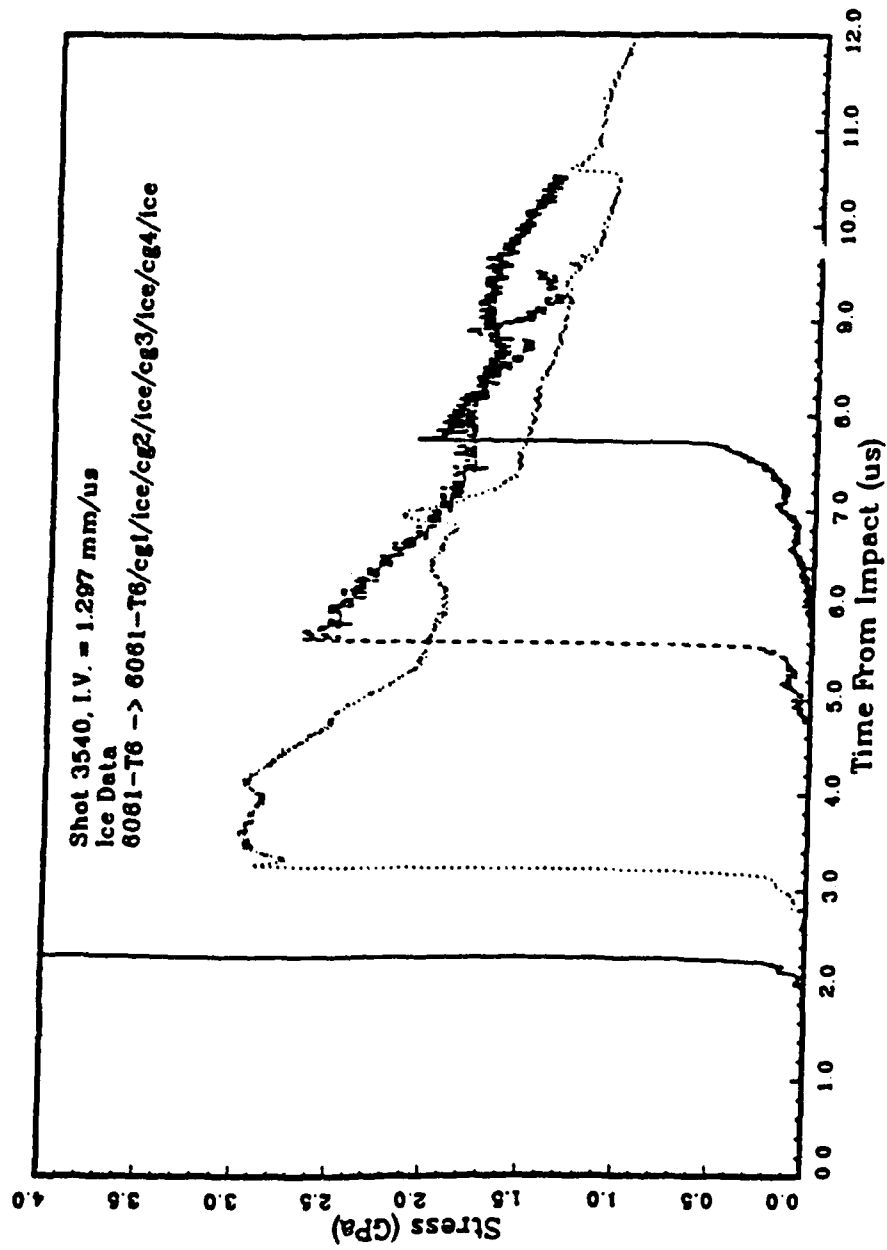


Figure 5-7. Shot 3540, stress-time data.

Shot 3538

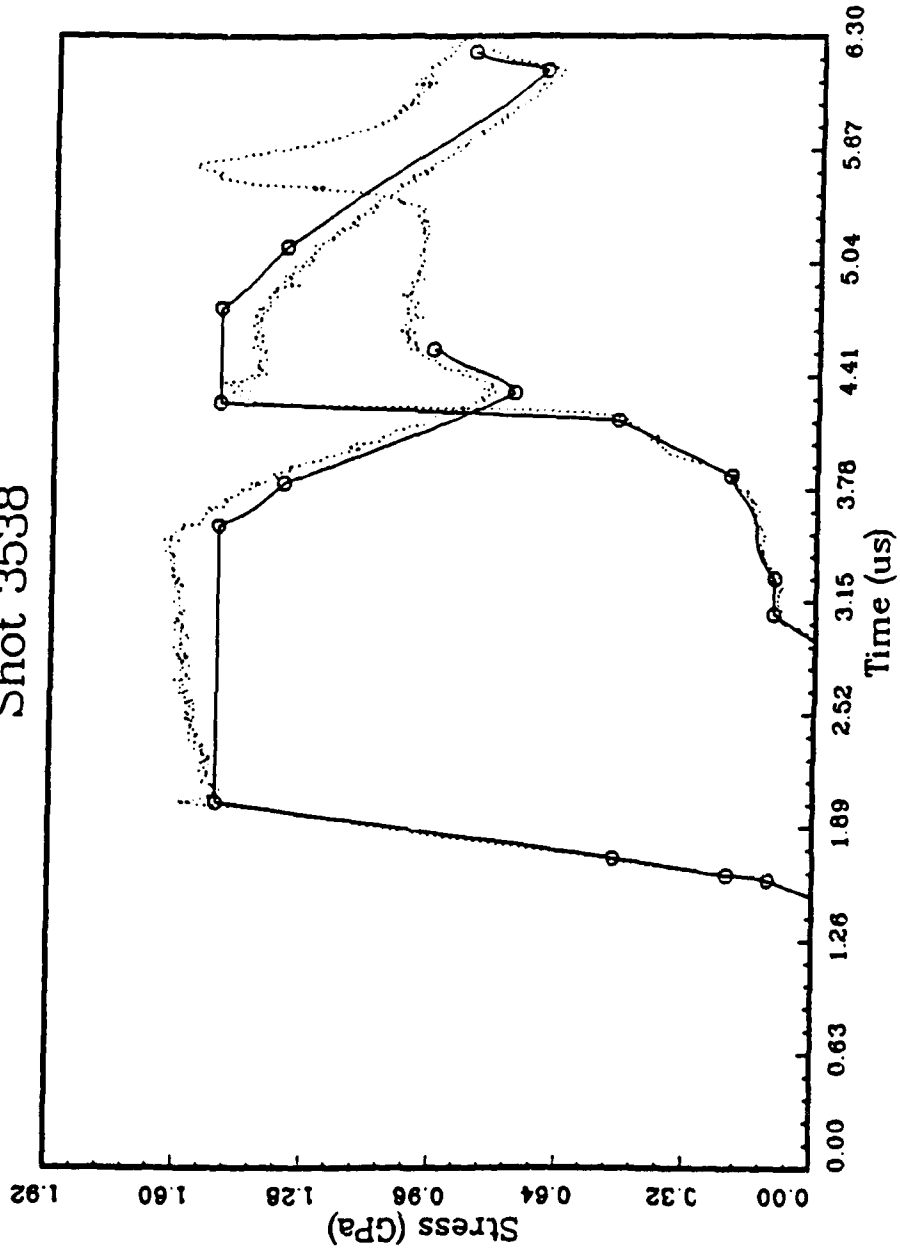


Figure 5-8. Stress histories (dotted line) and lagrangian code input (solid line) for gauges #1 and #2 on shot 3538.

3539, the Lagrangian analysis was conducted for the first and second gauges only up to the peak of the (attenuated) second gauge record. Although the results should be valid loading paths, they can not be compared directly to the impedance-match solutions because the same stress levels were not achieved.

5.2 DISCUSSION.

Shot 3538 provided good loading and partial unloading paths for ice to 1.5 GPa, and the peak state is consistent with the impedance-match Hugoniot point. Note that the two should not agree exactly because the Hugoniot point is derived from the state of stress at the interface which is achieved in a single (nearly instantaneous) compression step, whereas the Lagrangian analysis included the data from the second gauge which had a very pronounced precursor. These data are in good agreement with Larson's data (Gaffney, 1985) at 1.27 GPa and 1.62 GPa. The unloading data from this shot is also in good agreement for both Lagrangian and impedance-match analyses (see Figure 5-1).

The data from shot 3540 at about 3 GPa are consistent with the previous three results between 1.5 GPa and 3 GPa. The data over this range were obtained by three different experimental teams (including the present one) and utilized three different methods. The fact that the four data points define a fairly smooth curve lends credence to all of the results. Nevertheless, the fact that a good record was not obtained from gauge-1 in shot 3540 is disappointing since no unloading path could be derived. A Lagrangian analysis was attempted up to the peaks of the other three gauges, but the results are not consistent with the impedance-match solution, with the previous data, or with the known high-pressure properties of ice or water. The apparent shock velocity in the three records (about 2 km/s) is much too low. The reason for this anomalous result is not known.

The other two shots, 3539 and 3536, lie in a region where the previous results showed considerable scatter. Referring to Figure 5-2, the previous data between 0.55 GPa and 1.3 GPa fall into two distinct groups - one with a density between 1.1 to 1.2 g/cc and the others with densities between 1.3 and 1.4 g/cc. Our current data seem to favor the former group. The lack of information on the loading and unloading paths is again disappointing.

Although it was not discussed in detail above, it can be inferred by comparing the gauge records (Figures 5-4 through 5-7) with the Hugoniot elastic limit states in Figure 5-2 that much lower precursors were seen in this study than were seen in previous investigations. This is thought to be due to the quality of the ice studied. All the previous studies except Gaffney and Ahrens (1980) used ice samples prepared by the U.S. Army Cold Regions Research and Engineering Laboratories (CRREL) who have decades of experience in preparation of pure ice. Although our samples were frozen from distilled, de-aired water, some residual impurities or contamination could be present. This would be most apparent in the strength of the ice.

In conclusion, data for shocks in ice were reported from four experiments with peak stresses ranging from 0.7 GPa to 2.9 GPa. These results, when combined with the previously available data, provide a good definition of the Hugoniot of ice from 1.5 GPa to 3 GPa. As with previous investigations, the results between 0.7 GPa and 1.3 GPa are less satisfying. Good flat-topped records were not obtained on either shot in this stress range; therefore, good Lagrangian loading and unloading paths could not be derived. Such data probably would have assisted the interpretation of the test data in this region.

SECTION 6

EXPERIMENTAL RESULTS FOR JOINT EXPERIMENTS

An important consideration in the studies of shock wave propagation in porous frozen rocks is that real rocks are not continuous, but rather are masses of heterogeneous material separated by fractures which may be open. Alternatively, these fractures or joints may be filled with water or ice and/or other materials. All these alternatives result in a joint with an acoustic impedance much less than that of the rock. Consequently, the propagation of shocks across joints will modify the stress wave shape and amplitude. At pressures below 0.2 GPa, an ice-filled joint is expected to have less affect than a water-filled one because the impedance of ice is greater than water. But at higher pressures, the situation is reversed, and the ice-filled joint should have a greater affect than a water-filled one. In order to evaluate the effect of freezing on wave propagation in rock joints filled with ice or water, shock propagation experiments were conducted at ambient and -7°C temperatures on jointed, saturated samples made with multiple Danby marble samples separated by 1-mm gaps.

The experimental configurations for these joint samples are summarized in Table 6-1. High-impedance tungsten carbide (WC) and 4340 steel impactors were used in these experiments. Table 6-2 contains target material thicknesses and densities. Note that the material thickness may differ from those presented in Table 3-1 due to the lapping processes that were necessary to obtain adequately flat samples. The tests were conducted with incident stress amplitudes of 1.25 GPa and

Table 6-1. Danby marble joint experiment shot configuration summary.

Shot No.	Conf.°	Impactor			Target Temperature (°C)
		Velocity (mm/μs)	Material	Thickness (mm)	
3470	a	0.096	4340	3.19	Ambient
3471	a	0.509	WC	4.78	Ambient
3473	b	0.515	WC	4.77	Ambient
3474	a	0.096	4340	3.11	-7
3475	a	0.497	WC	4.78	-7
3476	b	0.507	WC	4.78	-7

Configuration:

a) Impactor → 6061-T6 /CG/Sample/ H₂O /CG/Sample/CG/Sample
 (9.35mm) (5mm) (1mm) (5mm) (10mm)

b) Impactor → 6061-T6/CG/Sample/H₂O/CG/Sample/H₂O/CG/Sample/H₂O/CG/Sample
 (9.35mm) (5mm) (1mm) (5mm) (1mm) (5mm) (1mm) (10mm)

Note: Fracture experiments were conducted to provide wave profiles to support modeling efforts. Lagrangian analysis was not done due to the alternate layers of rock and H₂O.

Table 6-2. Danby marble joint experiment target configuration data.

Shot No.	6061-T6 Buffer Thick	Thickness (mm) and Density (g/cc)														
		Sample 1			Sample 2			Sample 3			Sample 4					
		No.	Thick	ρ_s	Joint 1 Thick	No.	Thick	ρ_s	Joint 2 Thick	No.	Thick	ρ_s	Joint 3 Thick	No.	Thick	ρ_s
3470	9.354	DM-26	5.00	2.69	1.06	DM-25	5.00	2.70	--	DM-29	9.00	2.70	--	--	--	--
3471	9.420	DM-22	5.00	2.69	1.00	DM-23	5.00	2.69	--	DM-31	9.00	2.70	--	--	--	--
3473	9.397	DM-18	5.00	2.69	1.14	DM-17	5.01	2.70	1.24	DM-20	4.99	2.69	1.14	DM-33	8.99	2.70
3474	9.419	DM-19	5.01	2.69	1.34	DM-21	5.00	2.69	--	DM-32	9.00	2.70	--	--	--	--
3475	9.456	DM-15	5.01	2.69	1.00	DM-16	5.01	2.70	--	DM-34	9.00	2.70	--	--	--	--
3476	9.394	DM-13	4.99	2.69	1.32	DM-12	5.00	2.69	1.05	DM-11	4.99	2.69	1.06	DM-35	9.01	2.70

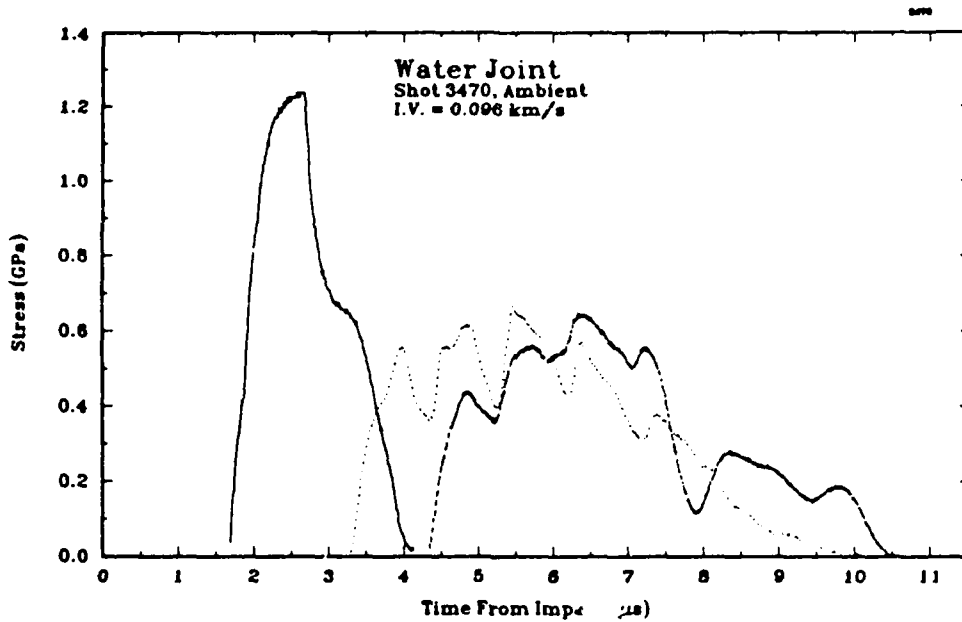
6 GPa. The same incident stress levels were used for water-filled joints and ice-filled joints in Danby marble. For 6 GPa incident shocks, both single-joint and triple-joint configurations were used.

Several observations were made based on the recorded stress histories shown in Figures 6-1, 6-2 and 6-3. The effect of a water-filled joint is very different at 6 GPa than at 1 GPa. Figure 6-2a illustrates the effect of a water-filled gap for an incident stress of about 6 GPa. These measured stress profiles should be compared to those measured for competent Danby marble (Figure 4-4b). The differences upon loading are not great, but unloading begins earlier for the jointed rock so that the impulse is lower. The precursor is suppressed in transit across the joint, but it quickly rebuilds to almost the same shape as in the rock with no gap.

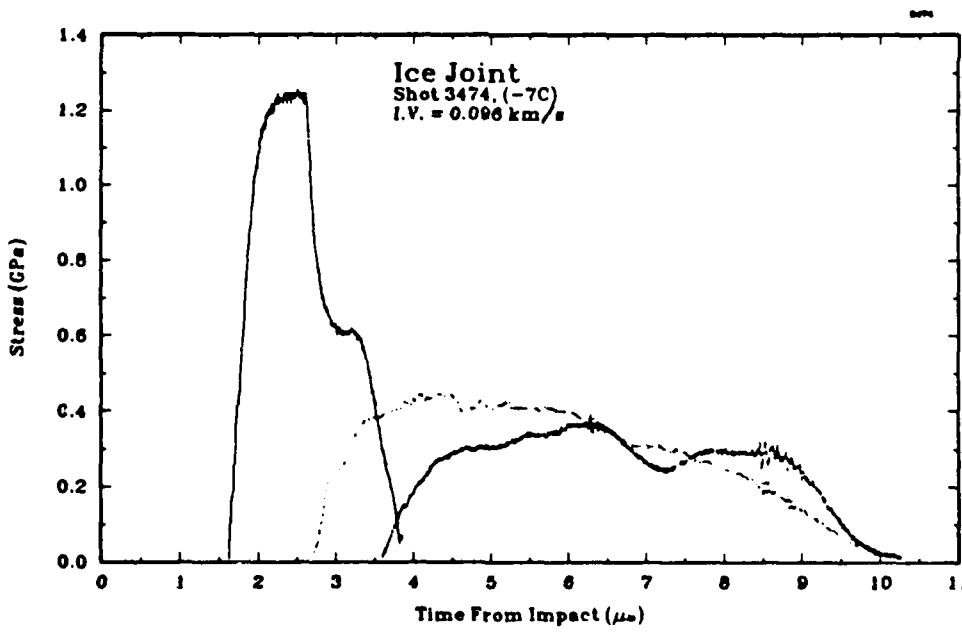
At lower stress the effect of the joint is greater. In the room temperature experiment, Figure 6-1a), the 1.25 GPa incident state is reduced to about 0.5 GPa (40 percent) and lengthened from about 2.5 μ s duration to about 6 μ s. The pressure in the joint oscillates by about ± 0.1 GPa for 3 μ s. When the frozen situation is compared to the water-filled one in Figure 6-1b, the wave transmitted through the ice is observed to attenuate faster.

The results of the high-pressure, triple-joint tests shown in Figure 6-3 are similar to those of the single-joint tests except that all the effects are more pronounced. The 6 GPa incident pulse is attenuated to about 70 percent of its initial value after traveling through 15 mm of marble and two 1-mm-thick water-filled joints. The same impact conditions with frozen joints results in the stress wave being attenuated to about 50 percent of its initial value. The lower transmitted amplitude can be attributed to the very high compressibility of ice. This high compressibility of ice is due to phase changes in the ice (solid-solid or melting). The pronounced precursor is also due to those phase changes.

At the lower stress (Figure 6-1), the effect of ice filling the joint is even more marked than for water. With ice-filled joints the transmitted stress is reduced to about 0.4 GPa (32 percent of its initial value), and the pulse length is even longer than observed with the water-filled joint. The oscillations on top of the transmitted wave seen in the water/joint experiment are almost completely absent in the ice joint experiment. As at higher pressures, the lower transmitted amplitude for frozen joints can be attributed to the very high compressibility of ice. The lack of oscillations may be due to damping associated with the phase changes. The increase in duration may be more apparent than real, i.e., a result of edge effects.

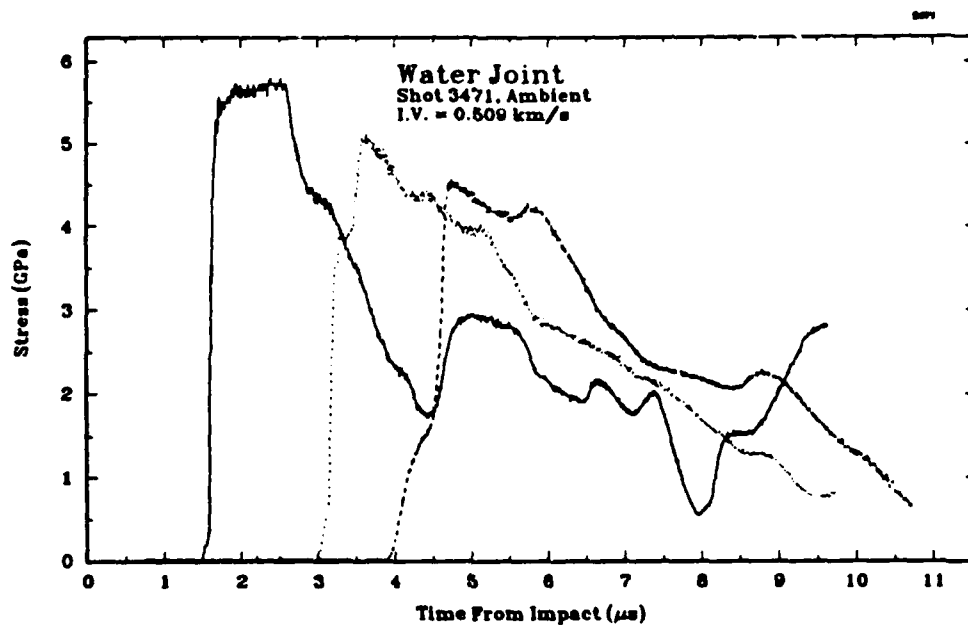


(a) Shot 3470, water joints.

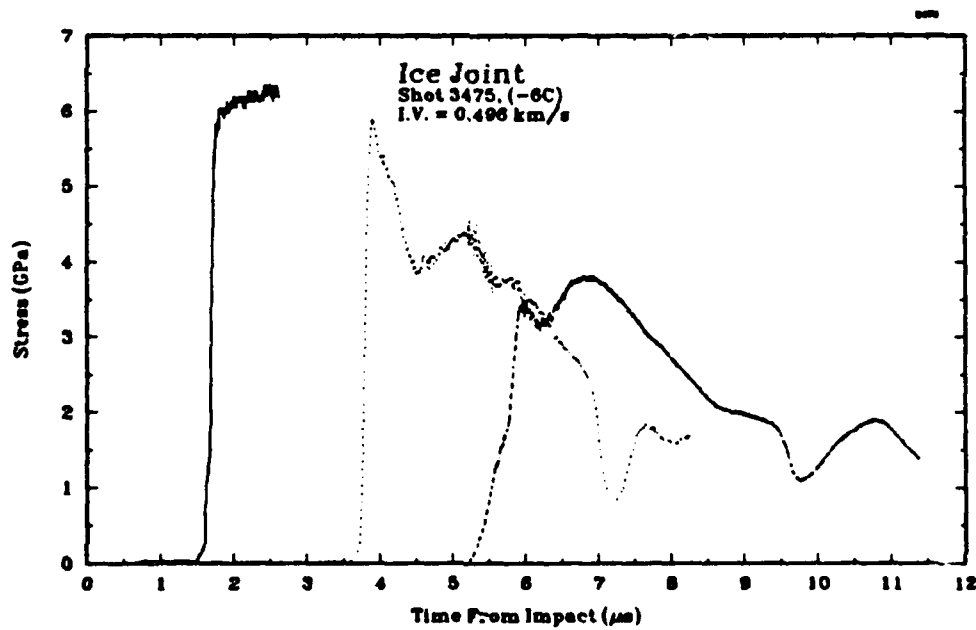


(b) Shot 3474, ice joints.

Figure 6-1. Stress wave profiles transmitted through single-jointed samples for 1.2 GPa input stress.

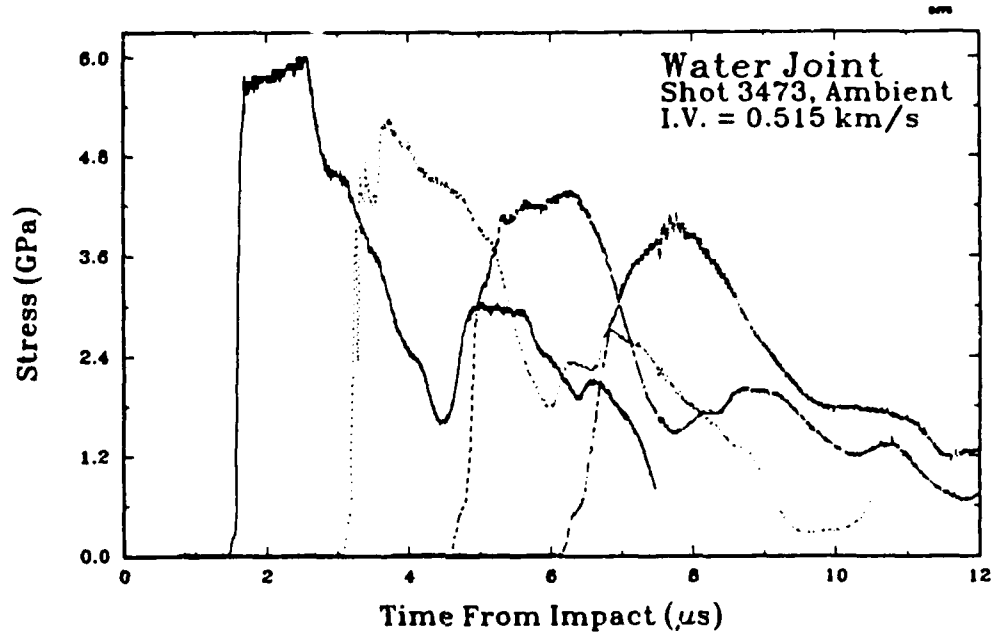


(a) Shot 3471, water joint.

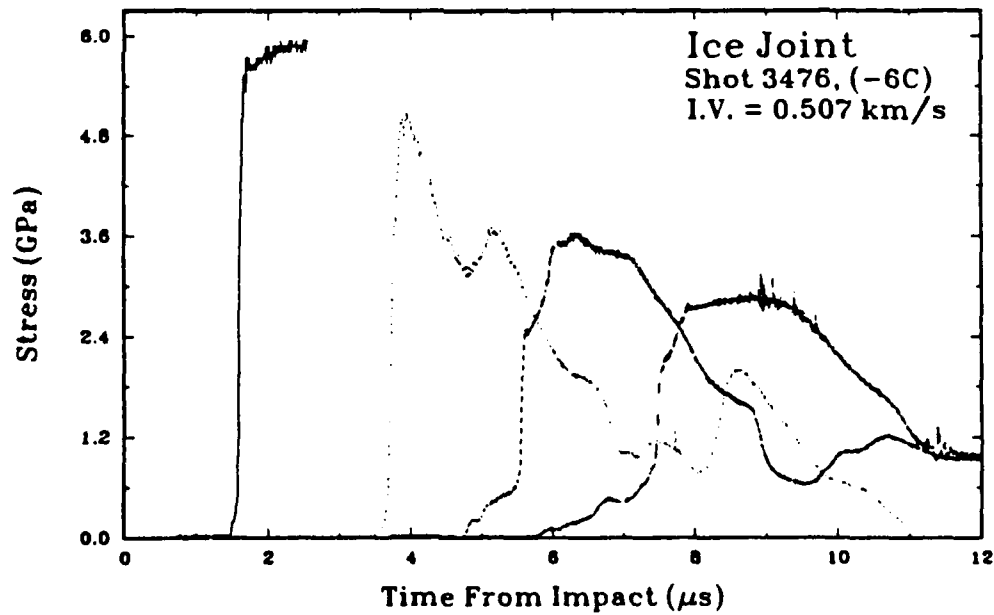


(b) Shot 3475, ice joints.

Figure 6-2. Stress wave profiles transmitted through single-jointed samples for 6 GPa input stress.



(a) Shot 3473, water joints.



(b) Shot 3476, ice joints.

Figure 6-3. Stress wave profiles transmitted through triple-jointed samples for 6 GPa input stress.

In summary, at low stresses (1 GPa) ice-filled joints result in about 30 percent greater attenuation than do water-filled joints. Even water-filled joints caused 60 percent attenuation of the peak stresses in these tests. At 6 GPa, water-filled joints are seen to have little effect, while ice-filled joints show 30 percent more attenuation than was observed in non-jointed Danby marble; but the rate of attenuation is diminished relative to 1 GPa because the same increase in attenuation is observed for three joints at 6 GPa as was noted for one joint at 1 GPa.

SECTION 7 CONCLUSIONS

Fifty-nine gas gun tests were conducted on 8 materials and 2 special target configurations to measure dynamic material properties required to support DNA's HYDROPLUS yield verification program. Equation of state data were obtained for 4 categories of materials: ice; MJ-2 (NSF-6) grout (a DISTANT ZENITH tuff-matching grout); DISTANT ZENITH tuff; HUNTERS TROPHY tuff; and 3 carbonate rocks: Danby marble, Ft. Knox carbonates, and Salem limestone. All of the rocks and the grout were tested in a water-saturated condition at ambient conditions. The Ft. Knox carbonates and the Salem limestone were also tested frozen. Only Salem limestone was tested dry.

The data presented here are sufficient to demonstrate that there is a significant difference between the Hugoniot of tuff from two sites at NTS even though the densities and ultrasonic speeds are virtually identical. Shock velocities in DISTANT ZENITH tuff are about 10 percent higher than they are in HUNTERS TROPHY tuff. The Hugoniots of DISTANT ZENITH and the MJ-2 (NSF-6) grout are close, even though the acoustic impedances differ by 30 percent. MJ-2 (NSF-6) grout has about a 10 percent greater impedance than DISTANT ZENITH tuff in the 4 to 10 GPa stress range. Clearly, for these materials acoustic impedances based on ultrasonic velocities should not be used to approximate the Hugoniot properties in the stress range of 1.5 to 12 GPa.

Four carbonate rocks were characterized: Danby marble from Proctor, VT; Louisville formation dolomitized limestone and Jeffersonville formation calcite limestone from Ft. Knox, KY; and Salem limestone from Bedford, IN. This set of data allows the effects of porosity, saturation, dolomitization, and temperature to be evaluated.

The Ft. Knox limestone had a porosity of only 1 to 2 percent while the Salem limestone had a 16 percent porosity. The dry Salem limestone showed classic porous material behavior at low stresses: (1) a 0.35 GPa precursor, resulting from cementation breakdown and particle crush-up, and (2) severe attenuation due to the leading edge of the rarefaction fan traveling at a higher velocity than the compressive wave.

The effects of saturation were dramatic for the high-porosity Salem limestone. While the precursor amplitude was approximately the same, the precursor velocity increased in the saturated materials (both water and ice) and the propagated wave forms shocked up earlier. These observed features of the measured stress profiles are consistent with the water- or ice-filled pores being less

compressible than the air-filled pores. However, the skeleton structure still fails compressively at about the same pressure.

Differences in the response of saturated Salem limestone at ambient temperature and -7°C were noted up to about 1.5 GPa; the effect was negligible above about 4.0 GPa. The precursors for the saturated and frozen samples had measured velocities of 4.23 and 5.03 km/s, respectively. Below 0.7 GPa higher wave speeds were measured in the frozen samples compared to those at ambient temperature. This is consistent with the higher wave speed of ice (~ 4 km/s) relative to water (~ 1.5 km/s). However, above 0.7 GPa the situation is reversed and the frozen sample wavespeeds are lower.

Two inflections at 2.5 and 1.7 GPa were noted in the unloading curves for both the water and ice saturated Salem limestones. This concave downward loading path results in a decompression shock front. The absence of this feature in the dry limestones suggests that this is a phase change involving or facilitated by water.

For Ft. Knox limestone (Jeffersonville formation) with only 1 to 2 percent porosity, there was little effect of freezing on the measured material properties above about 2 GPa. In the stress regime of 1.5 to 2 GPa, this frozen limestone was more attenuative than its ambient temperature counterparts.

The Danby marble, and the Jeffersonville formation limestone, all showed the development of a pronounced precursor with an amplitude of 1.2 GPa which was caused by the phase transition



The pronounced 1.2 GPa precursor was not observed in the Louisville formation dolomite limestone. This material is a higher impedance material than the Jefferson formation calcite limestones. Both materials are attenuative due to their high initial unloading wavespeeds.

EOS data for ice was obtained in the 0.5 to 3.0 GPa stress range. This data agrees well with previous data although the combined data set contains considerable scatter between 0.7 and 1.5 GPa. Ice compresses to densities of about 1.35 g/cc when shocked to 1.5 GPa. Unloading from this state trends toward the density of ices II and III, although the apparent modulus is too low for any of the high pressure phases. Further work will be required to determine the material response of ice below 1 GPa.

The studies with artificial joints, filled with ice or water, showed that both types of joints would increase the attenuation of stress waves with propagation distance. Water-filled joints severely attenuated the peak stress of shock waves propagating in Danby marble at stresses below 1.3 GPa in our laboratory studies. This indicates that numerous and wide joints could have similar effects on stress waves produced by nuclear explosions. Water-filled joints did not significantly attenuate the peak stress propagated in the marble at stresses near 6 GPa. Ice-filled joints in marble caused even greater attenuation than water at both 1.3 GPa and 6 GPa in our laboratory. The effect is about half as great at 6 GPa as at 1.3 GPa. The attenuation results must not be applied blindly to large-scale field testing because they are expected to be scale dependant. The ratio of the stress pulse width to the shock transit time through the joint is considered a good measure of scale. Our incident pulses were about 1 μ s long followed by a 3-6 μ s gradual or step-wise decrease to zero pressure, and the joint transit time was approximately 0.3 μ s. Thus, the scale parameter is 3. For scaling parameters greater than 3 the effects noted in these experiments are expected to decrease.

SECTION 8
REFERENCES

- Ahrens, T. J. and V. G. Gregson, Jr., Shock compression of crustal rocks: Data for quartz, calcite and feldspar rocks, *J. Geophys. Res.* 69, 4839-4874, 1964.
- Barker, L. M. and Hollenbach, R. E., "Laser Interferometer for Measuring High Velocities of Any Reflecting Surface," *J. Appl. Phys.*, Vol. 43, No. 11, Nov. 1972.
- Barker, L. M. and Hollenbach, R. E., "Shock-Wave Studies of PMMA, Fused Silica and Sapphire," *J. Appl. Phys.*, Vol. 42, No. 10, pp. 4208-4226, Sept. 1970.
- Butcher, B. M. and Cannon, J. R., "Influence of Work Hardening on the Dynamic Stress-Strain Curves of 4340 Steel," *AIAA Journal*, 2, No. 12, Dec. 1964.
- Christman, D. R., et al., Measurements of Dynamic Properties of Materials, Vol. III, 6061-T6 Aluminum, Final Report, Materials and Structures Laboratory, Warren, MI, Nov. 1971.
- Fowles, R. and Williams, R. C., "Plane Stress Wave Propagation in Solids," *J. Appl. Phys.*, Vol. 41, pp. 360-362, 1970.
- Furnish, M. D., "Measuring the Dynamic Compression and Release Behavior of Rocks and Grouts Associated with Hydro-Plus," Sandia National Laboratories, Report No. SAND92-0984, April, 1993.
- Gaffney, E. S., Equation of state of ice and frozen soil, *Lunar. Planet. Sci X*, 416-418, 1979.
- Gaffney, E. S., Hugoniot of water ice, pp. 119-148 in J. Klinger et al. (eds), *Ices in the Solar System*, Reidel, Dordrecht, 1985.
- Gagnon, R. E., H. Kiefte, M. J. Clouter, and E. Whalley, "Acoustic Velocities in Ice Ih, II, III, V, and VI, By Brillouin Spectroscopy," *J. de Physique*, Vol. 48, pp. 29-34, C1-1987.
- Gefken, P. R. and Florence, A. L., "Spherical Wave Experiments With Frozen Limestone," SRI International Technical Report (Draft), Menlo Park, CA, Nov. 1992.
- Grady, D. E., "Experimental Analysis of Spherical Wave Propagation," *J. Geophys. Res.* 78, (8), 1299 (1973).
- Greb, A. and Smith, E.A., Cryogenic Gas Gun Spall Testing, KTECH/TR-90/16, Ktech Corporation, Albuquerque, NM, Oct. 1990.
- Karnes, C. K., Private communications, Sandia National Laboratories, Albuquerque, NM 87185.
- Lee, L. M., Scotten, E. M. and Smith, T. W., Weapons Laboratory material Response Impact Facility Test Programs (June 1984 through June 1989), AFWL-TR-85-31 Vol. 2, Air Force Weapons Laboratory, Kirtland AFB, NM, Sept. 1989.
- Lee, L. M., Jenrette, B. D. and Newcomb, C. G., Carbon Stress Gauge Characterization, AFWL-TR-81-68, Air Force Weapons Laboratory, Kirtland AFB, NM, Aug. 1981.

McQueen, R. G., S. P. Marsh and J. N. Fritz, 1967, Hugoniot equation of state of twelve rocks, J. Geophys. Res. 72 (20), 4999-5036.

Marsh, S. P., LASL Shock Hugoniot Data, University of California Press, Berkeley, CA, 1979.

Seaman, L., "Lagrangian Analysis For Multiple Stress and Velocity Gauge In Attenuating Wave," J. App. Phys., Vol. 45, No. 10, Oct. 1974.

Seaman, L., "Analysis of Dynamic In-Situ Backfill Property Tests: Report 2. An Improved Lagrangian Analysis for Stress and Particle Velocity Gauge Arrays." Technical Report SL-87-11, U.S. Army Engineer Waterways Experiment Station, Vicksburg MS, 1987.

Smith, Eric A., WL Impact Facility Double-Delay-Leg. Push-Pull VISAR, KTECH/TR-89/11, Ktech Corporation, Albuquerque, NM, Nov. 1989.

Smith, E. A. and Davies, F. W., "High Pressure Equation of State Investigation of Rocks," KTECH TR93-05, Ktech Corporation, Albuquerque, NM, 1993. To be published.

Wise, J. L. and Chhabildas, L. C., "Laser Interferometer Measurements of Refractive Index In Shock-Compressed Materials," Shock Waves in Condensed Matter, 1986.

APPENDIX
STRESS AND PARTICLE VELOCITY WAVEFORMS

The figures in this Appendix contain stress-time and stress-particle velocity profiles for each experiment. The table below summarizes the contents of Appendix A and lists the order in which the profiles are presented along with page numbers. The order corresponds to the order in the Hugoniot Data Tables. Ice data profiles are not included here since individual wave forms for each shot were already presented with the experimental results (Section 5).

Material	Experiment Type	Shot No.	Page No.
HUNTERS TROPHY Tuff	Lagrangian	3520	A-3
	Lagrangian	3518	A-4
	Lagrangian	3519	A-5
	Lagrangian	3516	A-6
	Lagrangian	3517	A-7
	Lagrangian	3521	A-8
	Lagrangian	3522	A-9
DISTANT ZENITH Tuff	Lagrangian	3437	A-10
	Lagrangian	3447	A-11
	VISAR	3515	A-12
DISTANT ZENITH MJ-2(NSF-6) Grout	Lagrangian	3449	A-13
	VISAR	3506	A-14
	VISAR	3512	A-15
	VISAR	3514	A-16
	Lagrangian	3528	A-17
Danby Marble	Lagrangian	3467	A-18
	Lagrangian	3469	A-19
	VISAR	3513	A-20
	VISAR	3527	A-21
Ft. Knox Carbonate	Lagrangian	3489	A-22
	Lagrangian	3490	A-23
	Lagrangian	3499	A-24
	Lagrangian	3492	A-25
	Lagrangian	3491	A-26
	Lagrangian	3503	A-27
	Lagrangian	3505	A-28
	Lagrangian	3504	A-29
	Lagrangian	3497	A-30
	Lagrangian	3498	A-31

<u>Material</u>	<u>Experiment Type</u>	<u>Shot No.</u>	<u>Page No.</u>	
Salem Limestone	Lagrangian	3554	A-32	
	Lagrangian	3556	A-33	
	Lagrangian	3564	A-34	
	Lagrangian	3558	A-35	
	Lagrangian	3561	A-36	
	Lagrangian	3555	A-37	
	Lagrangian	3563	A-38	
	Lagrangian	3557	A-39	
	Lagrangian	3560	A-40	
	Lagrangian	3559	A-41	
	Lagrangian	3562	A-42	
	Lagrangian	3583	A-43	
	Lagrangian	3573	A-44	
	Lagrangian	3576	A-45	
	Lagrangian	3574	A-46	
	Lagrangian	3575	A-47	
	Lagrangian	3582	A-48	
	Lagrangian	3577	A-49	
	Danby Marble with Joints	Lagrangian Joints	3470	A-50
		Lagrangian Joints	3471	A-51
Lagrangian Joints		3473	A-52	
Lagrangian Joints		3474	A-53	
Lagrangian Joints		3475	A-54	
Lagrangian Joints		3476	A-55	

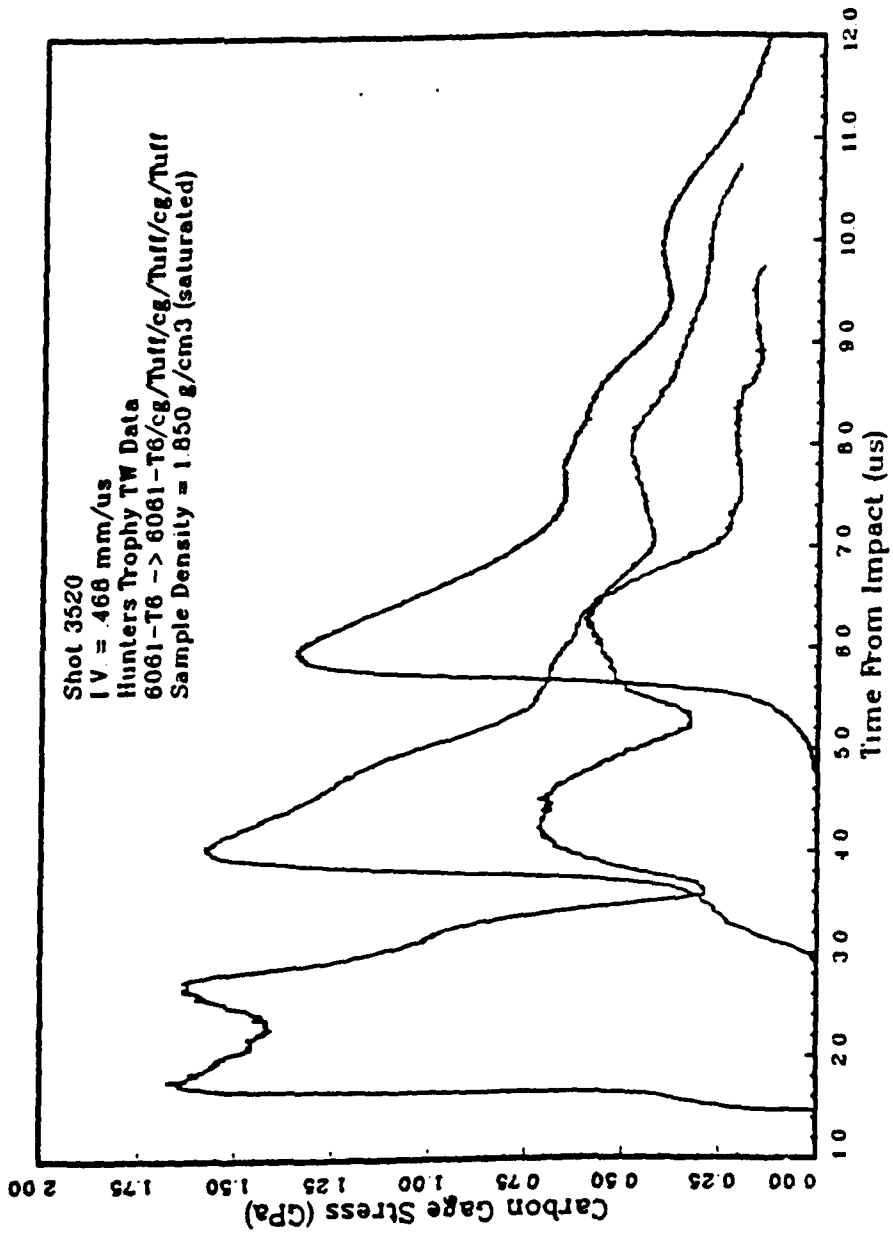


Figure A-1. HUNTERS TROPHY tuff shot 3520.

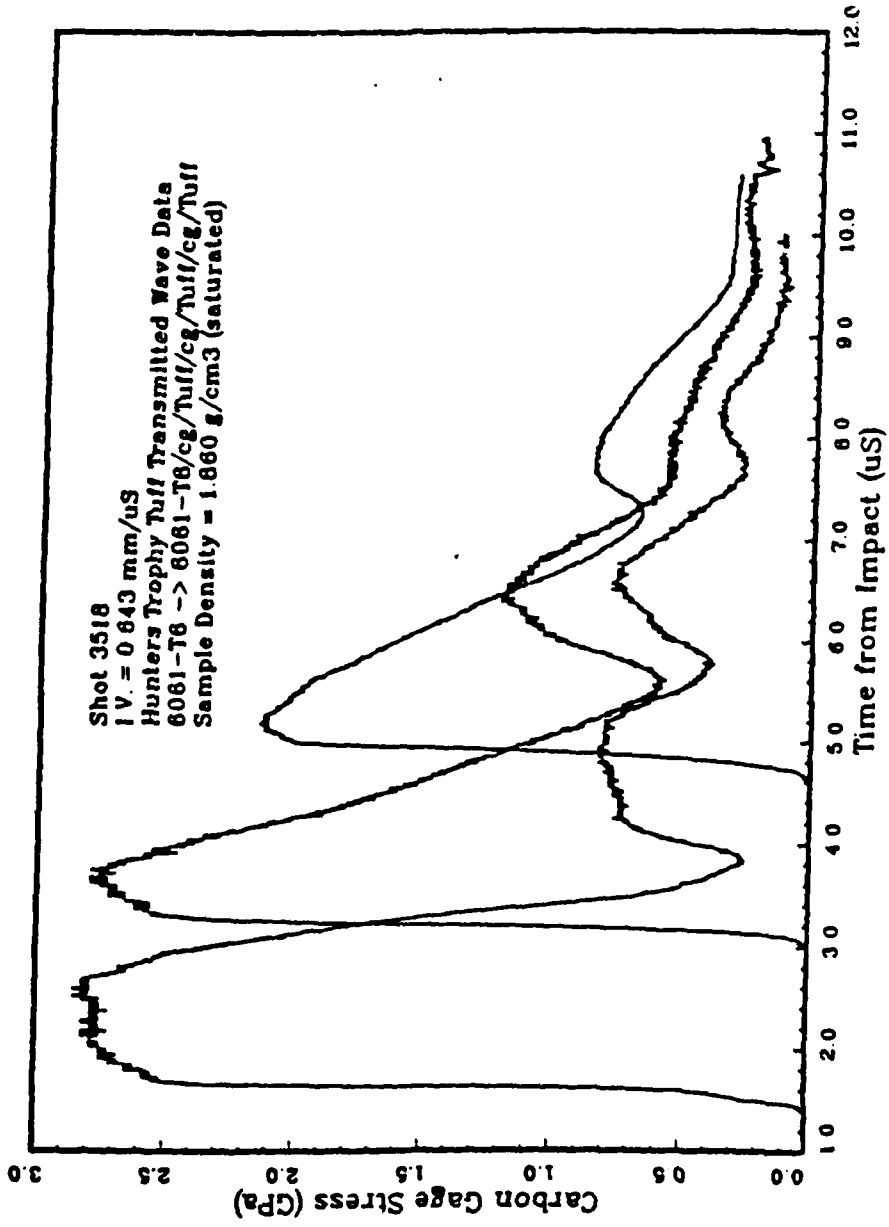


Figure A-2. HUNTERS TROPHY tuff shot 3518.

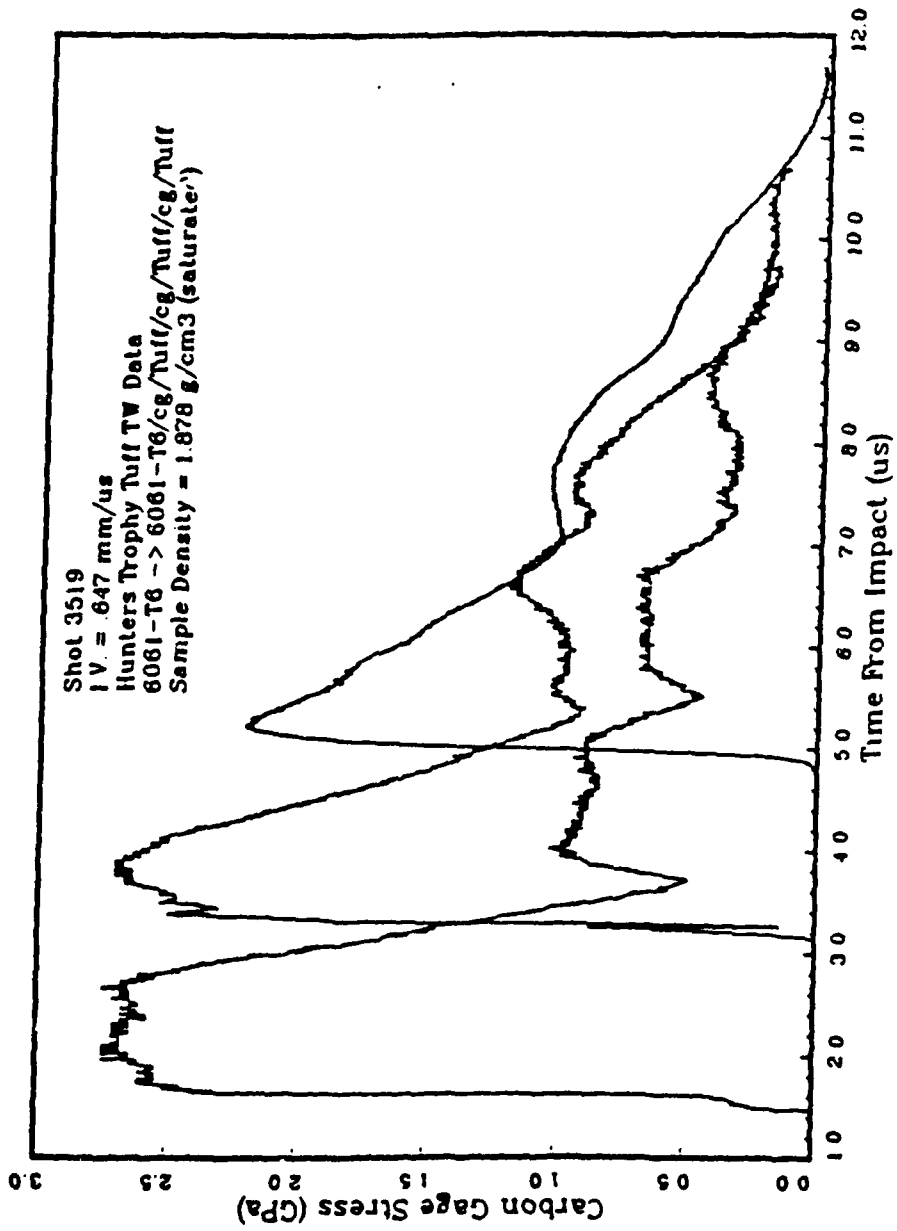


Figure A-3. HUNTERS TROPHY tuff shot 3519.

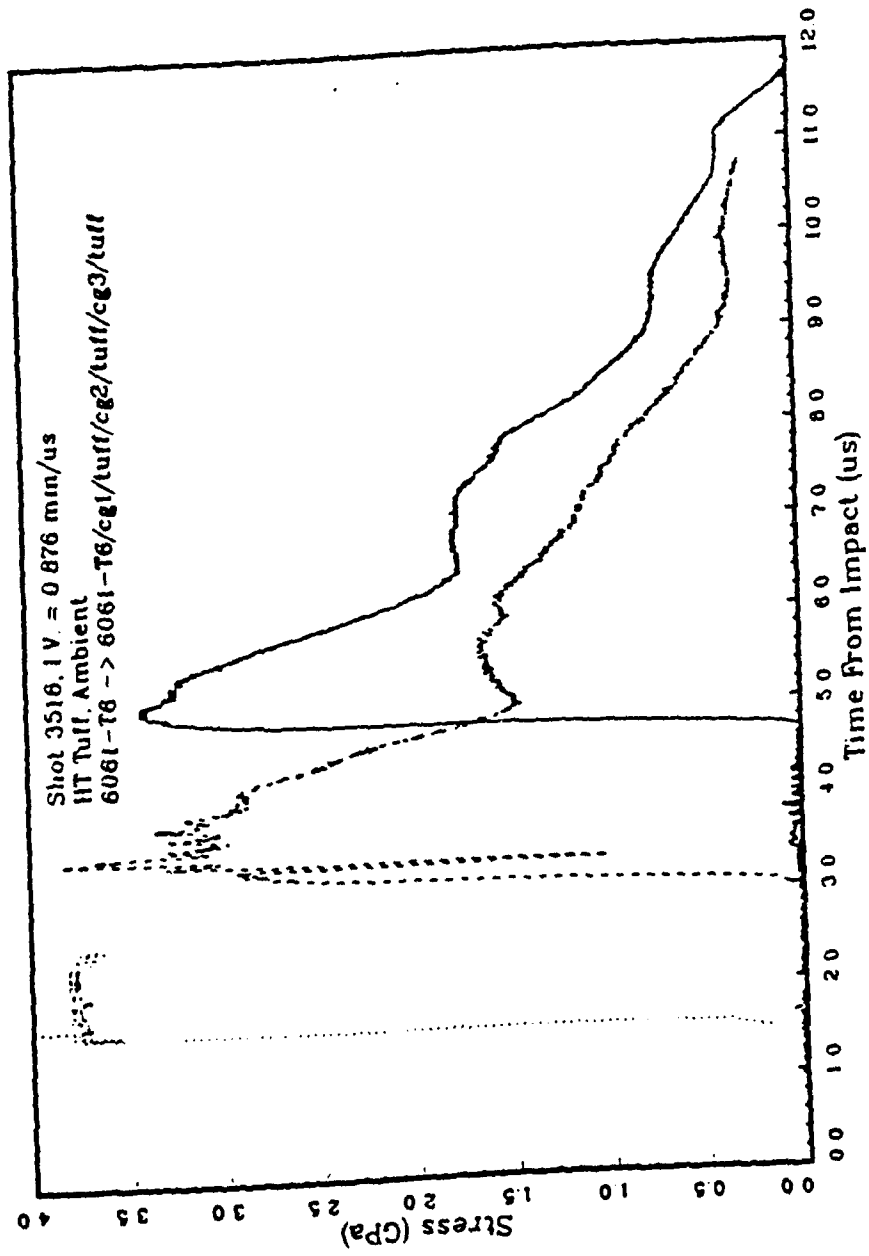


Figure A-4. HUNTERS TROPHY tuff shot 3516.

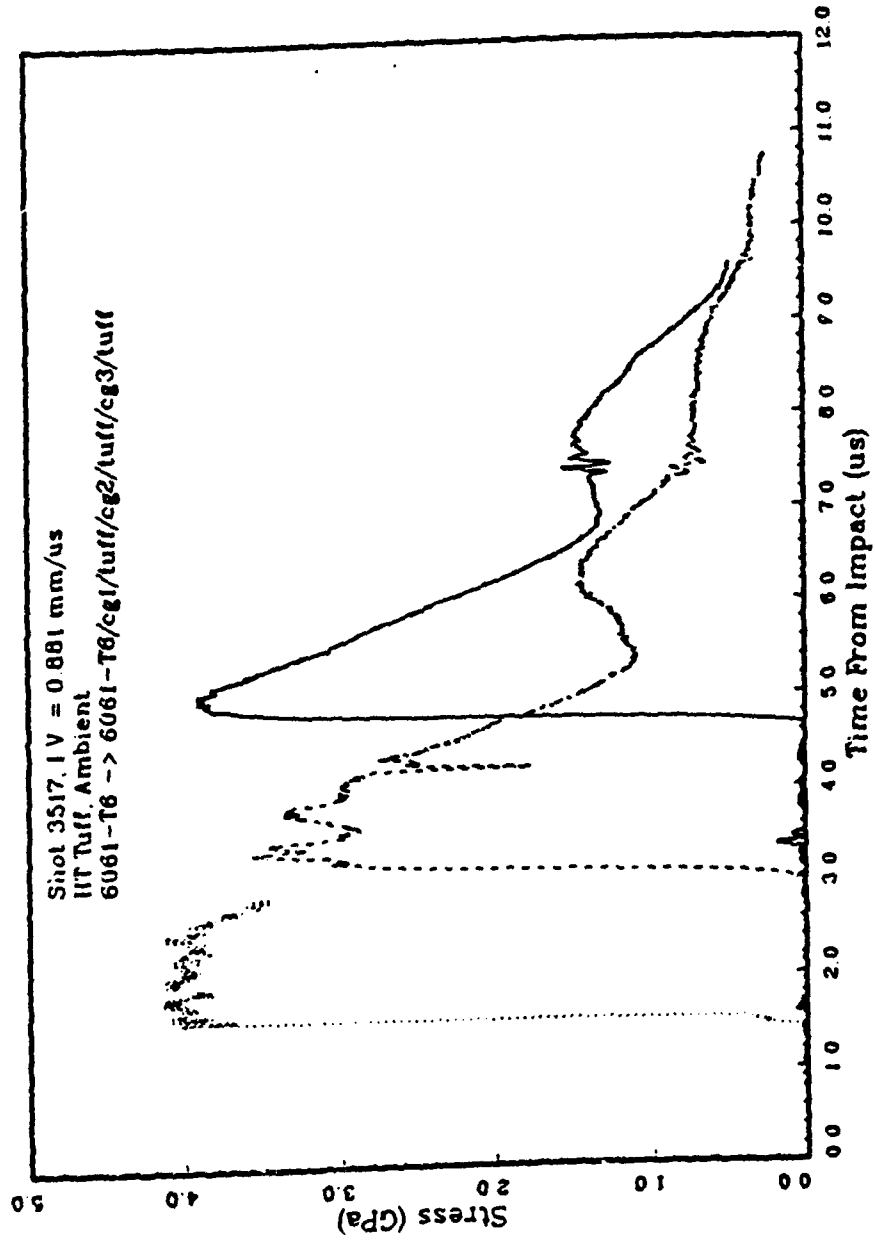


Figure A-5. HUNTERS TROPHY tuff shot 3517.

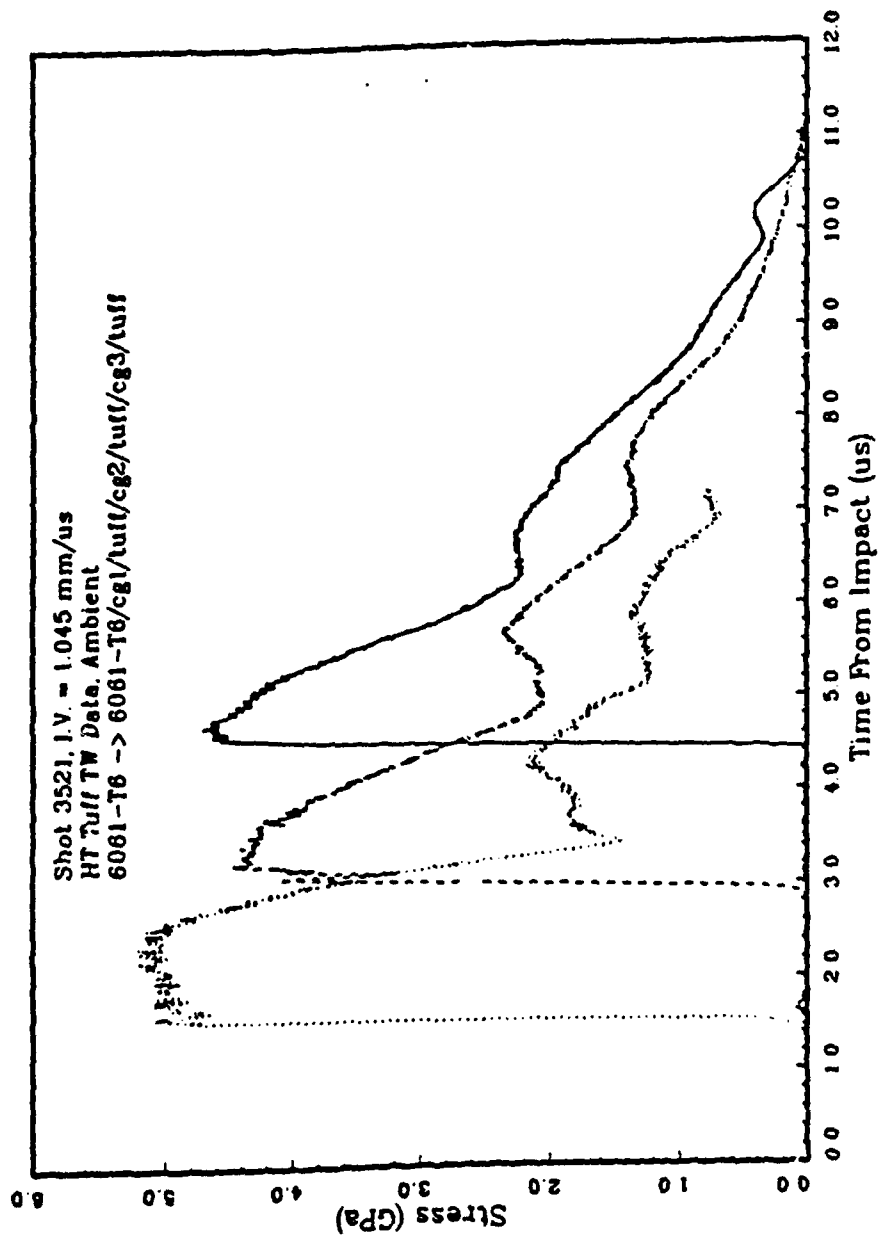


Figure A-6. HUNTERS TROPHY tuff shot 3521.

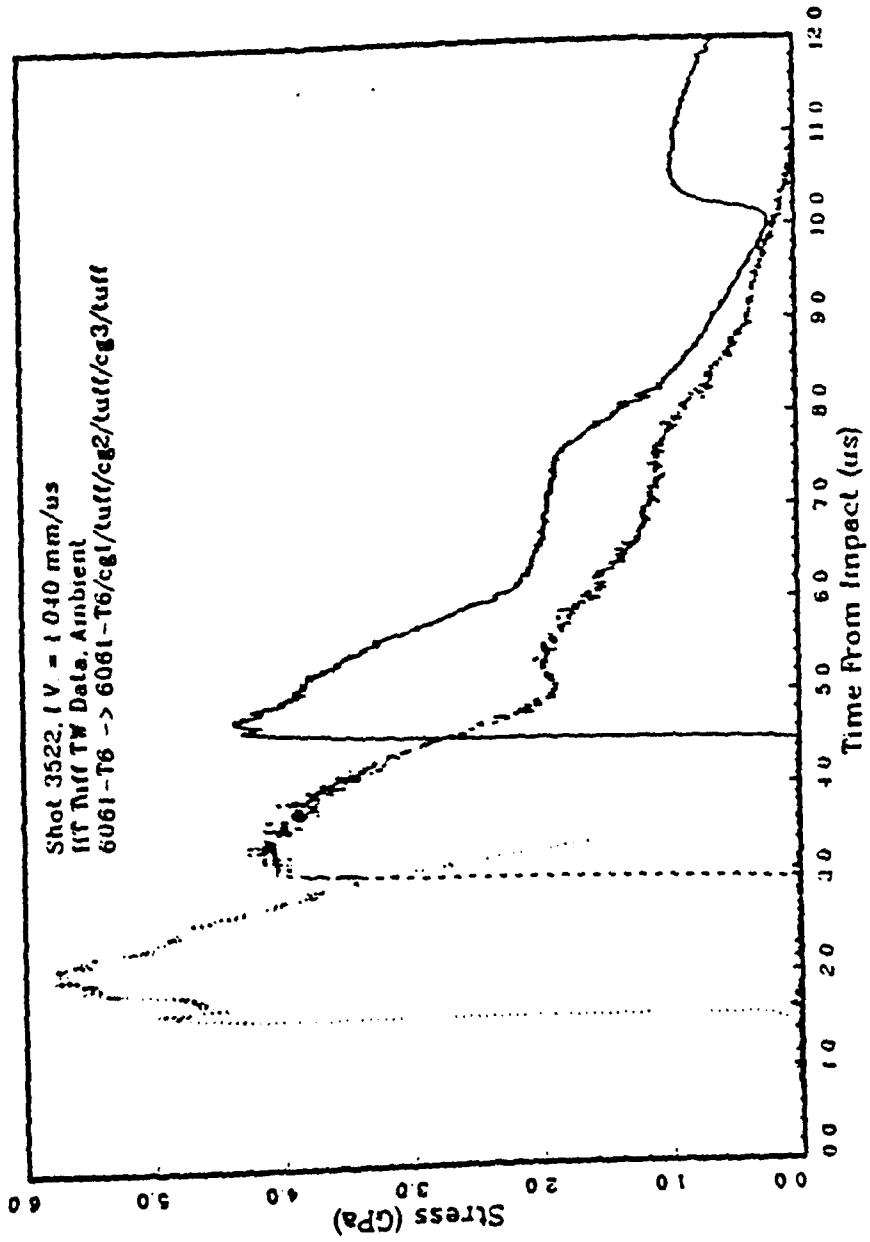


Figure A-7. HUNTERS TROPHY tuff shot 3522.

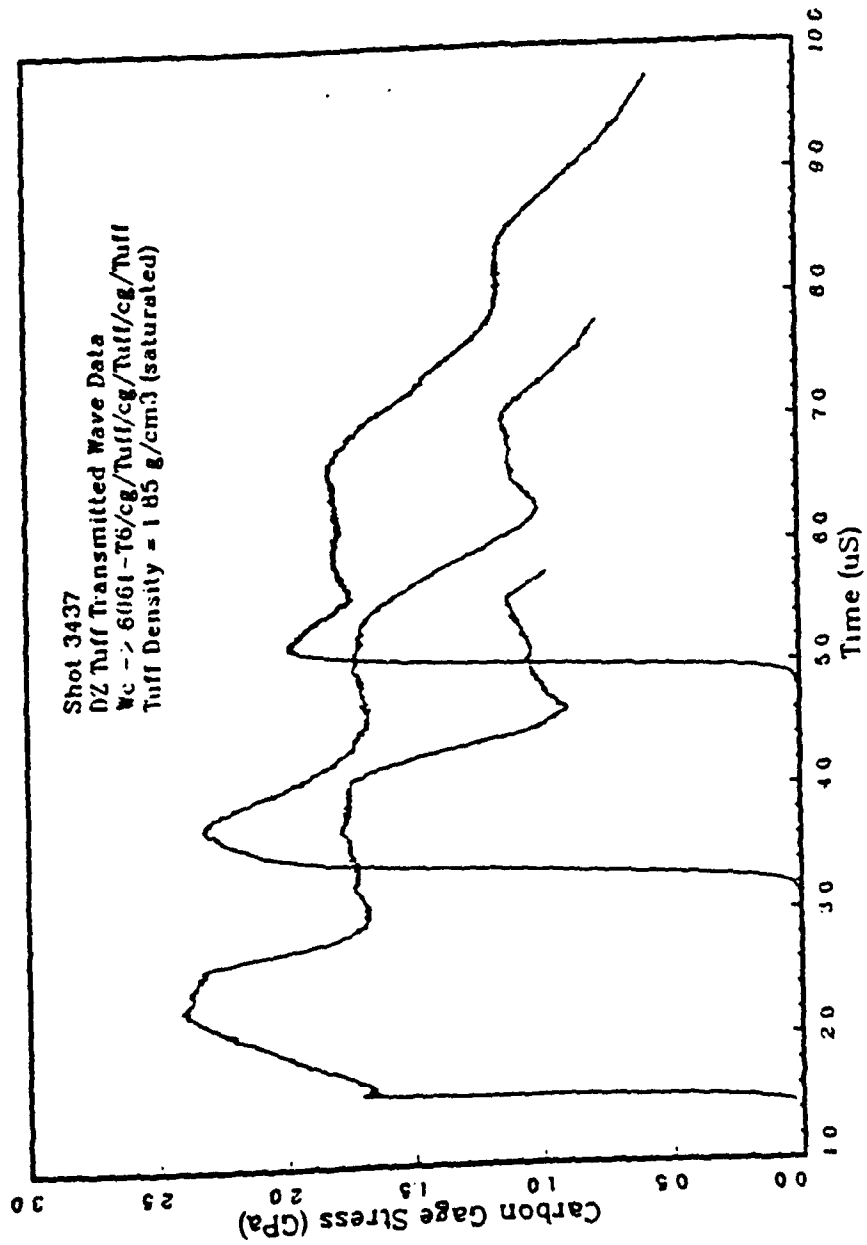


Figure A-8. DISTANT ZENTH shot 3437.

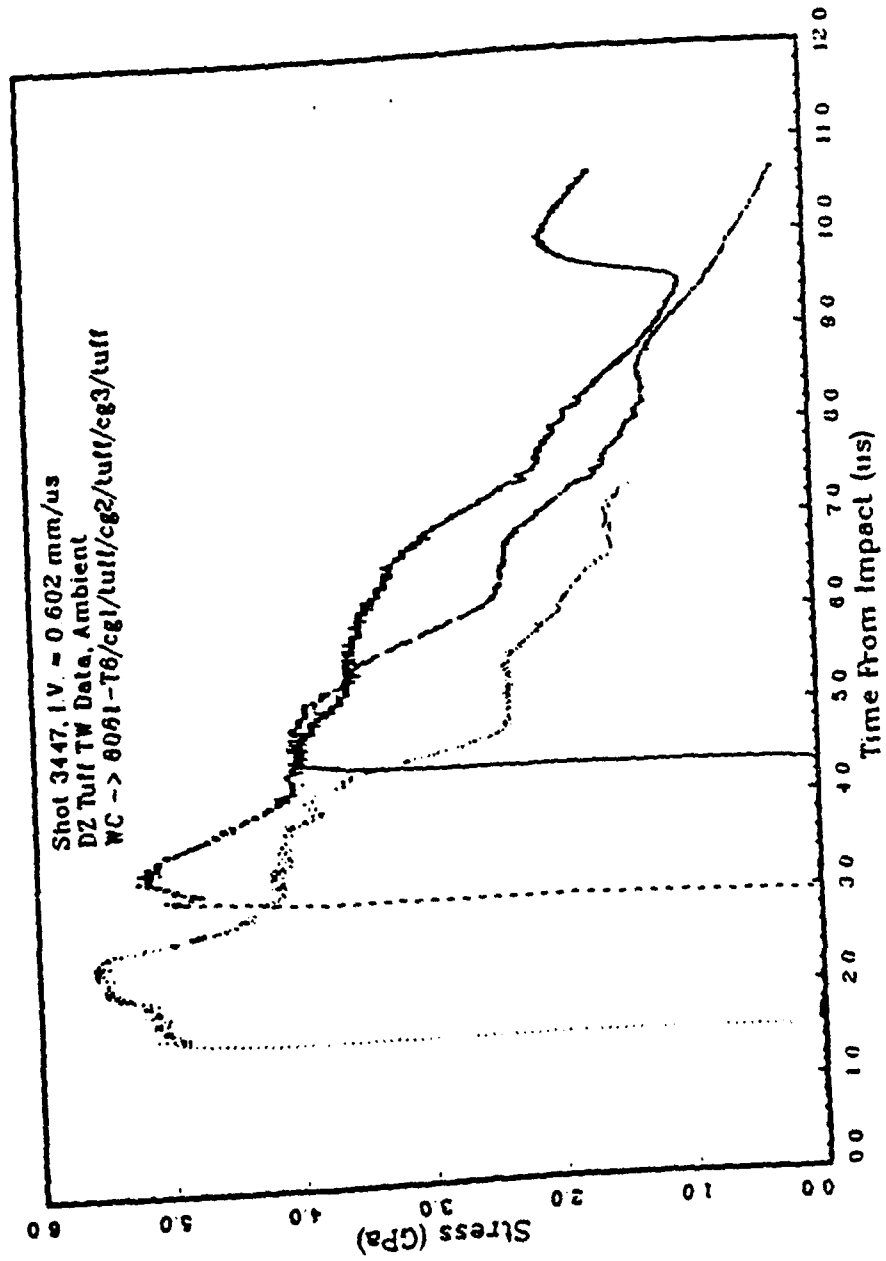


Figure A-9. DISTANT ZENITH shot 3447.

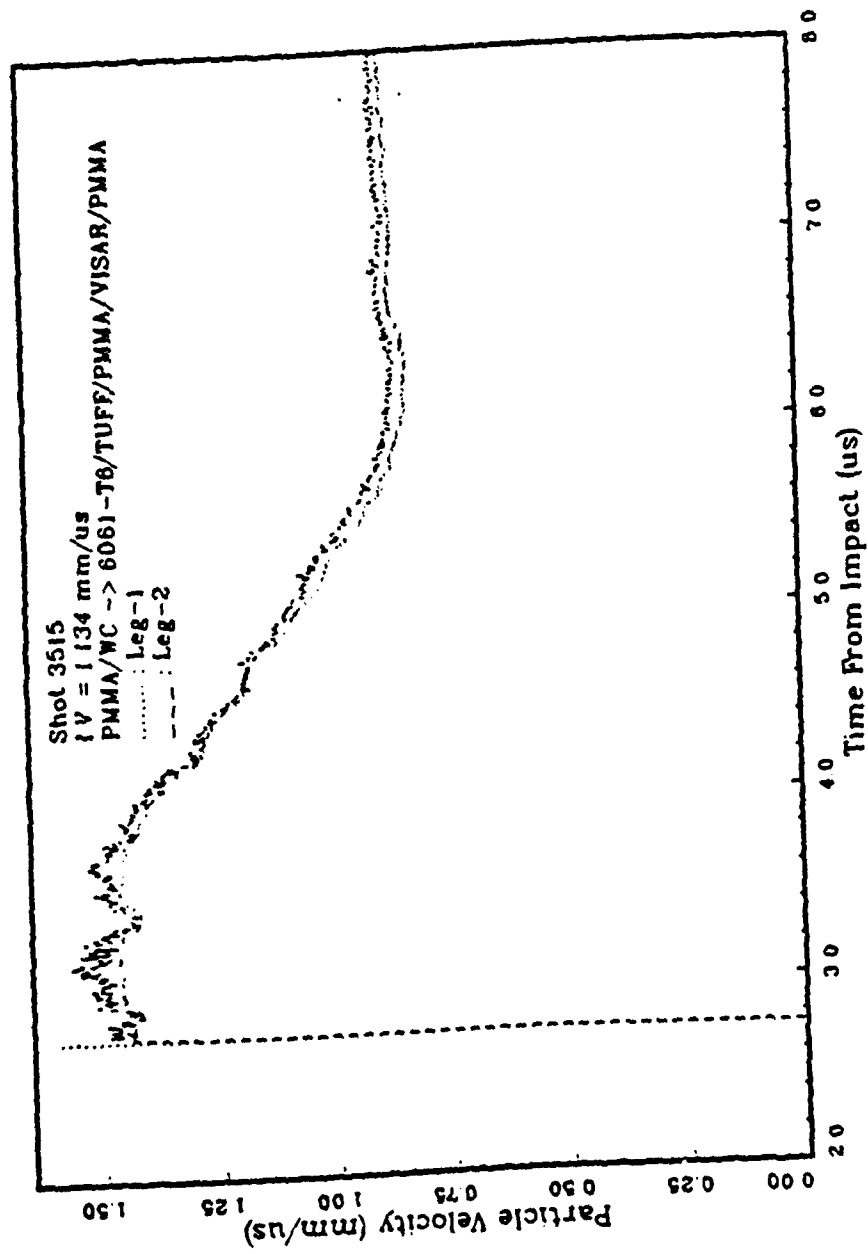


Figure A-10. DISTANT ZENITH shot 3515.

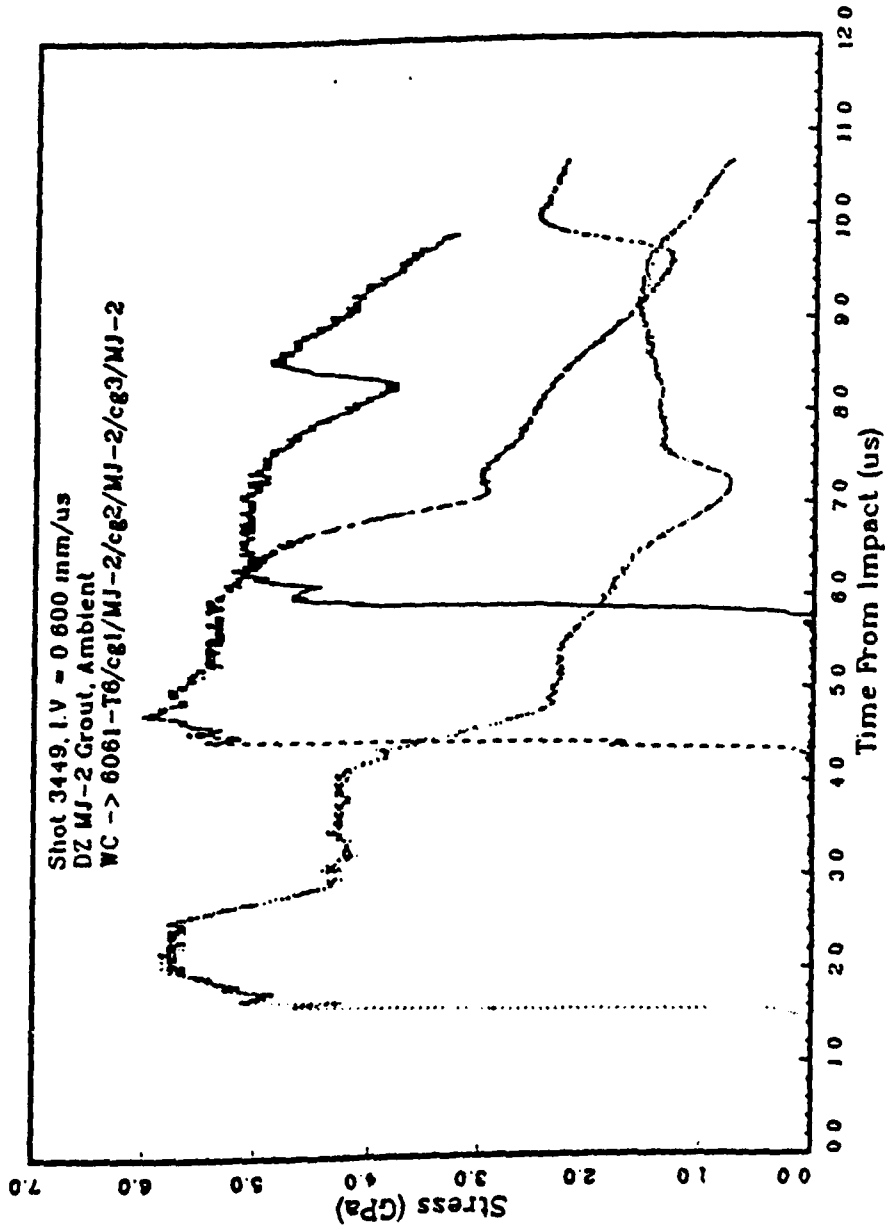


Figure A-11. MJ-2 (NSF-6) grout shot 3449.

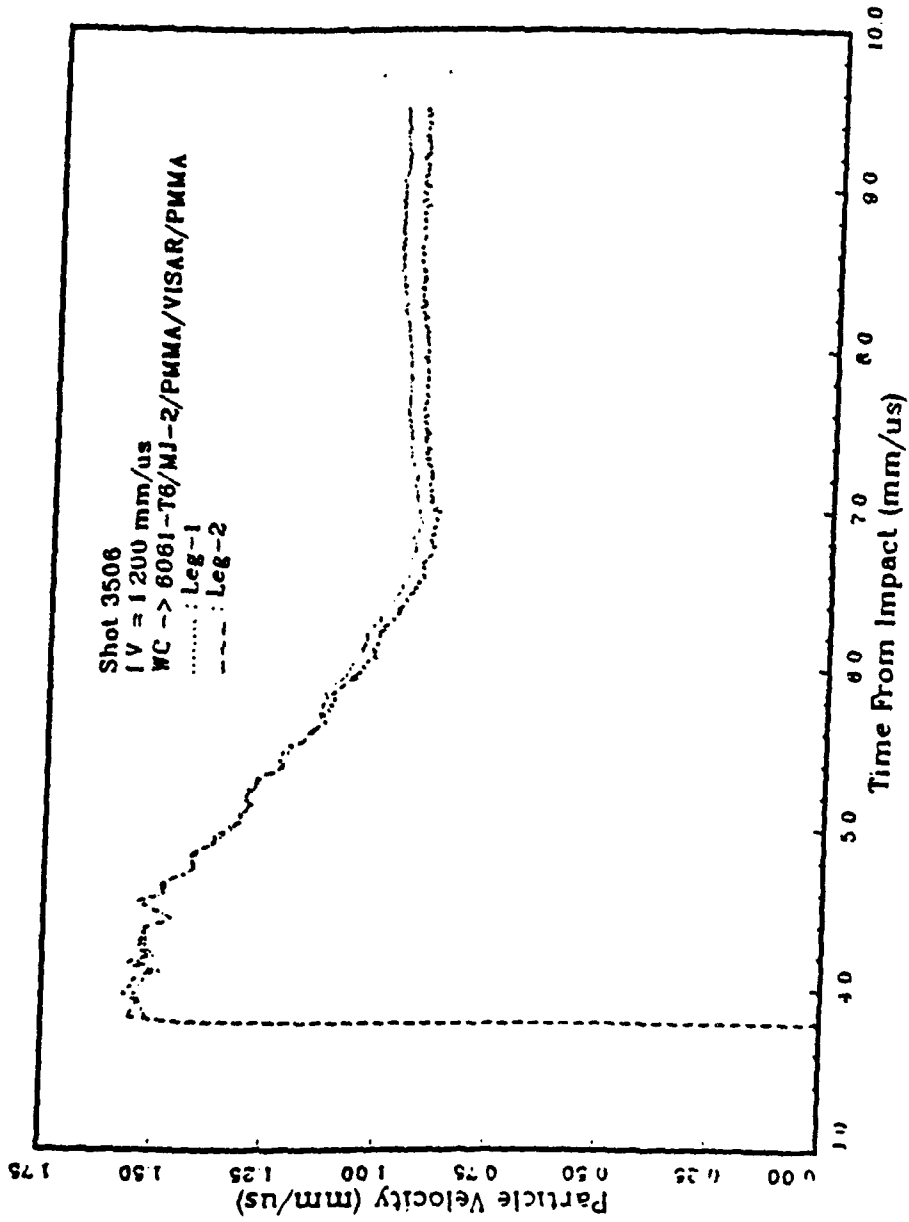


Figure A-12. MJ-2 (NSF-6) grout shot 3506.

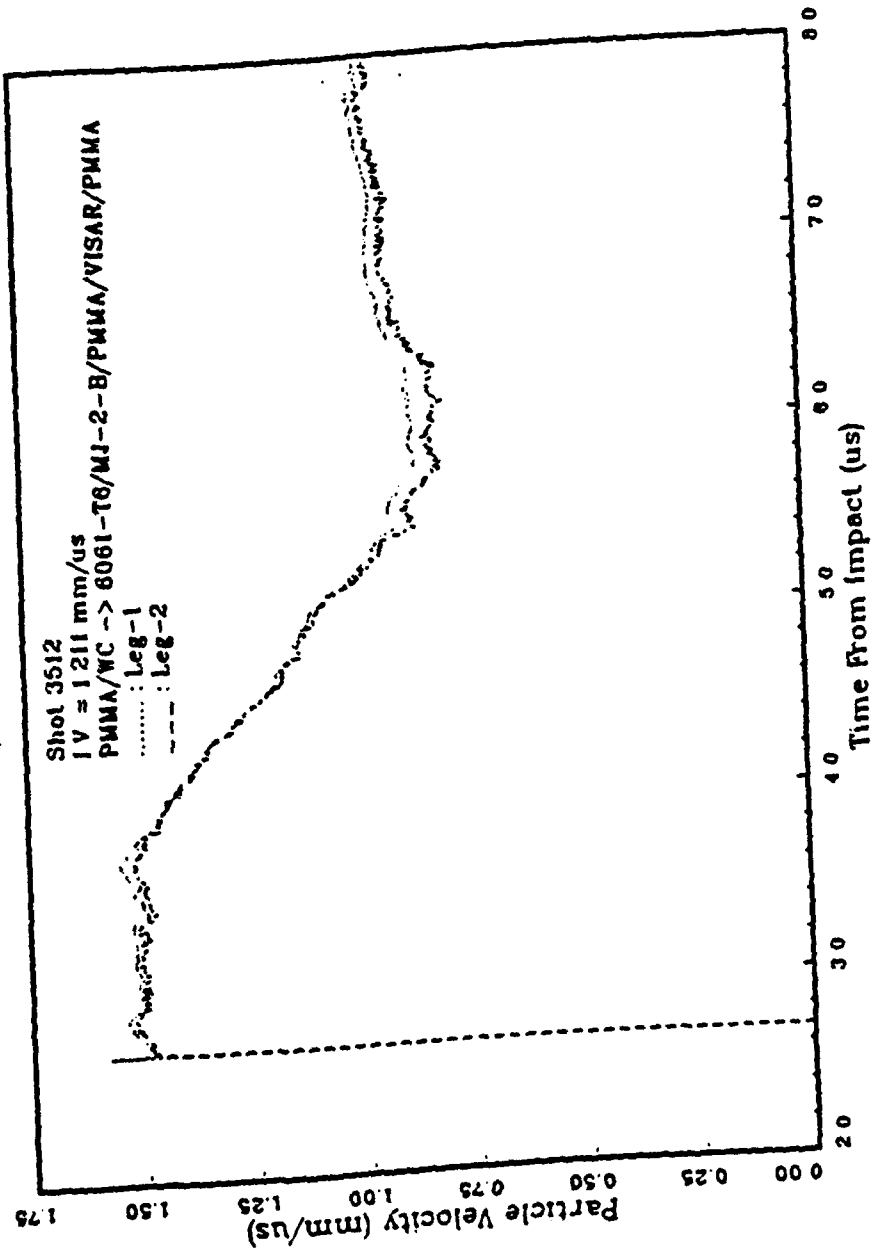


Figure A-13. MJ-2 (NSF-6) groud shot 3512.

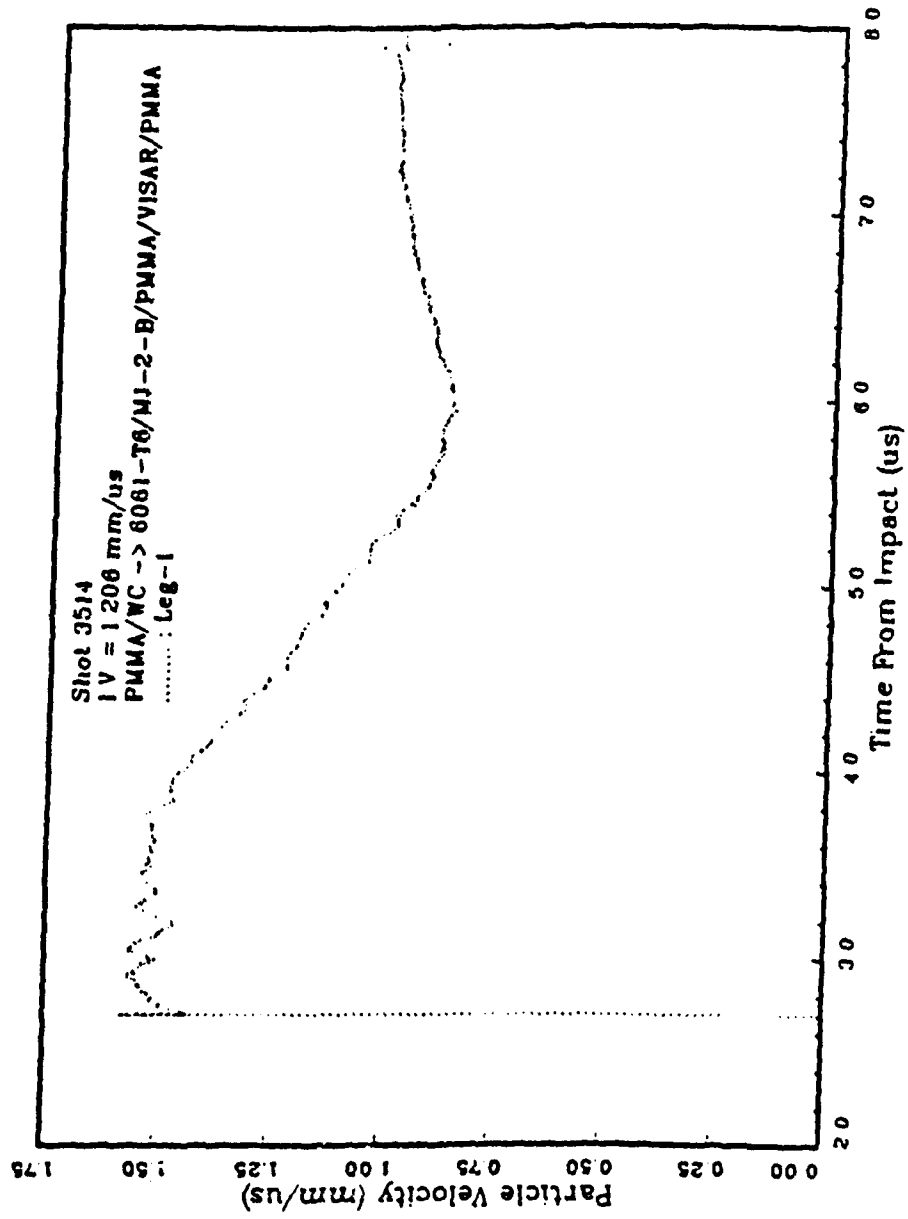


Figure A-14. MJ-2 (NSF-6) grout shot 3514.

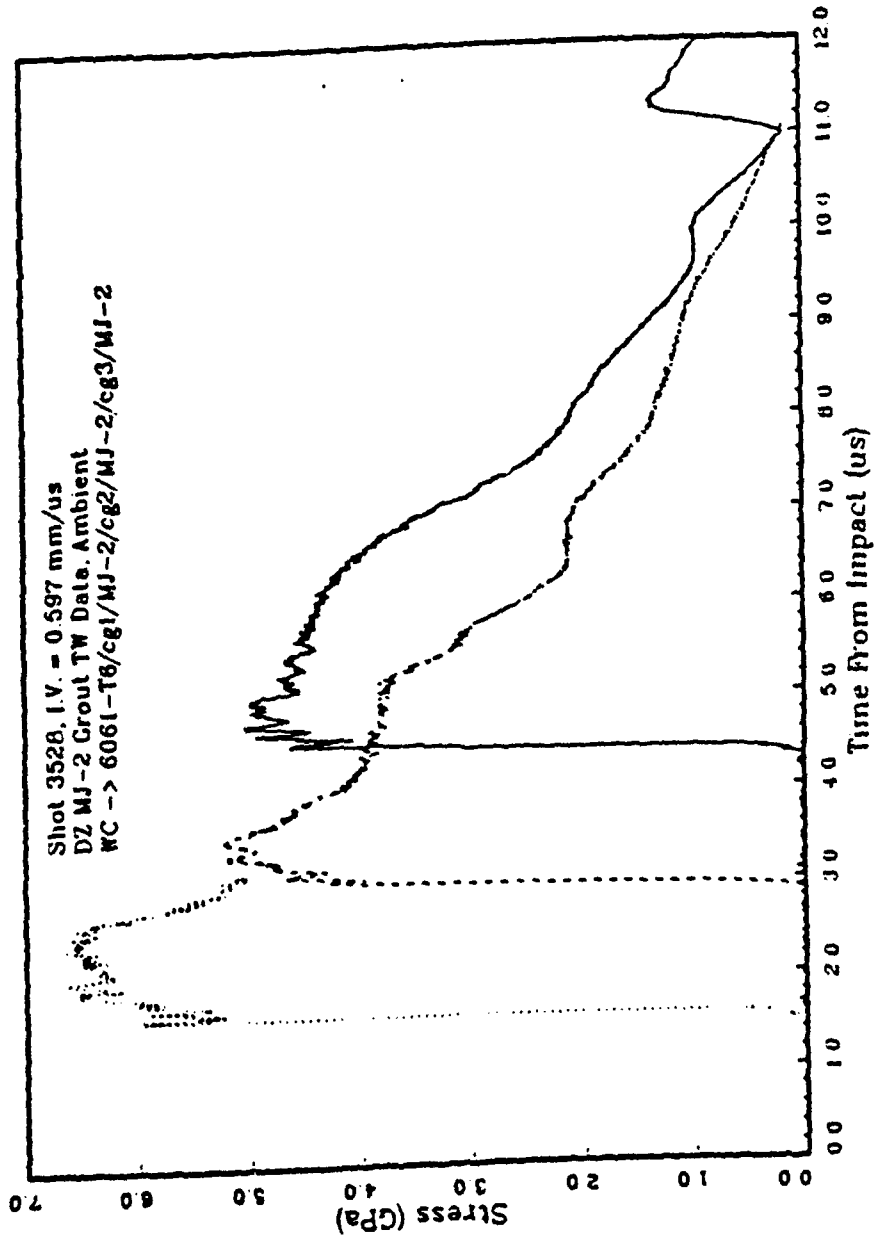


Figure A-15. MJ-2 (NSF-6) grout shot 3528.

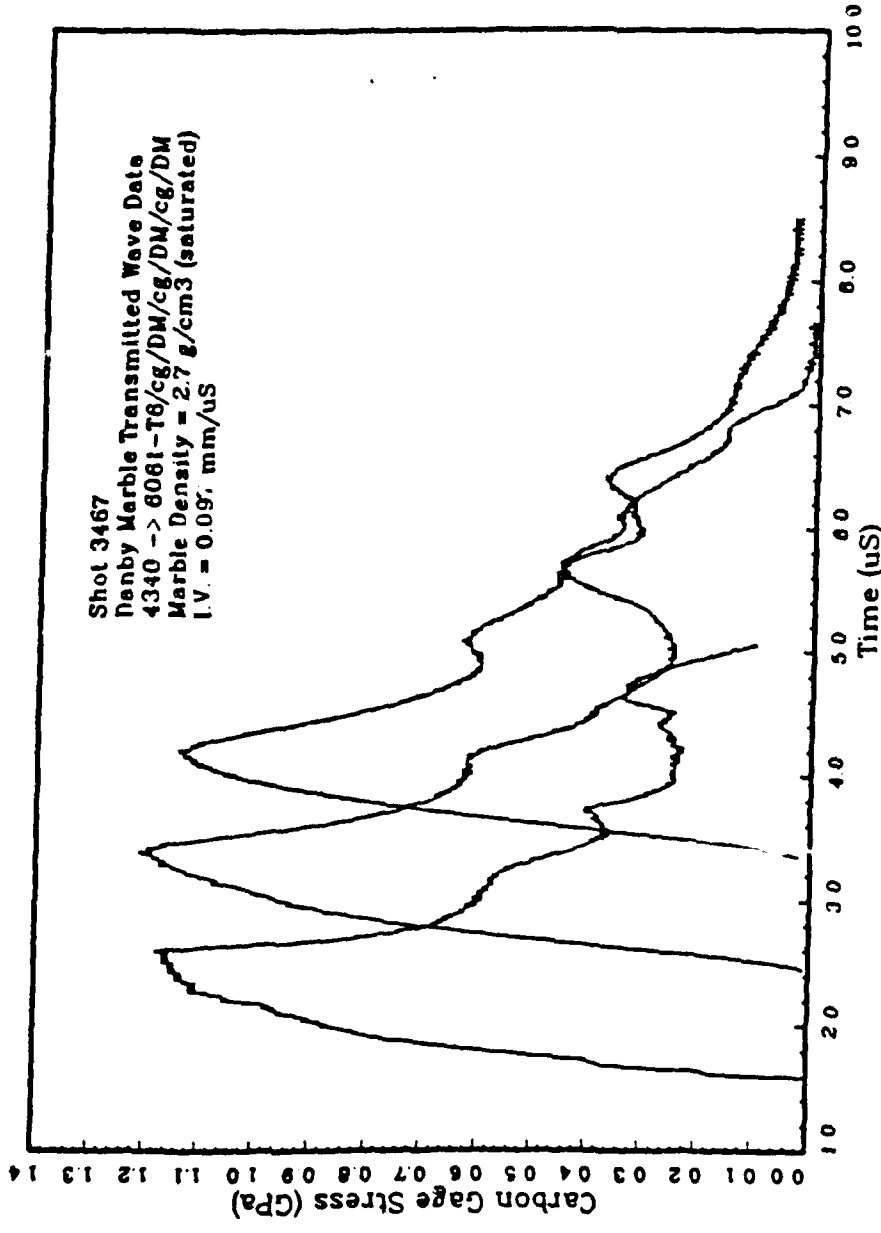


Figure A-16. Danby marble shot 3467.

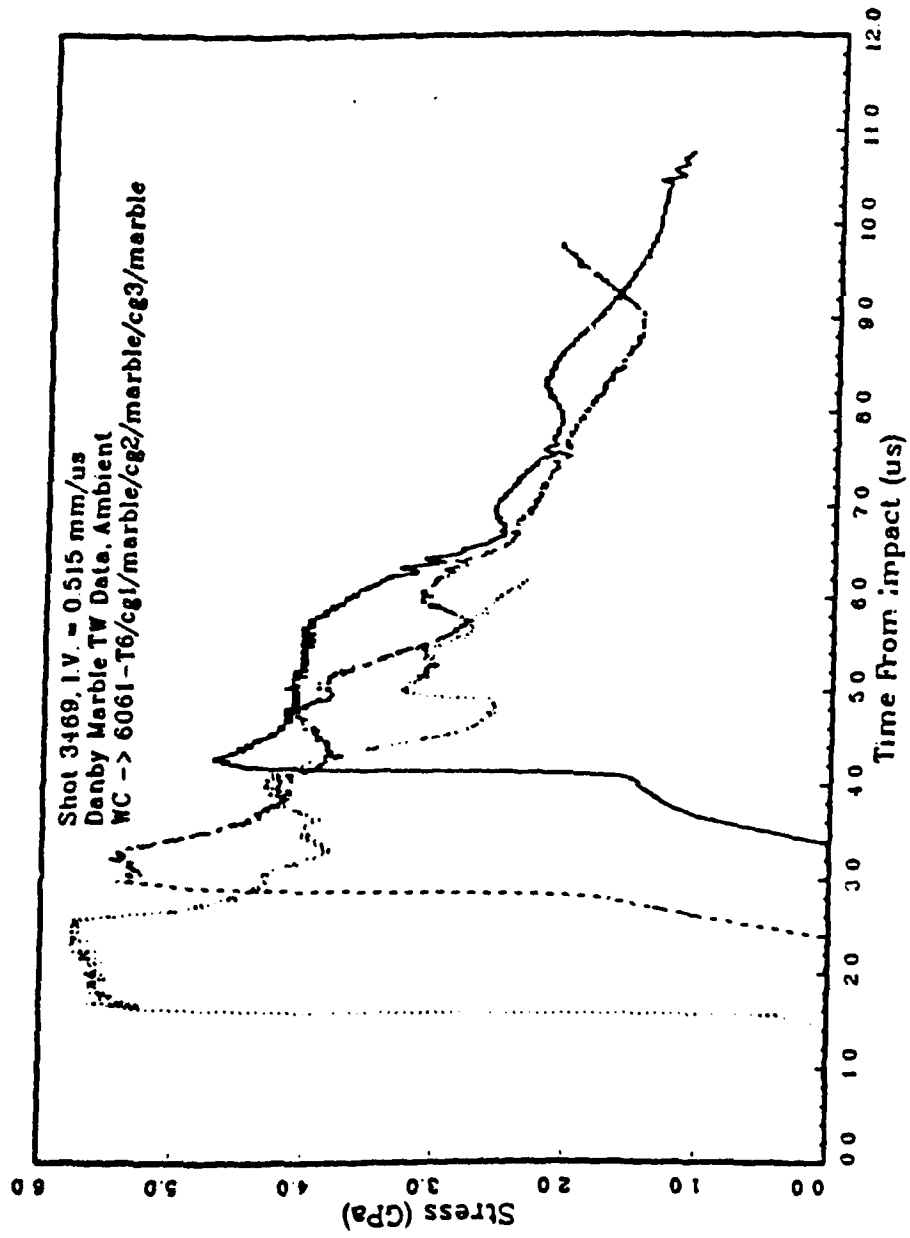


Figure A-17. Danby marble shot 3469.

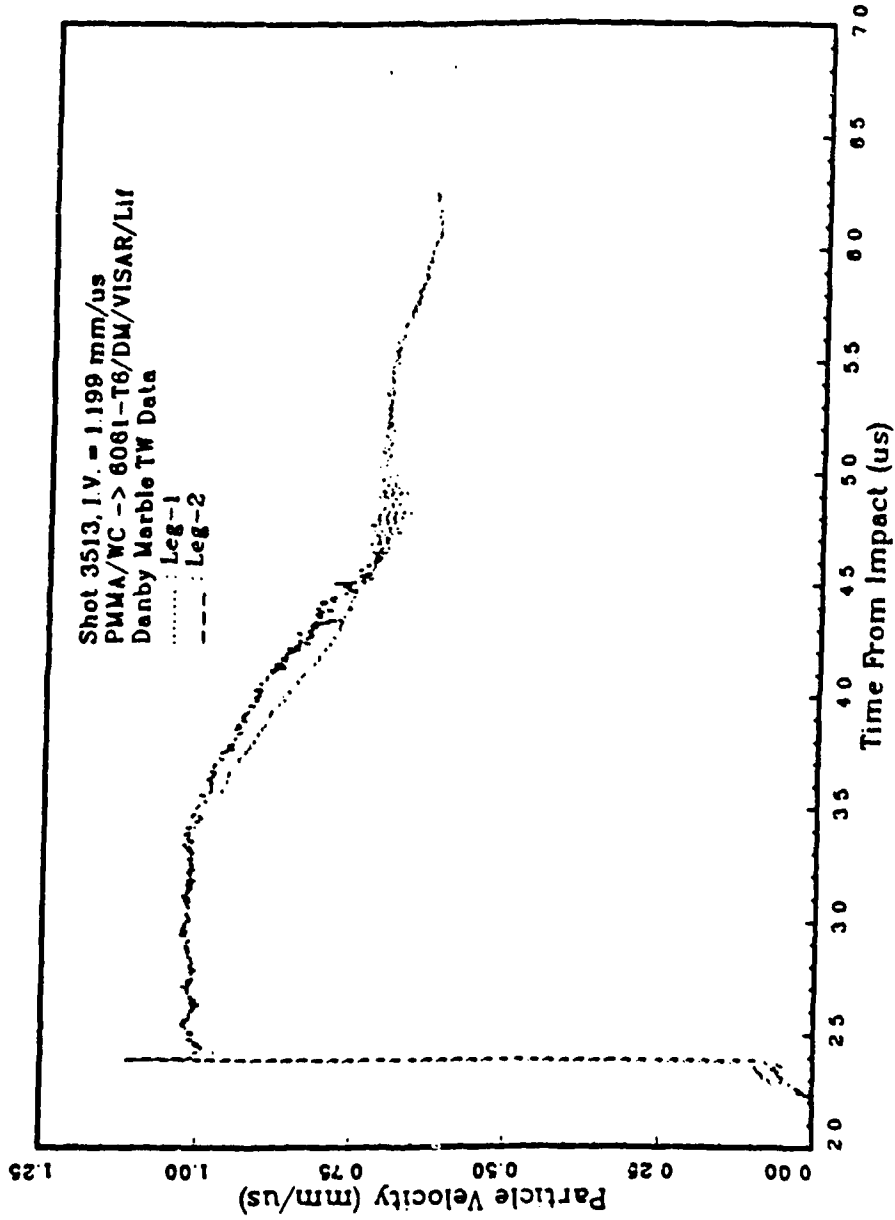


Figure A-18. Danby marble shot 3513.

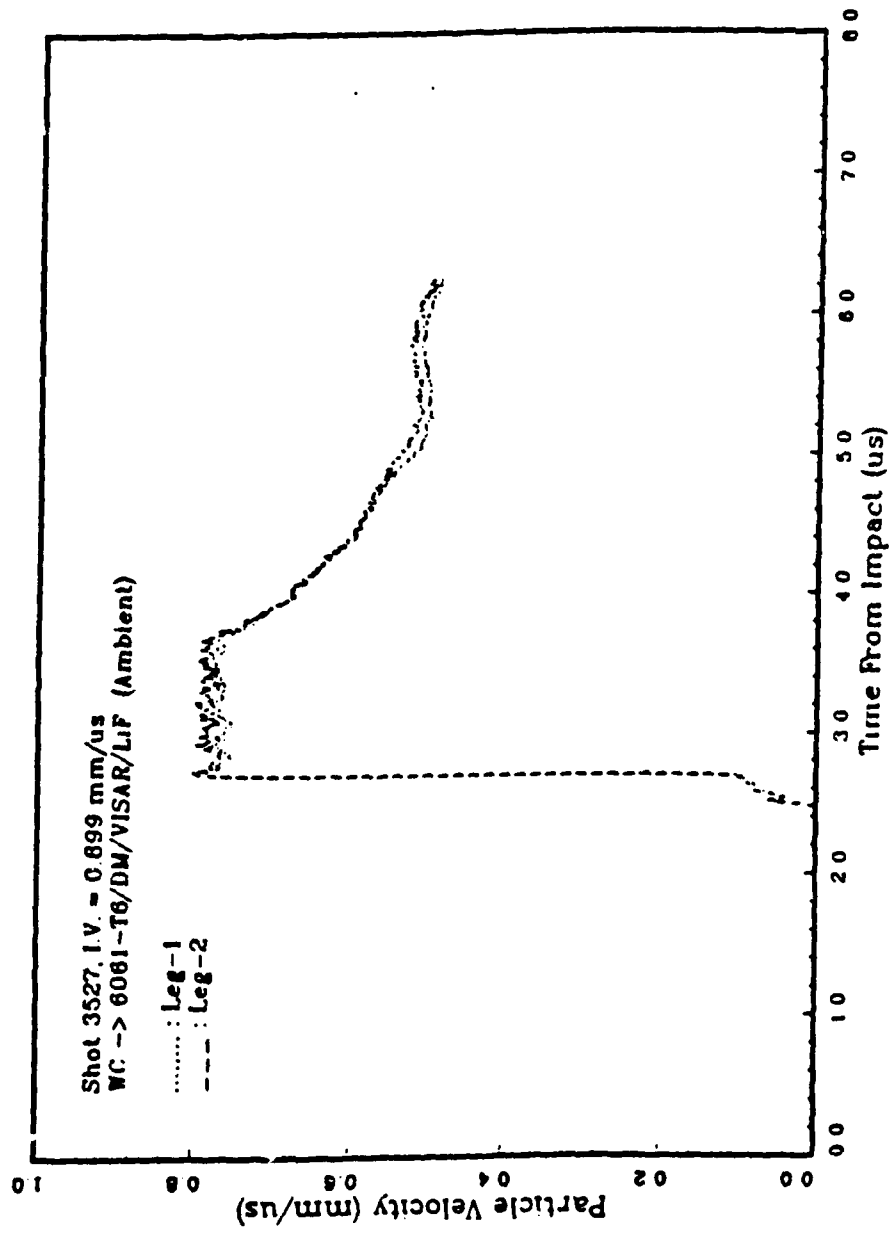


Figure A-19. Danby marble shot 3527.

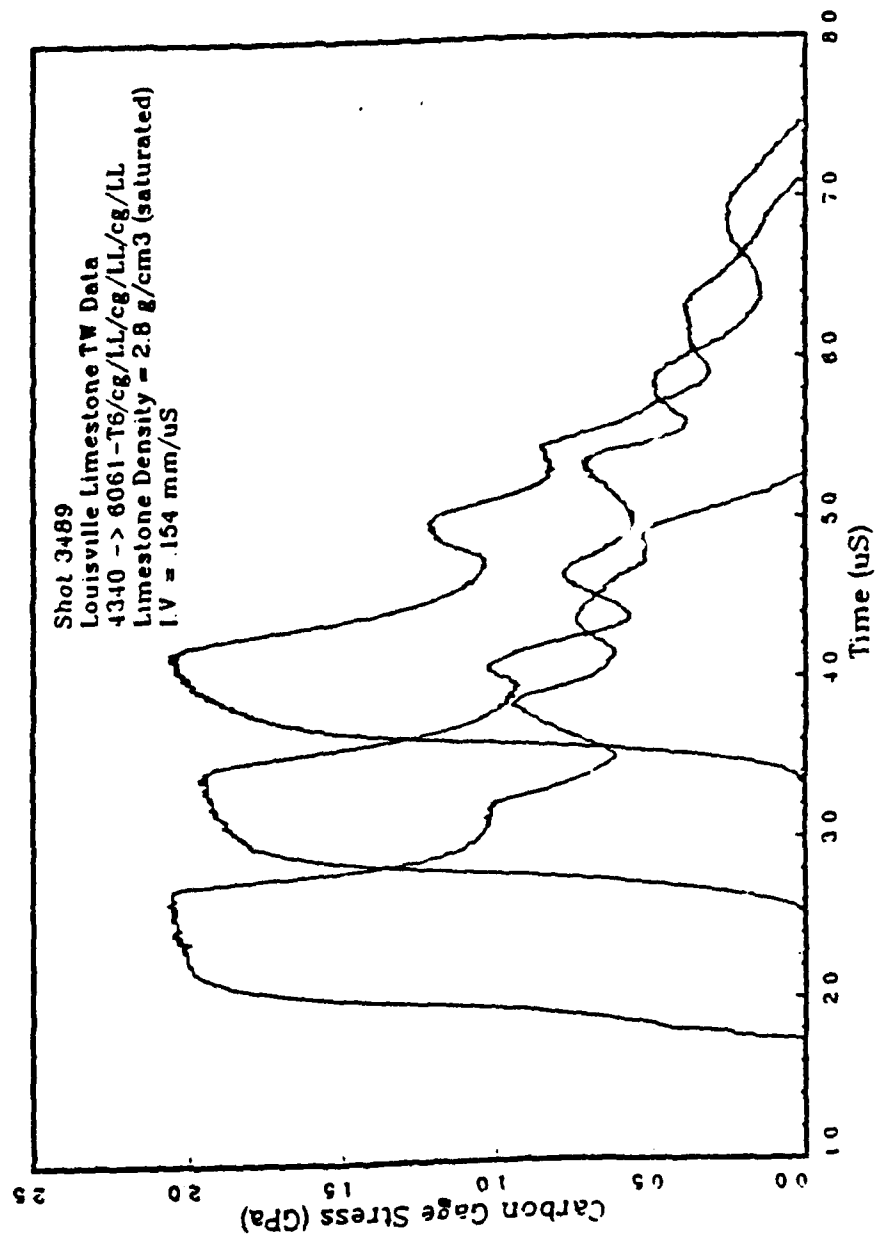


Figure A-20. Ft. Knox carbonates shot 3489.

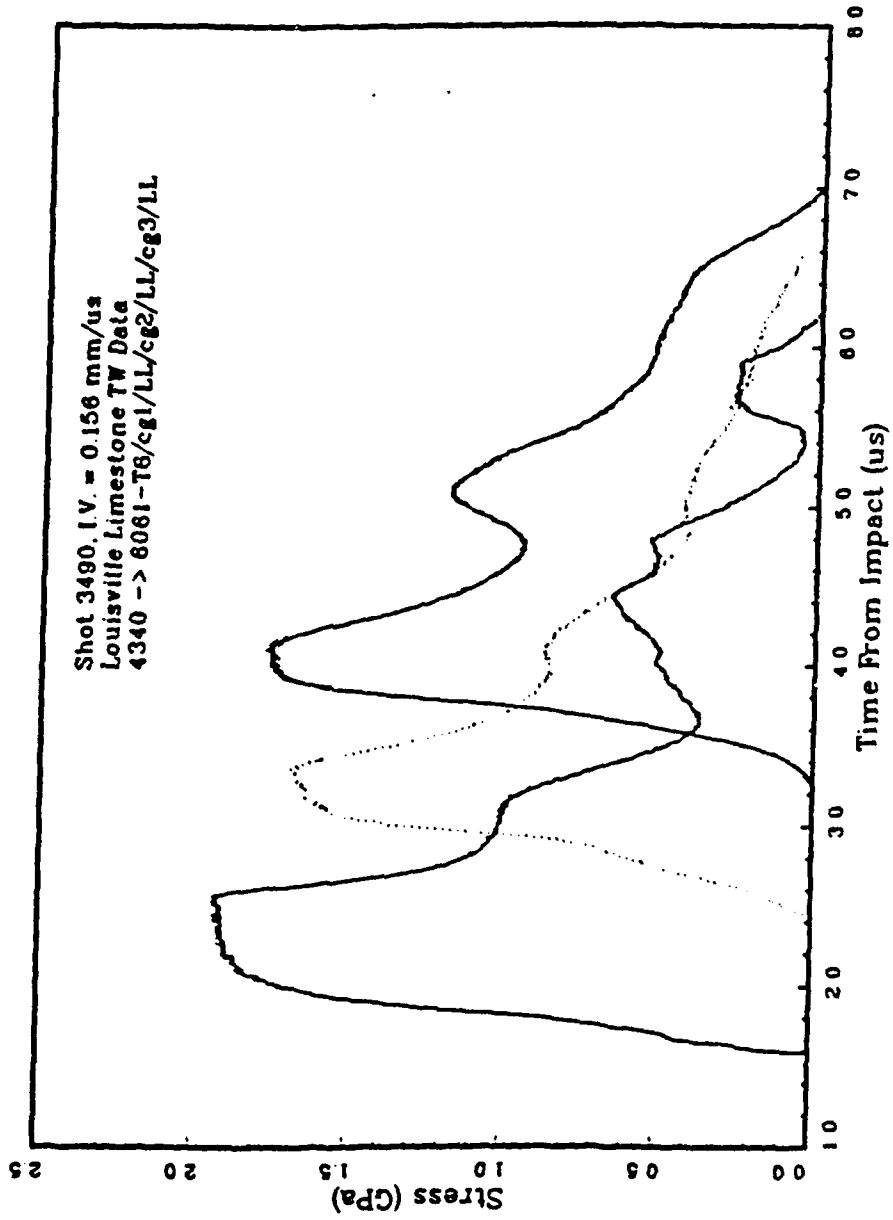


Figure A-21. Ft. Knox carbonates shot 3490.

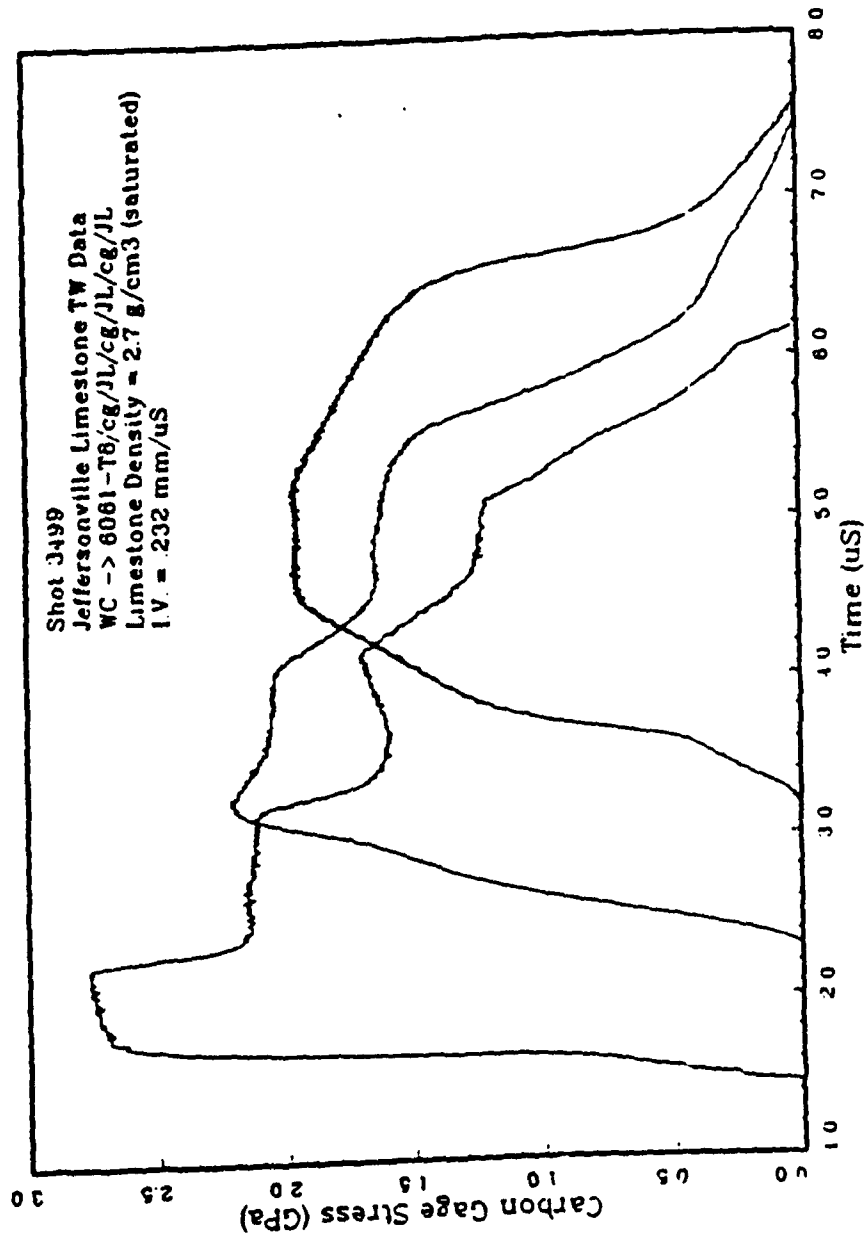


Figure A-22. Ft. Knox carbonates shot 3499.

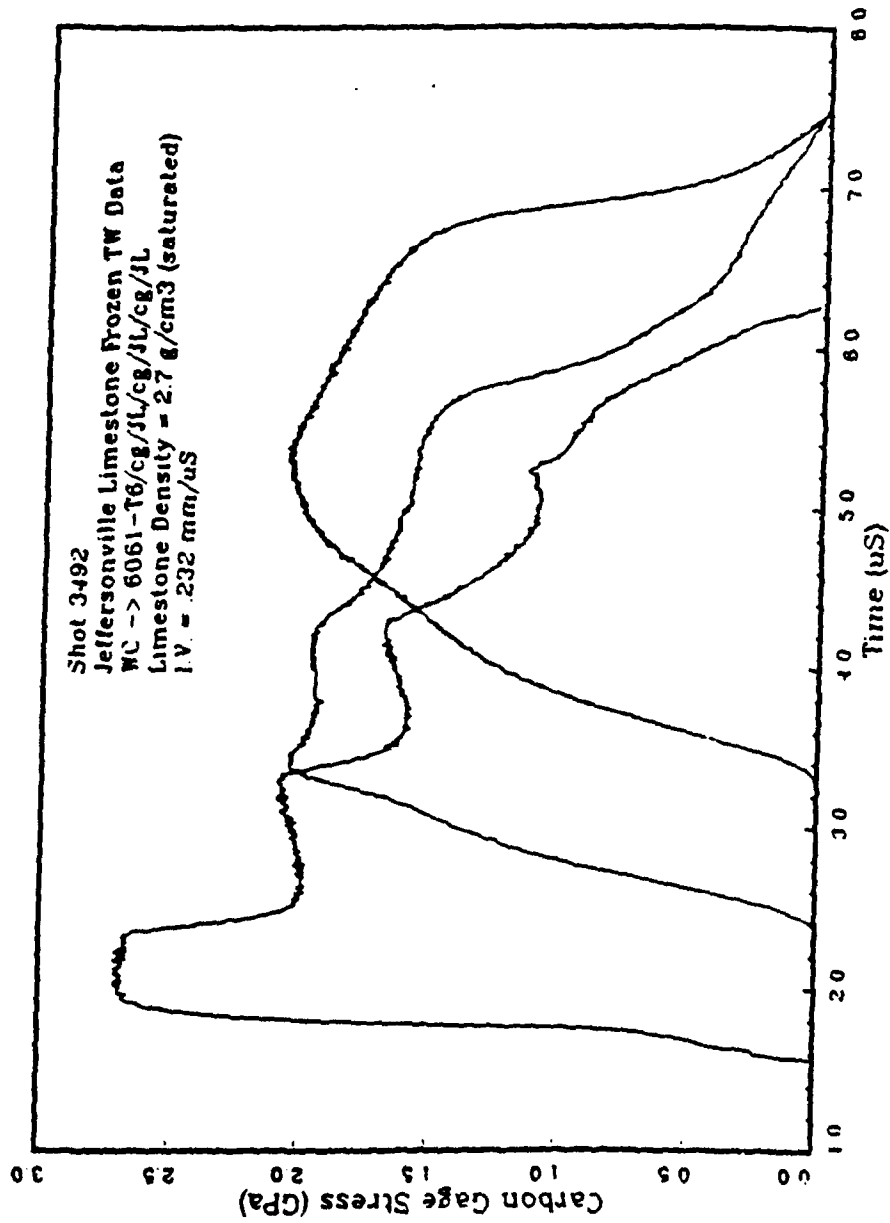


Figure A-23. Ft. Knox carbonates shot 3492.

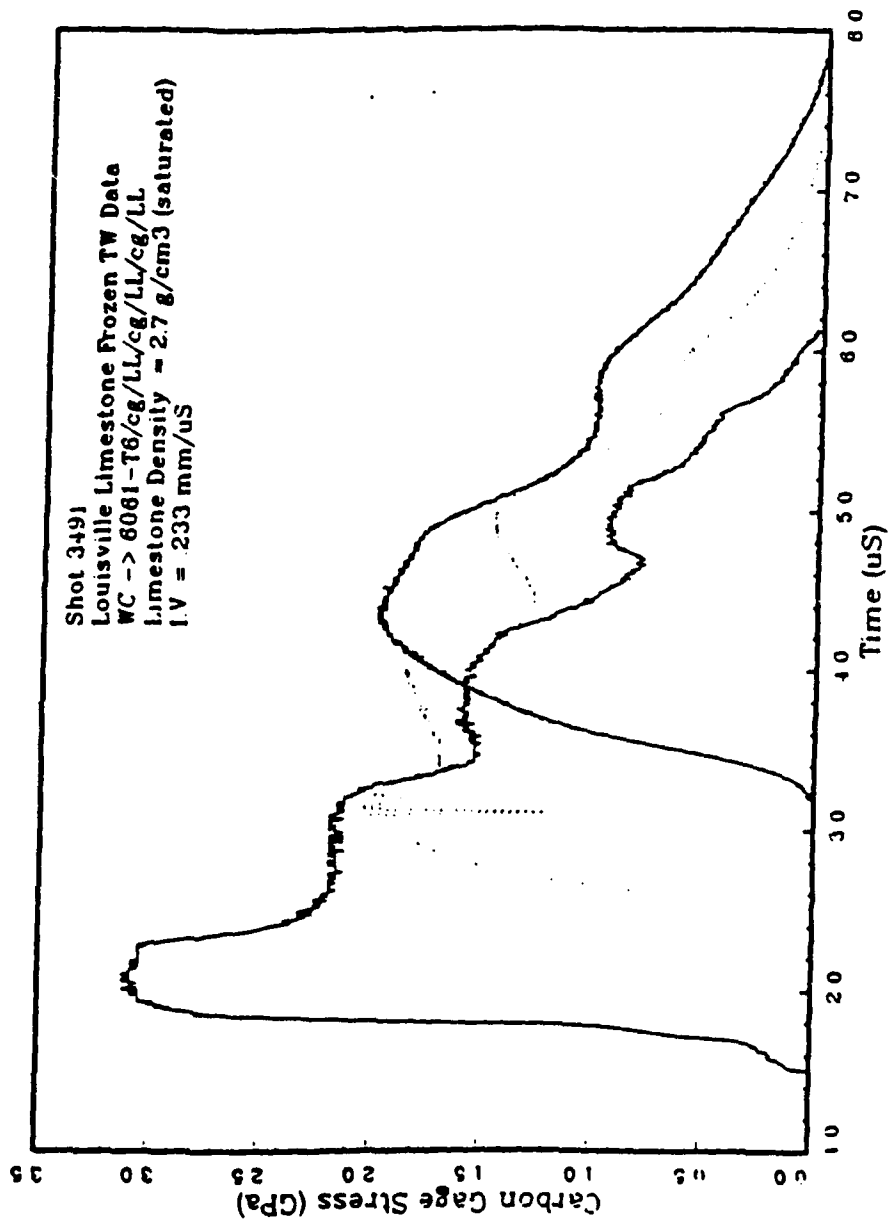


Figure A-24. Ft. Knox carbonates shot 3491.

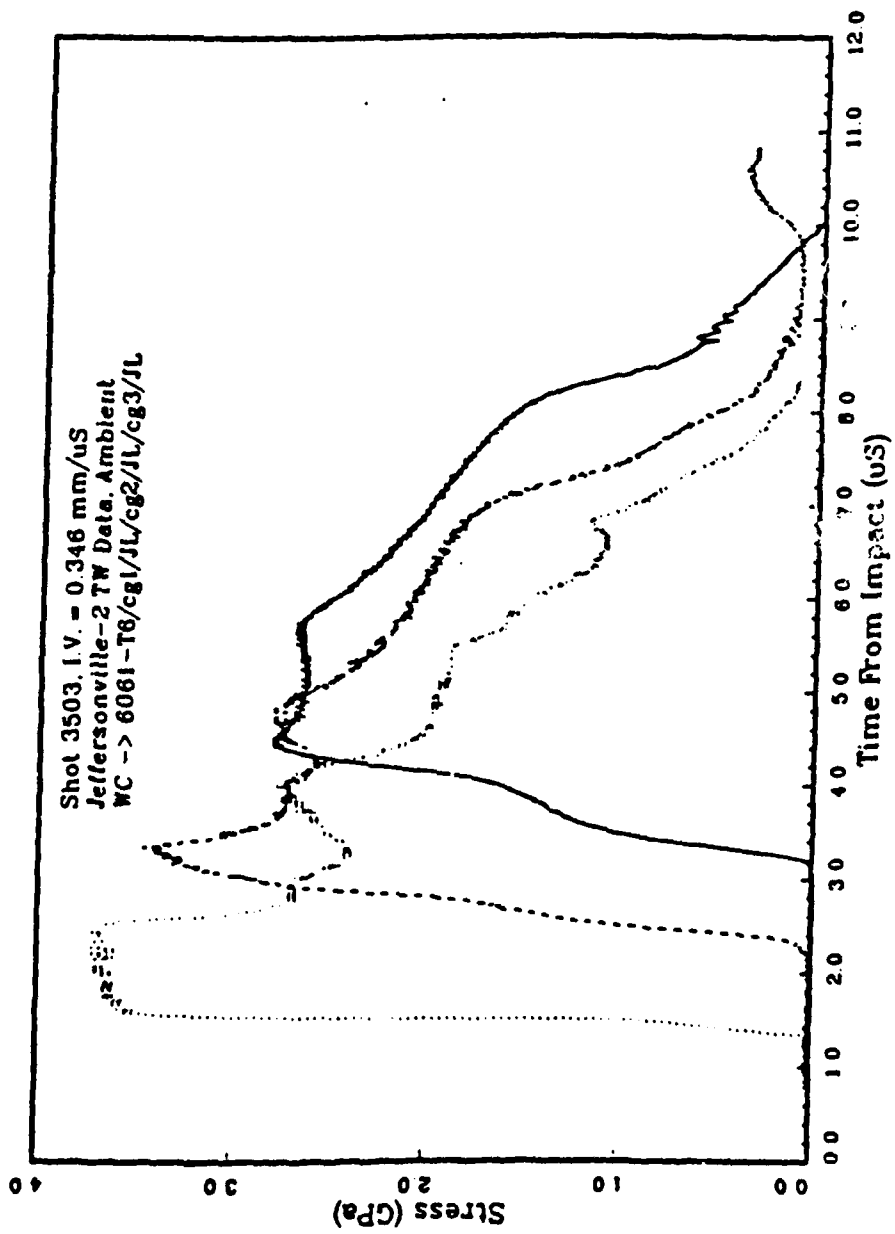


Figure A-25. Ft. Knox carbonates shot 3503.

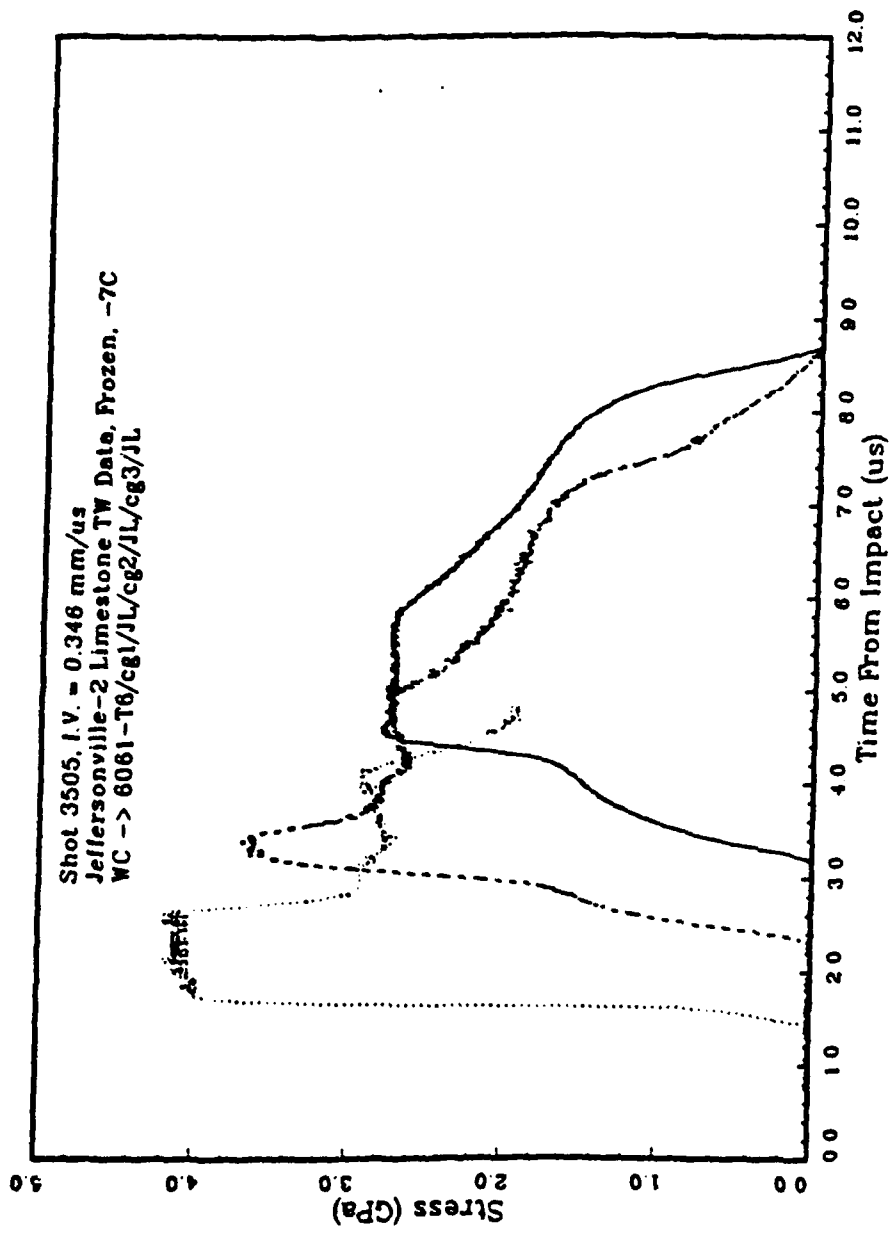


Figure A-26. Ft. Knox carbonates shot 3505.

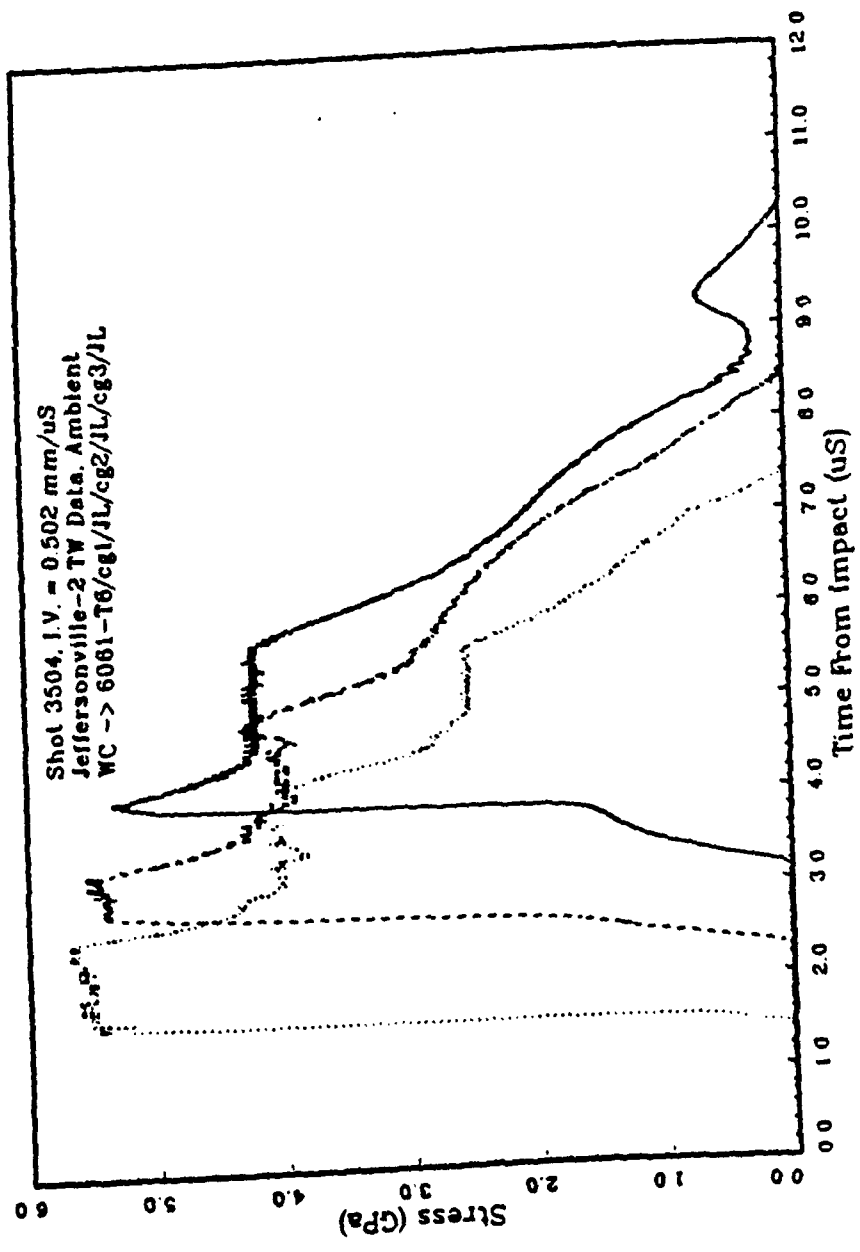


Figure A-27. Ft. Knox carbonates shot 3504.

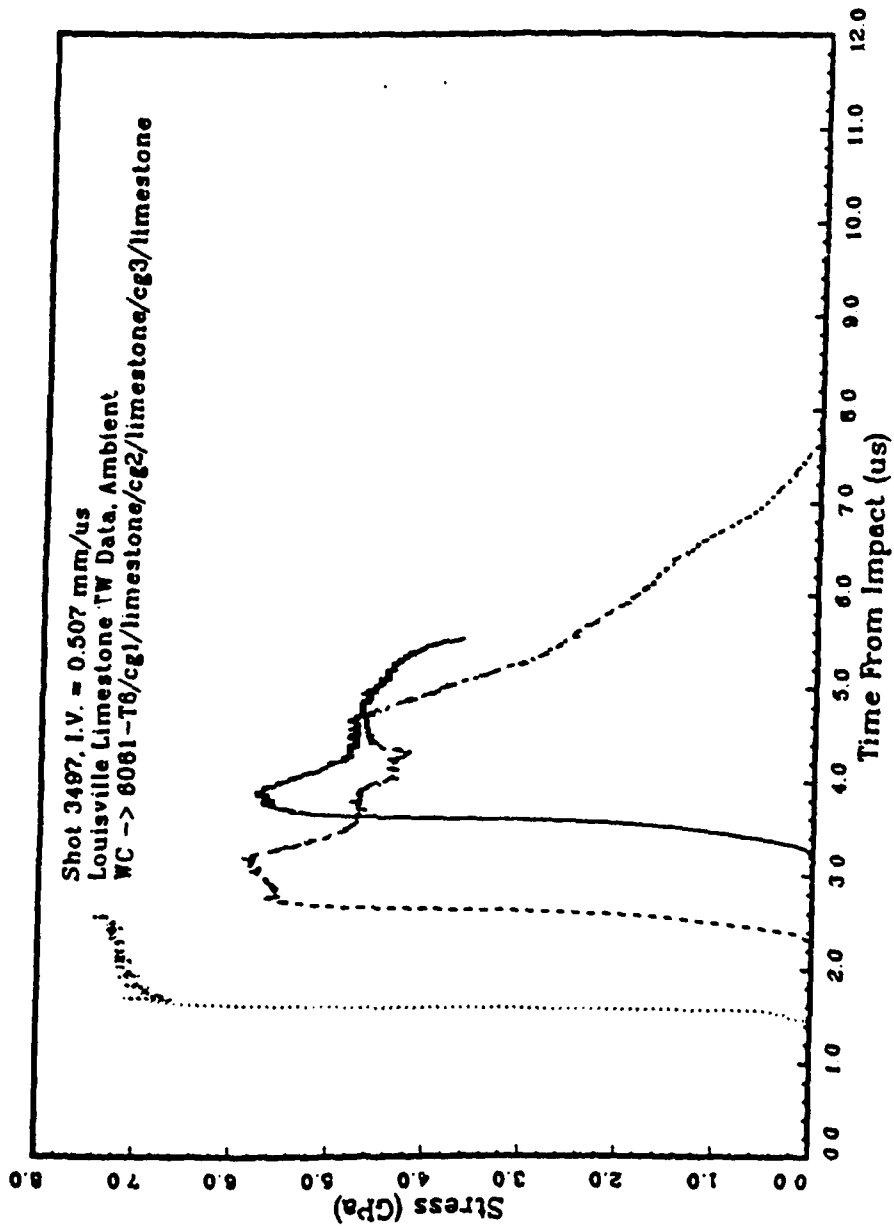


Figure A-28. Ft. Knox carbonates shot 3497.

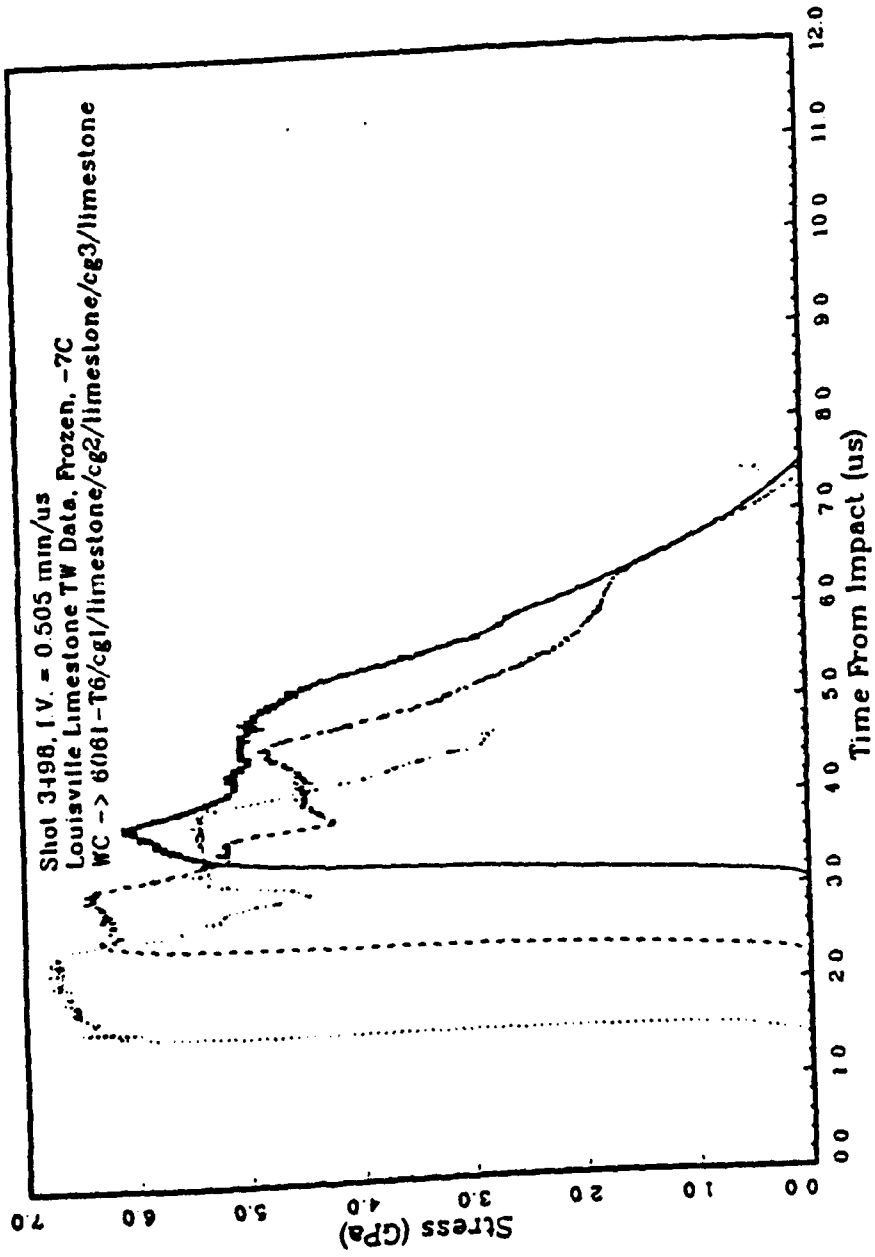


Figure A-29. Ft. Knox carbonates shot 3498.

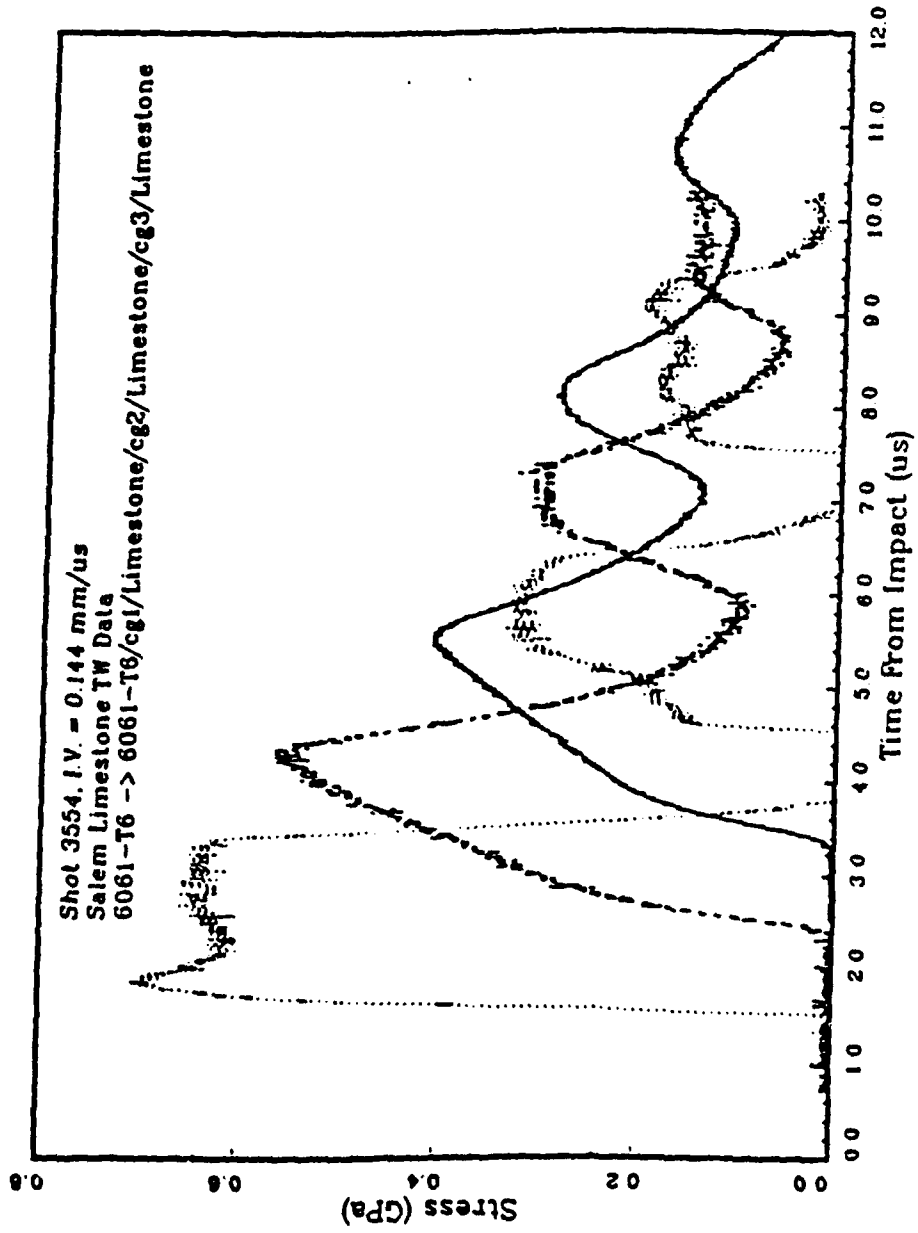


Figure A-30. Salem limestone shot 3554.

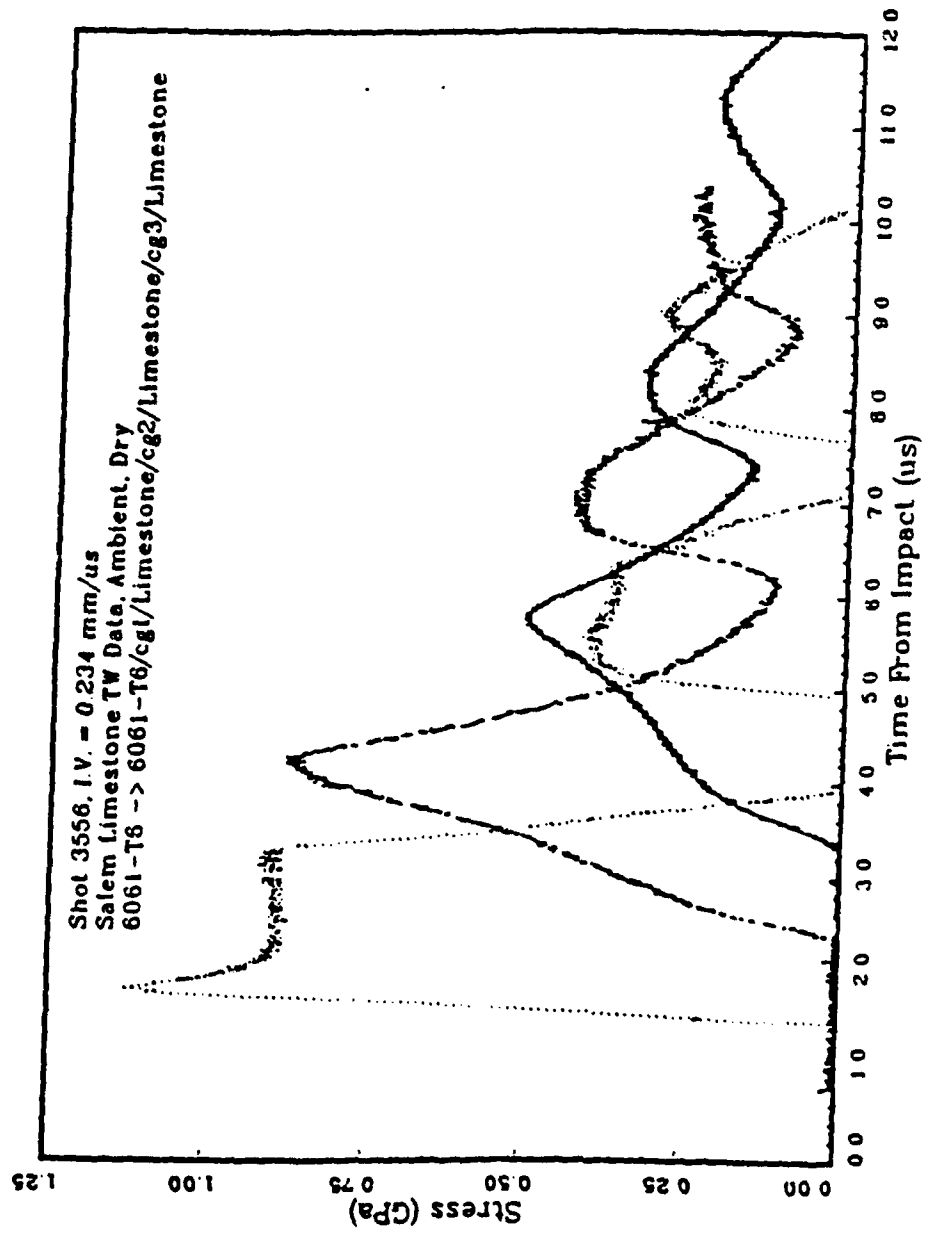


Figure A-31. Salem limestone shot 3556.

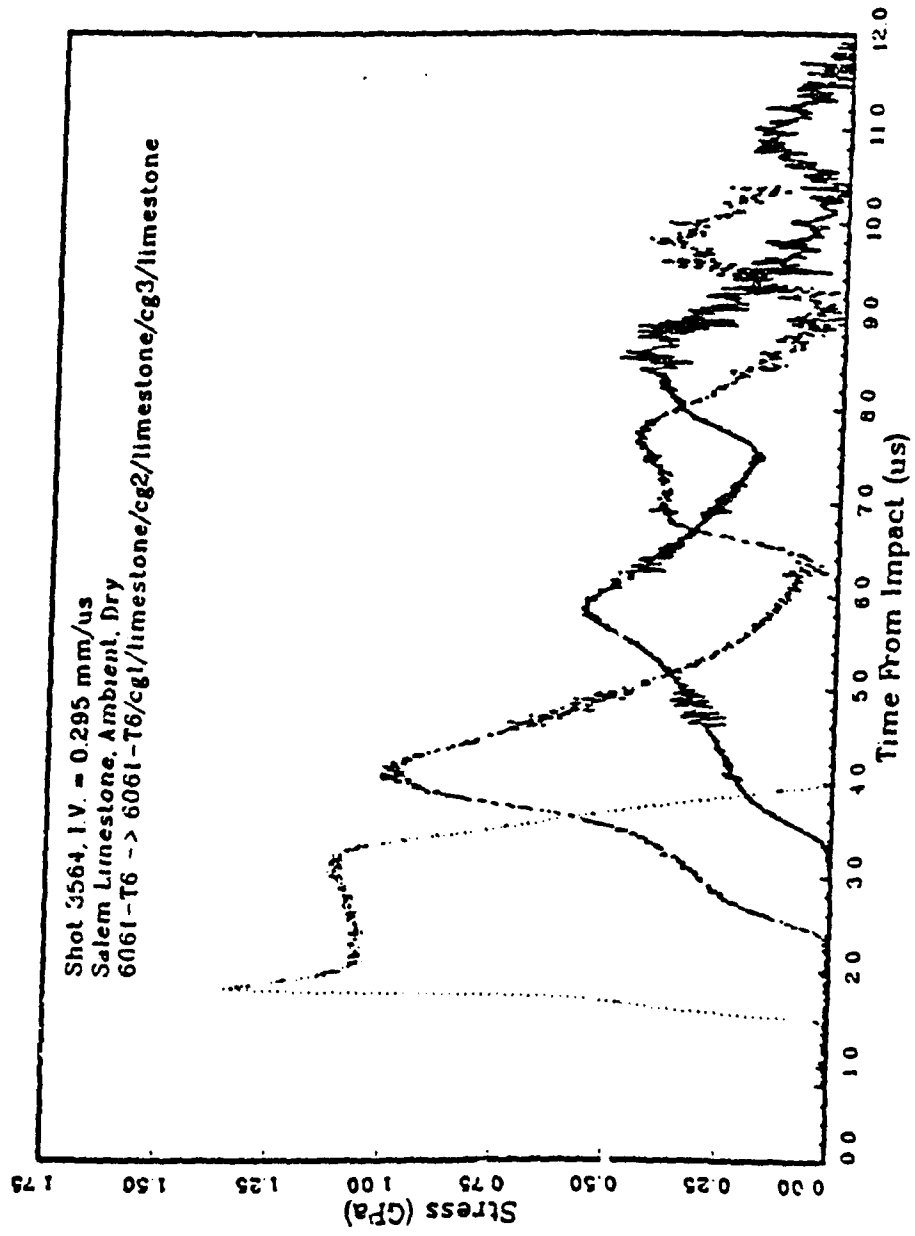


Figure A-32. Salem limestone shot 3564.

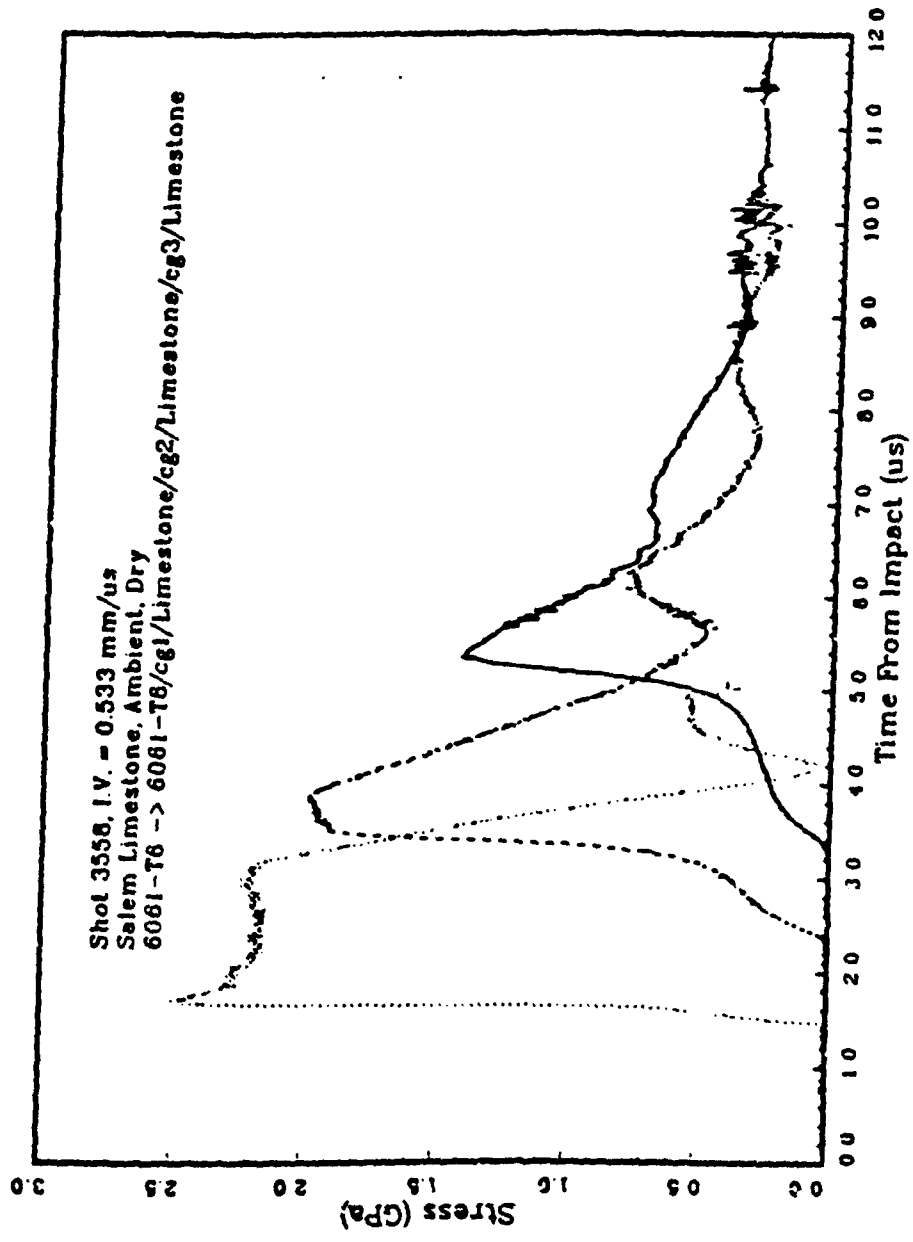


Figure A-33. Salem limestone shot 3558.

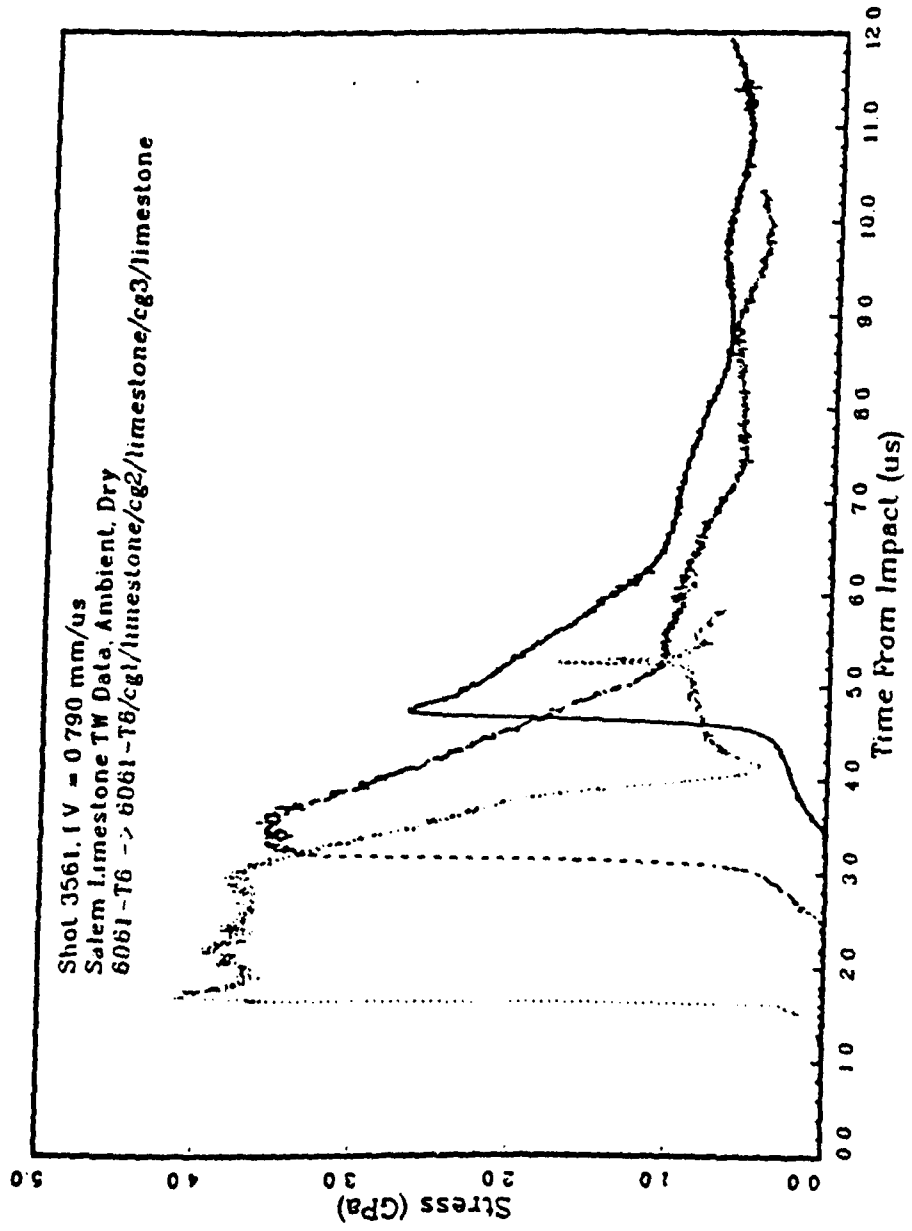


Figure A-34. Salem limestone shot 3561.

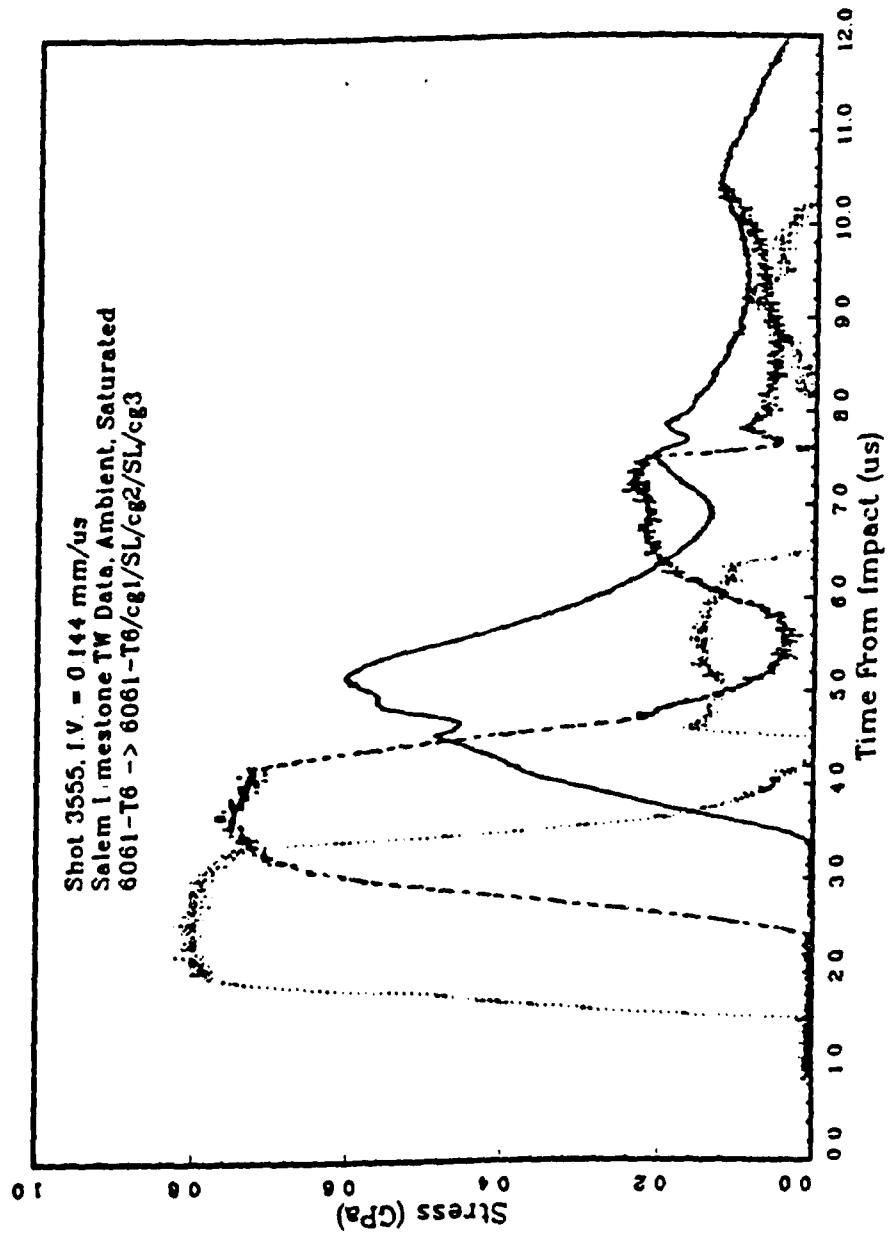


Figure A-35. Salem limestone shot 3555.

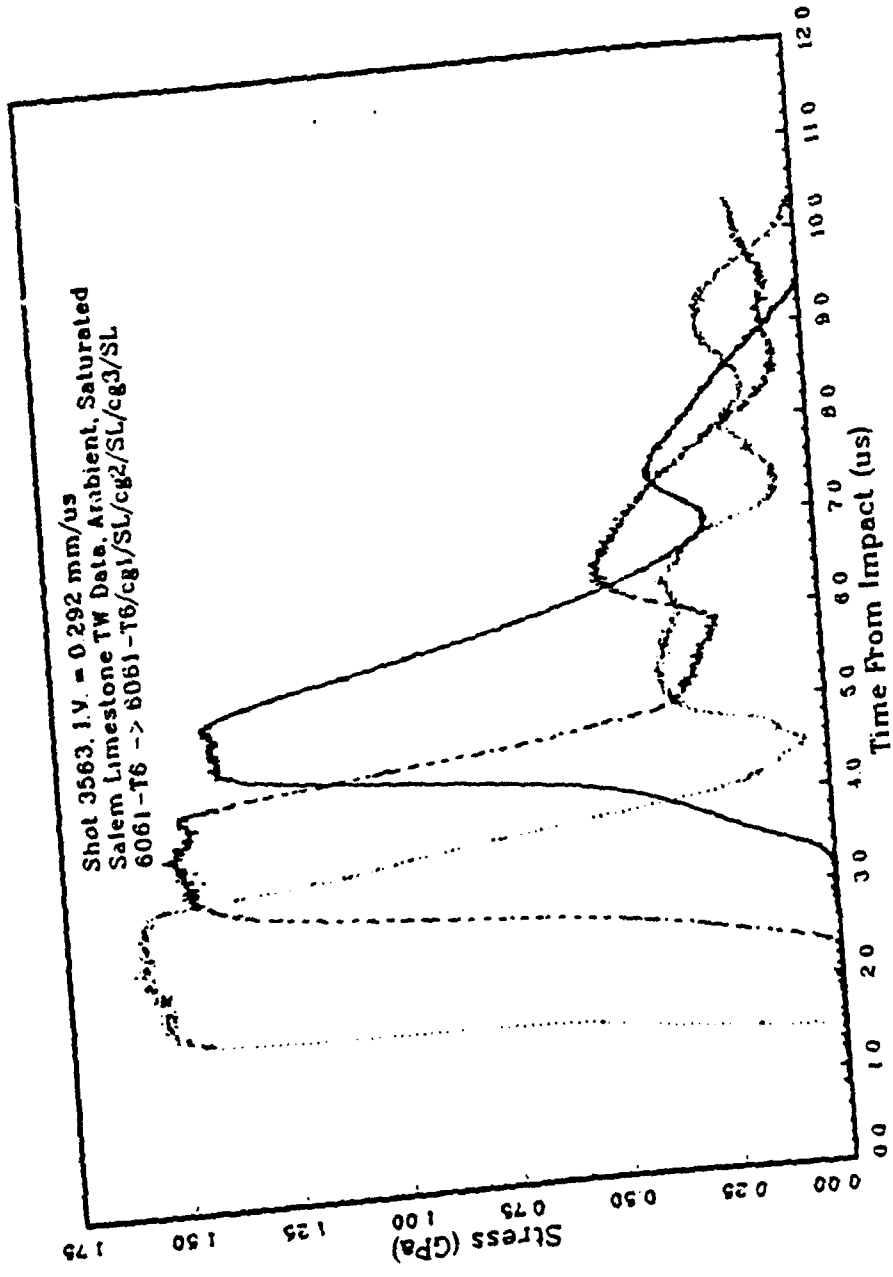


Figure A-36. Salem limestone shot 3563.

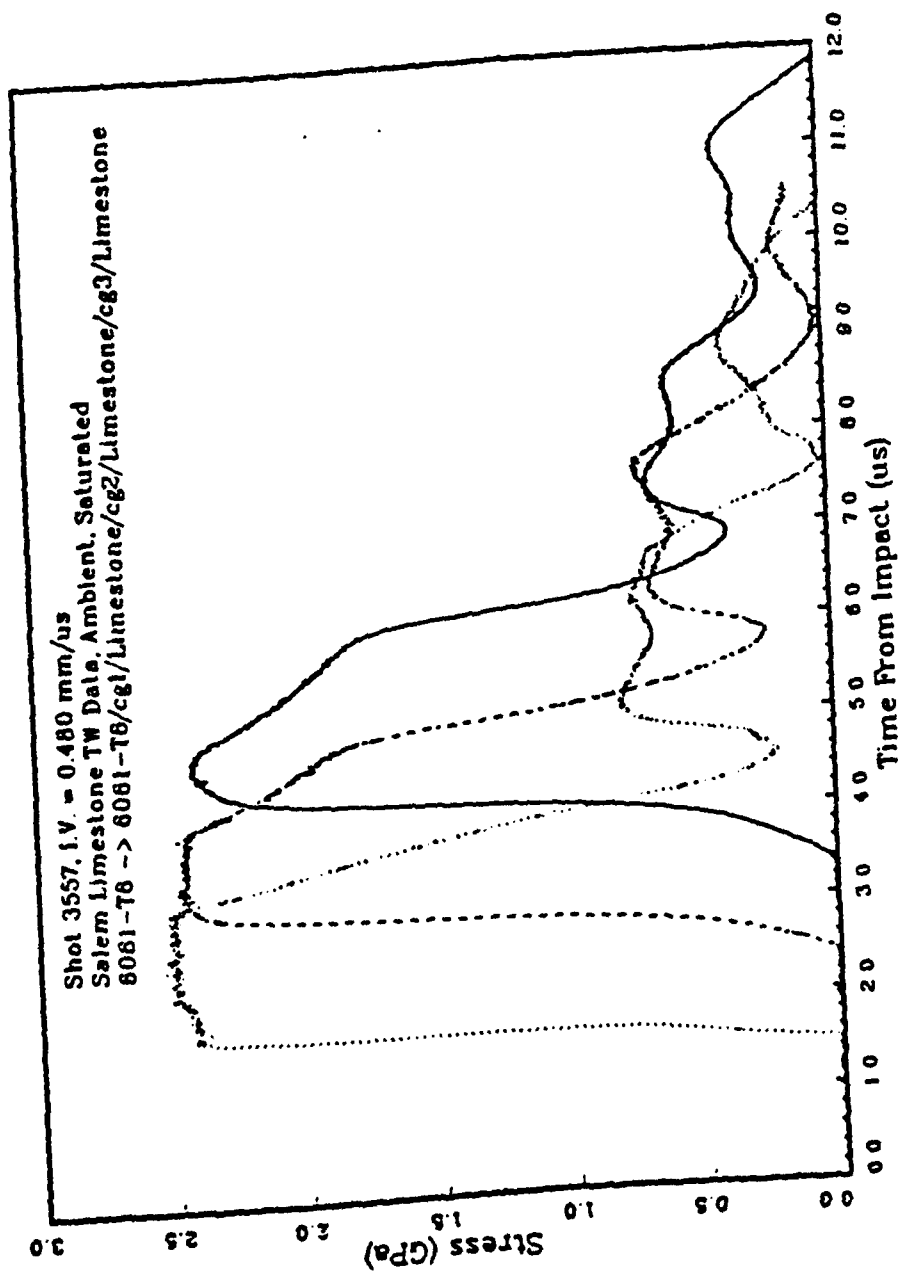


Figure A-37. Salem limestone shot 3557.

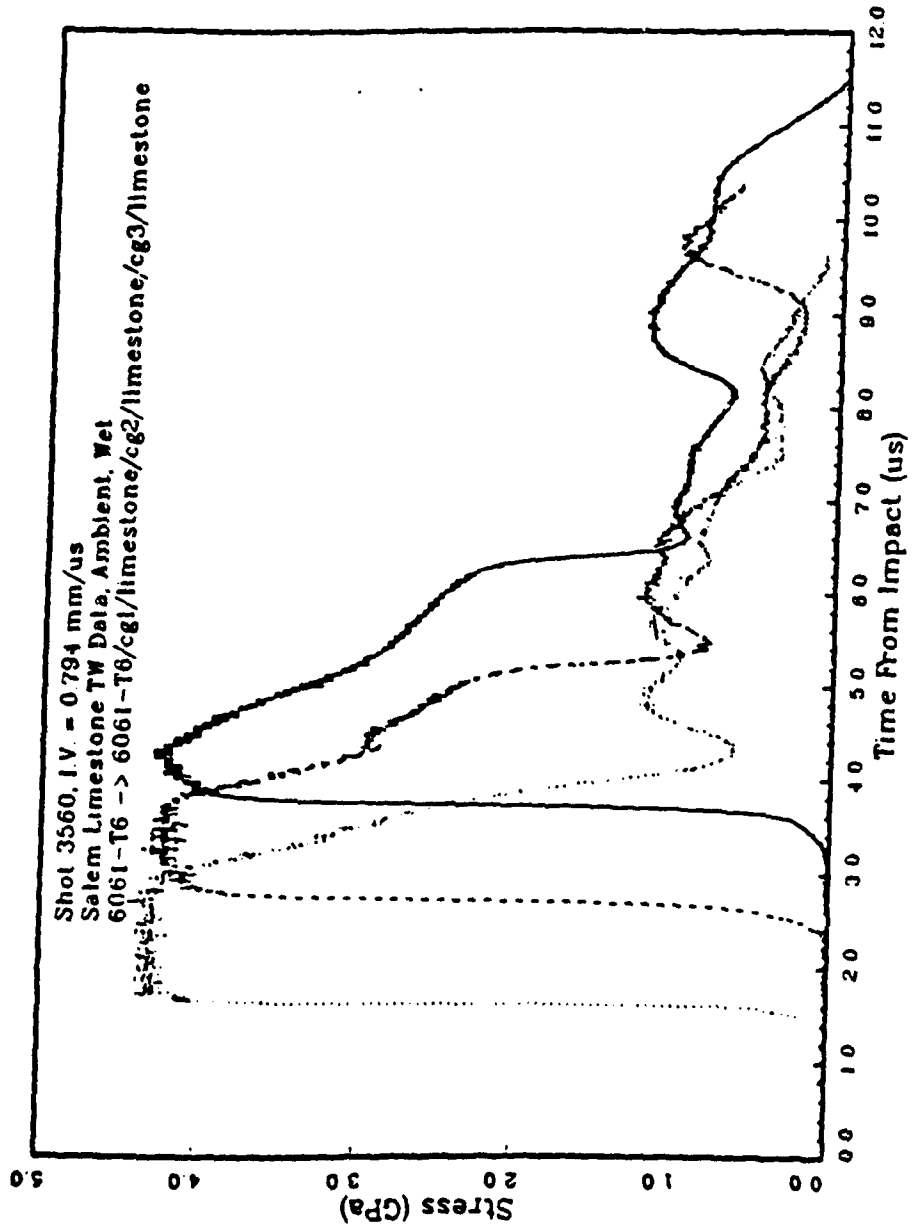


Figure A-38. Salem limestone shot 3560.

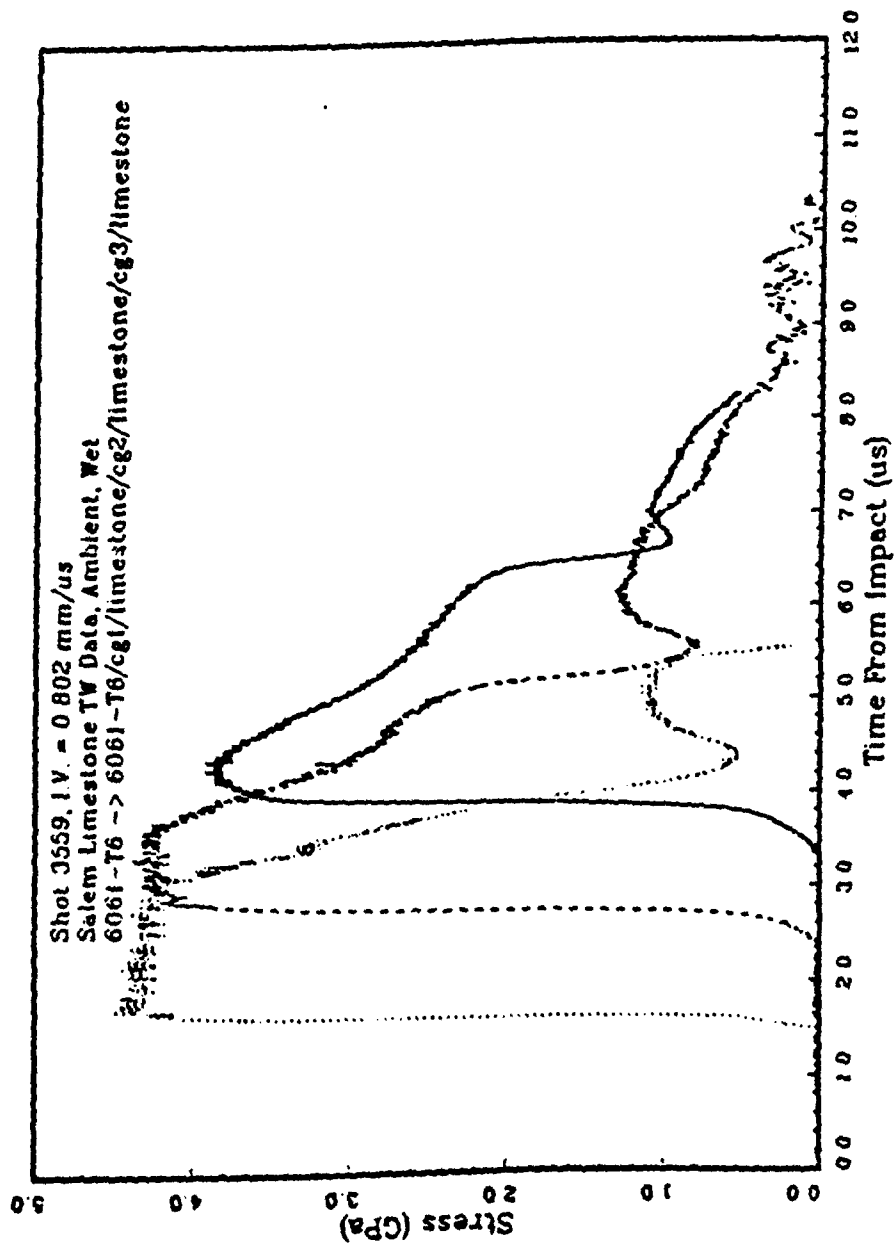


Figure A-39. Salem limestone shot 3559.

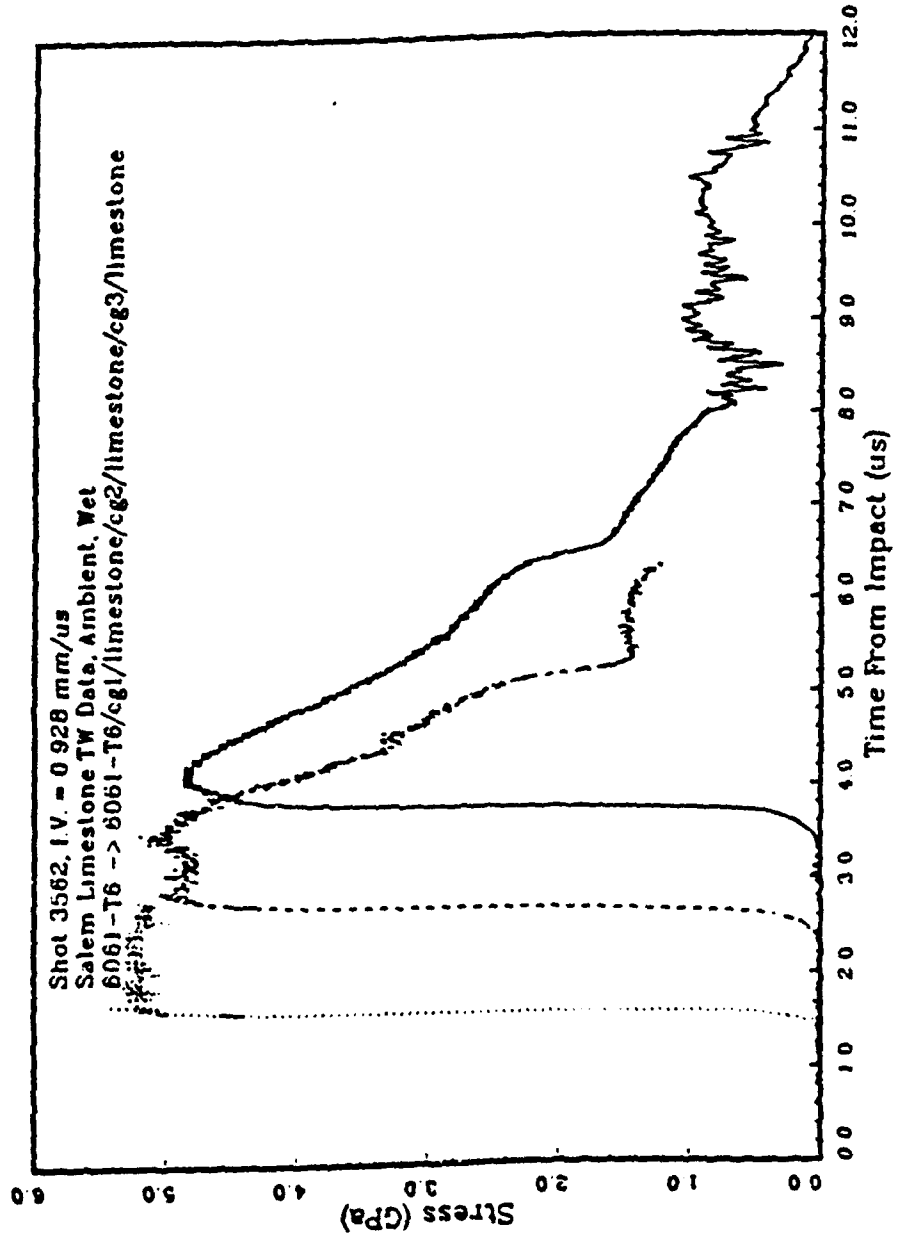


Figure A-40. Salem limestone shot 3562.

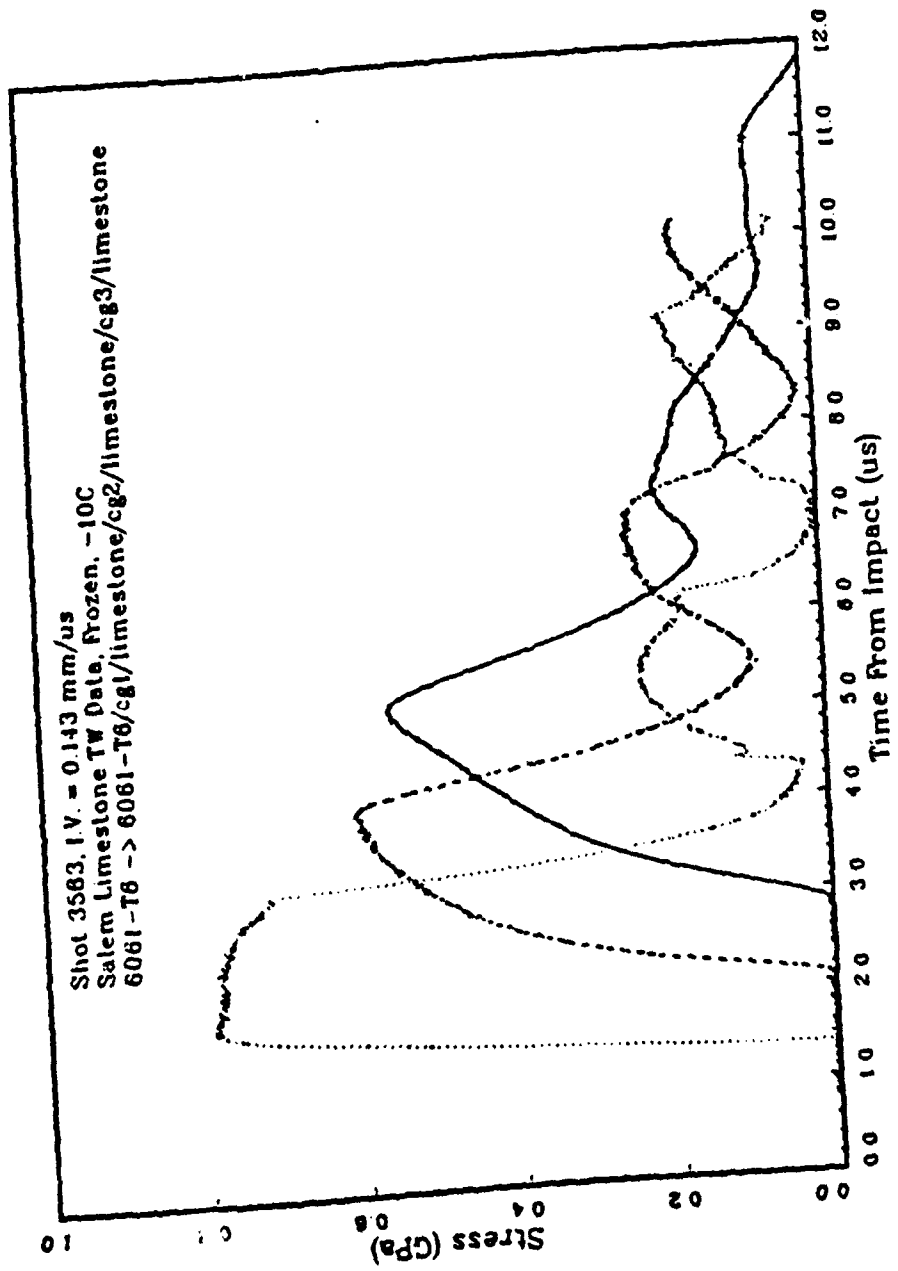


Figure A-41. Salem limestone shot 3583.

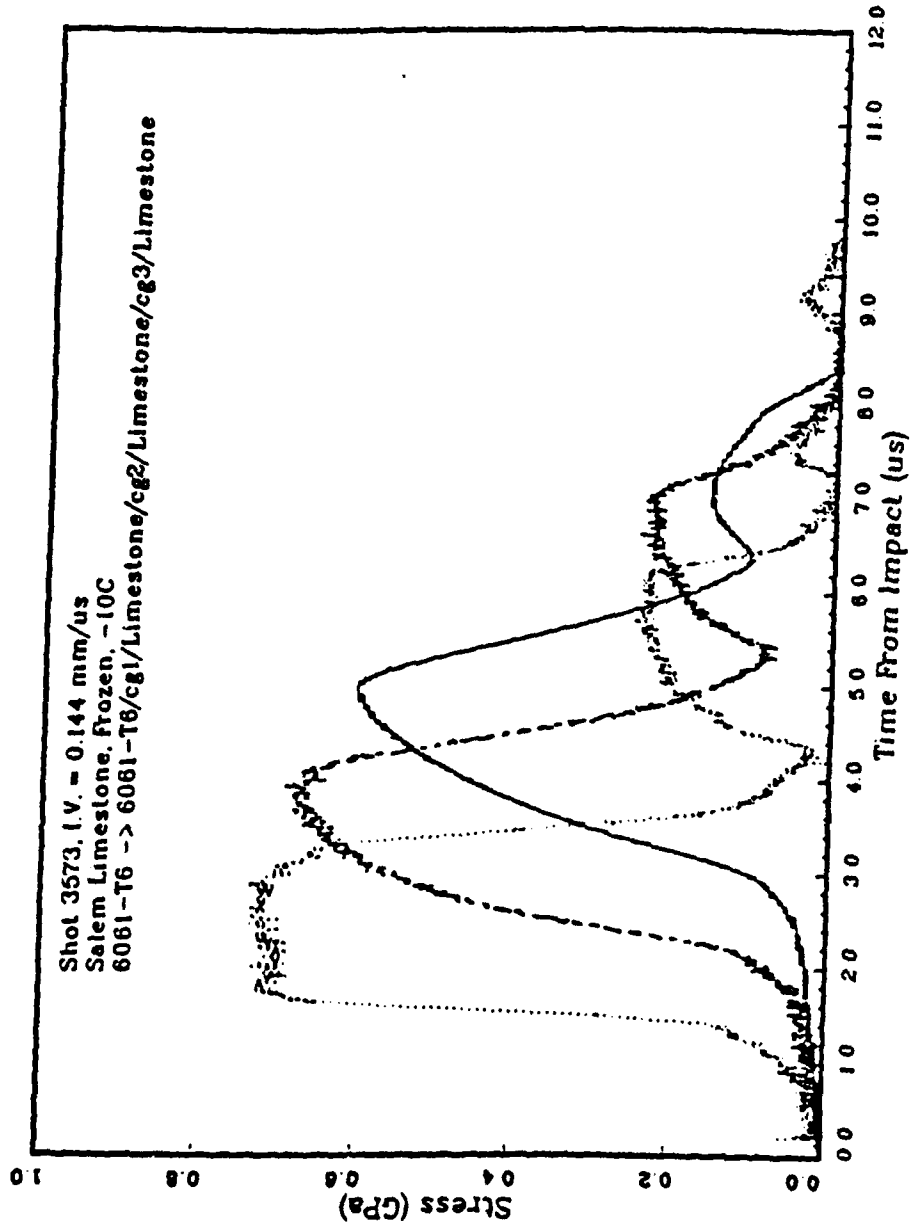


Figure A-42. Salem limestone shot 3573.

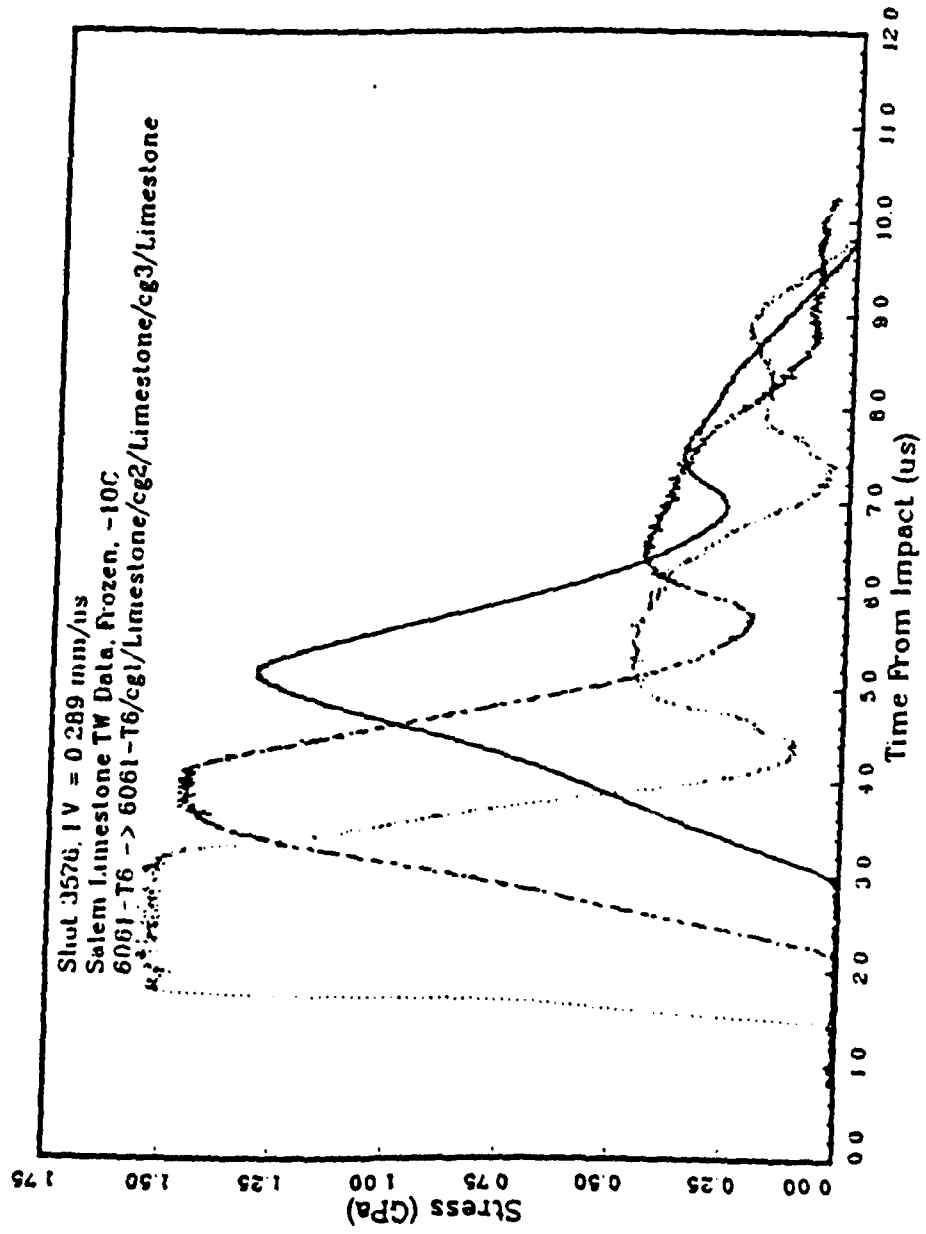


Figure A-43. Salem limestone shot 3576.

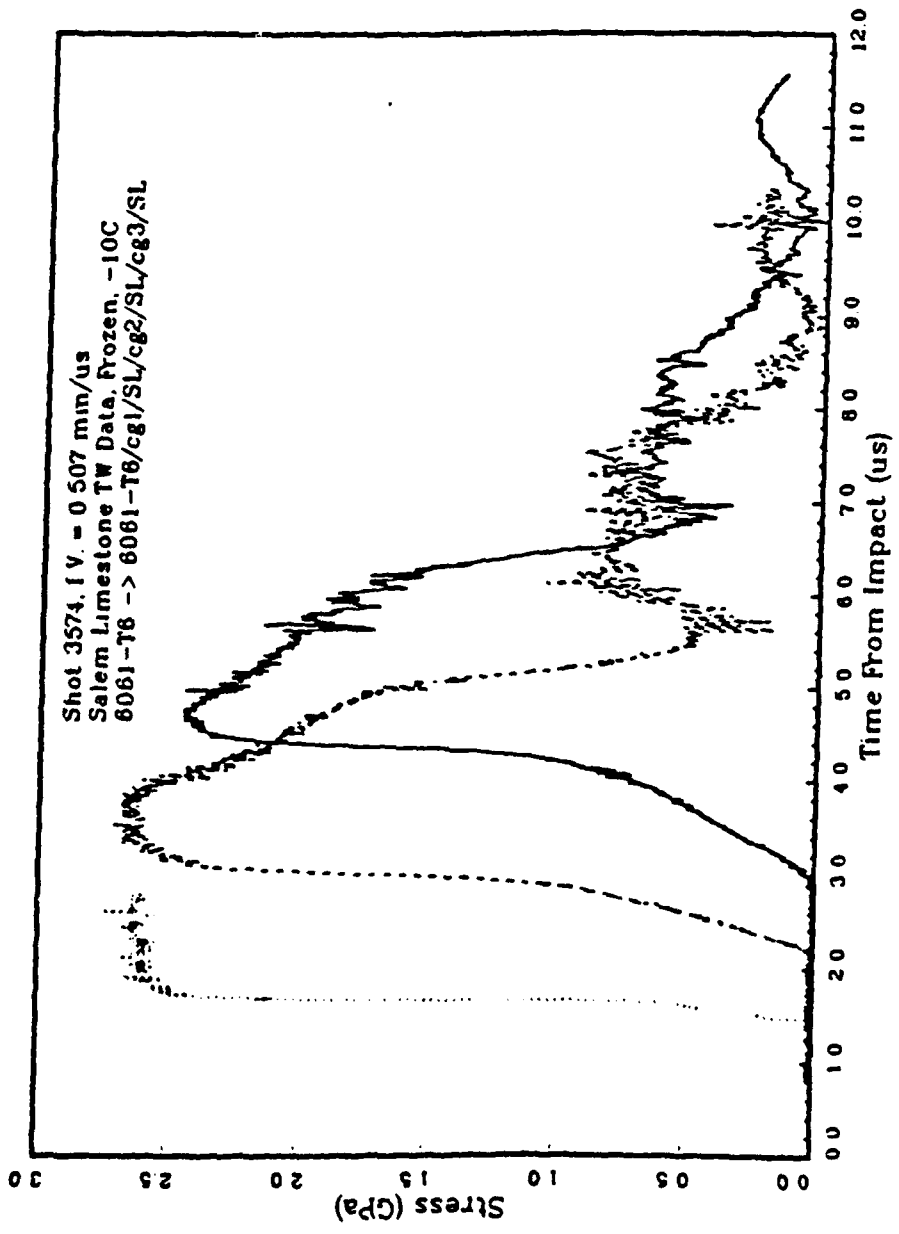


Figure A-44. Salem limestone shot 3574.

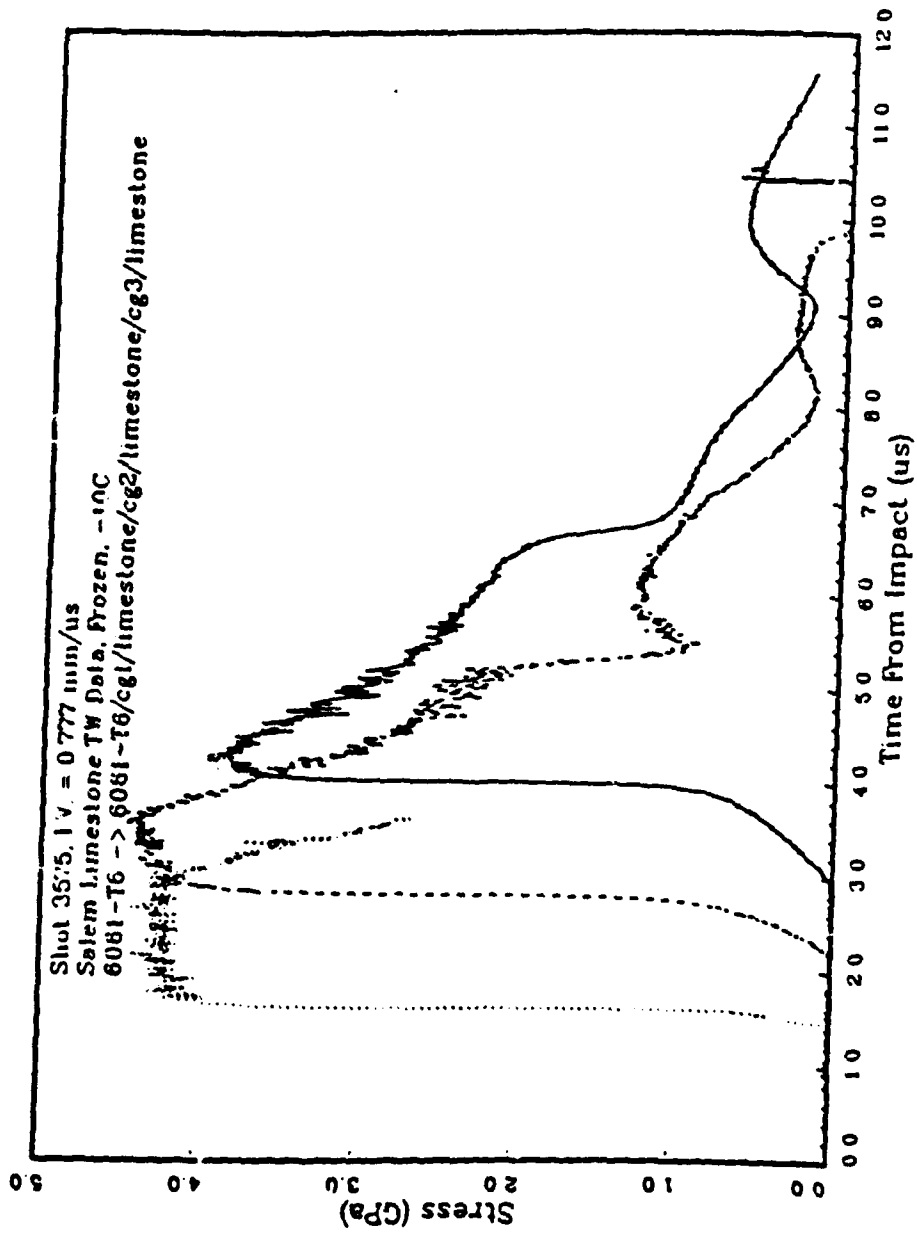


Figure A-45. Salem limestone shot 3575.

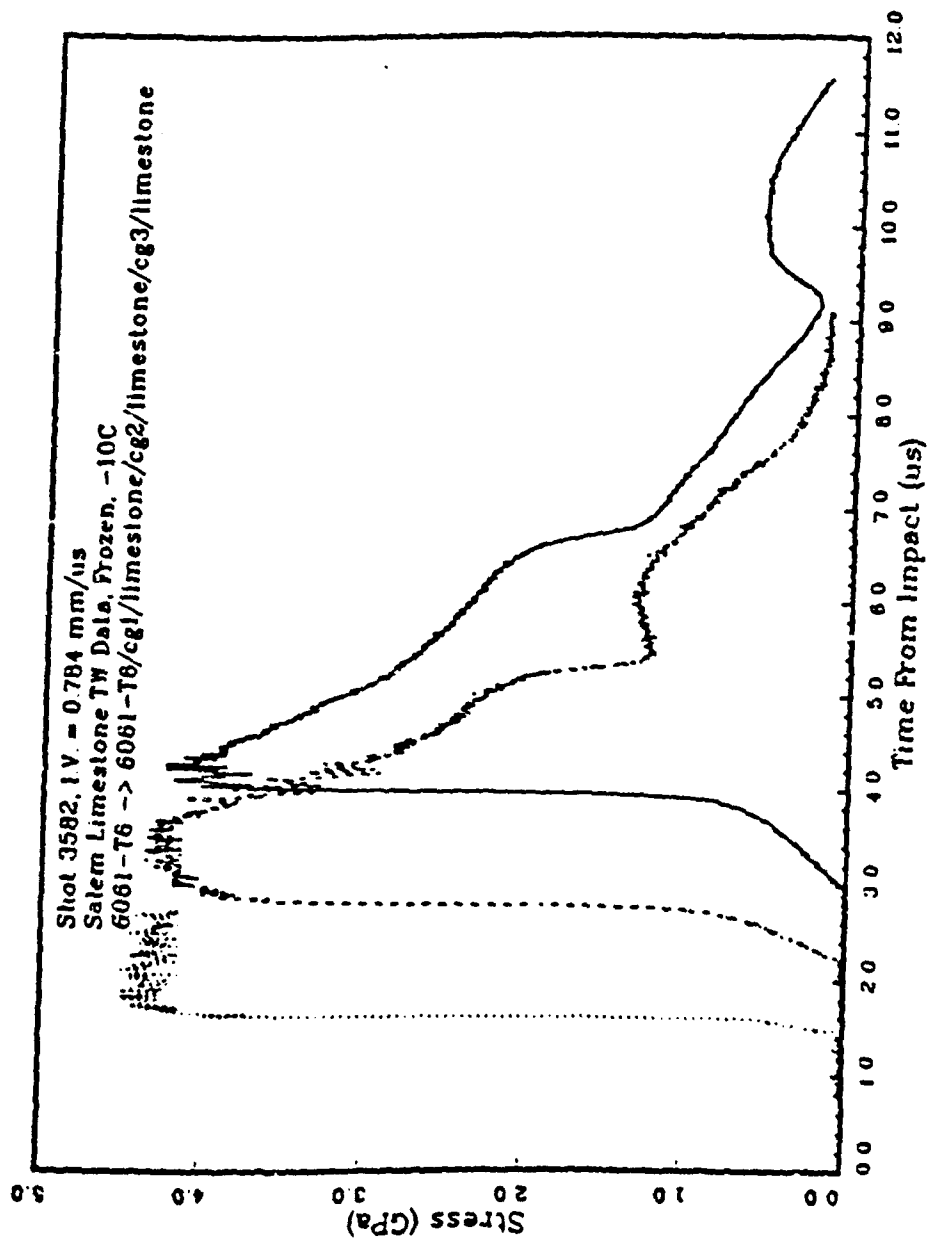


Figure A-46. Salem limestone shot 3582.

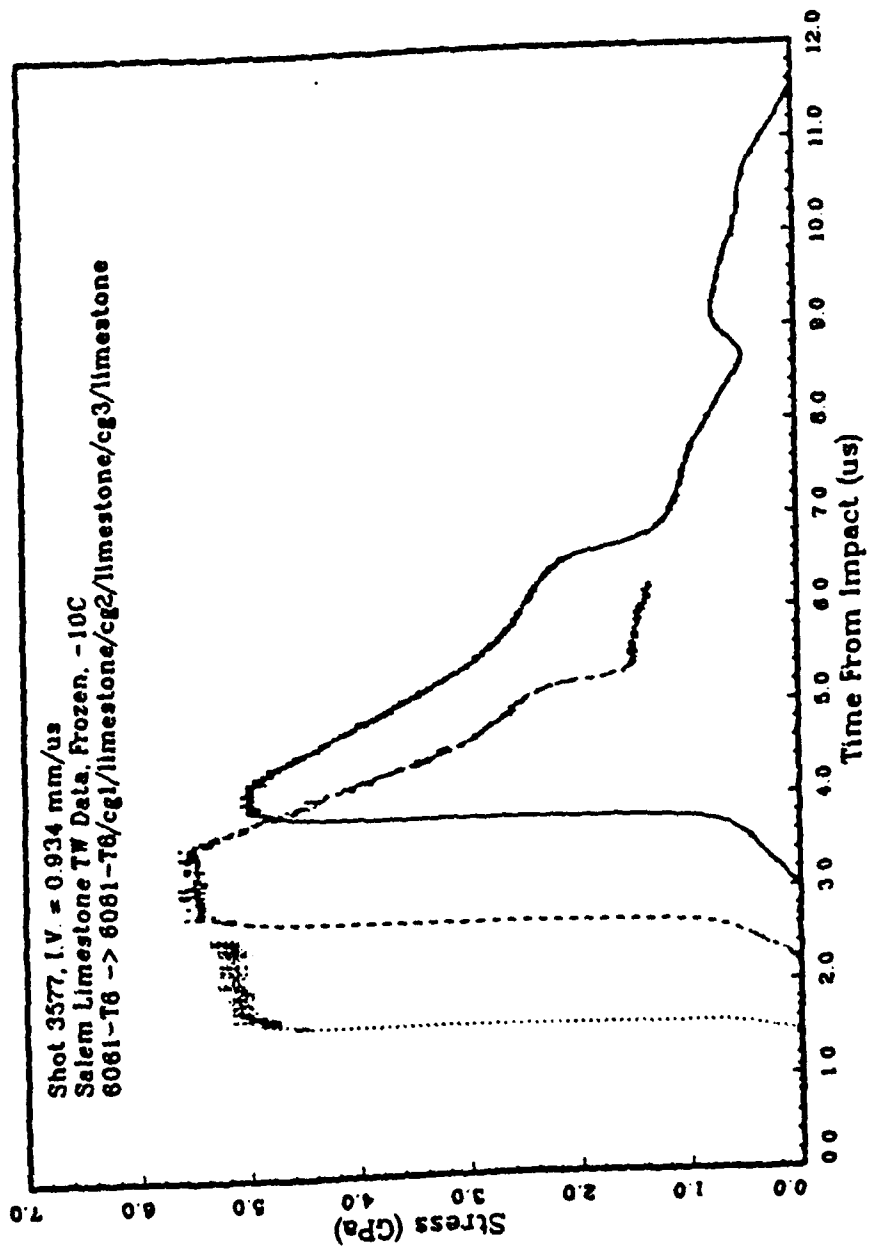


Figure A-47. Salem limestone shot 3577.

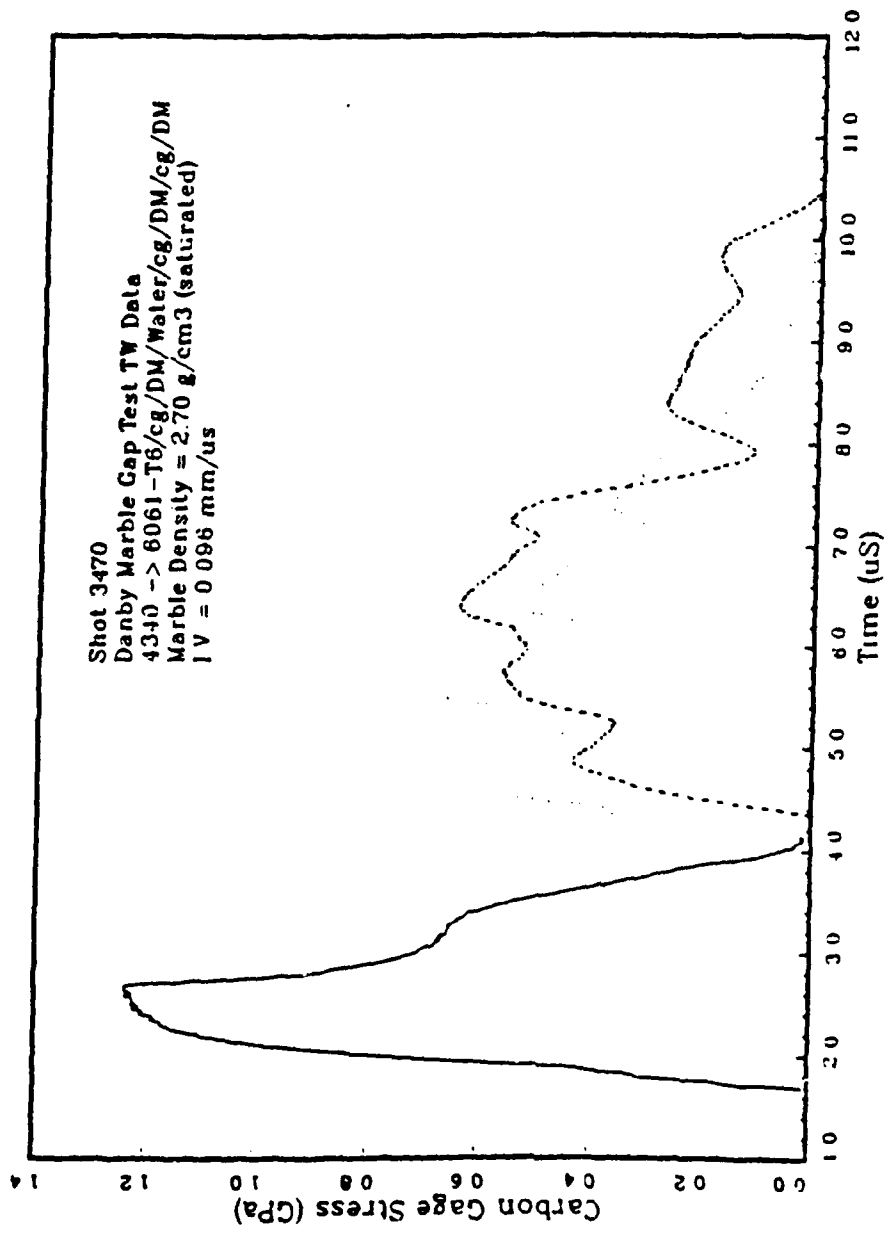


Figure A-48. Danby marble with joints shot 3470.

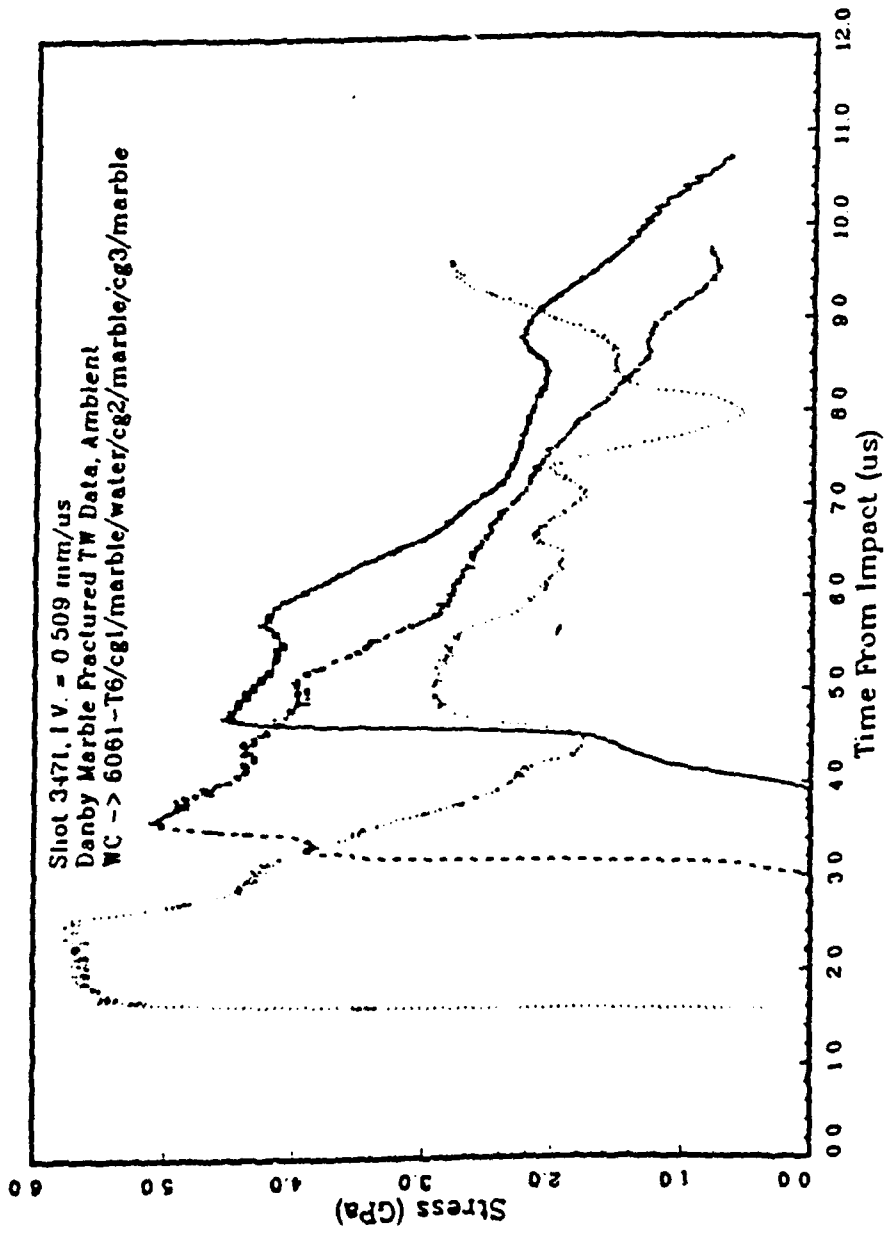


Figure A-49. Danby marble with joints shot 3471.

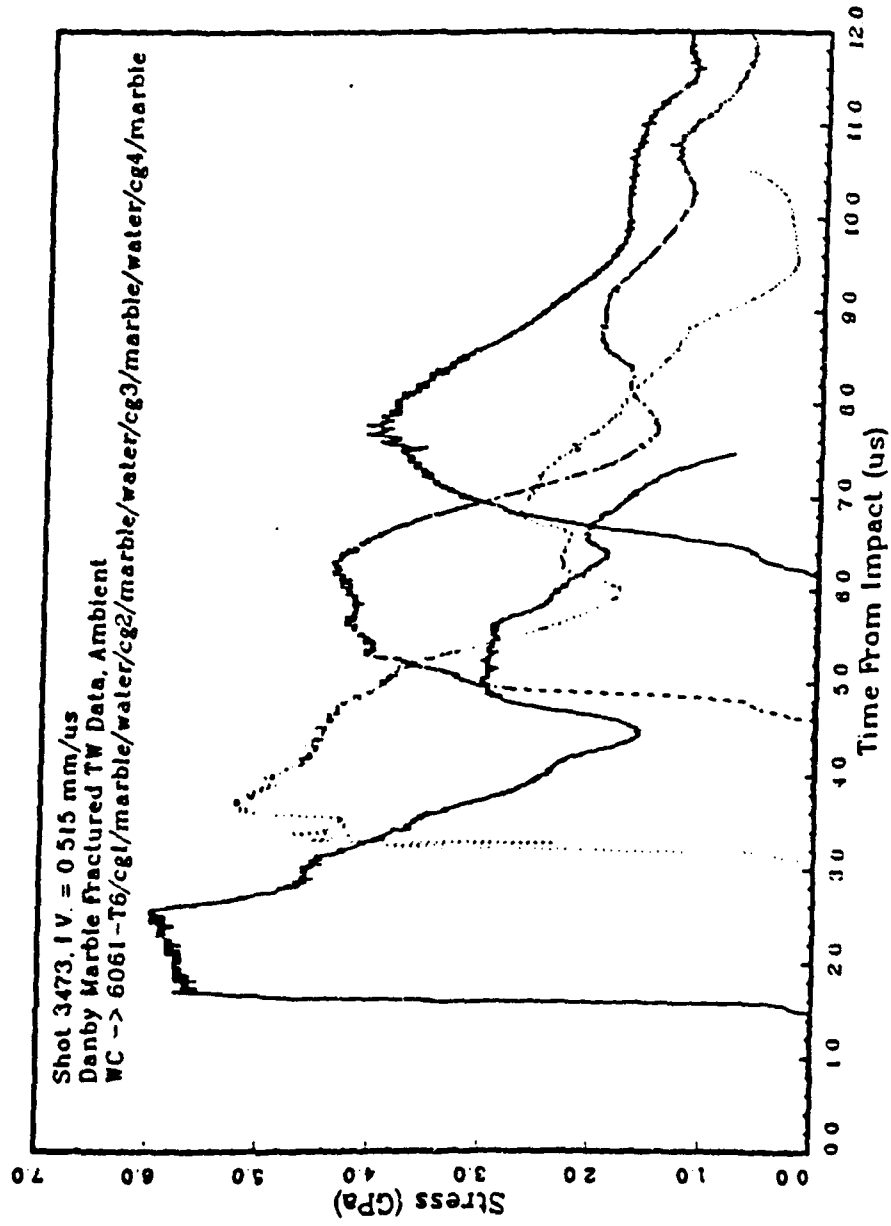


Figure A-50. Danby marble with joints shot 3473.

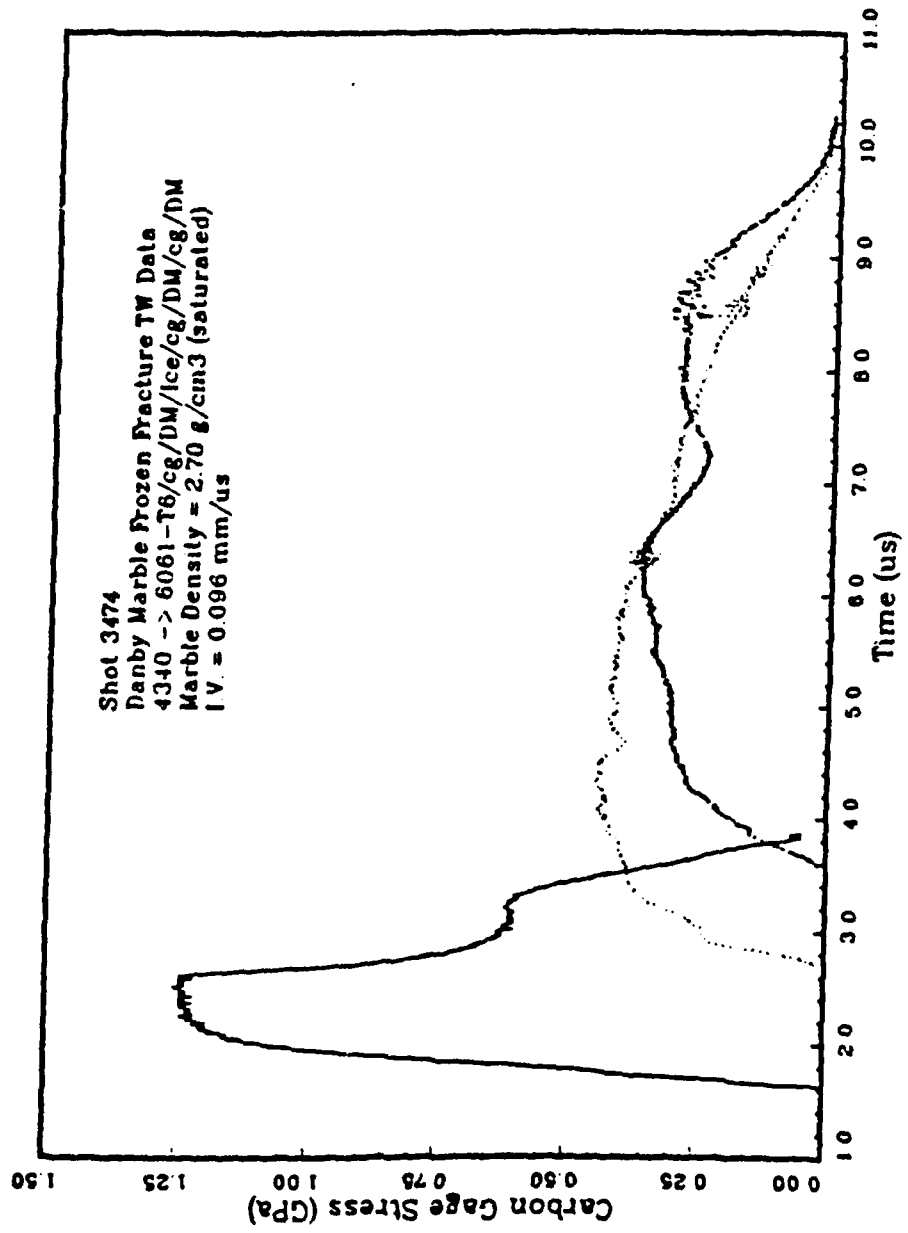


Figure A-51. Danby marble with joints shot 3474.

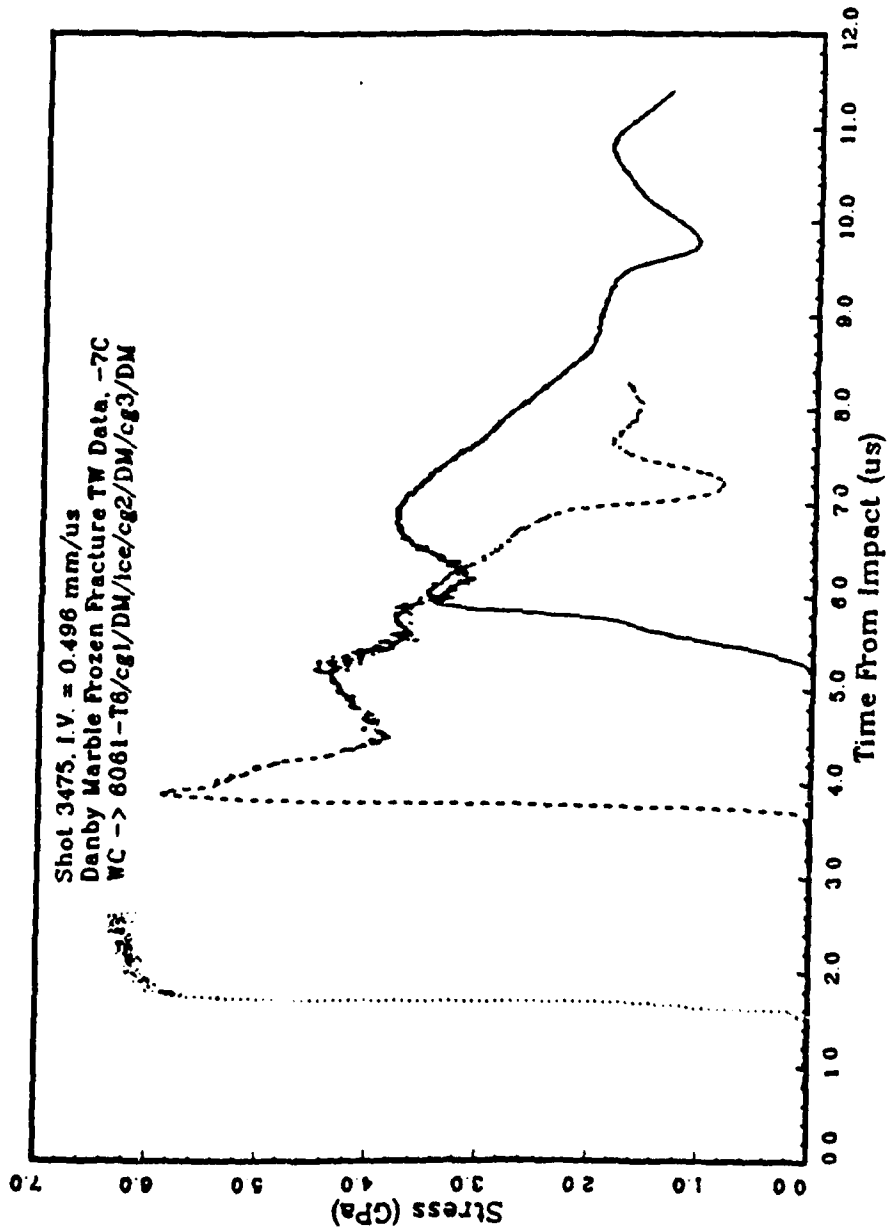


Figure A-52. Danby marble with joints shot 3475.

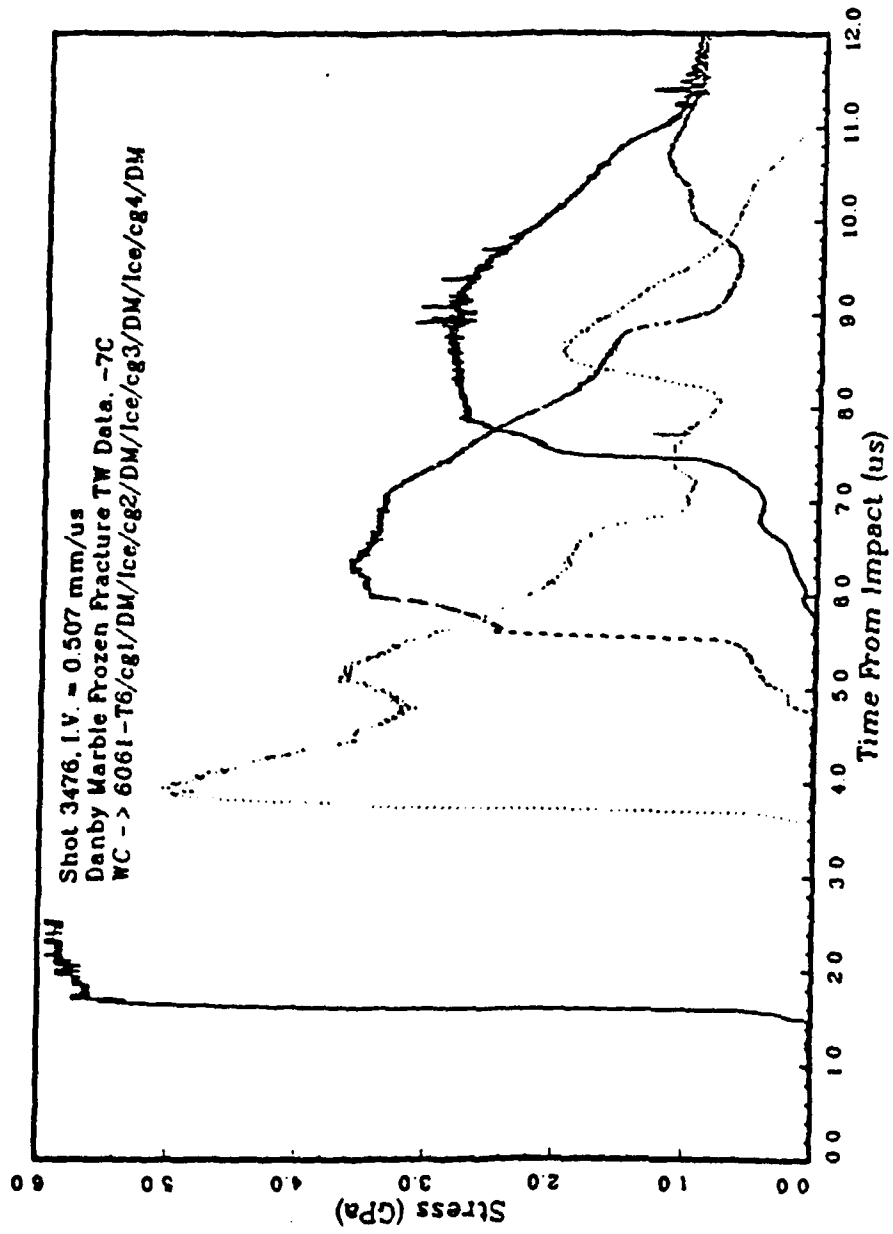


Figure A-53. Danby marble with joints shot 3476.

DISTRIBUTION LIST

DNA-TR-93-74

DEPARTMENT OF DEFENSE

ASSISTANT TO THE SECRETARY OF DEFENSE
2 CY ATTN: EXECUTIVE ASSISTANT

DEFENSE INTELLIGENCE AGENCY
ATTN: DT-1

DEFENSE NUCLEAR AGENCY
ATTN: DFSP
ATTN: DFTD D LINGER
ATTN: SPWE
ATTN: TDTR F RENSVOID
ATTN: TDTV F RENSVOID
2 CY ATTN: TITL

DEFENSE TECHNICAL INFORMATION CENTER
ATTN: DTIC/OC

FIELD COMMAND DEFENSE NUCLEAR AGENCY
ATTN: B HARRIS-WEST
ATTN: FCNV M O'BRIEN
ATTN: NVTV

FIELD COMMAND DEFENSE NUCLEAR AGENCY
ATTN: FCTT-T E RINEHART
ATTN: FCTT-T W SUMMA
ATTN: FCTT DR BALADI
ATTN: FCTTS
ATTN: FCTTS A MARTINEZ
ATTN: FCTTS D SEEMANN
ATTN: FCTTS DR BOB REINKE
ATTN: FCTTS J LEVERETTE
ATTN: FCTTS LTCOL LEONARD
ATTN: FCTTSP P RANDES
ATTN: MAJ C COOPER I CTT

UNDER SECRETARY OF DEFENSE (ACQ)
ATTN: G SEVIN

DEPARTMENT OF THE ARMY

U S ARMY ENGR WATERWAYS EXPER STATION
ATTN: CEWES-SD-CG J BOA
ATTN: E JACKSON CEWES-SD-R
ATTN: J ZELASKO CEWES-SD-R

DEPARTMENT OF THE AIR FORCE

PHILLIPS LABORATORY
2 CY ATTN: PUSUL

DEPARTMENT OF ENERGY

EQ&G, INC
ATTN: D EILERS

LAWRENCE LIVERMORE NATIONAL LAB
ATTN: DONALD LARSON
ATTN: F HEUZE
ATTN: B DUNLAP
ATTN: J RAMBO
ATTN: J WHITE
ATTN: W C MOSS
ATTN: R WARD

ATTN: B HUDSON
ATTN: LEWIS GLENN
ATTN: TECH LIBRARY

LOS ALAMOS NATIONAL LABORATORY

ATTN: B SWIFT
ATTN: DAVID KING
ATTN: FRED APP
ATTN: T MCKOWN
ATTN: J FRITZ
ATTN: C MORRIS
2 CY ATTN: REPORT LIBRARY
ATTN: J N JOHNSON
ATTN: R E HILL
ATTN: THOMAS DEY
ATTN: TOM WEAVER

SANDIA NATIONAL LABORATORIES

ATTN: DIV 9321 W BOYER
ATTN: MIKE FURNISH
ATTN: R BASS
2 CY ATTN: TECH LIB 3141

DEPARTMENT OF DEFENSE CONTRACTORS

ENSCO INC
ATTN: P FISHER

JAYCOR
ATTN: CYRUS P KNOWLES

JAYCOR
ATTN: R POLL

KAMAN SCIENCES CORP
ATTN: DASAC

KAMAN SCIENCES CORPORATION
2 CY ATTN: DASAC

KTECH CORP
2 CY ATTN: E GAFFNEY
2 CY ATTN: E SMITH
ATTN: FRANK DAVIES
ATTN: L LEE

LOGICON R & D ASSOCIATES
ATTN: B KILLIAN
ATTN: L GERMAIN

S-CUBED
ATTN: DR E PETERSON
ATTN: J BAKER
ATTN: J MORRIS
ATTN: MARK GROETHE
ATTN: P COLEMAN
ATTN: PERSONNEL OFFICE
ATTN: S PEYTON

SCIENCE APPLICATIONS INTL CORP

ATTN: DAN PATCH
ATTN: DR M MCKAY
ATTN: JACK KLUMP
ATTN: L SCOTT
ATTN: MARTIN FOGEL

DNA-TR-83-74 (DL CONTINUED)

**SCIENCE APPLICATIONS INTL CORP
ATTN: K SITES**

**SRI INTERNATIONAL
ATTN: D KEOUGH
ATTN: P DE CARLI**

**TECH REPS. INC
ATTN: F MCMULLAN
ATTN: R NAEGELI**

**TERRA TEK. INC
ATTN: W MARTIN**

**TITAN CORPORATION (THE)
ATTN: ANNE COOPER
ATTN: S SCHUSTER**

DIRECTORY OF OTHER

**MARYLAND UNIVERSITY OF
ATTN: RICHARD DICK**